Incorporation of Molybdenum in Nuclear Waste Glasses

By

Rick Short

Thesis
Submitted for the degree of Doctor of Philosophy

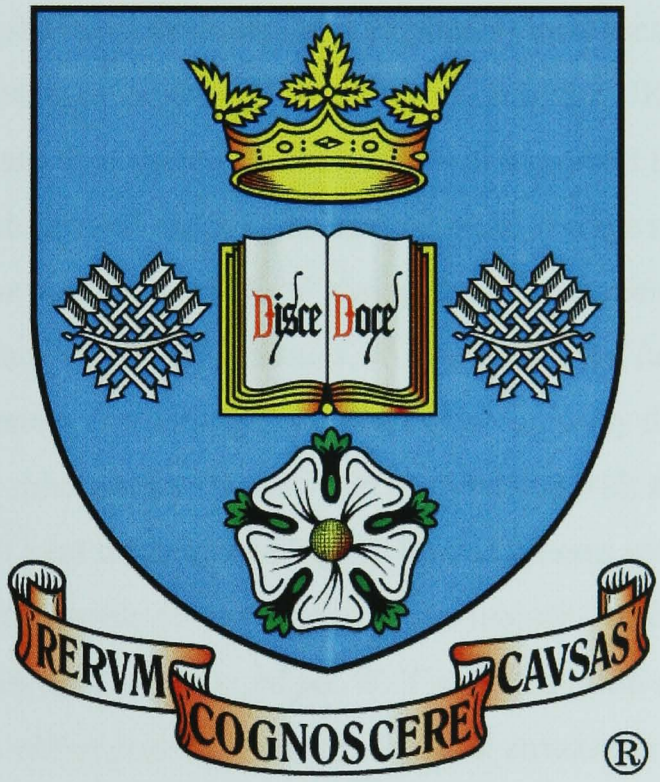

Immobilisation Science Laboratory
Department of Engineering Materials
University of Sheffield

Sponsored by EPSRC and BNFL

January 2004

Abstract

Alkali borosilicate glasses have been widely used as a matrix for the vitrification of high level radioactive waste (HLW) over the last 40 years. Increasing the waste loading of the HLW glasses could increase the efficiency of the vitrification process, but could also increase the tendency for devitrification, which could have a negative effect on the overall properties of the glass. Molybdenum (found in many HLW compositions) has a low (~1wt%) solubility in borosilicates, and when present in higher concentrations in HLW melts, tends to combine with other elements from the HLW to form crystalline material phases termed "yellow phase". Yellow phase (a mixture of alkali molybdates, chromates and sulphates) increases the corrosion rate of the inconel melting furnaces used in HLW vitrification in the UK, and can be water soluble in the solid state. It is therefore undesirable in a product that may eventually come into contact with ground water in an underground storage repository.

Simulated (non-radioactive) HLW glasses have been melted in various atmospheres, with a range of waste loadings, to investigate the factors influencing the formation of molybdenum containing crystalline phases. X-ray diffraction and transmission electron microscopy showed that molybdates with a powellite type structure formed upon heat treatment of highly loaded glasses melted in air, and that these molybdates were capable of incorporating the majority of mono, di and trivalent cationic species present in the simulated HLW. The distribution of the cationic species on the A sites of the powellite type molybdate structures was shown to be random using extended x-ray absorption fine structure (EXAFS).

Electron spin resonance and x-ray photoelectron spectroscopy were used to show that the oxidation state of the Mo in simplified simulated HLW glasses could be partially reduced by sparging the melt with a reducing (as opposed to a neutral or oxidising) gas. Heat treatments on these compositions showed that powellite molybdates were less likely to form in reduced melts, however sparging glasses containing a full simulated HLW with a reducing gas during melting increased the tendency for powellite type molybdate formation upon heat treatment. EXAFS was used to show that, regardless of the waste loading or sparge applied during melting, the Mo was predominantly present as $(MoO_4)^{2-}$ tetrahedra in the glasses, and also in a yellow phase sample taken from a full scale simulated HLW glass.

Published Work

A paper entitled "Molybdenum in Nuclear Waste Glasses – Incorporation and Redox State" was presented at the 2002 MRS Fall Meeting in Boston, USA, and will be published in Scientific Basis for Nuclear Waste Management XXVI. This paper contains work from Chapters 4, 5 and 6 of this thesis.

A paper entitled "An Investigation into the Oxidation State of Molybdenum in Simplified High Level Nuclear Waste Glass Compositions" was presented at the 2003 MRS Scientific Basis for Nuclear Waste Management XXVII Meeting in Kalmar, Sweden, and will be published in Scientific Basis for Nuclear Waste Management XXVII. This paper contains work from Chapter 6 of this thesis.

Parts of this work have been presented at a number of national and international conferences. The titles of the presentations, relevant abstracts and papers and the conferences at which they were presented are listed on the compact disc accompanying this thesis.

Acknowledgements

Firstly I would like to thank my supervisor, Dr Russell Hand, whose advice and support has been invaluable over the last 3 years. Many thanks also to Dr Neil Hyatt for his help with various experiments and his seemingly endless supply of enthusiasm and Mr Charlie Scales, my industrial supervisor and Cumbrian advisor.

For their help and technical support, I wish to thank Dean Headlock and Iron Watts (for making every melt a pleasure), Dr Paul Anderson and Mr Terry Green of the University of Birmingham (ESR), Dr Diane Holland of Warwick University (XPS), Mr Bob Bilsborow of Daresbury Labs and Prof Francis Livens of The University of Manchester (EXAFS), Dr Guenter Moebus (TEM) and all of the staff, technicians and students at The Engineering Materials department who have helped me out at one time or another.

On a more personal note, for all of you who were close during the writing up period… I want to thank Claire, Tony and James for ignoring my rages and resisting the urge to set fire to me whilst I was sleeping, all of my nearby friends for socialising with me, those in other parts of the world for the entertaining and pleasurably distracting emails (Miles). Mum, Dad, Cas and the rest of the family (yes, I very nearly have got a real job now). And most of all Suzy, for keeping me calm, focused, fed (in times of poverty), but mainly for being there.

Note to Reader

A table showing the compositions of the glasses melted for this thesis has been included on the last page, and can be folded out with the thesis open for ease of reference when perusing the text.

Also included in this thesis is a compact disc containing all of the raw x-ray diffraction data presented in this work. The data are in the format of text files which can be opened using Microsoft Excel, and most other charting and spreadsheet programs. The CD also contains a list of conferences at which parts of this work have been presented, along with the appropriate presentation titles, abstracts and papers. This information can be accessed using Microsoft Word.

Contents

1. Introduction

In 1938, Otto Hahn and Fritz Strassman discovered that by firing neutrons at uranium it was possible to split some of the atoms into 2 roughly equal parts, and termed this process "fission". Four years later, Enrico Fermi created a self sustaining fission reaction which paved the way for the development of ways to harness the vast quantity of potential energy locked up in the nuclei of atoms of ^{235}uranium. Unfortunately, the first ever practical use of the fission process was that of the atomic bomb, and that potential energy was used for destructive purposes. However, in 1951 the fission process was used to power 4 100W light bulbs, and the electricity for this was generated by Experimental Breeder Reactor-1, at the Argonne National Laboratory. This reactor was the first of more than 430 reactors that exist in the world today to generate electricity for public consumption. But, as well as generating electricity, these power stations also generate a form of waste that is today used by many people as the prime reason in their case for the cessation of all man made fission reactions, a waste generally termed "nuclear waste".

There are 3 main types of electricity generating nuclear reactors in operation today, gas cooled (**Figure 1.1**), water cooled (**Figure 1.2**) and fast breeder reactors (**Figure 1.3**). In gas cooled and water cooled reactors, neutrons split ^{235}U nuclei creating (at least) 2 smaller nuclei and releasing energy (in the form of heat) and a small number (usually 2 or 3) of free neutrons. These free neutrons may then go on to interact with other ^{235}U nuclei thereby creating a self sustaining reaction. If this is allowed to happen in an uncontrolled way and the quantity of fuel is great enough, then criticality is reached and a nuclear explosion occurs. To prevent explosions in power stations, moderators are used to slow down the neutrons. In gas cooled reactors the uranium fuel rods are encased in graphite to slow down the neutrons, and boron (alloyed with steel) rods can be inserted between the fuel rods to absorb excess neutrons. Pressurised CO_2 gas is pumped around the reactor which absorbs heat, and this heat is then transferred to water to create steam to drive electricity producing turbines. In a water cooled reactor, the fuel rods are contained in zirconium alloy tubes through which water is pumped at high pressure. This water absorbs the heat generated by the fission process and transfers it via heat exchangers to non-radioactive water which in

turn generate steam to drive turbines. The reactor itself is immersed in heavy water to moderate the neutrons.

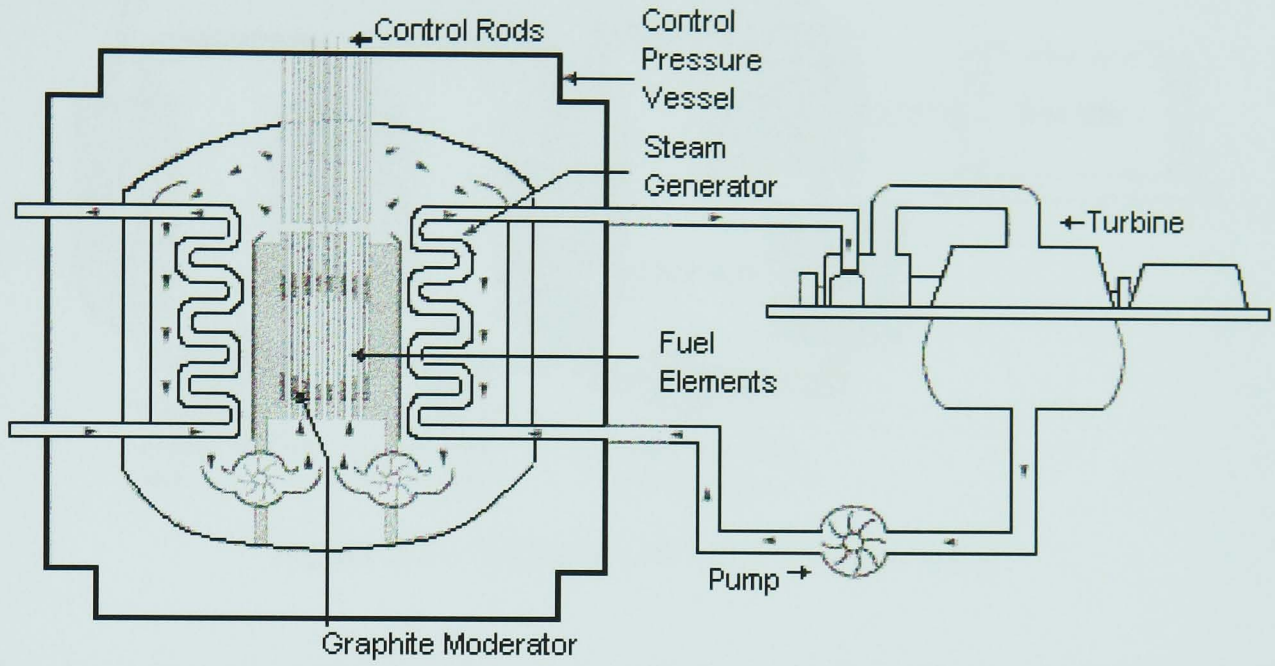

Figure 1.1 - Schematic of a gas cooled reactor[†]

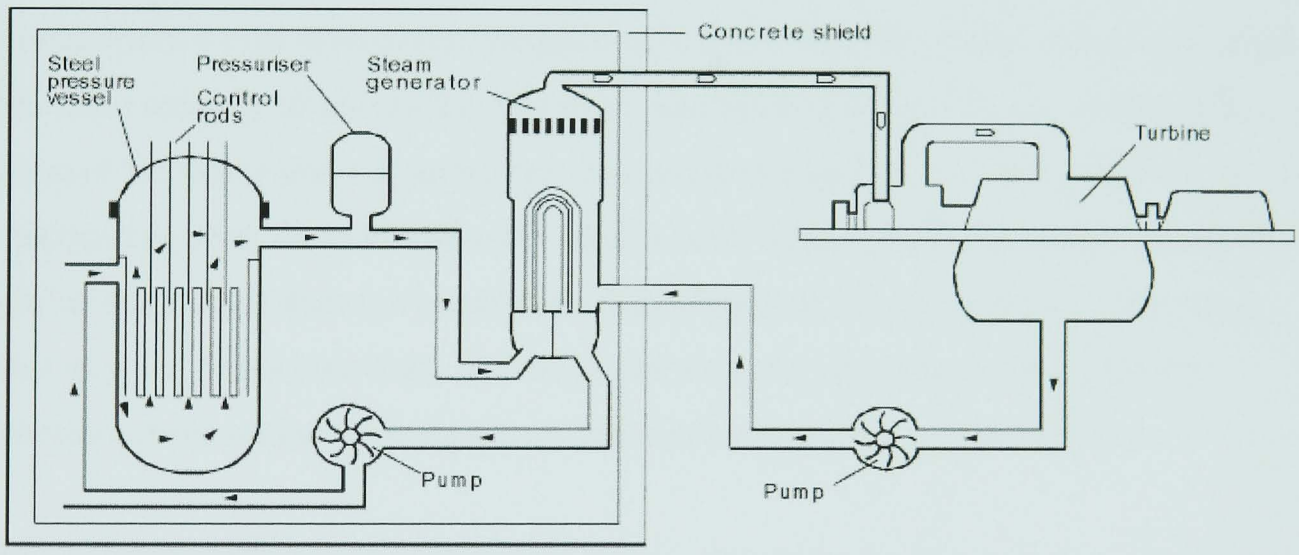

Figure 1.2 – Schematic of a water cooled reactor[†]

The fast breeder reactor has a core of either ^{239}Pu or ^{235}U and does not need to be moderated during normal operation, thus the neutrons in this type of reactor move at their normal speed. Around the core is a layer of ^{238}U which absorbs neutrons created by the fission of the ^{239}Pu or ^{235}U. The absorption of neutrons turns the uranium into plutonium, which can later be used as new core fuel. This type of reactor is cooled by the circulation of a liquid metal (usually sodium) around the core, and again the hot coolant is passed through heat exchangers to heat water and generate steam.

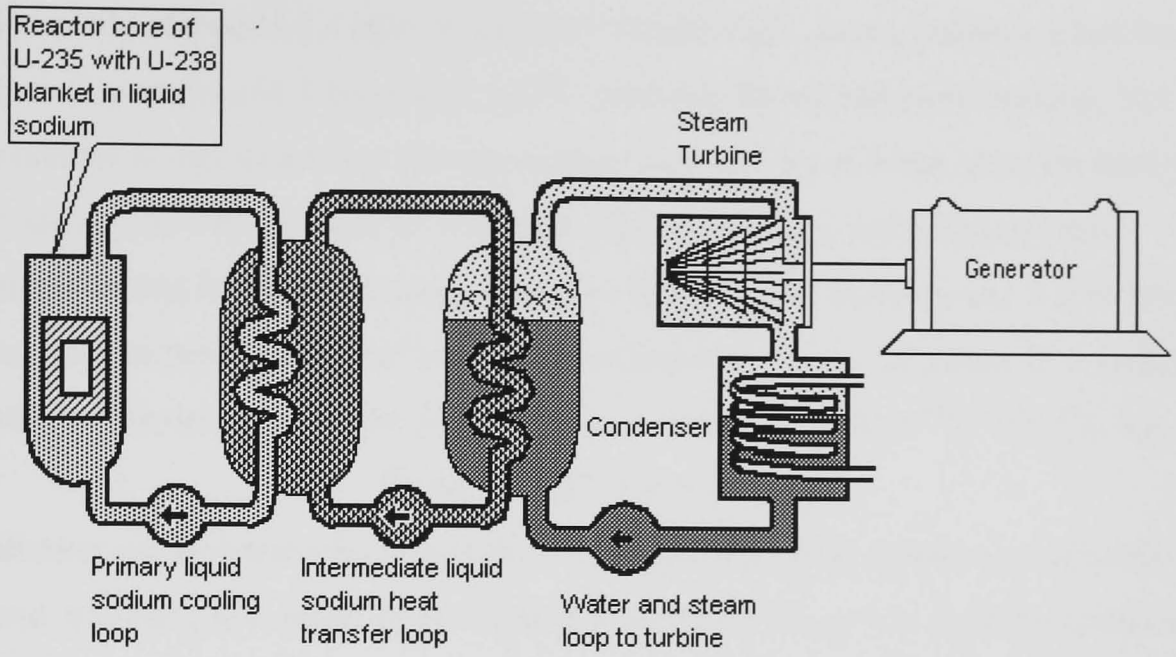

Figure 1.3 – Schematic of a fast breeder reactor[†]

The major benefit of nuclear power is the efficiency of the fuel – just 3kg of uranium can produce enough electricity to power a city of a million people for a whole day. In comparison, a coal fired power station would need over 150 tonnes of fuel to produce the same quantity of electricity. The main drawback of nuclear power comes in the form of the waste material generated. The primary waste form of fossil fuelled power stations is carbon dioxide, and whilst this is now recognised as the primary cause of global warming it does not cause immediate direct harm to living things (assuming that oxygen is also plentiful!). However, the majority of the waste generated by nuclear power stations is radioactive, and can be extremely hazardous to life.

The level of radioactivity will depend on how the waste is generated. For example, a latex glove worn whilst handling some unrefined uranium will be contaminated by a small amount of fissile material. It would be unlikely that any harm would come of interacting with the glove after use, but it would become a form of nuclear waste. At the other end of the scale is the waste generated inside the cores of nuclear reactors. If you were to try and directly interact with this form of nuclear waste, you would absorb a lethal dose of radiation. This is due to the quantity and types of ionising radiation generated by used nuclear fuel. The main types of ionising radiation generated by nuclear waste are α, β and γ radiation. α radiation is generally produced by the decay of heavy elements such as uranium, radium and thorium, e.g.

$$^{235}_{92}U \rightarrow {}^{231}_{90}Th + {}^{4}_{2}He + \text{energy}$$

and is easily stopped by a layer of paper or human skin. An α particle is a helium nucleus (2 protons and 2 neutrons), and is relatively heavy and slow moving. Yet, if an α emitter is ingested either through a body cavity or a cut in the skin, the heavy particles can do a lot of damage to human cells. β radiation is the expulsion of electrons arising from the decay of a neutron in an atomic nucleus, and is thus much faster (approaching 3 x $10^8 ms^{-1}$) and more penetrating than α radiation. It is generally emitted by the decay of lighter particles than α radiation such as ^{90}Sr and ^{35}S, e.g.

$$^{90}_{38}Sr \rightarrow {}^{90}_{39}Y + e^- + \text{energy}$$

β radiation can penetrate the skin down to the germinal layer where new skin cells are formed, but can cause much more damage if ingested. However, it can be stopped by relatively light shielding, for example clothing or wood. γ radiation is the most penetrating of the ionising radiations and is emitted by various isotopes such as ^{137}Cs and ^{99}Tc, and many of the α and β emitters, e.g.

$$^{137}_{55}Cs \rightarrow {}^{137}_{56}Ba + e^- + \gamma + \text{energy}$$

γ radiation is a form of electromagnetic radiation like light or x-rays, is very penetrating and can be very damaging to internal organs. Heavy shielding such as a thick concrete wall is needed to stop γ radiation. For the rest of this discussion, we will focus on the most dangerous type of nuclear waste - that generated in reactor cores.

Whilst a fuel rod is in a reactor, it is constantly being bombarded with neutrons and undergoing fission. Thus, the quantity of fissile uranium in the rod slowly decreases and is replaced by the fission products, the majority of which are radioactive. After a period of about 3 years, there is no longer enough ^{235}U in the rod for efficient fission to occur and so the rods are removed from the reactor and become nuclear waste. The rods are very hot when they are removed from the reactor as the fission process is still happening inside them, and will continue to happen (although at a regressive pace) until either all of the fissile uranium is used up, or the rods are disassembled. Therefore, they need to be stored in large cooling ponds until the outside temperature has dropped to a level where the rods are easier to handle. In some countries (Britain included), the rods are reprocessed after this cooling process. Reprocessing nuclear fuel involves dissolving the used fuel rods in highly concentrated nitric acid, and extracting unused fissile uranium using a tributyl phosphate solution. The extracted uranium can then be used to make new fuel rods thus increasing the efficiency of the

whole nuclear fuel cycle. Left over is a liquor of nitric acid and highly radioactive fission products, which is generally termed "High Level Waste" (HLW).

In the UK, HLW is currently stored in the liquid form in large double walled stainless steel tanks, surrounded by a thick layer of concrete to prevent the escape of γ radiation. The tanks have to be cooled internally as radiogenic heating occurs in the tanks via the decay of the fission products. If they were not cooled, the liquor would eventually boil which could lead to leaking. The liquor is piped from these tanks into a vitrification plant where it passes into a rotating tube furnace called a calciner. In this furnace it is heated to around 350°C and turned into a powder (or "calcine") resembling coffee granules. The calcine in then poured into an inconel glass melter along with an alkali borosilicate glass frit, and mixed by a compressed air sparge to form a homogeneous glass. The glass is then poured into stainless steel tubes (1.3m high and 30cm in diameter) which have lids welded onto them, and are then taken away for decontamination where any trace of radioactive material is removed from the outside. This whole process takes place within hot cells – large thick walled concrete buildings that prevent the escape of radioactivity – and all of the manipulation has to be performed using robotic arms called master slave manipulators. Thus, the whole process (summarised in **Figure 1.4**) is carefully controlled as any breakdown of machinery is very time consuming and costly to replace.

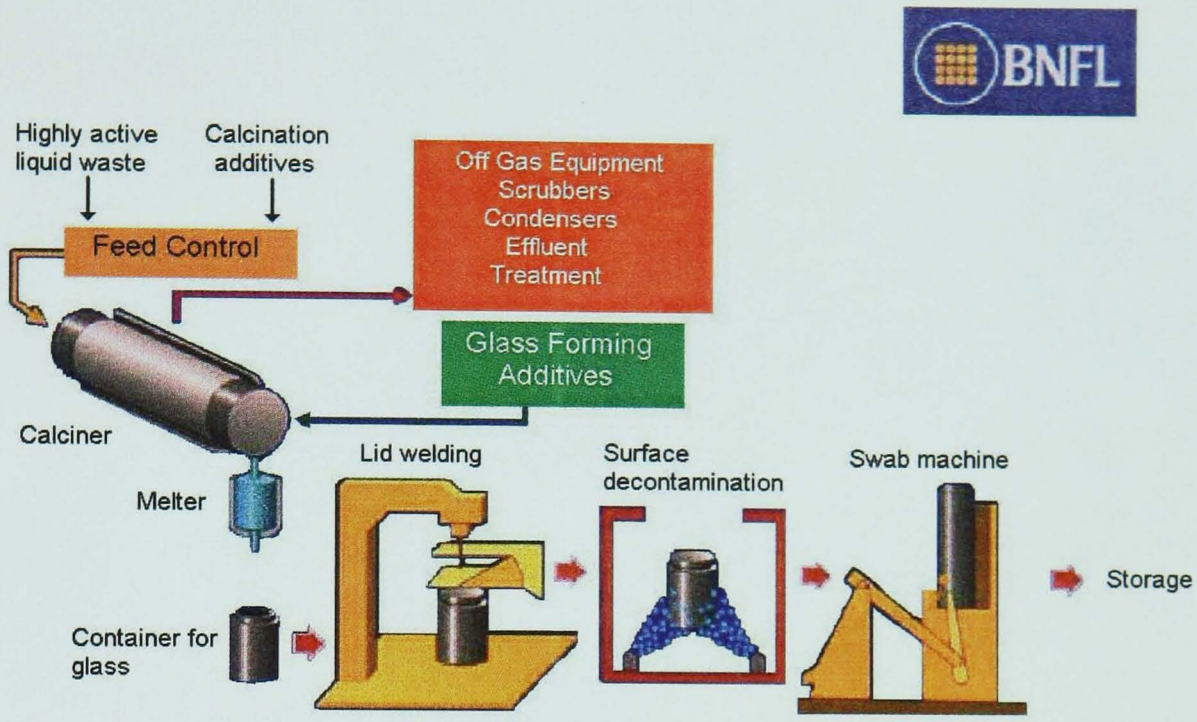

Figure 1.4 – Schematic of the continuous vitrification process*

After the steel canisters have been decontaminated, they are taken to a storage facility which comprises of a very large piece of concrete with verticle holes drilled in the top of it (**Figure 1.5**) that can hold approximately 8000 canisters. The canisters are inserted into these holes (which, like the liquid storage tanks, have to be water cooled) and are left awaiting eventual permanent storage in an underground repository. At the present time, no working repositories have been constructed due to the need to find a politically acceptable location that can be guaranteed to remain geologically undisturbed from its present state for (ideally) millions of years.

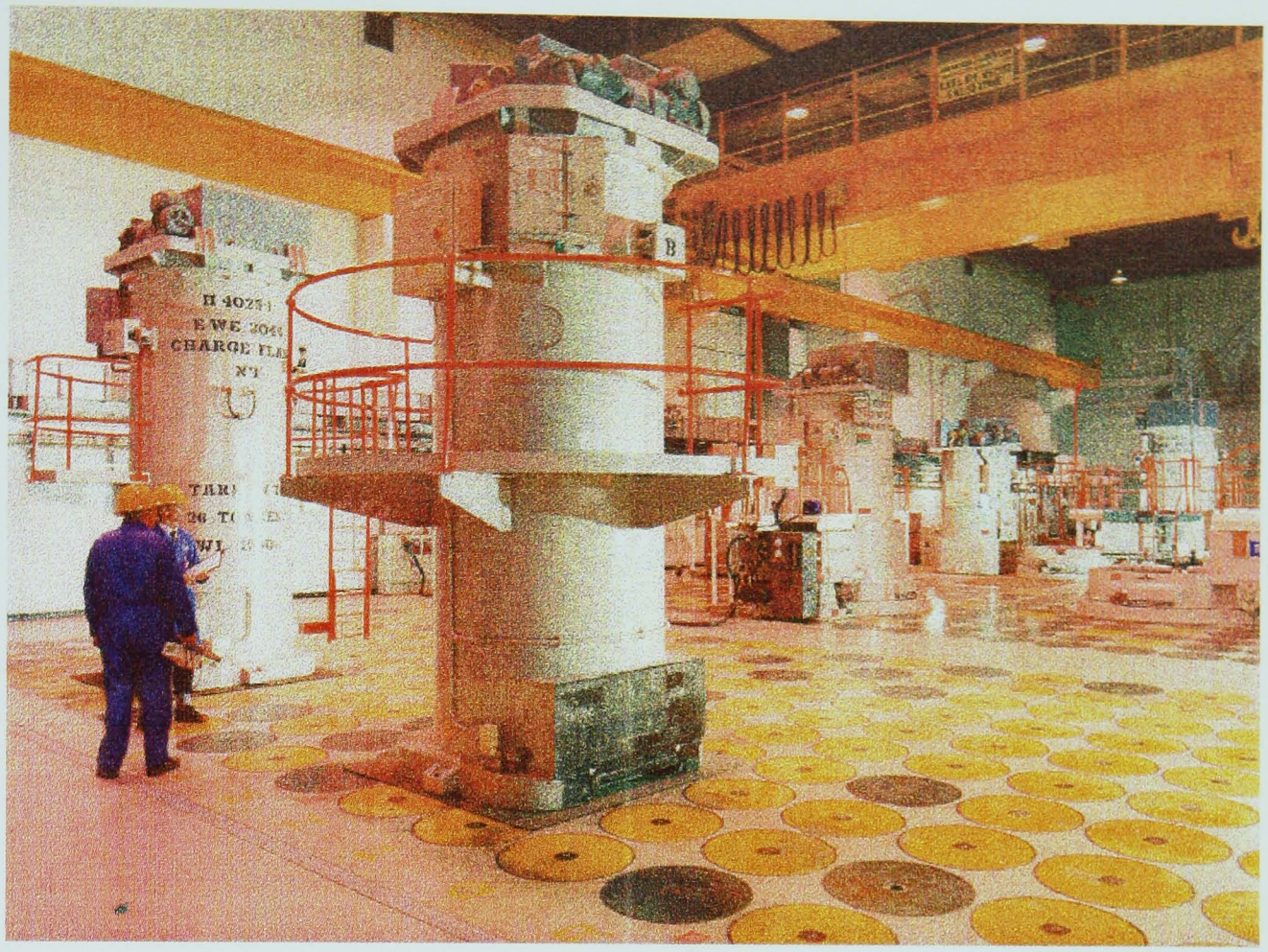

Figure 1.5 – The vitrification product store at Sellafield*

Should the product ever be moved to a permanent underground repository, it would be surrounded by various barriers to prevent isotope migration before the chamber was closed. For example, the steel canisters containing the glass would be over-packed with a layer of cement that should prevent the corrosion of the steel for several thousands of years. Once the canisters had been stacked in the repository and overpacked, the chamber in which they were placed would be back filled with bentonite clay, a material that would initially absorb water making it swell, and then become impermeable to water. It would also be able to absorb and retain radioactive isotopes should they be released from the glass. Also, the kind of sites that are currently being assessed for their suitability as repository locations are generally salt, clay or hard granite areas that are not very permeable to water or have low water flow rates through them. **Figure 1.6** illustrates a proposed repository in the United States. In this repository, the waste would be stored at a level above the water table where geological records indicate the water has never risen to before (even during the most extreme wet periods). In many of the proposed European repositories the waste would be stored below the water table to minimise the risk of contamination, or at levels

where the rock is saturated with static water containing very little dissolved oxygen in order to minimise the corrosion of the waste containers.

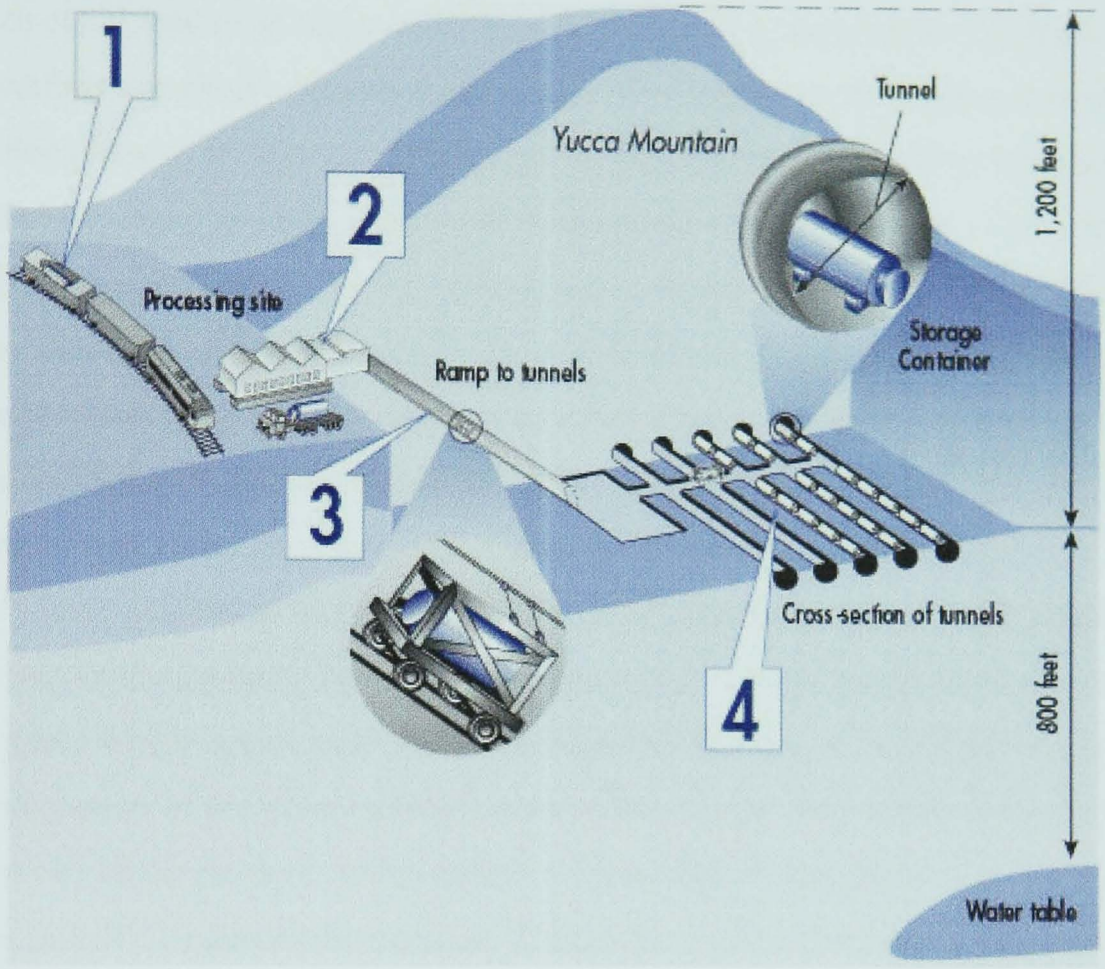

Figure 1.6 – Schematic of the proposed repository at Yucca Mountain in the United States.[‡]

1. Canisters of waste, sealed in special casks, are shipped to the site by truck or train.
2. Shipping casks are removed, and the inner tube with the waste is placed in a steel, multilayered storage container.
3. An automated system sends storage containers underground to the tunnels.
4. Containers are stored along the tunnels, on their side.

However, the vitrification process has to be carefully controlled to ensure that the glass product is of the required quality, as it is highly likely that water will eventually come into contact with the glass. Ideally this would not happen until the amount of radioactivity has dropped to within safe levels, but should it occur before that point then the glass has to be as chemically durable as possible to retain any remaining

radioactivity for as long as possible. Therefore, it should be homogeneous and free from cracks. A cracked (or worse, shattered) product would expose a much larger surface area to any leachant (should it be water or brine) that came into contact with it, which could lead to an increase in the rate of isotope removal from the glass. If the glass exhibits any phase separation either as 2 (or more) amorphous phases or if a crystalline phase is present (i.e. if the glass has devitrified during either temporary or permanent storage), this also could lead to an increase in leaching rate. For example, if the glass was to separate during melting into 2 distinct phases, one silica rich phase and one alkali rich phase, it would be likely that the alkali rich phase would be less durable to chemical attack (e.g. from water) than the silica rich phase, and thus any isotopes contained within the alkali rich area would be removed from the glass at an accelerated rate. If the glass devitrified, then the crystalline phase would almost certainly have a different thermal expansion coefficient to the glass which could lead to cracking of the product. The crystalline phase may also be less durable than the glassy phase which again could lead to accelerated leaching. It is difficult to guarantee the homogeneity of the glassy product at the present time. This is due to the level of radioactivity of the product, which makes it impossible to simply cut a random sample of tubes in half to examine the contents. Currently, quality control is performed by melting simulated HLW glasses on full scale vitrification lines. These glasses are melted under exactly the same conditions and contain chemically similar (but non radioactive) analogues of the isotopes that would be found in real HLW streams, which means that the resulting glass can be safely handled and examined by humans. However, this is not enough to satisfy every customer that uses the vitrification facility in the UK. Recently, a shipment of vitrified waste was returned to the UK from Japan amidst much controversy, as they were not satisfied that the required quality of product had been met.

It is the problem of devitrification of the glassy product that is addressed in this work, specifically the devitrification of a molybdenum containing phase generally termed "yellow phase". Yellow phase is actually a mixture of alkali sulphates, chromates (which give it its yellow colouration) and molybdates which forms during the melting process, and can incorporate ^{137}Cs and ^{90}Sr which produce the bulk of the radioactivity of HLW for the first few thousand years of its existence. It can be

present as striations in the glassy matrix, or as particles up to several centimetres across, which are often called "peanuts" (**Figure 1.7**).

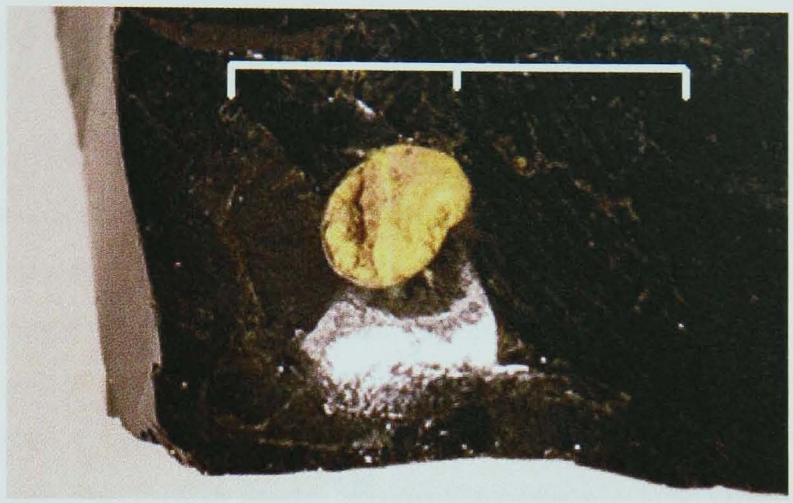

Figure 1.7 – Yellow Phase peanut found in a full scale simulated HLW glass
Scale bar = 2cm

In the liquid form in the melter, the yellow phase tends to enhance corrosion of the inconel furnace linings, and replacement of these furnaces is a very costly and difficult operation as it has to be performed using the master slave manipulators in the hot cells. In the solid form, yellow phase tends to be less chemically durable than the amorphous matrix which could lead to accelerated leaching of radio isotopes. The effects of altering the melting conditions and base glass composition on yellow phase production in a simulated HLW glass are examined in the following chapters.

† Taken from the World Nuclear Association website
http://www.world-nuclear.org/info/inf32.htm

* Courtesy of BNFL

‡ Taken from U.S. Nuclear Regulatory Commission website
http://www.nrc.gov/waste/hlw-disposal/design.html

2. Literature Survey

2.1 Background

There are several operations used today that are sources of nuclear waste, and each source produces a different type of waste. For simplicity, the different sorts are broadly categorised into one of four groups - high, intermediate, low and very low level wastes - depending upon the radioactive hazard they present. Very low level wastes are produced by sources such as hospitals, research institutions and university research laboratories. Generally, these facilities will use radioactive isotopes which have short half-lives, and so the waste, which for example may consist of gloves, aprons and storage containers, can be disposed after short storage times in general use landfill sites, or diluted in liquid form and put into public sewers. The official UK classification rates very low level waste as material which contains less than 400 kBq of beta/gamma activity per $0.1m^3$ or 40 kBq per single item (DEFRA, 2001). Organic low level wastes (paper towels, clothing etc) are generally produced from the same sources as very low level wastes, but some inorganic material such as soil, metals and rubble from redundant nuclear facilities also falls into this category. These materials are classified in the UK as having activities that exceed those of very low level waste, but which do not exceed 4 GBq per tonne of alpha or 12 GBq per tonne of beta/gamma activity (DEFRA, 2001). Low level wastes are usually accepted for shallow controlled burial at Drigg, Dounreay or other licensed sites. Intermediate level wastes generally consist of material that has come into contact with strong sources of radioactivity such as building materials used near the active parts of nuclear reactors, or chemicals used to treat radioactive material. This type of waste usually requires more sophisticated treatments and longer storage times to be made safe. They are classified as materials that exceed low level waste activity limits, but do not need radiogenic heating to be taken into account when designing the storage facilities (DEFRA, 2001). Most of the UK's intermediate level waste originates at Sellafield. High level wastes (HLW) are produced by the decommissioning of nuclear weapons and by the reprocessing of spent nuclear fuels from nuclear power plants. HLW are classified in the UK as materials which generate significant amounts of heat from the radioactive decay process, which has to be taken into account when designing storage and disposal facilities (DEFRA, 2001).

Thus, nuclear reactors are the major source of HLW in the UK. In nuclear reactors, ^{235}U atoms are bombarded with slow moving neutrons, and this causes the nuclei to split into smaller nuclei and release large amounts of energy. It is this energy in the

form of heat which is used to make steam, and thus to drive the turbines and then turn generators to produce electricity. However, the fission products that arise from this process vary widely in atomic number (see **Figure 2.1**) and many of them have unstable nuclei, and thus decay further over time generating various types of potentially harmful radioactivity, as well as significant amounts of energy in the form of heat. **Table 2.1** gives the composition of a typical HLW (after some initial reprocessing) produced in the UK, in the form of oxides.

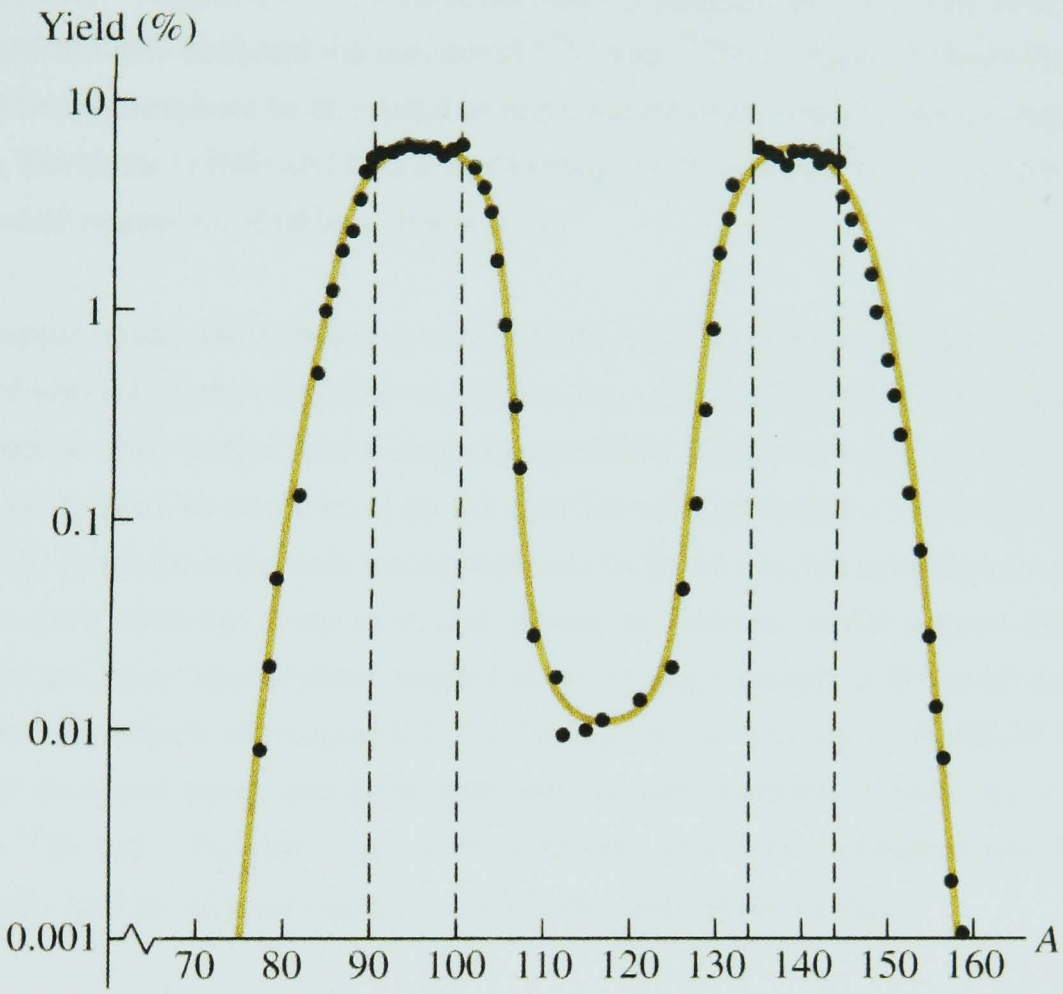

Figure 2.1 – Graph showing the atomic weights of the ^{235}U fission products (taken from Young and Freedman, 2004)

Oxide	Weight %	Oxide	Weight %	Oxide	Weight %
MoO_3	14.3	Pr_6O_{11}	4	Rb_2O	1.1
ZrO_2	13.8	Tc_2O_7	3.8	Pm_2O_3	0.5
Nd_2O_3	13.1	PdO	3.3	Eu_2O_3	0.3
Cs_2O	9.3	SrO	2.9	Sb_2O_3	0.2
CeO_2	8.4	Sm_2O_3	2.6	Ag_2O	0.1
RuO_2	7.8	Rh_2O_3	2.2	In_2O_3	0.1
BaO	4.6	Y_2O_3	1.7	Gd_2O_3	0.1
La_2O_3	4.2	TeO_2	1.6	Total	100

Table 2.1 - Composition of calcined Magnox fission products

Once the UO_2 fuel rods (that are composed of approximately 95% ^{238}U and 5% of the fissile isotope ^{235}U) have been in the reactor for about 3 years, they have to be removed as the build up of fission products creates a neutron poison. Thus, the neutrons that are aimed at the fuel to induce the fission process are slowed down meaning less nuclei are split, and thus reducing energy production to an unprofitable level. At this point, the rods are composed of approximately 95% ^{238}U, 3% fission products, 1% ^{235}U and 1% ^{239}Pu (from neutron irradiation of ^{238}U). The rods are dissolved in nitric acid and the unreacted ^{235}U and ^{239}Pu is extracted from the solution using tributylphosphate to be reused in fresh mixed oxide (MOX) fuel. Amphlett (1961), Berkhout (1990) and Lutze and Ewing (1988) all give good accounts of the origins and treatment of radioactive wastes.

After reprocessing, the remaining solution (the high level liquid waste) contains a range of species, many of which are radioactive. Those species with short half-lives (a few hours or less) do not pose a long term problem for the industry as they have generally decayed to a safe level by the time the storage period of the waste (usually around 10 years from the rods being removed from the reactor until the reprocessed waste is dealt with) has come to an end. However, isotopes which require much more attention are those intermediate length half-lives (e.g.1 month to 30 years) such as ^{90}Sr and ^{137}Cs which are responsible for the bulk of the activity in the HLW for the first few thousand years, and those with half-lives of hundreds to millions of years such as ^{99}Tc and ^{107}Pd plus many of the actinides, that emit α radiation which is potentially structurally damaging to HLW immobilisation matrices.

Any isotope that emits α, β, or γ radiation (i.e. is radioactive) has the potential to disrupt cells in any biological organism, with the worst effects being caused by the ingestion of α emitters. Therefore the waste has to be contained safely until the amount of radiation emitted has dropped to a level which no longer poses a threat to the ecosystem, a period of hundreds of thousands of years. Several possible solutions to this problem have been put forward, such as depositing the waste on the bed of a deep ocean (Johnson & Marples, 1979), or placing it in geologically stable formations such as disused salt mines, clay or hard rock (Donald *et al*, 1997) such as at Yucca Mountain in the United States. A method of containment proposed more recently is very deep borehole disposal (Gibb, 1999) in which the waste would be placed in a borehole sunk several kilometres into the earth. The method relies on a solid HLW package that would generate temperatures of the order of 850°C (which could be achieved, for example, by mixing a current vitrified waste material with fissile

material from decommissioned nuclear weaponry). At these temperatures, the earth's crust itself would melt around the waste package due to the radiogenic heat and eventually solidify to become a natural barrier to isotope migration. However, before any of these solutions can be utilised, the waste has to be "locked up" in a suitable matrix. If is not, then the potential for leakage (if the waste is stored in a liquid form) or aqueous dissolution (should any water come into contact with a waste stored in solid form) of radioactive material is greatly increased, which could pose a serious environmental hazard. Also, intermediate term storage of HLW in liquid form requires regular tank maintenance to be performed to prevent leakage of radioactive material, and this is an added cost to the reprocessing industry.

Many methods of encapsulating nuclear waste have been investigated (and are summarised in **Table 2.2**), and all have various advantages and disadvantages. However, the method chosen by BNFL (and majority of other nuclear users in the world) for dealing with the HLW arising from nuclear fuel reprocessing is vitrification in an alkali borosilicate glass matrix, and it is this matrix which is the subject of this thesis.

Type of Wasteform	Use
Borosilicate glasses	Fission product vitrification, high Pu and U wastes, defence wastes
Phosphate glasses	High actinide waste, Pu waste
Sodium aluminophosphate glasses	High sulphur content wastes
Rare earth oxide glasses	U, Pu, and Am immobilisation
Aluminosilicate glasses	High UO_2 wastes
SYNROC (TiO_2) ceramics	Defence wastes
Phosphate ceramics	High lanthanide and actinide wastes
Natural clays and minerals	Studies still in progress for high U, Pu and Zr wastes
Ba-Al-Si glass ceramics	Limited HLW use
Ba-Ti-Si glass ceramics	Limited HLW use
Ca-Mg-Si glass ceramics	High waste loadings for HLW
Ca-Ti-Si glass ceramics	CANDU wastes, and up to 50wt% UO_2 loadings
Basaltic glass ceramics	Up to 50wt% HLW loadings
Alkali-Ti-Si glass ceramics	Up to 75wt% simulated HLW loadings

Table 2.2 - A compilation of the major HLW immobilisation matrices which are either in use or are currently being studied.

2.2 Vitrification Matrices

Borosilicate compositions were chosen as host matrices for HLW vitrification in the UK for several inter-connected reasons. Marples (1988) lists these as the ability to incorporate all of the oxides that comprise the HLW in relatively high proportions, the relatively low formation temperature, the capacity to tolerate variations in the HLW composition (which can occur due to settling in the liquid storage stage), the chemical durability and radiation hardness of the glass, the capability of the glass to withstand slow cools (in the canisters) with only small amounts of crystallisation, and the ease and (relatively) low cost of borosilicate glass production. The decision to use borosilicate glass in the UK was made after an extensive research programme which began in the 1950s, a detailed summary of which is given by Lutze (1988). Initial research looked into melting natural soils as a host matrix. The high melting temperatures (~1500°C) required to give bubble free homogeneous products using this material encouraged researchers to move to alkali borosilicate and phosphate compositions which could give a homogeneous bubble free product at considerably lower temperatures (1000-1200°C). In the early 1960s, the FINGAL (Fixation in Glass of Active Liquors) vitrification process was being developed, in which active liquor was fed into a stainless steel tube along with glass forming additives, and the whole vitrification process (evaporation, denitration, calcination of the waste and melting and cooling of the glass) took place within this tube. It was at this stage that phosphate glasses were eliminated as a vitrification matrix due to their attack of the metal tubes, along with their inferior leach resistance (in comparison to the borosilicate compositions). After tens of runs on a pilot scale FINGAL facility (some of which were with active wastes), several important lessons had been learned regarding vitrification of active liquors, not least the importance of keeping melting temperatures low to minimise the emission of gasses and volatiles (especially Ru). In 1975, a scaled up and modified version of the FINGAL process known as HARVEST (Highly Active Residue Vitrification Experimental Studies) was begun in Harwell, during which several borosilicate compositions (with melting temperatures in the 900-1000°C range) were developed that could cope with ~25wt% waste loadings. The chemical durability of many of these compositions was also improved when high concentrations of Al and Mg (two elements which are present in the fuel assemblies in high concentrations) were present, which was beneficial to the vitrification process as it meant that the fuel assemblies did not have to be separated from the fuel prior to reprocessing.

However, in the early 1980s BNFL compared the HARVEST process and the French AVM (Atelier de Vitrification de Marcoule) process, which had been vitrifying active wastes since 1978. The AVM process is a continuous process in which active liquor is fed into a calciner where it is evaporated and partially denitrated, then fed into a melting furnace along with glass frit where the remainder of the denitration and the formation of the matrix takes place. The molten active glass is then poured into a steel canister and left to cool. BNFL decided to adopt this process for the vitrification of HLW rather than to continue with the HARVEST process, as AVM was a proven technology (very similar technology had been used for active waste vitrification in France since 1969) which meant the move to vitrifying active waste in a full scale plant could happen more quickly. It was also envisaged that the AVM process provided more scope for processing the increased volumes of waste which were expected should more nuclear power stations have been built in the UK.

Once the AVM process had been chosen, work concentrated on refining the borosilicate glass composition to optimise the incorporation of Magnox waste. Particular attention was paid to the ability of the glasses to incorporate molybdenum, transition metals such as chromium, and metals such as ruthenium and palladium, all of which tend to have very low solubility in silicate glasses. The glass composition that was eventually chosen was that with the greatest capacity for dealing with the low solubility elements, met all of the processing requirements and had the best leach resistance.

As the majority of waste streams present similar problems to those posed by wastes from the UK, it is perhaps unsurprising that nearly every other country with active waste vitrification facilities also chose a borosilicate composition for their host matrices. For example, in the United States extensive research programmes were carried out during the 1960s and 70s looking into many different types of waste form. The results of these studies indicated that borophosphates and borosilicates were likely be the most suitable amorphous wasteforms for vitrification of HLW, and in the late 70s a review panel set up by the Department of Energy ranked borosilicates as the most appropriate wasteform. In France, both amorphous and crystalline host matrices, such as calcium and potassium aluminosilicates, borosilicates and synthetic micas were studied in the 1950s. By 1961, borosilicates had been selected as the most suitable candidates and further studies focused mainly on these compositions. The major notable exception to this trend is in Russia, where phosphate based glasses are still being extensively studied.

Alternatives to the borosilicate matrix are discussed by Marples (1988), and also by Hayward (1988, glass ceramics), and Donald, Taylor and Metcalfe (1997, glasses and ceramics) who summarise the properties of the majority of possible wasteforms in one table, reproduced here in **Table 2.3**.

Wasteform	Principal Application	Processing Temperature[1]	Waste Loading[2]	Mechanical Properties[3]	Thermal Expansion[4]	Thermal Conductivity[5]	Chemical Durability[6]	Radiation Stability[7]	Economics[8]
Hydrated Inorganics									
Clay based	LLW-ILW	Low	Int	Low	Low	Low	Low	Low	Low
Cement	LLW-ILW	Low	Int	Low	Low	Low	Low	Low	Low
Concrete	LLW-ILW	Low	Int	Low	Low	Low	Low	Low	Low
FUETAP	ILW-HLW-TRU	Low-int.	Int	Low	Low	Low	Low	Low	Low-int
Glasses									
Alkali borosilicate	HLW-TRU	High	Int	Int	Int	Low	Int	Int	Int
High silica	HLW-TRU	V.High	Int	Low-int	Low	Low	High	High	High
Aluminosilicate	HLW-TRU	V.High	Int	Int	Int	Low	High	High	High
Lanthanide silicate	TRU	V.High	Int	Int	Int	Low	High	Int	High
Sintered glass	HLW-TRU	Int	High	Low-int	Int	Low	Int	Int	Low
Alkali phosphate	HLW-TRU	Int	Int	Low	High	Low	Low	Int	High
Aluminophosphate	HLW-TRU	Int	Int	Low	Int	Low	Int	Int	High
Zinc phosphate	HLW-TRU	Int	Int	Low	Int	Low	Low	Int	Int
Iron lead phosphate	HLW-TRU	Int	Int	Low	High	Low	Int	Int	Int
Iron phosphate	HLW-TRU	Int	Int	Low	High	Low	High	Int	Int
Glass Ceramics									
Barium aluminosilicate	HLW	High	Int	Int	Int	Low	Int	Int	Int-high
Magnesium aluminosilicate	HLW	V.High	Int	Int	Int	Low	High	Int	Int-high
Barium titanium silicate	HLW	High	Int	Int	Int	Low	Int	Int	Int-high

Wasteform	**Principal Application**	**Processing Temperature**[1]	**Waste Loading**[2]	**Mechanical Properties**[3]	**Thermal Expansion**[4]	**Thermal Conductivity**[5]	**Chemical Durability**[6]	**Radiation Stability**[7]	**Economics**[8]
Calcium magnesium silicate	HLW	High	Int	Int	Int	Low	High	Int	Int-high
Calcium titanium silicate	HLW	V.High	High	Int	Int	Low	High	Int	Int-high
Basaltic	HLW-TRU	V.High	High	Int	Int	Low	High	Int	Int-high
Phosphate	HLW-TRU	Int	Int	Int	Int	Low	Low	Int	Int
Ceramics									
SYNROC-B	HLW	High	Int	High	Int-high	Int	High	Int	Int-high
SYNROC-C	HLW	High	Int	High	Int-high	Int	High	Int	Int-high
SYNROC-D	HLW	High	Int	High	Int-high	Int	High	Int	Int-high
SYNROC-E	HLW	High	Int	High	Int-high	Int	High	Int	Int-high
SYNROC-F	HLW-TRU	High	Int	High	Int-high	Int	High	Int	Int-high
SYNROC-FA	HLW-TRU	High	Int	High	Int-high	Int	High	Int	Int-high
Calcium silicate	HLW	Int	Int	Int	Int	Int	Int	Int	Int
Titania	HLW	Int-High	Int	Int	Int	Int	High	Int	Int-high
Monazite	HLW-TRU	High	Int	Int	Int	Int	Int	High	Int-high
Sodium zirconium phosphate	HLW-TRU	Int	High	Int	-	Int	High	High	Int
Sodium titanium phosphate	HLW-TRU	Int	High	Int	-	Int	High	Int	Int
Rare earth pyrochlore	TRU	High-V.High	High	Int	-	Int	Int	Int	Int
Lanthanum zirconate	TRU	V.High	High	Int	-	Int	High	High	Int
Zirconolite	TRU	High-V.High	High	Int	High	Int	High	High	Int

Wasteform	Principal Application	Processing Temperature[1]	Waste Loading[2]	Mechanical Properties[3]	Thermal Expansion[4]	Thermal Conductivity[5]	Chemical Durability[6]	Radiation Stability[7]	Economics[8]
Zircon	TRU	V.High	Low-high	Int	-	Int	High	Int-high	Int
Inorganic ion-exchange media									
Titanate	ILW-HLW	Int	High	-	Int-high	Int	Int	Int	Int
Zeolite	ILW-HLW	Int	High	-	Int-high	Int	Int	Int	Int
Sodalite	ILW-HLW	Int	High	-	Int-high	Int	Int	Int	Int
Encapsulants									
Cement matrix	HLW-TRU	Low	High	Low	Low	Low	Low	Low	Low
Metal matrix	HLW-TRU	Int	High	Int	High	High	High	Low-int	Int
Ceramic matrix	HLW-TRU	Int-high	High	Int	Int	Low-int	High	Int	Int-high
Glass matrix	HLW-TRU	Int	High	Int	Int	Low-int	Int	Int	Int
Coated particles	HLW-TRU	Int	High	Int	Int	Low-int	Int	Int	Int
Sol-gel particles	HLW-TRU	Int	High	Int	Int	Low-int	Int	Int	Int

Table 2.3 – Comparison of the properties of the major types of wasteform by Donald *et al*, 1997
Int = Intermediate, V.High = Very high, TRU = Transuranic elements
[1]*Processing Temperature*: Low, $\leq 200^{\circ}C$; Intermediate, 200-1000°C; High, 1000-1250°C; Very high, >1250°C
[2]*Waste Loading*: Low, <10%; Intermediate, 10-20%; High, 20-40%; Very high, >40%
[3]*Mechanical Properties*: Low, <50MPa; Intermediate, 50-200MPa; High, >200Mpa
[4]*Thermal Expansion*: Low, $<5x10^{-6}K^{-1}$; Intermediate, $5\text{-}10x10^{-6}K^{-1}$; High, $>10x10^{-6}K^{-1}$
[5]*Thermal Conductivity*: Low, $<2.0Wm^{-1}K^{-1}$; Intermediate, $2.0\text{-}5.0Wm^{-1}K^{-1}$; High, $>5.0Wm^{-1}K^{-1}$
[6]*Chemical Durability*: Low, <Borosilicate glass; Intermediate, Comparable to borosilicate glass; High >Borosilicate glass
[7]*Radiation Stability*: Low, <Borosilicate glass; Intermediate, Comparable to borosilicate glass; High >Borosilicate glass
[8]*Economics*: Low, <Borosilicate glass; Intermediate, Comparable to borosilicate glass; High >Borosilicate glass

Many of the alternatives offer superior qualities in one or more of the areas mentioned above (for example Hayward found the chemical durability of aluminosilicate glass ceramics to be ten to a hundred times better than that of borosilicate glass compositions), but none of the options studied so far offer such good overall performance along with the relative low cost and ease of production as borosilicate compositions.

Clark *et al.* (1982) found that the chemical durability of a borosilicate base glass composition was significantly improved when any of the three simulated waste streams investigated (a high alumina stream, a high iron stream and a Savannah River Plant simulant) were added to the glass batches in quantities up to 30wt%. However, Calestani *et al.* (1984) took base glass frits (similar in composition to that used in this study) and added varying amounts SrO, Cs_2O, U_3O_8 and ZnO to simulate nuclear waste additions. The glasses were then powdered and subjected to 24 day leach tests, and only those glasses with added zinc showed an improvement in the chemical durability. Raman (1997) found in one study that an increase in the amount of boron and alkali in the base glass composition helped to dissolve a greater amount of high calcium simulated waste into the glass, and also improved the chemical durability. He attributed this to an increase in the amount of polymerized tetraborate rings, and a decrease in the concentration of metaborate rings. However, the author does state that increasing the alkali and borate loading in waste glasses, although lowering the viscosity of the melt at a given temperature and increasing the solubility of many waste species, does tend to decrease the chemical durability of the glass. A very detailed summary of the available data on the chemical durability of many of the popular vitrification matrices is given by Trocellier (2001) and is reproduced in **Table 2.4**. Trocellier also includes data on the crystalline forms that can be used for the "specific immobilisation" of radionuclides after they have been separated from the fission products.

Material	Waste loading (wt%)	Waste nature[†]	Leaching test	Dissolution rate for the crystalline/ amorphized form ($gm^{-2}d^{1-}$)[‡]	Activation energy (kJ/mol)
Alkali-borosilicate glass	≤15	Cs,Sr, Ln,An, metals	90°C, static, monolith	$1x10^{-3}$ – $3x10^{-3}$ (bulk)	65
Phosphate glass	6-16	Ln,An	90°C, static, monolith	$1x10^{-4}$ – $1x10^{-3}$ (Pb, Fe, P)	
Alumino-silicate oxy-nitride glass	10-20	Cs,Sr, Ln,An, metals	90°C, static, monolith, pH 5.5	$7x10^{-6}$ – $8x10^{-5}$ (bulk)	
SYNROC		Cs,Sr, Ln,An, metals	90°C, static, monolith,	$1x10^{-5}$ – $1x10^{-4}$ (Tc,An)	15 - 30
Alumina		metals	250°C	$1x10^{-9}$ – $1x10^{-8}$	
Zirconia			150°C, deionised water	$1x10^{-6}$ – $1x10^{-5}$	
Thorianite		Ln,An	25°C, pH 7, deionised water	$7.7x10^{-10}$	
Uraninite		Cs,Sr, Ln,An, metals	25°C ox/ 25°C red	$1.9\text{-}9.6x10^{-4}$ / $9.3x10^{-8}$ – $7x10^{-7}$	
Fluorapatite	10	Ln,An	25°C pH 4	1.1/100 (bulk)	
Monazite	≤20	Ln,An	95°C soxhlet	$2.7x10^{-4}$ – $3.3x10^{-2}$ (bulk)	
Sodium zirconium phosphate	≤20	Cs,Sr, Ln,An,	100°C soxhlet, powder	$1x10^{-6}$ – $1x10^{-5}$ (bulk)	
Thorium phosphate diphosphate		Ln,An	90°C, pH 7	$3x10^{-6}$ (Cm,Am)	42
Nepheline		Cs	90°C, pH 7	0.5 (bulk)	53 – 77
Zircon	8-10	Ln,An		$3x10^{-4}$/ 0.018(Si)	23
Sphene		Ln,An	90°C deionised water	$9x10^{-3}$ – $1x10^{-1}$ (bulk)	

Material	Waste loading (wt%)	Waste nature†	Leaching test	Dissolution rate for the crystalline/ amorphized form ($gm^{-2}d^{1-}$)‡	Activation energy (kJ/mol)
Perovskite		Cs,Sr, Ln,An	100°C	0.2 (Ca)	
Hollandite	10	Cs,Sr	9≤pH≤11, 90°C	0.6 – 2.5 (Cs)	
Zirconolite	10-20	Ln,An	90°C powder	$2x10^{-7}$ – $7x10^{-5}$ (Ca)	19 – 25
Pyrochlore		Ln,An	75°C 6≤pH≤8/ 90°C static monolith/ 90°C pH 7	$2x10^{-6}$ – $6x10^{-5}$ (x10 to 30)/ $8x10^{-6}$ – $3x10^{-5}$/ $2.7x10^{-5}$ (Pu)	5 – 7
Brannerite		Ln,An	75°C 6≤pH≤8	$1x10^{-5}$ – $1x10^{-4}$ (x10 to 30) (U)	5 - 7
Sphene glass		Cs,Sr, Ln,An	100°C, brine	$1.3x10^{-4}$ (bulk)	
Hollandite glass	10	Cs	90°C 9≤pH≤11	$2x10^{-3}$ – $1x10^{-2}$ (Cs)	
Zirconolite glass		Ln,An	90°C, deionised water	$1x10^{-7}$ – $6x10^{-5}$ (Ce)	

†Ln and An = Lanthanide elements and actinide elements (including U and transuranium elements) respectively

‡The amorphisation is obtained through the incorporation of an alpha emitter within the matrix

Table 2.4 – Summary of the chemical durability of the major HLW waste forms taken from Trocellier (2001)

Upon examining **Table 2.4**, it seems apparent that there are several waste forms with substantially higher chemical durabilities than the standard alkali borosilicate composition (which is of the order of 10^{-3} $gm^{-2}d^{-1}$). For example, Trocellier writes that the dissolution rate of SYNROC waste forms is 10 to 100 times less than that of alkali borosilicate, and that of Thorianite is around 1,000,000 times less. However, there are several factors that need to be considered when addressing the issue of chemical durability via leach testing. The most important of these is that there are several different types of standard leach test applicable to nuclear waste glasses, many of which have been developed to simulate the particular modes of aqueous attack that could be found in specific repository environments (Strachan, 2001). The Materials

Characterisation Centre at the Pacific Northwest National Laboratory developed 5 different forms of leach test (known as MCC-1 to MCC-5) each one designed to measure dissolution rates under different conditions. For example, MCC-1 was designed to measure dissolution rates of glass in static water at room temperature in an open atmosphere, whereas MCC-3 measures the dissolution of glass powder that is being stirred in water in a closed system. Other tests such as the vapour phase hydration test and autoclave tests are designed to simulate long term corrosion by the acceleration of the dissolution process using high temperatures and pressures, whilst the pressurised unsaturated flow (PUF) test was developed to simulate the repository conditions of Yucca mountain and Hanford soils specifically. A summary of the major types of test and their applicability is given by Strachan (2001) and is reproduced in **Table 2.5**. As these tests often vary considerably in their methodology, direct comparisons of leach rates (as in **Table 2.4**) can often be misleading. For example, a bulk glass sample in static water is likely to leach much more slowly than the same glass in powdered form placed in a constantly flowing and refreshed leachate solution. Similarly a glass is likely to dissolve at a greater rate in a solution at 90°C than the same glass in the same solution at room temperature. These basic examples highlight the need for a single international standard leach test that is applicable to all potential waste forms. Still, if we compare all of the materials in **Table 2.4** that were subjected to the same leach test as the alkali borosilicate composition (90°C, static solution, monolithic glass block) we find that they all out performed alkali borosilicate. However, if the same waste forms are compared in **Table 2.3**, we can also see that they all require higher processing temperatures and cost more than the alkali borosilicate composition, and thus are not used for the bulk of HLW vitrification. As mentioned above, all of the factors that define the performance of a host matrix have to be considered before that matrix will go into large scale production.

Test	Conditions†	Use
MCC-1	Static. S/V usually $10m^{-1}$. Open.	To compare waste forms. Normally a closed test, but solution equilibrates rapidly with the ambient atmosphere when performed in a Teflon vessel
MCC-2	Static. High temperature, >90°C. Closed.	A high temperature version of MCC-1, normally performed in a Teflon lined stainless steel vessel.
MCC-3	Stirred with glass powder. Closed .	Used to accelerate the glass water reaction
MCC-4	Open, single pass flow through and atmosphere	Used to determine the dissolution as a function of flow rate
MCC-5	Open to both flow and atmosphere	Used for forward dissolution rate measurements. Boiling water and reflux used to obtain flow.
PUF	Open to flow and atmosphere, (flow is unsaturated over powdered specimen surface)	Used for accelerated alteration under open system conditions, and hydraulic properties measurements. Unsaturated conditions of water flow in Yucca mountain and Handford soils are simulated.
Pulsed flow	Open with some percent of the leachant replaced with fresh leachant, or the specimen removed and placed in fresh leachant. Can be open or closed.	Used for very low flow conditions and/or to obtain solution data with the same specimen.
Vapour phase hydration	Closed. Only water vapour is present. Monolithic specimen	Used to accelerate alteration product formation. Reaction is between condensed water on the specimen surface and the specimen itself.
Autoclave tests	Usually run at >100°C. Closed. Usually run in stainless steel or titanium vessels with gold or other tube.	Used to determine equilibrium phase assemblages, kinetics of alteration and solubility.

†"Open" refers to tests performed in systems open to the atmosphere. "Closed" refers to tests performed in systems closed to the atmosphere.

Table 2.5 – Summary of the standard leach tests commonly used for analysis of HLW glass, taken from Strachan (2001).

Jantzen (1992) evaluated the long-term corrosion characteristics of nuclear waste glasses by constructing Pourbaix diagrams. This method relates the pH of the aqueous system with which the glass is likely to come into contact with in an underground repository, to the oxidation potential of the glass, to extrapolate the likely dissolution qualities of the glass. The technique draws upon modern leach testing results performed under laboratory conditions, and also on data obtained by studying ancient man made glasses (such as those made in Egypt over 3500 years ago) and natural glasses that are hundreds of thousands of years old. The study concludes that the borosilicate waste glasses studied would be likely to be either thermodynamically inactive, or would become covered by a passive surface layer in any ground waters to which they are liable to be exposed.

In selecting a suitable glass composition, Marples (1988) compares the limits of waste incorporation, the ease of manufacture, the speed with which the glass is able to incorporate the calcined waste, the viscosities of the glass frit and of the final glass, and the durability of the final glass. He goes on to discuss in detail the radiation effects on glasses and the leaching process, and concludes that even after hundreds of thousands of years the radiation effects will be minimal with small (<1%) changes in density and increases in leach rates, and that, in the conditions under which it is proposed that the glass is to be disposed, the leaching of the dangerous radioactive isotopes will be very slow. Matzke (1984) indicates a beneficial increase in fracture toughness in waste glasses doped with a short-lived radioactive Cm isotope to simulate the long-term α particle bombardment that would be experienced by real vitrified products. However, he also states that in another test to simulate long-term radiation effects (bombardment by Pb ions), the glasses showed a decrease in fracture toughness. It was also noted that many crystalline phases present in the simulated waste glasses became amorphous after undergoing long-term radiation damage. A very comprehensive summary of radiation effects in many types of nuclear waste forms is given by Ewing *et al.* (1995). The authors conclude that the effect of long-term radiation on amorphous matrices is not well understood and requires more investigation.

Soper *et al.* (1983) performed a series of experiments to determine an optimum base glass composition for vitrification of nuclear waste from the Savannah River plant. The criteria used to judge the glasses were leachability, viscosity at 1150°C (the upper limit of melting temperatures for nuclear wastes due to the volatilities of elements such as Cs and Ru), liquidus temperature and coefficient of expansion. The team used

different "worse case scenario" waste streams depending upon the property being judged. For example, to optimise the viscosity, a high alumina waste stream was used as this tends to increase the viscosity of a melt at a given temperature. By rating the compositions on a scale of 0 – 1 depending upon how well they performed in each area, an optimum composition was chosen after only 25 trials. However, it must be remembered that only 4 criteria were examined for the glass, and a trial that considered all of the criteria for a good vitrified product would have made the experiment exponentially more complicated. The experiments were also optimised for a slurry fed melter which can induce sufficient homogenisation of waste components in higher viscosity melts than can be achieved in the calcine fed melters used by BNFL.

Nuclear waste vitrification in America has a limitation stating that, "no foreign materials must be released or generated as a result of exposure of the canistered waste form to the glass transition temperature of the glass". Harbour (1992) took samples of a simulated waste glass from the Savannah River plant and subjected them to thermogravimetric analysis with a hold of 4 hours close to the T_g of the glass. The experiments were performed in atmospheres of helium, oxygen and air. The author found that those samples heated in oxygen or air underwent a net weight gain, and those heated in helium lost a small amount of weight. The weight loss was found to be due to loss of absorbed moisture from the powdered glass samples, whereas the weight gain was attributed to the oxidation of FeO to Fe_2O_3 (i.e. by the uptake of one molecule of oxygen for every four molecules of FeO). The only effect this oxygen uptake would have on a full size glass canister would be a weight gain of a few milligrams. This is not deemed to be a significant effect in a canister weighing 1.7 tonnes.

2.3 Yellow Phase and Other Molybdenum Compounds

A high weight percentage (i.e. >1%) of MoO_3 or sulphur (in the form of Na_2SO_4, SO_3, etc.) can lead to the formation of a yellow phase which is immiscible with the bulk of the glass (Lutze and Ewing, 1988). As this phase is of lower chemical durability than the bulk homogeneous phase it is undesirable in the manufacture of the finished product. Schiewer et al. (1982) performed a detailed analysis of yellow phase revealing that it is a molybdenum compound that obtains its yellow colour from the presence of chromates. Altering the oxidation state of molybdenum in the melt could lead to the ability to incorporate a higher percentage of waste into the final glass, as Mo^{5+} and Mo^{3+} are more readily dissolved into the matrix than the more stable Mo^{6+}. Camera *et al.* (1980) and Horneber *et al.* (1982) investigated the effect of iron on the oxidation state of molybdenum, and found that small additions of Fe_2O_3 lead to an increase in the concentration of Mo^{3+}, but higher additions lead to the reoxidation of Mo^{3+} back to Mo^{6+}. Horneber *et al.* also discovered that as the basicity of the melt is increased (achieved by substituting sodium with caesium in the glass frit) it becomes more difficult to reduce molybdenum to the 3+ state. Kawamoto *et al* (1981) experimented with a simple sodium borosilicate glass with small molybdenum additions to investigate the phase separation tendencies of the system. They found that when molybdenum is present in the +4 valence state, it has a great tendency to form MoO_2. Whilst this phase has a reasonable chemical durability (the authors state that it is not completely soluble in HF solution), it is not desirable in vitrified wastes because of thermal expansion mismatches between the glass and the MoO_2 (which could lead to cracking of the waste form on cooling) and enhanced melter "heel" formation. A heel is a layer of dense glass that forms at the bottom of the melting furnace containing elevated levels of refractory oxides and reduced metals. Eventually the heel grows so deep that it prevents the pouring of glass from the furnace, requiring replacement of the melting vessel. In a paper related to that of Kawamoto *et al*, Bando *et al* (1980) used scanning electron transmission microscopy to investigate the location of Mo in sodium borosilicate glasses doped with 1% Mo. They found that upon 1 hour heat treatments, small (0.1μm) silica rich droplets developed within the matrix of the glasses, and that these droplets were about 4 times poorer in Mo than the matrix. However, at the droplet/glass interface the Mo concentration was 4 times greater than that of the matrix, and this tended to encourage the growth of MoO_2 "whiskers" on the edges of the droplets.

Molybdates which have the powellite (calcium molybdate, $CaMoO_4$) structure (see **Figure 2.2**) have been studied by Teller (1992) and Stedman *et al* (1994). In these

molybdates, the calcium ion positions are taken up by a random distribution of +1 and +3 cations (and are sometimes vacant, with the charge difference being balanced by an excess of +3 ions). These observations combined with information obtained from the ICDD database indicate that the +1 positions can be occupied by sodium, silver or lithium ions, and the +3 sites can host a range of lanthanide ions (all of which have similar radii in the +3 oxidation state), yttrium or bismuth ions, as summarised in **Table 2.6**.

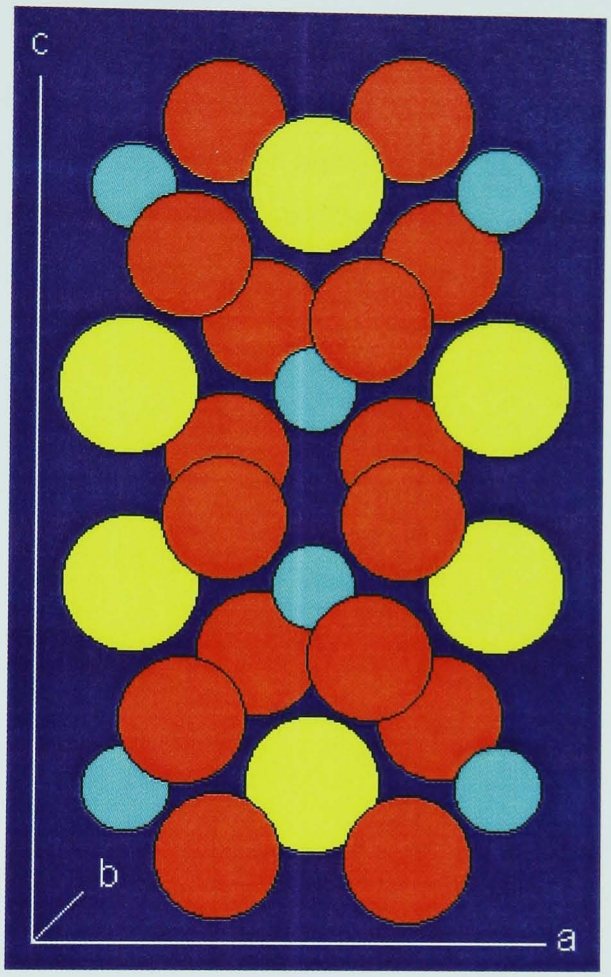

Figure 2.2 – $CaMoO_4$ unit cell. Space group $I4_1/a$. ICDD card [29-351]
Mo^{6+} ion Ca^{2+} ion O^{2-} ion

$LiY(MoO_4)_2$	$NaY(MoO_4)_2$	$AgY(MoO_4)_2$
$LiLa(MoO_4)_2$	$NaLa(MoO_4)_2$	$AgLa(MoO_4)_2$
$LiCe(MoO_4)_2$	$NaCe(MoO_4)_2$	$AgCe(MoO_4)_2$
$LiNd(MoO_4)_2$	$NaNd(MoO_4)_2$	$AgNd(MoO_4)_2$
$LiSm(MoO_4)_2$	$NaSm(MoO_4)_2$	$AgSm(MoO_4)_2$
$LiGd(MoO_4)_2$	$NaGd(MoO_4)_2$	$AgGd(MoO_4)_2$
$LiBi(MoO_4)_2$	$NaBi(MoO_4)_2$	$AgBi(MoO_4)_2$

Table 2.6 - Different types of feasible powellite structured molybdates.

As all of the crystals in the literature have been produced from known precursors, the structure is fixed. It is not reported in the literature, but it seems reasonable to assume that it is possible for these scheelite structures to form and incorporate several different but similarly sized +1 and +3 cations. It is also clear that all of the necessary

ions will be present in high level waste glasses, and so these structures are probably closely related to yellow phases as described above.

Simple molybdates can also cause problems in vitrified wastes. Horenber *et al.* discovered that in glass containing >3% MoO_3 melted under neutral conditions, sodium molybdates (Na_2MoO_4 and $Na_2MoO_4.2H_2O$) which are water soluble and therefore easily leached, were present. It is likely (although not proven) therefore, that the caesium molybdate of this type would also be present under such conditions, which is problematic as the caesium isotope Cs^{137} is one of the most undesirable elements in the radioactive waste (for the initial 300 years at least) due to its high heat generating capacity and short half life. However, under reducing conditions induced by adding tannic acid to the batch, the precipitates were not observed as Mo^{6+} was reduced to Mo^{3+}.

2.4 Redox

Many factors are known to influence the redox state of glasses. Temperature, atmosphere, pressure, melting time, melt additions and batch origin can all affect the overall oxidation state of glasses, which in turn can significantly alter the final properties of the glass. In turn, foaming of the melt, precipitation of metals and crystalline species, volatility of some elements and melter corrosion can all be influenced by controlling the redox chemistry.

The Ellingham diagram (see **Figure 2.3**) relates the free energy of formation of different pure oxides of the same element to temperature. It can be a useful tool for glass scientists as it gives a good indication of which oxides are likely to undergo a redox reaction and which are not. For example, the AgO line has a much higher ΔG value at any given temperature that the SiO_2 or B_2O_3 lines have, thus indicating that silver oxide is much more likely to undergo a redox reaction than either of the conventional glass forming oxides silicon and boron. However, Paul (1990) points out that the diagram was compiled from data obtained from the pure oxides of the elements covered, and that modifications have to be made to the positions of the lines when the oxides are being considered as part of a mixture of other oxides, such as are present in a glass melt. Paul also postulates that mutual interaction between two (or more) different redox couples can only take place during the cooling of the melt down to the fictive temperature, and not whilst the melt is held at equilibrium conditions (i.e. constant temperature, pressure etc.). Thus, it can be inferred that if the redox pairs have not reached an equilibrium during the cooling of the melt, further redox interactions will take place if the glass is subjected to heat treatments at or around the fictive temperature.

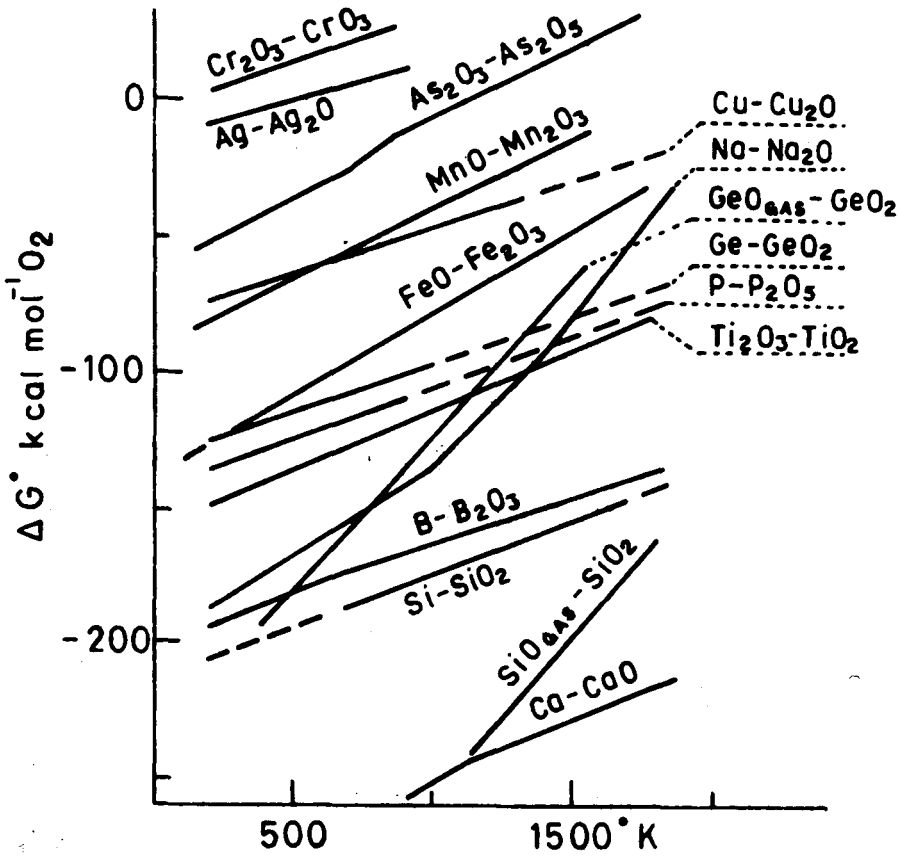

Figure 2.3 – An Ellingham diagram for some oxides

The amount of oxygen above the melt can significantly affect the redox states of the components of the glass. If conditions are too oxidising, foaming may occur (due to the release of oxygen from oxidation-reduction reactions) which will interfere with heat transfer in the melt. Meanwhile heavily reducing conditions can lead to the formation of conductive metal phases in the melt, which could potentially short circuit submerged electrodes (Goldman, 1986). Krause and Luckscheiter (1991) investigated the formation of RuO_2 needles in the sludge which collects in the bottom of HLW vitrification tanks over long periods of time. The needles make the sludge highly conducting which increases the chances of an electrical short. In this case they found that applying reducing conditions or bubbling air through the melt inhibited the formation of these particles on a laboratory scale.

Schreiber *et al.* (1984) compiled a chart (reproduced in **Figure 2.4**) showing the redox state of many of the common redox couples found in HLW borosilicate glasses, against the oxygen fugacity over the melt.

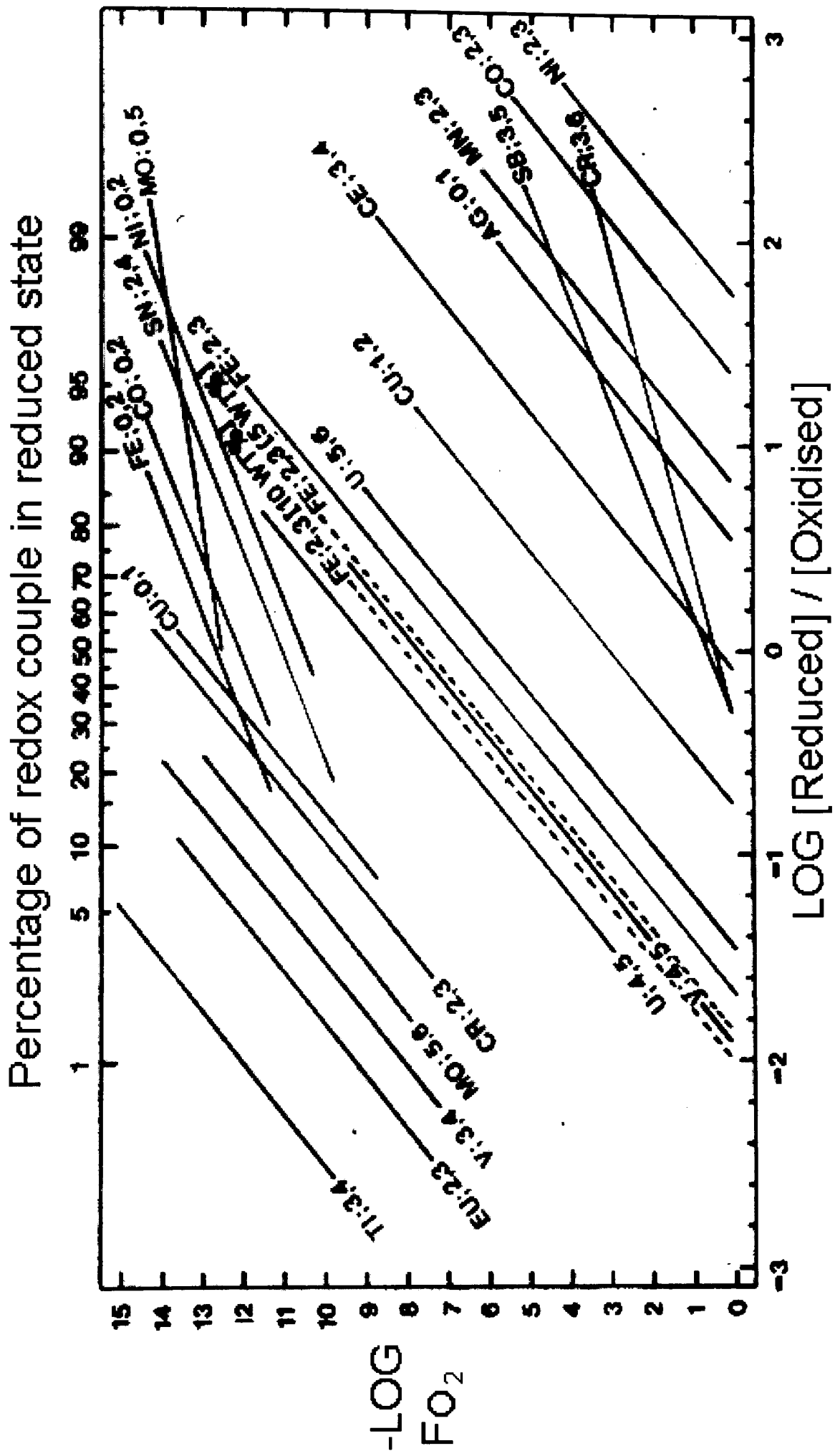

Figure 2.4 – Chart showing redox state with changing oxygen fugacity

They concluded that temperature and base glass composition have little effect on the overall redox potentials of the elements, but it must be remembered that a waste stream will contain many redox couples that are capable of interacting with one another. This would make it difficult to apply the ferrous/ferric (Fe^{2+}/Fe^{3+}) redox couple ratio, which has long been used to determine the overall redox state of many types of glass. Goldman and Brite (1986) investigated this problem using a simulated West Valley glass - an alkali borosilicate base glass containing a simulated HLW stream high in iron. They found that the Fe^{2+}/Fe^{3+} ratio vs. O_2 partial pressure deviated substantially from its predicted linear behaviour, but only at $P_{O_2}<1$ kPa, where they suspected that the Cr^{3+}/Cr^{6+} redox couple begins to interact with the iron couple. Thus, they concluded that the ferrous/ferric couple can be used to quantify the redox state of a nuclear waste glass that contains several other redox couples. This theory was utilised by Iwase *et al.* (1998) in their investigation into the redox equilibrium of a Japanese waste glass candidate. Buhler (1999) used a mathematical approach to determine the thermodynamic properties of two polyvalent elements in relation to a fixed oxygen partial pressure and melt temperature. The equations show that the position of the equilibrium of the redox state of one polyvalent element depends on the melt composition and the activity of the second polyvalent element in question. If the interaction of all polyvalent elements found in a melt containing nuclear waste, and their effects upon the activity coefficients of all of the corresponding polyvalent elements were taken into account, the series of equations would become unworkably large. The results would also only be applicable for a defined temperature and oxygen partial pressure, and the exact composition of the melt would be required, a property that cannot be measured on a real vitrification line (see above).

Medlin *et al.* (1998) used square wave voltammetry (SWV) to analyse individual reduction potentials of components in glass melts *in situ*. The compositions used were the same as those used by Schreiber, and they found that the redox state of the melt correlated with that of the glass. SWV was also used by Clauβen and Rüssel (1996) to investigate the redox equilibria of some transition metal ions in a borosilicate glass melt. However, SWV cannot directly monitor individual redox ion concentrations. In a paper examining the redox state of cerium (used as a surrogate element for plutonium in model defence wastes), Fortner *et al.* (1997) used electron energy loss spectroscopy (EELS) to determine the valence state of the element. They reported that changing the proportions of the alkali elements in the base glass composition can have a significant effect on the redox state of the cerium, and thus can affect its solubility

in the glass. They also concluded that EELS analysis could be applied to any material that can be prepared for TEM analysis, and could be used to determine the valence states of elements in multivalent systems. The technique is however limited when applied to materials that are beam sensitive. Tilquin *et al.* (1998) made a comparison between electrochemical and spectrophotometric (visible light absorption) methods of measuring the redox state of chromium ions at high temperature in a sodium borosilicate melt under different oxygen partial pressures. Whilst there is an upper limit on the quantity of chromium in the melt for the spectrophotometric analysis to work, a good correlation between the results from the two methods was obtained. However, the authors do not comment on whether the methods are applicable to melts that contain more than one multivalent species.

Duffy (1999) points out that increasing the basicity of the melt usually encourages higher oxidation states of the cationic species. He also describes how a cation (or anion) can only be in its full oxidation state when in the gaseous form, where the separation between individual ions is effectively infinite. In a melt or a solid, a cation will share some negative charge with the anions around it (usually O^{2-}), as the electron orbitals of the anions overlap the empty electron orbitals of the cationic species.

Schreiber *et al.* (1993) investigated the use of sulphate as a selective redox buffer for melts. The team added sodium sulphate to the borosilicate waste glass SRL-131 (a Savannah River waste composition) and found that at 1150°C the sulphate formed an immiscible layer above the borosilicate melt. They discovered that this layer altered the redox state of the chromium ions in the melt, but did not affect iron, cerium or manganese ions. This effect is attributed to isomorphic substitution of the chromate ions with the sulphate ions in the immiscible layer, and can stabilise chromates and molybdates in oxidising conditions. This has important implications for waste streams high in sulphates as sulphur can play a major part in yellow phase formation.

Silicon metal, sugar and carbon (in the form of graphite) have long been known as reducing agents that can be used in glass manufacture. Wang *et al.* (2000) investigated the effects of adding sugar to 3 different batch compositions that had previously been melted to produce homogeneous glasses containing 20/25% high level waste. They found that as little as 0.2wt% sugar addition could cause reduced metals to precipitate out of the melt (and be left in the crucible after casting), and that >0.5wt% sugar addition led to devitrification of the melt on cooling. This may have been due to reduced metals acting as nucleation centres for crystalline phases.

Smith *et al* (1995) investigated the effects of sugar, nitrate and formic acid additions on a glass containing a simulated neutralized current acid waste (a radioactive wasteform with high Fe content under consideration for vitrification in the United States) which contained a similar range of waste oxides to the compositions examined in this work (although at a much lower waste stream content). They found that the addition of sugar resulted in a much more reduced glass based on the Fe^{2+}/Fe^{3+} ratio than either the formated or nitrated glasses. The added sugar pyrolyzed at 665°C in the melter resulting in the release of CO and H_2. The redox ratio of the nitrated samples were found to be almost identical to those of the untreated and formated samples, although this does not agree with other work carried out on the topic of nitration.

Feng *et al* (1989) investigated the effects of redox state on the chemical durability of West Valley nuclear waste glasses. The West Valley wastes contain a large proportion of iron oxide, and the $Fe^{2+}/\sum Fe$ ratio (determined using a combination of colourimetry, Mossbauer spectroscopy and wet chemical analysis) was used to determine the redox state of the glass samples. Feng *et al* used several glass compositions and found that glasses containing a high percentage of alumina (nearly 10wt%) displayed a two-fold increase in chemical durability as the furnace atmosphere was changed from highly reducing to oxidising. However, in the lower alumina glasses (around 3wt%), the change was much more pronounced with a twelve-fold increase in durability as the atmosphere was changed from reducing to oxidising. Feng *et al* concluded that glasses which have an excess of network formers, (the high alumina glasses in this case) which are in general the more durable base glass compositions, are insensitive to reducing atmospheres, whereas those glasses with network former deficits are generally much more sensitive to even small melting atmosphere alterations.

2.5 Molybdenum and Glass

The vast majority of papers on the subject of Mo in relation to glass melting in general concern the dissolution rate of Mo electrodes in glass melts, as Mo electrodes are the most commonly used type of electrodes for electric glass melting. Mo metal has a high melting point (>3000°C) and is thus an ideal material for the manufacture of electrodes that have to withstand glass melting temperatures. Tantalum has a similar melting point to Mo and Ta electrodes are also used for some glass melting operations, but the high cost of this material generally restricts its use to specialist melts. The electric melting procedure itself is also becoming more popular.

Min'ko *et al* (2000) gives the benefits of electrical melting over more conventional gas furnaces as greater ease of control, greater efficiency, promotion of homogeneity, and a reduction in the quantity of raw materials (especially alkali containing materials) needed and atmospheric pollution produced. Also, electrical furnaces are generally smaller and simpler to build than open-flame furnaces, and therefore come at a reduced cost. The largest problem with this method seems to be the corrosion of the Mo electrodes, and the best way to minimise it. Corrosion of the electrodes can cause unwanted colouration of the melt, and eventually will lead to a furnace shut down to replace them. Min'ko *et al* studied data from the Zarya Glass Works in Kharovsk, Russia and determined the redox potential of the melt was the controlling factor in the dissolution of the electrodes. The redox potential depends on the chemical oxygen minimum of the batch/cullet, and the chemical species contained within it. A high redox potential was found to increase the rate of electrode dissolution via the formation of molybdenum dioxide and molybdenum sulphides. In a similar paper, Holzwarth *et al* (1991) investigated the corrosion of Mo electrodes in an aluminosilicate glass melt doped with various polyvalent ions. They found that electrode dissolution occurred via oxidation of the Mo metal by the formation of a redox couple with one of the polyvalent ions. This then led to the formation of molybdenum [tri]oxide on the surface of the electrode, which eventually evaporated into the furnace atmosphere.

Bobkova *et al* (1989) point out that addition of MoO_3 can improve the properties of n-type semiconductor glasses and can be efficient at reducing viscosity and surface

tension in glasses generally. They relate these improvements to the structure, valence and coordination states of the Mo ions in the glasses and investigated these properties using Raman scattering and electron spin resonance techniques on CdO-PbO-MoO_3-Al_2O_3-SiO_2-B_2O_3 glasses. They discovered both Mo^{6+} and Mo^{5+} ions in the glasses, and determined that the Mo^{6+} was mainly 4-fold coordinated, although there was a tendency to 6-fold coordination at higher MoO_3 and CdO concentrations.

Van Der Wielen *et al* (1968) investigated the glass forming properties of alkali molybdate systems primarily, it seems, in order to make a comparison with the glass forming properties of alkali tungstates. They found that by melting batches of MoO_3 and M_2CO_3 (where M=alkali metal) and cooling at rates of ~8000°C/second, glasses could be formed given the correct Mo/alkali ratios, and that in the solid state the coordination of the Mo ions moved from tetrahedral to octahedral with decreasing alkali content.

Johnson *et al* (1999) investigated the properties of $MoSi_2$ for use as an alternative to normal refractories in glass furnaces, due to its special corrosion resistant properties in molten glass. Below the glass line, it tends to form Mo rich regions near the surface which have high corrosion resistance, whilst above the glass line Si rich areas form which have good oxidation resistance. Johnson *et al* compared the corrosion rates of $MoSi_2$ with alumina-zirconia-chrome-silicate refractories in a molten alkali borosilicate glass, and found that above the glass line a protective layer of SiO_2 formed on the $MoSi_2$, whilst below the glass line a layer of various Mo rich molybdenum silicates formed giving the $MoSi_2$ corrosion resistant properties comparable to those of the alumina-zirconia-chromia-silica (AZCS) refractory blocks. However, at the glass line, Si tended to dissolve rapidly into the melt and Mo tended to oxidise and vaporise, giving much more rapid corrosion than was noted in the AZCS.

Some work has been performed investigating the glass forming ability of silicates containing MoO_3. Stemprock *et al* (1974) melted sodium silicates with various quantities of MoO_3 in Pt crucibles at 1400°C. They found that homogeneous glasses with an 8wt% MoO_3 content could be formed in the metasilicate region, but as the system moved towards the di and trisilicate region, the solubility of MoO_3 dropped to

around 4wt%. At higher MoO_3 contents, Na_2MoO_4 and $Na_2Mo_2O_7$ phases formed in the melt and sank to the bottom of the crucible.

Some authors have investigated glasses with small (≤3.5%) MoO_3 additions, often during studies on crystallisation aspects of various systems. Schlesinger and Lynch (1988) melted a series of lithium disilicate glasses containing small substitutions of MoO_3 for SiO_2 at 1445°C for 2 hours in Pt-Rh crucibles to investigate the nucleation effects of the MoO_3 substitutions. They found that with a 3% substitution of MoO_3 for SiO_2, the glass crystallised despite a splat quench pour, and that even with a 2% substitution the glass appeared cloudy (indicating some phase separation). Only a composition with a 1% substitution was found to be homogeneous upon quenching, indicating a low solubility of MoO_3 in lithium disilicate compositions. Donald *et al* (1994) melted a $Li_2O.3.5B_2O_3$ glass containing 5wt% SiO_2 and 1.5mol% MoO_3 additions in a Pt-Rh crucible at 1000-1100°C as part of an investigation into the properties of some lithium borate based glasses. They rated the Li-B-Si-Mo composition as having a good glass forming ability, i.e. when poured onto a metal plate to a thickness of >10mm, there was no visible crystallinity in the glass. Donald, Metcalfe and Morris (1992) found that a 2mol% addition of MoO_3 could be dissolved in a lithium zinc silicate glass melted at 1450°C during their study of the influence of transition metal ions on the crystallisation kinetics, microstructures and thermal expansion characteristics of the glass. However, with a 3.5mol% addition of MoO_3 the glass appeared a milky opal colour in the as cast state, indicating a heterogeneous glass (as the homogeneous glasses of this composition containing Mo were colourless)

2.6 Summary

Over the last 50 years, many different types of matrices have been suggested and investigated as possible hosts for HLW. Of these, dissolution of the waste in borosilicate glass has become the most popular method of immobilisation, due to the superior overall qualities of the vitrified product. Much research has been performed on borosilicate glasses of varying compositions in the areas of chemical durability, radiation stability and optimising composition for maximum waste loadings whilst retaining a low viscosity at melting temperatures and maintaining an amorphous structure during slow cools.

However, there are still several areas of waste vitrification using borosilicates that are capable of being refined. Molybdenum is a major component of Magnox reactor HLWs, and at high waste loadings tends to form yellow phase, a generic term which is applied to crystalline material composed of molybdate compounds and other elements of the HLW that devitrifies during the slow cools experienced in canisters of HLW glass. Previous studies have shown that the formation of yellow phase can be suppressed by reducing Mo^{6+} ions in the melt to lower oxidation states, thereby giving them a higher solubility in the glass, although the solubility limit of Mo in most of the studied glass compositions is <3%.

The oxidation state of elements in a glass melt can be affected by the melting atmosphere, temperature and pressure, the batch composition and melt additions. Highly oxidising conditions can lead to melt foaming, whereas highly reducing conditions can cause the formation of metallic particles in the melt, both of which are detrimental to glass production. The Ellingham diagram is often used as a guide for judging which elements are likely to undergo redox reactions, but due to the high number of interacting redox couples in a typical HLW melt the true oxidation state has to be measured either *in-situ* in the furnace or after the glass has been cast. Square wave voltammetry and spectrophotometric analysis have both been used to measure the redox potentials of species in a melt, but to obtain the actual concentration of a given redox state, wet chemical methods (usually titrations) are used on the glass after it has been cast and has cooled. To obtain the overall oxidation state of the waste

glass, the ratio of ferrous to ferric iron is often used. These methods have been used to quantify the effects of redox agents (such as sulphates, nitrates, sugar, silicon, graphite) on many glass melts over long periods of time in both HLW vitrification experiments and research on commercial borosilicates.

3. Experimental Procedures

3.1 Batch preparation

The glasses melted for this work were all based on the standard MW glass frit used in the Waste Vitrification Plant at Sellafield. The composition termed "HM4" was specified by BNFL and is shown in **Table 3.1**.

Oxide	Weight %	Mole %	Supplied as	Purity %	Supplier
SiO_2	49.44	56.10	SiO_2 (Loch Aline sand)	99.8	Tilcon
B_2O_3	17.52	17.16	B_2O_3	99	Sigma Aldrich
Na_2O	8.80	9.68	Na_2CO_3	99.95	Sigma Aldrich
Li_2O	4.24	9.67	Li_2CO_3	99.95	Sigma Aldrich
Waste	20	7.39	-	-	See **Table 3.2**
	Total	Total			
	100	100			

Table 3.1 - Nominal composition of HM4 glass

The component listed as "waste" represents the non-active simulated HLW stream used for these experiments. The composition of this stream as oxides of the HLW elements was specified by BNFL and is shown in **Table 3.2**. All compositions reported are nominal compositions. Chemical analysis (Inductively Coupled Plasma Atomic Emission Spectroscopy) had been requested for some samples, but was unavailable at the time of print. Chemicals were supplied by Tilcon Ltd, West Avenue, Talke, Stoke on Trent, ST7 1TU, UK and Sigma-Aldrich Company Ltd., The Old Brickyard, New Rd, Gillingham, Dorset, SP8 4XT, UK.

Oxide	Weight %	Mole %	Supplied as	Purity %	Supplier
AgO	7.05	5.61	Ag_2O	99	Sigma Aldrich
BaO	4.68	5.63	$BaCO_3$	99	Sigma Aldrich
CeO	6.65	7.86	Ce_2O_3	99.9	Sigma Aldrich
Cs_2O	6.54	4.28	Cs_2CO_3	99.9	Sigma Aldrich
Gd_2O_3	13.87	7.06	Gd_2O_3	99.9	Sigma Aldrich
La_2O_3	3.55	2.01	La_2O_3	99.9	Sigma Aldrich
MoO_3	11.97	15.34	MoO_3	99.5	Sigma Aldrich
Nd_2O_3	14.98	8.12	Nd_2O_3	99.9	Sigma Aldrich
Rb_2O	0.82	0.81	Rb_2CO_3	99	Sigma Aldrich
RuO_2	7.47	10.36	N/A	N/A	N/A
Sm_2O_3	2.20	1.16	Sm_2O_3	99.9	Sigma Aldrich
SrO	2.07	3.69	$SrCO_3$	99.9+	Sigma Aldrich
TeO_2	0.60	0.69	TeO_2	99+	Sigma Aldrich
TiO_2	2.67	6.17	TiO_2	99.9	Sigma Aldrich
Y_2O_3	1.23	1.01	Y_2O_3	99.99	Sigma Aldrich
ZrO_2	11.02	16.50	ZrO_2	99.5	Sigma Aldrich
Fe_2O_3	1.66	1.92	Fe_2O_3	99.9	Sigma Aldrich
NiO	0.47	1.16	NiO	99.9	Sigma Aldrich
Cr_2O_3	0.50	0.61	Cr_2O_3	99+	Sigma Aldrich
Total	100	100			

Table 3.2 - Composition of simulated HLW stream.

N.B. RuO_2 was omitted from the waste stream on the grounds of cost.

This simulated HLW waste stream represents a stream that is based on the projected fission products of a 4:1 blend of high burn up (HBU) UO_2 fuel and mixed oxide (MOx) fuel, a composition that BNFL is considering for possible future reprocessing. Whilst an active HLW stream of this type would contain upwards of 40 different elements in the form of oxides and nitrates (of which the latter would become oxides during melting), many of these components have been replaced by a single oxide with similar chemistry in the simulated stream to simplify the reproduction and analysis of the HLW glasses and avoid use of radioactive isotopes. For example, many of the rare

earth elements such as Pr and Eu have been simulated by increasing the amount of Nd_2O_3, and AgO has been used to represent Rh, Pd and Cd oxides. TiO_2 was used to model TcO_2. The high proportion of Mo and Zr in the waste stream originates from the electrochemical dissolution of the fuel assemblies and the Gd_2O_3 has been added as a neutron poison, not a fission product.

In some cases the waste loading of the glass and the components added to represent the simulated waste stream were changed depending on the particular experiment for which the glasses were prepared. These compositional variations are expanded upon in the relevant chapters. For the purpose of all of these experiments, RuO_2 was omitted from the simulated HLW stream due to the high cost of the compound. Although RuO_2 is a waste stream component that causes some concern in HLW vitrification, it is thought to have little effect on the behaviour of Mo in these systems and so it was agreed with BNFL to omit it from the compositions studied here. Precious metals are known to act as nucleating agents in some glass melts and RuO_2 crystals have been found in high concentrations in melter heels from full scale simulated HLW melts. However the available literature does not mention RuO_2 acting as a nucleating agent for yellow phase, possibly because this phase is less dense than the HLW glass and therefore tends to form on or near the surface, whereas RuO_2 has a greated density than the melt and tends to sink to the bottom.

The necessary chemicals for a given composition were weighed to an accuracy of ±0.01g and placed in stainless steel vessel. They were then intimately mixed using a PVC spatula and transferred to a batch scoop ready for "filling-on" for the melts performed in Pt crucibles (see **Chapter 3.2.1**), or an alumina crucible for preheating for those melts performed in alumina crucibles (see **Chapter 3.2.2**).

3.2 Glass Melting

All of the glasses were melted in a 147.5cm^3 (internal volume) electric furnace with Kanthal SiC elements. The temperature of the glass furnace was regulated by a Eurotherm controller and a melting temperature of 1150°C was used for the majority of the experiments. This temperature was sometimes altered to attain the desired viscosity of the glass or to observe the effects of melting at different temperatures on specific compositions. The total melting time for all melts was 5.5 hours (i.e. a 1 hour batch free time and 4.5 hours stirring/bubbling time) and all the glasses were poured into a preheated steel block mould to form a rectangular glass block approx. 2x2x10cm in size. This block was then transferred to an annealing furnace where it was held at 550°C for 1 hour and then cooled to room temperature at 1K/min to relieve the stresses in the glass. In some cases a gob of glass was rapidly quenched between 2 cold steel plates to form a "splat".

The total melting time of 5.5 hours with 4.5 hours of either sparging or stirring for each 100g batch was considered ample for homogenisation. In comparison, the batch in the real vitrification procedure is of the order of 2 x 10^3 times greater in size and is given a total melting time of 8 hours in which to homogenise.

3.2.1 Platinum Crucible

Due to the small size of the Pt crucible used (approximately 0.2l capacity), a whole 100g batch would not fit into the crucible in one go. Therefore, the crucible was filled with batch using a scoop to a depth of approximately 1cm from the brim and placed into the glass furnace at the appropriate temperature (nominally 1150°C). After the batch had begun to melt (approx. 10 mins), the resulting reduction in volume allowed more batch to be added so the crucible was withdrawn from the furnace using iron tongs and more batch poured on to the top of the melt until again the crucible was nearly full. This process was repeated until the entire batch had been added to the crucible, which usually involved 3 "fill-ons" in total. The melt was then allowed 1 hour batch-free time before a rectangular Pt stirring paddle was inserted to a depth of approx. 1cm from the base of the crucible and rotated at 60rpm for the remainder of

the melting period (4.5 hours). The stirrer was necessary to compensate for the lack of convection currents in full scale glass melts which help to homogenise the glass.

3.2.2 Alumina Crucible

It was suspected that the batches with high waste loadings and those to be melted under reducing conditions could potentially damage Pt crucibles. Due to the high cost of these items, it was decided to use alumina crucibles (approximately 0.4l in capacity) for any melt that was a potential threat to the integrity of the Pt crucibles (and also any associated melts to keep experimental conditions constant). For these melts, the entire batch was poured into the crucible and preheated to a temperature of 1000°C at 1K/min in a Lenton 1500W muffle furnace and then transferred to the melting furnace. The preheat was necessary to prevent thermal shock and cracking of the alumina crucible from expansion on transfer to the glass furnace. The melt was allowed one hour batch-free time, and then an alumina stirring paddle was inserted into the crucible to a depth of approx. 1cm from the base of the crucible, and rotated at 60rpm for the remainder of the melting time (4.5 hours)

3.2.3 Gas Sparging

To control the redox conditions in some melts, a gas was bubbled through the melt, a process known as sparging. In all cases where sparging was used, the melts were performed in alumina crucibles. To create a strongly reducing atmosphere, N_2 gas containing 5% H_2 was used, Ar gas was used for mildly reducing atmospheres, compressed air for neutral atmospheres and for the oxidising atmosphere, pure oxygen was employed. All gas cylinders were supplied by BOC gases (The Priestley Centre, 10 Priestley Rd, Surrey Research Park, Guildford, Surry, GU2 7XY, UK) and are specified as ≥99.5% pure. For the melts performed with pure oxygen, a flow back arrester was placed between the tube and the cylinder to remove the possibility of explosion.

One end of a hollow pure alumina rod was connected to the gas cylinder via a plastic tube. The other end of the alumina rod was positioned in the melt so that it was approx. 1cm from the bottom of the crucible, and the gas control valve set at a level

where the melt was gently bubbling- i.e. enough gas to create a stirring effect, but not so much as to push the molten glass out of the crucible. At this level the flow rate was usually between 2-5l/min depending upon the viscosity of the melt. This was done for all but the first hour of the 5.5 hour melts to correlate with those melts which were mechanically stirred with alumina paddles.

3.2.4 Annealing

The melts were poured into a preheated steel block mould and annealed at 550°C (an appropriate temperature as determined during initial experimentation) for one hour, then cooled to room temperature at 1K/min. The annealing was done in a Lenton 1500W muffle furnace.

3.3 Heat Treatments

Some of the glass samples were heat treated for various times and temperatures to simulate the slow cools that the actual vitrified product experiences in the steel containment vessels used in HLW vitrification. The samples to be heat treated were cut into cubes approx. 1x1x1cm using a diamond saw and placed in an alumina boat crucible. This crucible was then inserted into a Lenton 3000W tube furnace and heated to the required temperature at 5K/min, held for the required period of time and then cooled back to room temperature at 5K/min. The heat treatment times and temperatures are detailed in the relevant sections of this thesis.

N.B. The temperatures of all the furnaces used were checked occasionally with a calibrated Pt-Rh thermocouple, and in all cases was found to be within ±2K of the stated temperature.

3.4 X-ray Diffraction (XRD)

XRD is a technique widely used to identify crystalline compounds. The technique is based on Braggs Law

$$n\lambda = 2\,d\,\sin\theta$$

where n is an integer, λ is wavelength, d is the crystalline lattice spacing and θ is the angle of incidence.

The sample to be analysed is placed in the path of a beam of x-rays of known wavelength (λ) which is diffracted by a certain angle (θ) depending upon the spacing of the lattice planes of the sample (d). This is illustrated in **Figure 3.1**.

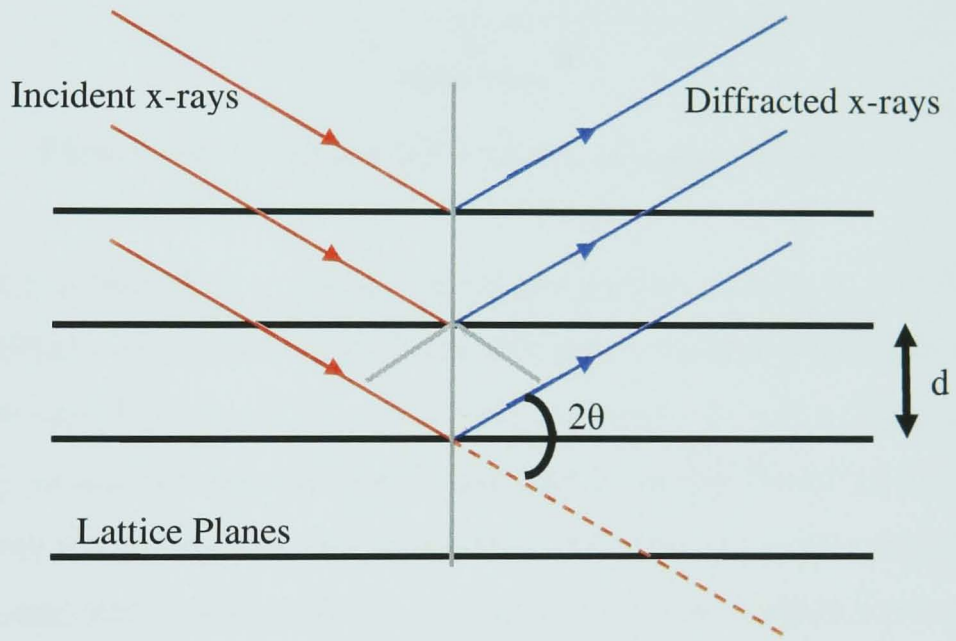

Figure 3.1 – Schematic of basic x-ray diffraction

In most powder XRD machines (such as the one used for the majority of the experiments performed during this work) the x-ray source remains still, whilst the sample is rotated about a point (the axis of which lies perpendicular to the direction of the x-ray beam) at θ^{o}/min. The detector moves around the sample with the same axis of rotation at a speed of $2\theta^{o}$/min (so that the angles of incidence and diffraction are maintained equal) and measures the number of counts caused by the diffraction of the

x-ray beam. The distance between the x-ray source target to the sample, and from sample to detector is equal to maintain the correct focusing of the diffracted beam, and therefore prevent peak broadening.

An example of the pattern produced by a powdered glass ceramic sample is shown below in **Figure 3.2**

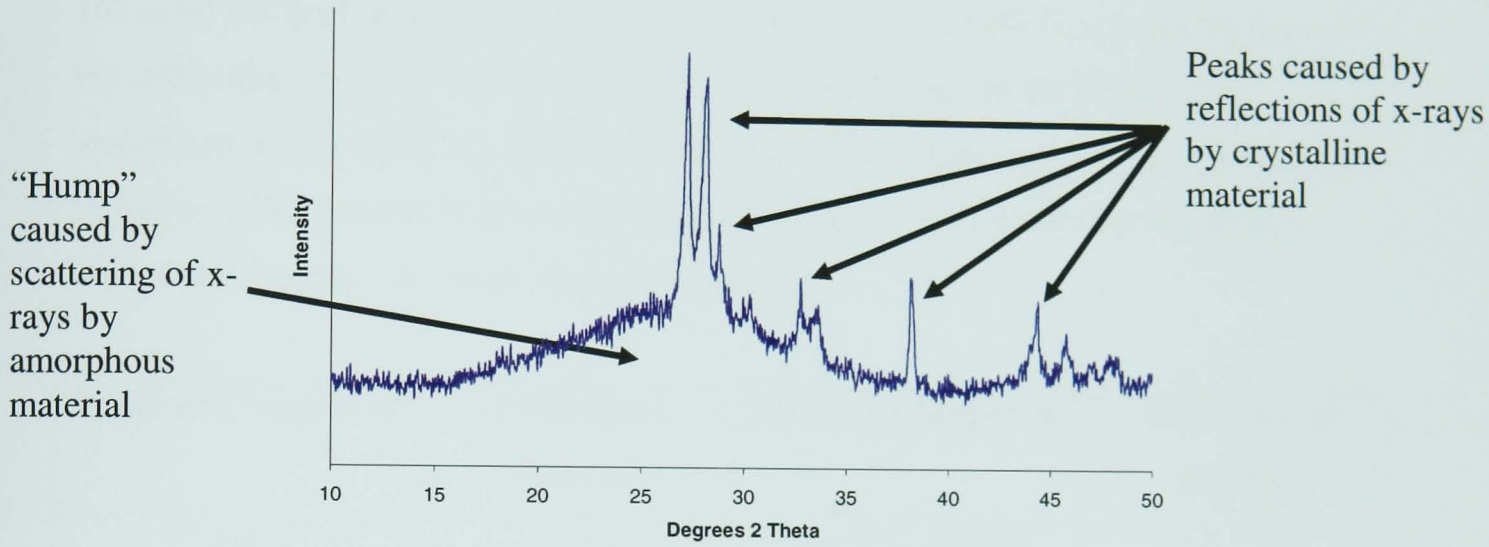

Figure 3.2 – A typical XRD pattern of a glass ceramic

As the sample is powdered in a mortar using a pestle prior to analysis, it is assumed that the crystallites (and therefore the crystal planes) are randomly oriented when loaded into the sample holder. Thus, a full XRD pattern with correct intensities should be obtained by simply moving the detector around the sample. However, this assumption does not always hold true as the front-filled sample holder preparation process can sometimes lead to preferred orientation of the crystallites in the sample. This will affect the intensities of the crystalline peaks on the resulting pattern, but should not lead to a shift in the peak positions, and thus peak matching can still be performed using the International Centre for Diffraction Data (ICDD) database. If accurate peak intensities are required then backfilled sample holders can be used, which avoid preferred orientation as the sample does not need to be smoothed after the sample holder has been filled. More information on x-ray diffraction can be found in Guinier, 1994.

Samples for analysis using a Philips PW1373 X-ray Powder Diffractometer, were first broken down into a coarse powder using a percussion mortar. The powder was then

ground to a fine enough size for diffraction (<200μm) in an agate mortar using a pestle. In all cases where the agate mortar and pestle was used, it was cleaned after each sample by grinding Loch Aline sand and wiping with acetone so as not to contaminate the next sample. The powder for analysis was then front loaded into an aluminium sample tray, and scanned using CuKα radiation at 50kV. The step size used was 0.02°, and the scanning speed was nominally 2°/min (although this was sometimes slowed to 0.5°/min if a more detailed scan was required) over a range of 10° to 60°2θ. The patterns obtained were matched to the ICDD files using the Stoe x-ray diffraction computer analysis software WinXPOW. All of the ICDD cards referenced in this thesis are listed in **Table 3.3**. Some of the samples were ground and sieved to ≤75μm and re-scanned to check for particles size effects. No significant differences between the scans could be observed.

Element/Compound	**ICDD Card Number**	**Element/Compound**	**ICDD Card Number**
Ag	4-783	$Li_{0.5}Nd_{0.5}$ MoO_4	23-1195
$Ag_{0.5}La_{0.5}$ MoO_4	49-384	$Li_{0.5}Sm_{0.5}$ MoO_4	18-745
$Ag_{0.5}Ce_{0.5}MoO_4$	49-381	$Li_{0.5}Gd_{0.5}$ MoO_4	18-728
$Ag_{0.5}Nd_{0.5}(MoO_4)$	49-380	Mo	42-1120
$Ag_{0.5}Sm_{0.5}$ MoO_4	49-383	$Na_{0.5}Y_{0.5}$ MoO_4	82-2368
Al	85-1327	$Na_{0.5}La_{0.5}$ MoO_4	79-2243
$BaMoO_4$	29-193	$Na_{0.5}Ce_{0.5}$ MoO_4	79-2242
$CaMoO_4$	85-546	$Na_{0.5}Nd_{0.5}$ MoO_4	25-852
$Cs_{0.5}Nd_{0.5}(MoO_4)$	49-1015	$Na_{0.5}Gd_{0.5}$ MoO_4	25-828
$K_{0.5}Nd_{0.5}(MoO_4)$	32-817	$Nd_2(MoO_4)_3$	73-1212
$LiCsMoO_4$	72-2479	$(Nd_2(MoO_4)_3)_{1.333}$	73-489
$Li_{0.5}Y_{0.5}$ MoO_4	17-773	SiO_2 (Quartz)	85-335
$Li_{0.5}La_{0.5}(MoO_4)$	18-734	$SrMoO_4$	85-586 and 8-482
$Li_{0.5}Ce_{0.5}$ MoO_4	84-539	$Sr_{0.5}Ba_{0.5}$ MoO_4	30-157

Table 3.3 – ICDD database cards referenced in this thesis

N.B. Due to mechanical machine failure, some of the redox effect glasses (**Chapter 4.3.2**) were x-rayed using a Co kα source as opposed to the Cu kα source used for the majority of these experiments. For ease of comparison, the Co traces have been converted to Cu traces using the formula:

$$2\theta_2 = 2\{\sin^{-1}(\lambda_2/\lambda_1.\sin[2\theta_1/2])\}$$

where $2\theta_1$ and λ_1 are the original Co diffraction angles and Co kα wavelength, and $2\theta_2$ and λ_2 are the Cu diffraction angles and Cu kα wavelength. The values used for the wavelengths were 1.78896Å and 1.54060Å for Co and Cu respectively.

3.5 Electron Microscopy

The basic principals of electron microscopy are similar to those of optical microscopy, in that lenses are used to magnify an image of an object. In optical microscopy, the lenses are made of curved pieces of glass which magnify and focus divergent rays of light (or photons) that have either been reflected from the surface of the object, or transmitted through the object. In electron microscopy, magnetic fields are used as lenses for magnification and electrons are aimed at the object, reflected (in scanning electron microscopy) from the surface of the object or transmitted (in transmission electron microscopy) through the object, and then focused and to form an image (either by phosphorescence on a coated screen or by digital conversion). The benefit of using electrons over light is due to the much shorter wavelength of electrons. The resolution (the smallest distance between two distinct points that can be observed) is a function of wavelength and improves (i.e. the smallest resolvable distance is reduced) with decreasing wavelength. The best resolution that can theoretically be obtained using an optical microscope is ~0.15μm, assuming perfect lenses and very large apertures (which minimise the diffraction of the light). However, if we make the same assumptions for electron microscopy and consider 100kV electrons (typical of those used in many electron microscopes), we can theoretically resolve distances of 0.02nm, which is smaller than the radius of an atom. Whilst these kinds of resolution are never likely to be achieved in real microscopes, it is possible to see that using electrons one can achieve resolutions 10^4 times better than can be achieved with light. For an in depth discussion on the basic principals and applications of electron microscopy see, for example, Williams and Carter (1996) or Watt (1985).

3.5.1 Scanning Electron Microscopy

A scanning electron microscope (SEM) was used with an Energy Dispersive X-ray Spectroscopy (EDS) attachment to obtain chemical analysis from some samples. The basic principal of EDS is illustrated in **Figure 3.3** below.

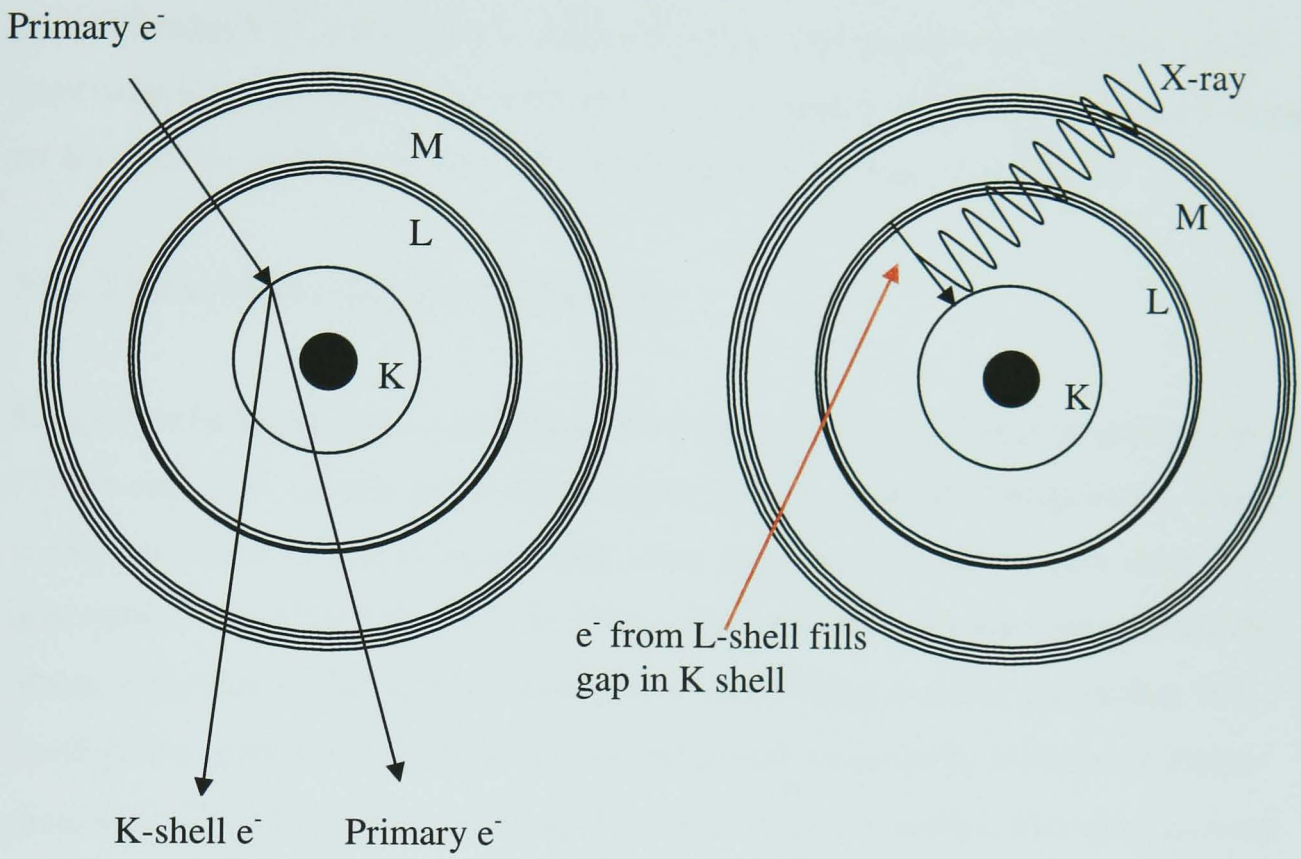

Figure 3.3 – Schematic diagram showing typical electron (e^-) movement in an atom during EDS.

When an electron is knocked out of an inner shell of an atom (e.g. the K shell in **Figure 3.3**) by an incoming (primary) electron from the microscope source, the atom is left in an excited (high energy) state. This state is unstable and will relax back to its lower energy state by filling the inner shell vacancy with an electron from an outer shell (e.g. the L shell in **Figure 3.3**). For this relaxation to occur, energy has to be released from the atom, and this happens in one of two forms. Either a valence shell electron (e.g. from the M shell in **Figure 3.3**) is emitted from the atom carrying the excess energy caused by the initial excitation (this is known as Auger electron emission), or an x-ray will be emitted. If an x-ray is emitted, the energy of the x-ray will be determined by the difference in energy of the two states between which the electron moves, and this difference is unique to every particular atom. Thus, by measuring the energies of the x-rays produced in this way, one can obtain a compositional analysis of a sample.

Samples that were to be examined using the EDS function of the CamScan scanning electron microscope were mounted in epoxy resin and left under vacuum during setting. They were then ground using 120, 240, 400, 600, and 1200 grit wheels, and polished using 6, 3, and 1 micron diamond pastes. The samples were carbon coated prior to analysis to prevent charging, and were examined in backscattered mode using an accelerating voltage of 20kV. The working distance was set at 25mm.

3.5.2 Transmission Electron Microscopy

Samples to be viewed under the Philips EM 420J transmission electron microscope (TEM) were first cut into 1mm thick sections using a diamond cutting wheel. These sections were then stuck to a glass slide using wax, and polished on both sides alternately using 120, 240, 600, and 1200 grit papers until they were approximately 30μm in thickness. The samples were then cleaned using acetone, and broken into small pieces approximately 3mm across, and glued using epoxy resin to a 3.05mm diameter copper ring with a 1000μm diameter hole in the middle. The samples were then further ground using a Gatan ion beam miller until perforation gave a small hole in the centre of the disc surrounded by thin (~30nm) area. The samples were then carbon coated before being viewed in the microscope, using an accelerating voltage of 120kV. The EDS function of this microscope was also employed for some samples, and required no further sample preparation. Samples of glass 2 were examined using this microscope.

All other samples subjected to TEM were viewed under a Jeol JEM-2010F Field Emission Gun TEM. The samples were prepared using the same method as stated above for the Philips EM 420J samples. An accelerating voltage of 200kV was used, and a Gatan Digiscan imager connected to this system was used to acquire images of samples. Images were taken in Scanning TEM (STEM) mode. In normal TEM images, it is the electrons that pass through the sample and do not get scattered over large angles that are used for image formation. However, in STEM, an annular detector is used that only detects electrons that have been scattered through relatively large angles and these electrons are used to form an image. As the inelastic scattering power of an atom is proportional to its atomic number, heavier atoms appear brighter

in the image as they scatter more electrons over the angles that the STEM detector covers. For more information on STEM, see Williams and Carter Vol. III (1996). An Oxford Link Isis EDS system was also connected to this system and was used to acquire EDS analysis from some samples.

3.6 Differential Thermal Analysis

Differential thermal analysis (DTA) was performed using a Stanton Redcroft DTA 673-4, calibrated using aluminium (atomic weight 26.98, melting point 660.1°C) and gold (atomic weight 196.97, melting point 1063.0°C) standards in air, and the Perkin Elmer thermal analysis software Pyris V.5. The sample to be analysed was ground to a fine powder (<75μm) using an agate pestle and mortar. Approximately 0.1g of the powder was weighed out using an electronic balance, and the weight recorded to ±0.0001g. Then an equivalent amount of finely divided fired alumina was weighed to an accuracy of ±0.0005g as a reference, and the powders were placed into two identical DTA crucibles. Alumina crucibles were used as platinum crucibles would have been damaged by the samples. The samples were placed in the furnace and heated to 850°C at 10K/min, with temperature and ΔT measurements taken every 0.1secs. The cooling curves were not recorded. Glass transition (T_g) temperatures were indicated by the mid-points of the endothermic dips on the resulting DTA trace, and were used to set heat treatment temperatures. All DTA analysis was performed in static air. Mackenzie (1970) discusses the fundamental aspects of DTA.

3.7 Electron Spin Resonance

Electron spin resonance (ESR) is an analysis technique which can be used to detect paramagnetic species in samples, and thus help to identify oxidation states of some species. A sample is placed in a microwave radiation chamber and irradiated with microwaves of varying frequencies. Any unpaired electrons in the sample will absorb the microwave radiation at specific frequencies (depending on the atom or ion with which they are associated) and be promoted to a higher energy level. By measuring the frequency at which absorption takes place to obtain a *g*-value, the atom or ion to which the unpaired electrons belong can be identified. Obviously, one of the main limitations of this technique is that species that contain no unpaired electrons will exhibit no resonance, and therefore cannot be identified. For more information on ESR, Wertz (1986) details the elementary theory and practice of the ESR technique. A typical ESR trace from a paramagnetic species is shown in **Figure 3.4**. A trace from a diamagnetic species would only show background noise.

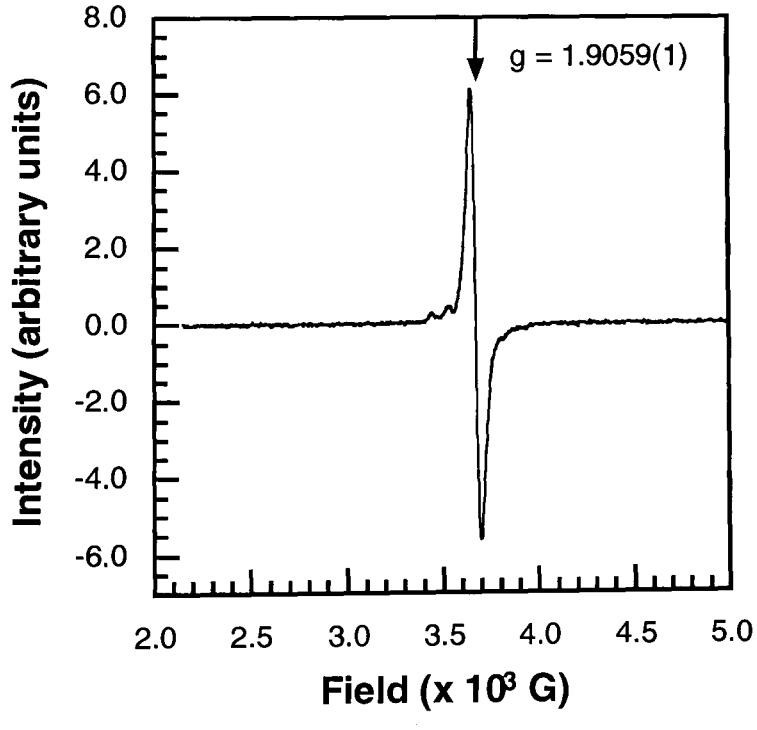

Figure 3.4 – A typical ESR trace of a paramagnetic species

Some glass samples were examined using the ESR technique to determine the oxidation state of the Mo in these glasses. ESR samples were ball milled using alumina balls to a fine powder (<75μm). Prior to milling each ESR sample, the mill

was cleaned by milling 2 samples of the base glass for 5 minutes each. The ESR samples were loaded into glass ESR sample tubes and then inserted into the microwave cavity of a Bruker ESP 300 spectrometer at the University of Birmingham School of Chemical Sciences and scanned at a frequency of 9.89GHz over a range of 2149.63-5149.63 Gauss (0.214963 – 0.514963 Tesla). The microwave power was set at 1.01mW.

3.8 Extended X-ray Absorption Fine Structure

Extended x-ray absorption fine structure (EXAFS) can be used to examine the immediate environment of particular elements (i.e. within a sphere of ~12Å from the element of interest). High energy photons (x-rays) from a synchrotron radiation source are directed towards the sample, some of which interact with the element of interest. When the energy of the x-rays is at a certain value (the "photoionisation energy"), a core electron from a 1s or 2p orbital can be ejected from the element of interest and escapes from the element into the sample. This electron behaves as a wave radiating in a sphere from the central atom and interacts with the electrons of neighbouring atoms, causing it to be partially backscattered. When the backscattered and outgoing waves interfere, a modulation of the absorption cross-section of the target element occurs, and changing the x-ray energy causes this modulation to become periodic over the photoionisation range. EXAFS spectra record this periodic modulation, which is dependant on (and can be used to identify) the atoms causing the backscattering. More information on the basic EXAFS theory and application can be found in Teo and Joy (1981). A typical EXAFS pattern is shown in **Figure 3.5**.

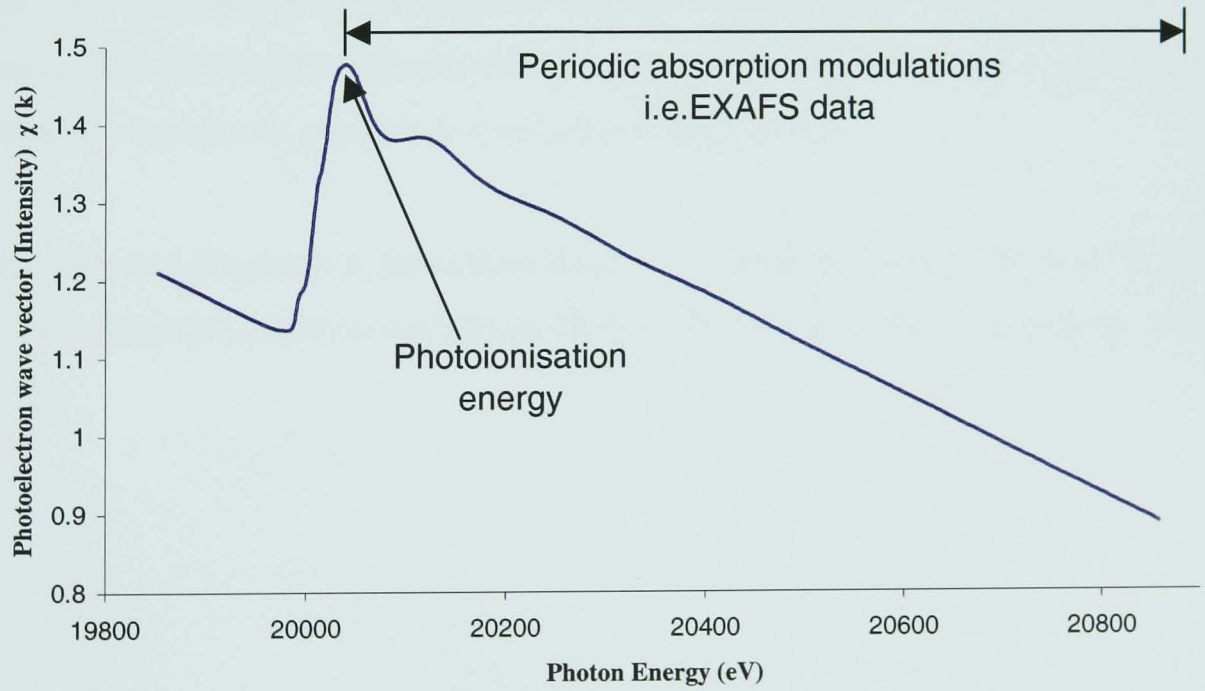

Figure 3.5 – A typical EXAFS data set

Mo K-edge X-ray absorption spectra were collected on Station 16.5 at the Synchrotron Radiation Source, Daresbury, UK. The storage ring operates at 2 GeV with a typical beam current of 150 mA. A double crystal Si (220) monochromator

was used detuned to 50% of maximum intensity for harmonic rejection. The Mo K absorption edge was calibrated by measuring the K-edge from a Mo foil at 20005 eV. Spectra were recorded at ambient temperature in transmission mode using ion chambers filled with a mixture of Ar (69800 Pa) / balance He (incident beam, I_o) and Kr 36800 Pa / balance He (transmitted beam, It). The samples, in the form of fine powders, diluted where necessary with BN (in a ca. 1:10 volume ratio), were packed into aluminium sample holders. At least two data sets were acquired per sample, over the energy range 19850 – 20850 eV. The spectral data were summed, calibrated and background subtracted using the programs EXCALIB, EXSPLINE and EXBACK. The background subtracted EXAFS data were analyzed using EXCURV98. Theoretical fits were obtained by adding shells of backscattering atoms around the central absorber atom (Mo) to create a theoretical model of the possible environment around the Mo. Refinments of the Fermi energy, E_f, the absorber-scatterer distances, r, and the Debye-Waller factors, $2\sigma^2$ were then carried out using EXCURV98 in order to minimize the sum of the squares of the residuals between the experiment and the theoretical fit. Shell occupancies were fixed at the integral values which gave the best fit as indicated by the EXAFS goodness of fit parameter, or R-factor, as calculated by EXCURV98. An R factor between 20 and 35 is normally accepted as a good fit, greater than 40 would be considered a poor fit, and less than 15 is rarely obtained on unfiltered data due to electronic noise and sample effects.

The estimated precision in the refined absorber – scatterer contact distances is ± 0.02 Å, the relative precision in the refined Debye Waller parameters is estimated to be ± 25 %.

3.9 Molybdate Synthesis

Some molybdate powders were synthesized by reacting appropriate oxides and carbonates (see **Table 3.4**) to help interpret the data obtained from the glass samples.

Oxide/Carbonate	Purity (%)	Supplier
MoO_3	99.5	Sigma Aldrich
Li_2CO_3	99.5	Sigma Aldrich
Na_2CO_3	99.95	Sigma Aldrich
K_2CO_3	99.99	Sigma Aldrich
Rb_2CO_3	99	Sigma Aldrich
Cs_2CO_3	99.9	Sigma Aldrich
$CaCO_3$	99.95	Sigma Aldrich
$SrCO_3$	99.9 +	Sigma Aldrich
$BaCO_3$	99	Sigma Aldrich
Ag_2O	99	Sigma Aldrich
La_2O_3	99.9	Koch-Light Laboratories
Ce_2O_3	99.9	Sigma Aldrich
Nd_2O_3	99.9	Sigma Aldrich
Gd_2O_3	99.9	Sigma Aldrich

Table 3.4 – Purity of oxides and carbonates used for molybdate synthesis

Stoichiometric quantities of the appropriate oxides or carbonates of the necessary elements (supplied by either Sigma Aldrich, address given above or Koch-Light Laboratories (now NBS Biologicals, 14 Tower Square, Huntingdon, Cambridgeshire, UK) were weighed out to accuracy of ±0.005g, to produce 10g of the end products (shown in **Table 3.5**). The chemicals were mixed using a spatula for approximately 5 minutes, and then ground using an agate mortar and pestle to aid mixing. The batch was then transferred to a small alumina crucible, topped with an alumina lid to minimise volatilisation and prevent contamination and then placed into a Lenton 1500W muffle furnace. The batch was held at a temperature of 700°C for 10 hours, with heating and cooling rates from and to room temperature of 5K per minute. The

batch was then removed from the crucible, reground to enhance reactivity, and refired using the same schedule as described above. This firing schedule was established by using a batch of Ag_2O, Ce_2O_3 and MoO_3 to produce 10g of $Ag_{0.5}Ce_{0.5}MoO_4$. This composition was chosen as the compound that was produced by sintering could be compared to the reference for $Ag_{0.5}Ce_{0.5}MoO_4$ in the ICDD database (card [49-381]). A good single phase product was obtained using the above firing schedule and thus it was used for all subsequent experiments. Once the powders had been fully fired, they were again ground using an agate mortar and pestle, and then analysed using x-ray diffraction. In some cases, the computerised crystallography programme Carine 3.1 was used to generate theoretical unit cells of the synthesised molybdates. The atomic positions for the component atoms were obtained from data on powellite, and the cell dimensions were obtained from the d-spacings of the (200) and (004) planes(from XRD of the synthesised molybdates). Carine was then used to generate theoretical XRD patterns for the theoretical unit cells, which could be compared to the real XRD patterns to judge the uniformity of the synthesised molybdate.

Ag Series	$AgGd(MoO_4)_2$
	$AgLa_{0.5}Gd_{0.5}(MoO_4)_2$
	$AgCe(MoO_4)_2$
Nd Series	$LiNd(MoO_4)_2$
	$NaNd(MoO_4)_2$
	$KNd(MoO_4)_2$
	$RbNd(MoO_4)_2$
	$CsNd(MoO_4)_2$
Di-alkali Series	$Li_{0.5}Na_{0.5}Nd(MoO_4)_2$
	$Li_{0.5}K_{0.5}Nd(MoO_4)_2$
	$Li_{0.5}Rb_{0.5}Nd(MoO_4)_2$
	$Li_{0.5}Cs_{0.5}Nd(MoO_4)_2$
	$KBa_{0.5}(MoO_4)_2$
Triple Valency Series	$K_{0.25}Ba_{0.5}La_{0.25}(MoO_4)_2$
	$Na_{0.25}Sr_{0.5}Nd_{0.25}(MoO_4)_2$
	$Na_{0.25}Ba_{0.5}Nd_{0.25}(MoO_4)_2$
Standards	$CaMoO_4$
	$SrMoO_4$

Table 3.5 - Composition of synthesised molybdates

3.10 X-ray Photoelectron Spectroscopy

X-ray photoelectron spectroscopy (XPS) is a surface analysis technique that is capable of determining the oxidation states of particular elements and the ratios of different oxidation states of individual elements. In XPS, monochromated x-rays are directed towards a freshly exposed surface of the sample to be analysed. Wherever possible, the surface is exposed by breaking the sample under vacuum in the XPS chamber so as to minimise any surface contamination. Some of the x-rays (photons) will be absorbed by atoms or ions in the sample, and will ionize the atoms (or further oxidize the ions) by causing them to emit inner shell electrons. These emitted electrons (photoelectrons) have a range of kinetic energies and are detected by an electron energy analyser. As the kinetic energy of the photoelectron leaving the atom or ion is proportional to its binding energy (a value specific to electrons in individual elements and ions), the technique can be used to identify atoms or ions in the sample. The oxidation state of the photoelectron emitter can also be determined from the energies of the photoelectrons. Fully quantitative analysis using XPS requires careful calibration and the use of standards, but semi-quantitative information (in the form of redox ratios of a given element) can be obtained from most XPS equipment given that the resolution is greater than ~1eV. However, the technique is only surface sensitive, as photoelectrons emitted from more than ~30nm depth will lose energy on the way out of the solid via inelastic scattering. A typical XPS result id shown in **Figure 3.6** below. Briggs and Seah (1990) discuss the principals and practice of XPS in depth.

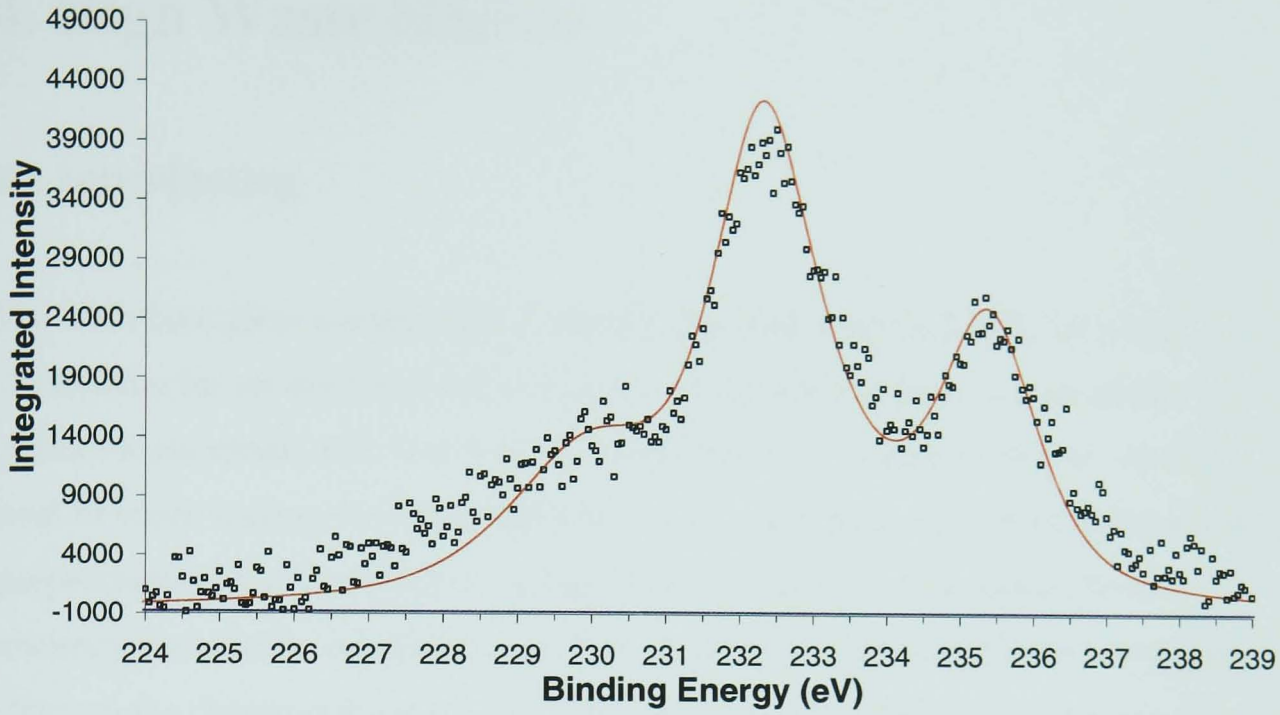

Figure 3.6 – A typical XPS data set

XPS samples were cut into bars measuring 6 x 6 x 30mm and mounted in copper sample holders. The glasses were then fractured immediately prior to insertion in the spectrometer (as the glass could not be broken under vacuum inside the machine) and analysed using a Scienta ESCA 300 at Daresbury Laboratories, with a pass energy of 150eV, slit width of 0.8mm and a take off angle of 45°. The number of scans acquired depended upon the concentration of Mo in the sample and the range of binding energies analysed. The data were corrected for the effect of sample charging by reference to O K_α. The data were fitted using the Origin curve fitting program, and as the parameters differed for each sample, the charge shifting corrections and other values used for fitting are given with the results.

4. High Waste Glasses

4.1 Introduction

The HM4 base glass composition is one that has been used by BNFL for waste vitrification for several years and is known to form a homogeneous amorphous product when mixed with simulated HLW streams to a loading of 20wt%. At this level of waste loading HM4 also tends to remain amorphous upon heat treatment at temperatures above T_g. However, at higher waste loadings these glasses have a tendency to devitrify, especially upon heat treatment, which usually has a negative effect on the chemical durability of the glass as the crystalline phases that develop tend to be highly water soluble. It was suspected that changing the base glass composition could influence the probability of the glass devitrifying. Thus, several glasses were melted with high (35%) waste loadings and varying base glass compositions to observe the effects.

One of the base glass variables examined was the Li_2O content. Li is an important factor in HLW vitrification in the UK, as the concentration of Li in the glass batch is a variable that can be affected by more than just the exact composition of the initial frit which is mixed with active HLW in the vitrification lines at Sellafield. This is because a quantity of the Li that makes up the overall concentration in the final glass is added to the active liquor (in the form of lithium nitrate) just prior to it being calcined. The Li is added to prevent the formation of refractory oxides (via the formation of Li-refractory complexes) during the calcination process, but it is a procedure that is currently under consideration for redundancy. This is because the lithium nitrate feed tank has to be located in the active liquor storage tank, which takes up valuable space that could otherwise be used for HLW storage. Also, should the lithium nitrate feed be interrupted, a costly delay is caused to the whole vitrification process. Thus, if the proposal to dispense with the Li additions comes into effect, it will be important to understand fully how HLW glasses with reduced Li contents behave.

Another factor that could influence the probability of devitrification is the redox conditions during glass melting. Lutze (1988) suggests that if the Mo in HLW glasses

can be reduced from a +6 oxidation state (the valency in which it is introduced to the batch) to a +3 oxidation state, the solubility of the element in the borosilicate matrix will increase, and thus the tendency for devitrification will decrease. Therefore, to test this theory with respect to the waste loading of the glasses, several glasses were melted with loadings between 20% and 35% using compressed air and $N_2/5\%H_2$ sparges (instead of stirring) to create neutral and reducing conditions respectively during melting.

4.2 Experimental

4.2.1 Glass Compositions

4.2.1.1 *High Waste Loading Glasses*

Glass	1	2	3	4	5	6
	HM4 20%	HM4 35%	HM4 35% 3/4Li_2O	HM4 35% 1/2Li_2O	HM4 35% No Li_2O	HM4 35% No Na_2O
Oxide	Wt (g)	Wt (g)	Wt (g)	Wt (g)	Wt (g)	Wt (g)
SiO_2	49.44	40.17	40.73	41.29	42.42	40.17
B_2O_3	17.52	14.24	14.43	14.63	15.03	14.24
Na_2O	8.80	7.15	7.25	7.35	7.55	0
Li_2O	4.24	3.45	2.58	1.72	0	6.9
Waste†	20	35	35	35	35	35

Table 4.1 - Compositions of high waste loaded glasses

† See **Table 3.2** for full details

As can be seen from **Table 4.1**, the initial glass melted (glass1) was the standard HM4 composition with a 20% waste loading. For glass 2, the waste loading was boosted to 35% (which raises the MoO_3 content to 4.19wt%) and it was expected that the matrix would at least partially devitrify at this waste loading. For the remaining glasses, the quantities of the Li and Na oxides in the glass were altered to investigate the effect on the devitrification products of varying the alkali content of the glasses. In the case of the reduced Li glasses, the quantities of the remaining base glass components were proportionally boosted to keep the overall weight of the batch to 100g. In the case of glass 6, the quantity of Li_2O has been doubled and the Na_2O omitted from the batch completely.

4.2.1.2 *Redox Effect Glasses*

The glass compositions of those glasses with various waste loadings for melting under differing redox conditions are shown in **Table 4.2** below. The prevailing redox

conditions were determined by the gas sparge applied during melting, as opposed to glasses 1 – 6 which were all melted in air atmospheres and stirred during melting.

Glass	**7 air/red**	**8 air/red**	**9 air/red**	**10 air/red**
	HM4 20%	HM4 25%	HM4 30%	HM4 35%
Oxide	Wt (g)	Wt (g)	Wt (g)	Wt (g)
SiO_2	49.44	46.35	43.26	40.17
B_2O_3	17.52	16.43	15.33	14.24
Na_2O	8.80	8.25	7.7	7.15
Li_2O	4.24	3.98	3.71	3.45
Waste	20	25	30	35

Table 4.2 – Compositions of full waste stream glasses sparged with neutral (air) and reducing (red) gasses during melting.

4.2.2 Melting and Heat Treatments

4.2.2.1 *High Waste Loading Glasses*

A summary of the high waste glass melting experiments is shown below in **Table 4.3**.

Glass	Crucible type	Melting temperature	Annealing temperature	Heat Treatment Temperature
1	Platinum	1150°C	430°C	600°C for 6hrs 680°C for 6hrs
2	Platinum	1150°C	500°C	600°C for 6, 12, 24 & 48hrs
3	Alumina	1175°C	500°C	650°C for 48hrs
4	Alumina	1200°C	500°C	665°C for 48hrs
5	Alumina	1300°C	500°C	680°C for 48hrs
6	Alumina	1300°C	500°C	635°C for 48hrs

Table 4.3 - Summary of glass melting and heat treatment temperatures.

Glasses 1 and 2 were melted in platinum crucibles to avoid contamination of the melt by, or reaction of the melt with, the crucible. However, after melting glass 2 micro

cracks were discovered in the platinum crucible upon cleaning. These cracks were thought to have been caused by interactions with the melt, therefore alumina crucibles were used for the remaining melts with high waste loadings.

4.2.2.2 *Redox Effect Glasses*

Two batches of each composition shown in **Table 4.2** were mixed. During melting, one batch of each glass was sparged with compressed air to create neutral redox conditions (as occurs during the real HLW vitrification process at Sellafield) and one with a mixture of N_2 and 5%H_2 to create a strongly reducing atmosphere during melting. Henceforth, glasses sparged with compressed air will be denoted glass #(air), and those sparged with N_2/5%H_2 as glass #(red). All of these glasses were melted in alumina crucibles at 1150°C, and annealed at 550°C. They were also all heat treated at 600°C for 48 hours.

4.3 Results

4.3.1 As Cast High Waste Loading Glasses

4.3.1.1 *Glass 1*

The composition of this glass is the standard HM4 composition, as would be used for real HLW vitrification. The glass produced was a homogeneous transparent dark green block (as can be seen in **Figure 4.1a**), and a rapidly quenched "splat" showed no sign of phase separation or precipitation of crystalline phases. The glass block was amorphous to x-ray diffraction (**Figure 4.2**) The platinum crucible was "clean" (i.e. contained only residual glass, no unmelted batch or reduced metals) after pouring.

Figure 4.1 – As cast samples of (**a**)glass 1, (**b**)glass 2, (**c**)glass 3, (**d**)glass 4, (**e**)glass 5, (**f**)glass 6

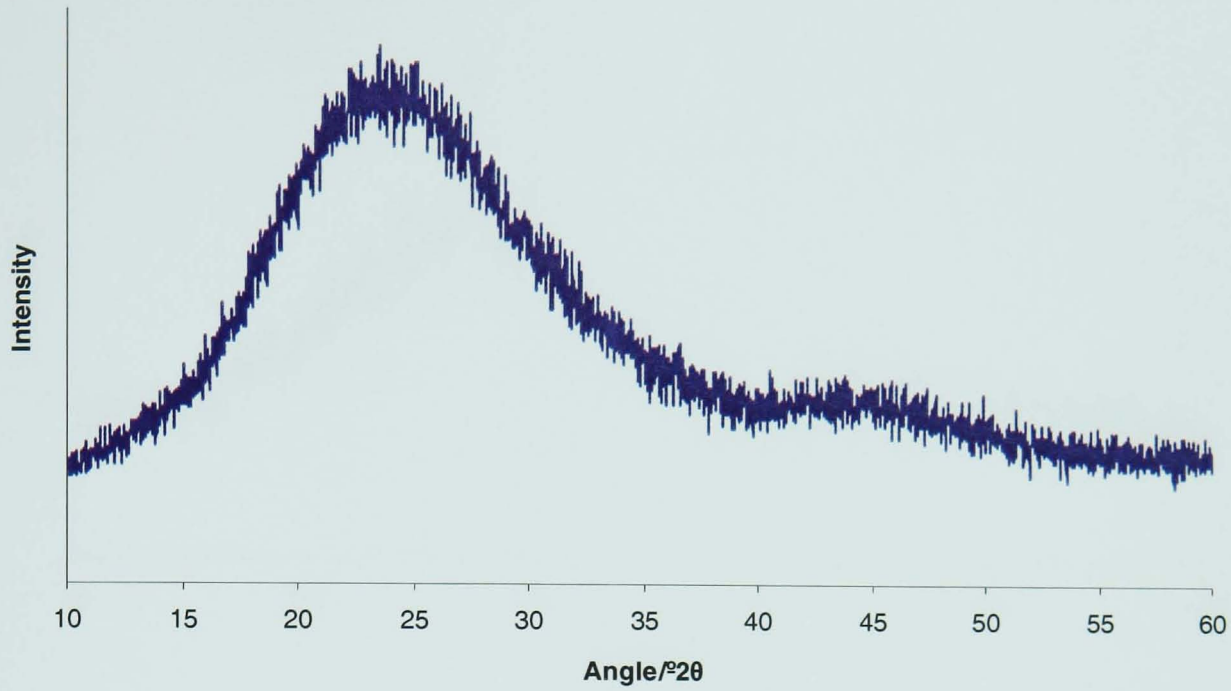

Figure 4.2 – XRD of glass 1 as cast

4.3.1.2 *Glass 2*

The cast block was mainly purple in colour, but also had some lighter purple streaks partly exposed on the surface but mainly distributed in the centre of the block (see **Figure 4.1b**). There were also some yellow streaks found in the very centre of the sample. The glass was therefore clearly not homogeneous. X-ray diffraction showed that there was some crystalline material present in the sample (labelled "x" in **Figure 4.3**), although not enough was present to enable identification of the phase.

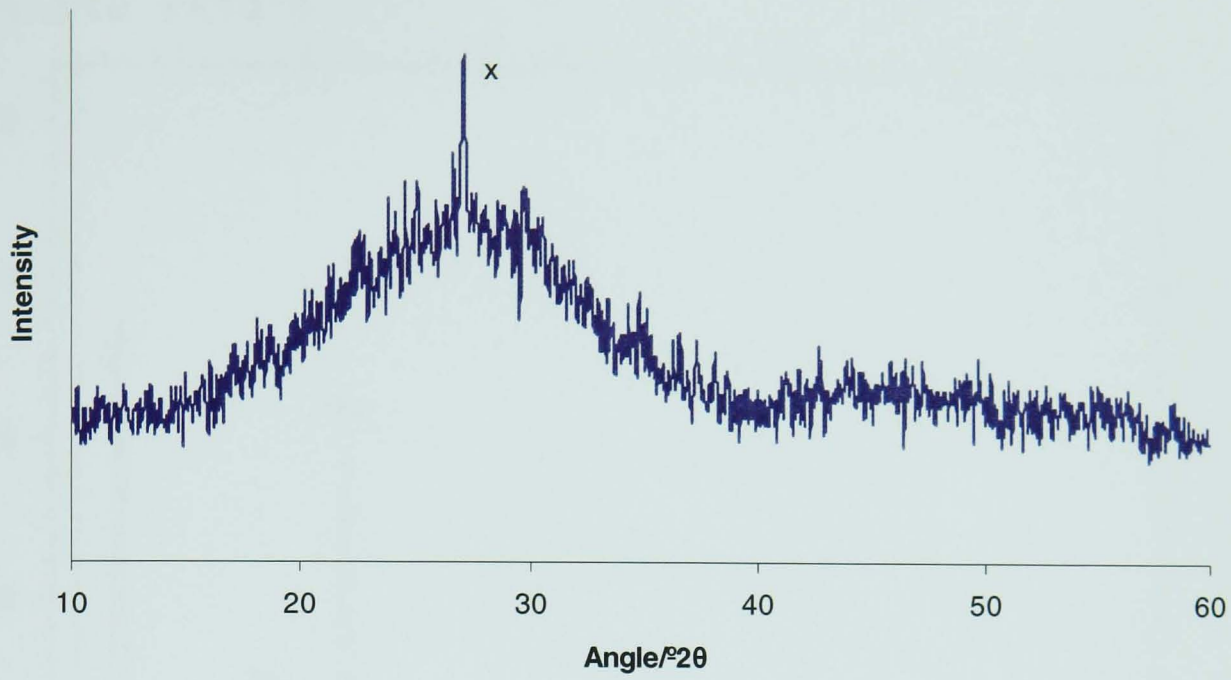

Figure 4.3 – XRD of glass 2 as cast

Neither optical nor scanning electron microscopy were capable of resolving the crystals, but TEM showed the presence of spherical crystallites approximately 0.2μm in diameter (**Figure 4.4**)

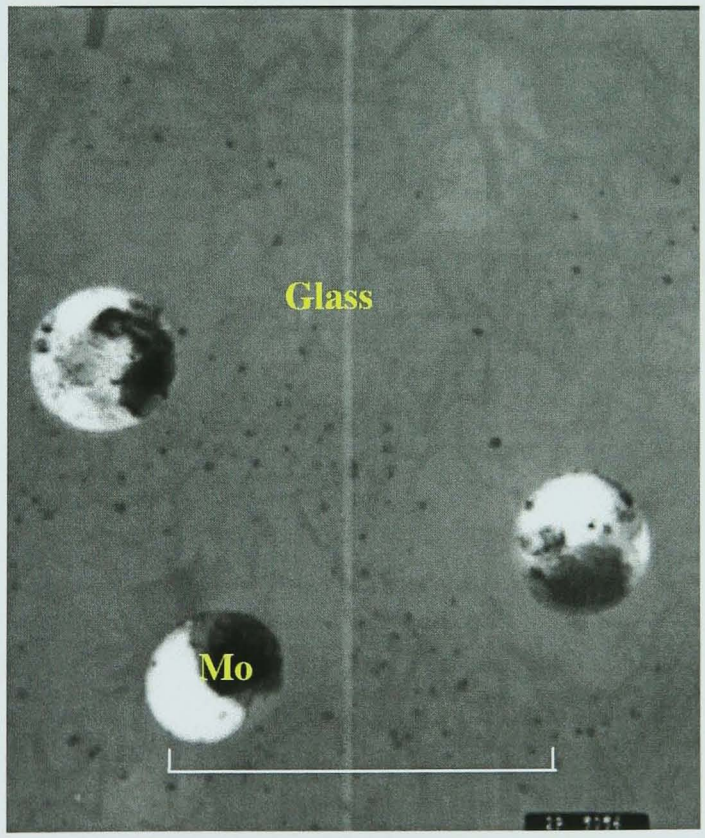

Figure 4.4 – Bright Field TEM image of spherical particles in glass 2 matrix. Scale bar = 0.5μm

EDS analysis (**Figure 4.5a**) of the crystals labelled "Mo" in **Figure 4.4** showed that they were higher in molybdenum than the surrounding glass matrix (**Figure 4.5b**).

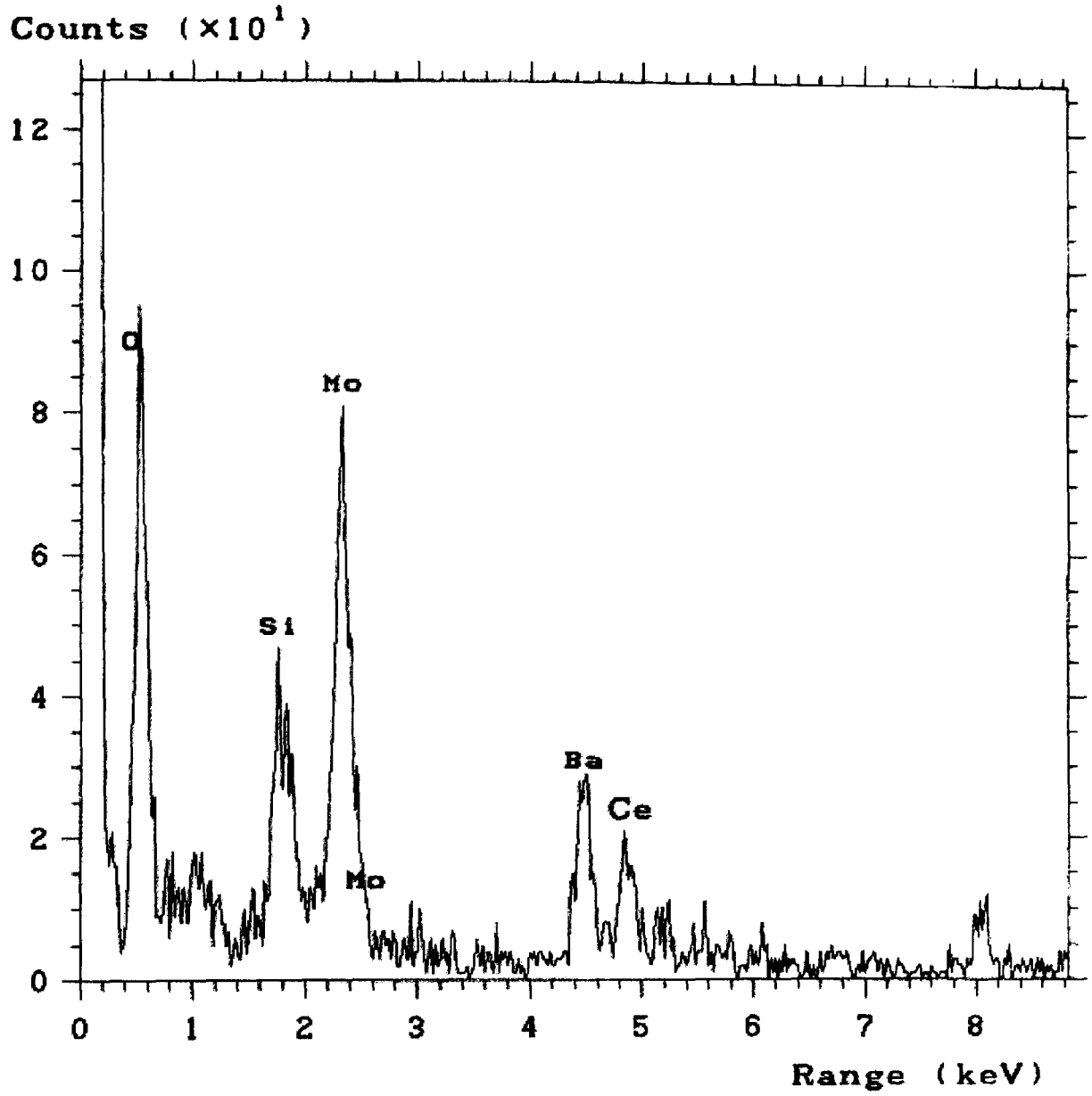

Figure 4.5a – EDS of spherical particles (labelled "Mo" in **Figure 4.4**) in glass 2

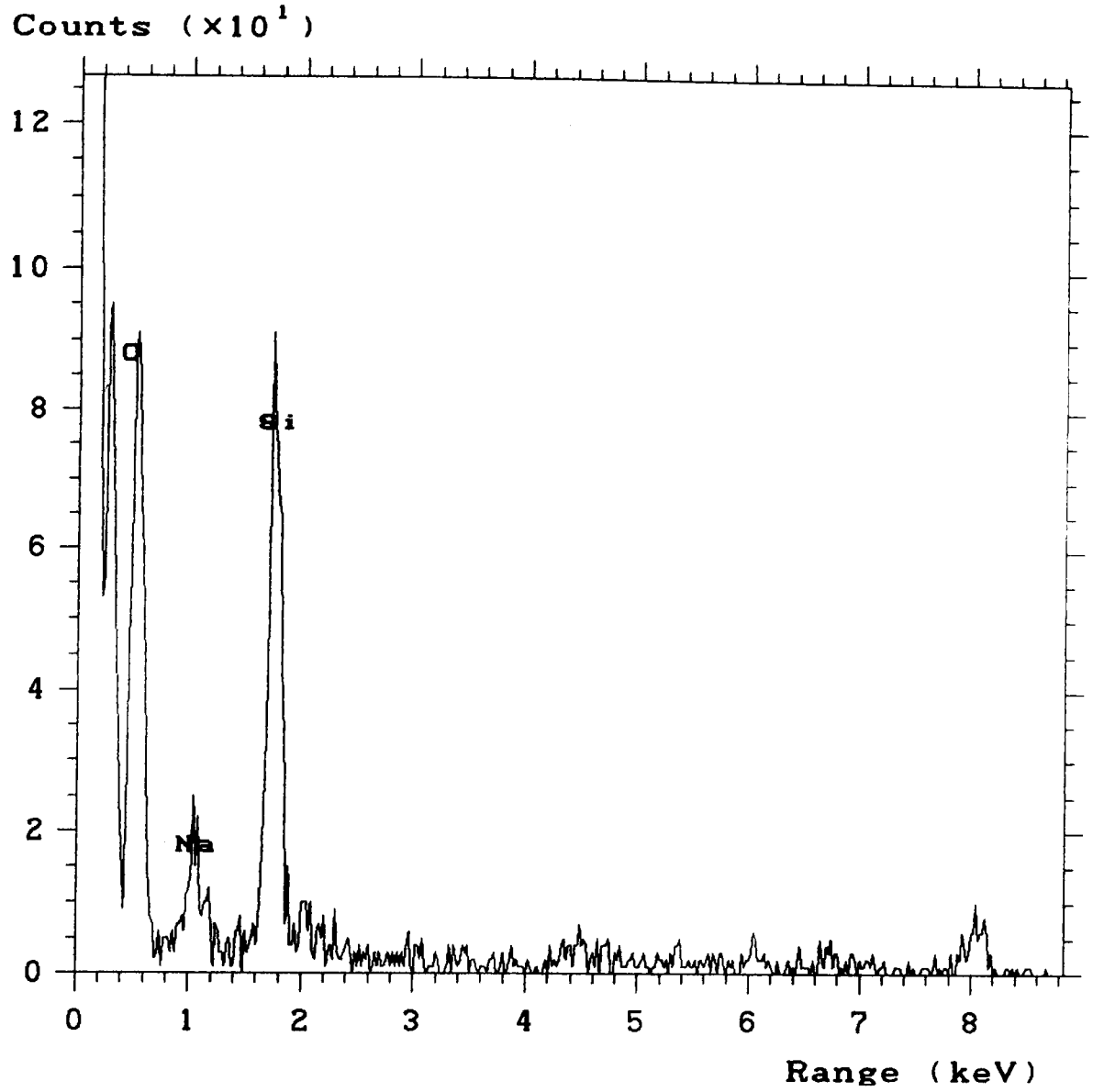

Figure 4.5b – EDS of glassy region (labelled "Glass" in **Figure 4.4**) of glass 2

4.3.1.3 *Glass 3*

As this glass was melted in alumina, the crucible and batch were preheated to 1000°C prior to insertion into the melting furnace. It was noted that at this temperature the batch had already liquefied, a consequence which applied to all batches that required preheating. The glass was observed to be more viscous than glass 2 on pouring, despite an increase in the melting temperature of 25°C. This was due to the reduced amount of Li_2O in the batch, a compound that acts as a flux during glass making (Weyl, 1964). The increase in melting temperature was however insufficient to fully counter the reduction in alkali content. Unfortunately, no viscometers were available at the time of these experiments with which to quantify the melt viscosities, hence all viscosity related comments refer to observations made at the time of pouring.

Examination of the cast block after annealing, and the crucible when cool, revealed a great deal of phase separation (with both yellow and light blue phases being apparent in the dark green matrix, as can be seen in **Figure 4.1c**). The presence of some undissolved batch was also noted in the crucible, along with the presence of silver coloured particles ranging from approximately 0.5 to 3mm in diameter. These particles were subjected to EDS analysis (**Figure 4.6**) and found to be metallic silver.

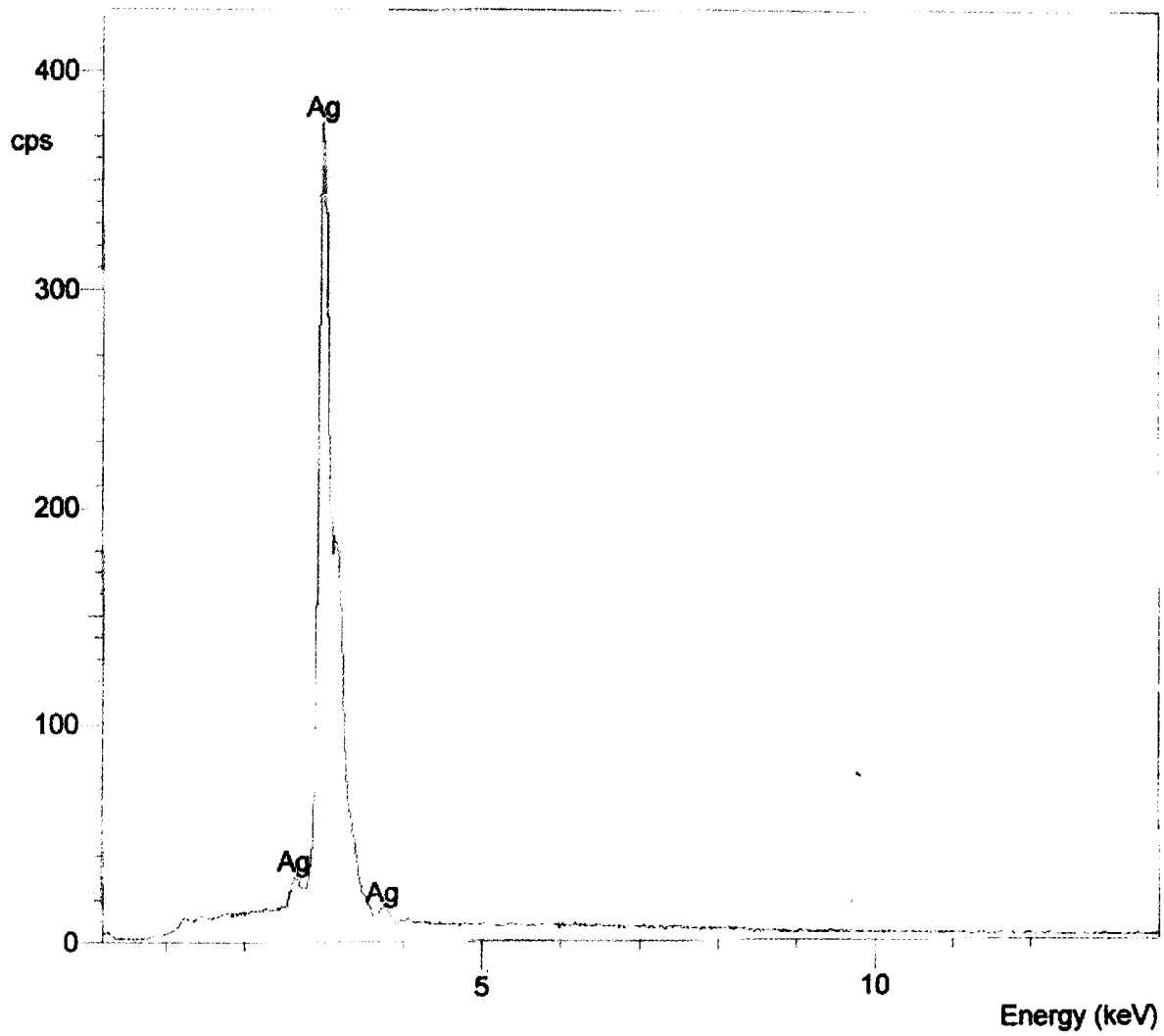

Figure 4.6 – EDS of metallic particle in glass 3 as cast

A splat quench (a rapid cooling performed by pressing a molten gob of glass between 2 large cold steel plates) of this glass had a shiny mirrored surface, and it is likely that this layer was composed of silver metal [Volf, 1984] that produced a dichroic effect. XRD analysis of the as-cast block showed it to be amorphous (**Figure 4.7**) indicating that any metallic silver in the glass block that did not aggregate into the 0.5-3mm particles mentioned above, must have been very finely dispersed. In **Chapter 4.3.4**,

TEM indicates that the silver particles were ~0.2μm in size post heat treatment, which suggests that smaller particles than this would have been present in the as cast glass.

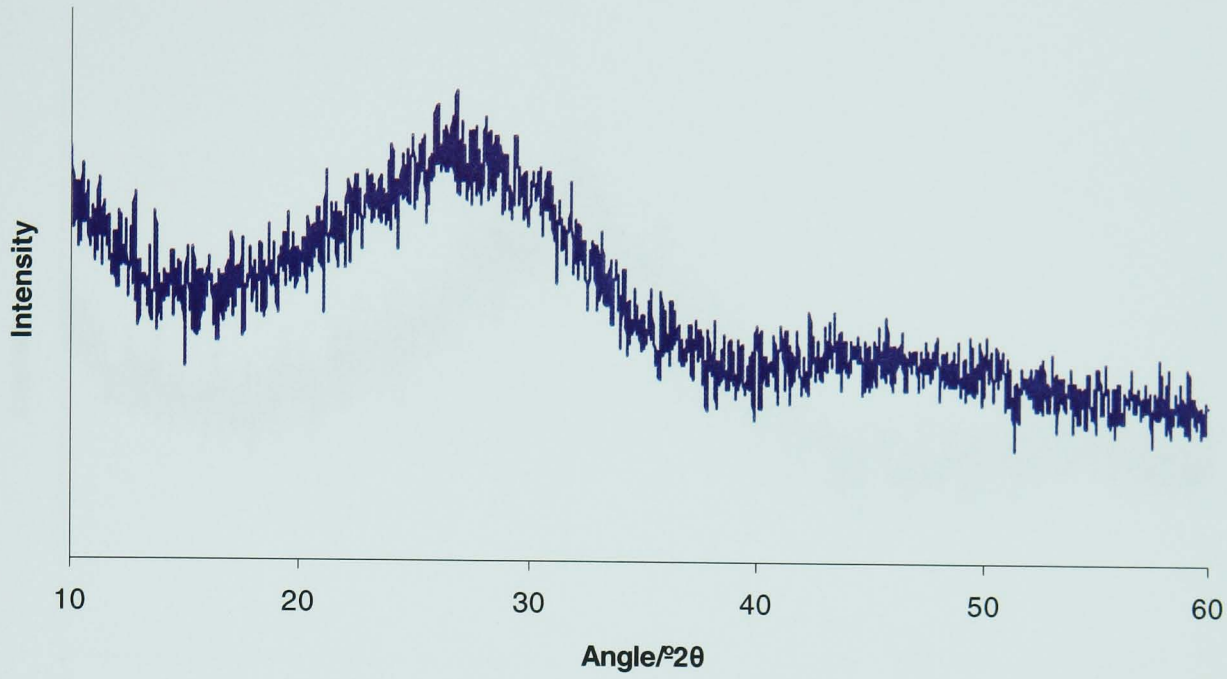

Figure 4.7 – XRD of glass 3 as cast

The presence of blobs of metal in the melt can result in a drilling effect on the walls and bottom of the crucible. This is where the blob, being moved by the motion of the stirrer and the thermal currents in the crucible, mechanically attacks the alumina thus chipping off small particles that can then only be incorporated in the melt. Therefore, any melt in which this phenomenon has taken place will have an altered composition from the batch composition (i.e. will contain some alumina). However, no significant corrosion of the alumina stirrer or crucible was observed for this melt.

4.3.1.4 *Glass 4*

This glass had a further reduction in Li_2O content and thus the melting temperature was increased by another 25°C. However, despite the further increase in melting temperature, glass 4 was more viscous than glasses 2 and 3. The bright yellow and blue phases were not present (see **Figure 4.1d**), although some phase separation was visible in cross section. A splat quench was performed and showed the same mirror effect apparent in the rapidly quenched sample of glass 2. A particle of silver approximately 3mm in diameter was also discovered on cutting open the glass block. This glass appeared amorphous to XRD (**Figure 4.8**), indicating that any silver metal

that had not aggregated into larger particles must have been very finely dispersed in the glass (as for glass 3, particles were likely to have been <0.2μm).

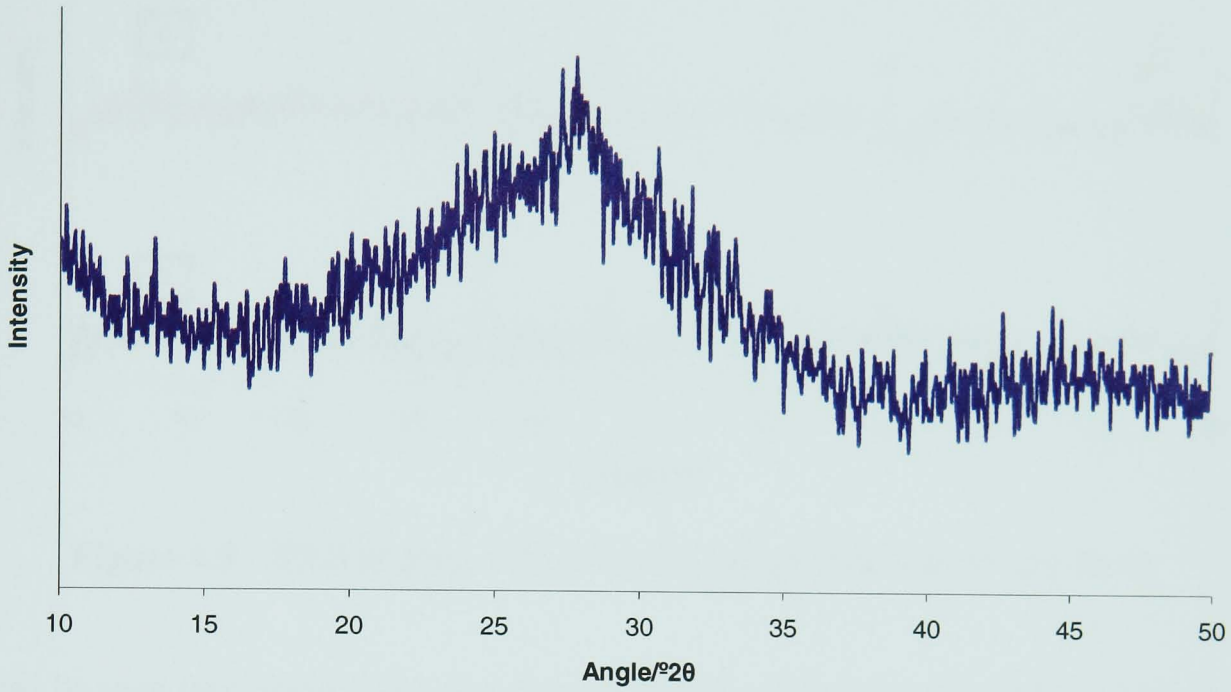

Figure 4.8 - XRD of glass 4 as cast

4.3.1.5 *Glass 5*

Glass 5 was melted at 1300°C due to the absence of Li_2O to act as a flux. There was a small quantity of undissolved batch left in the crucible after pouring, and a previously unseen light green phase was apparent in the cast block (**Figure 4.1e**), along with some metallic silver particles approximately 2mm in diameter. The alumina stirring paddle exhibited a significant amount of corrosion. Due to a colour difference between the residual glass in the crucible and the cast block, x-ray diffraction patterns were obtained from samples of both (**Figures 4.9a and 4.9b**).

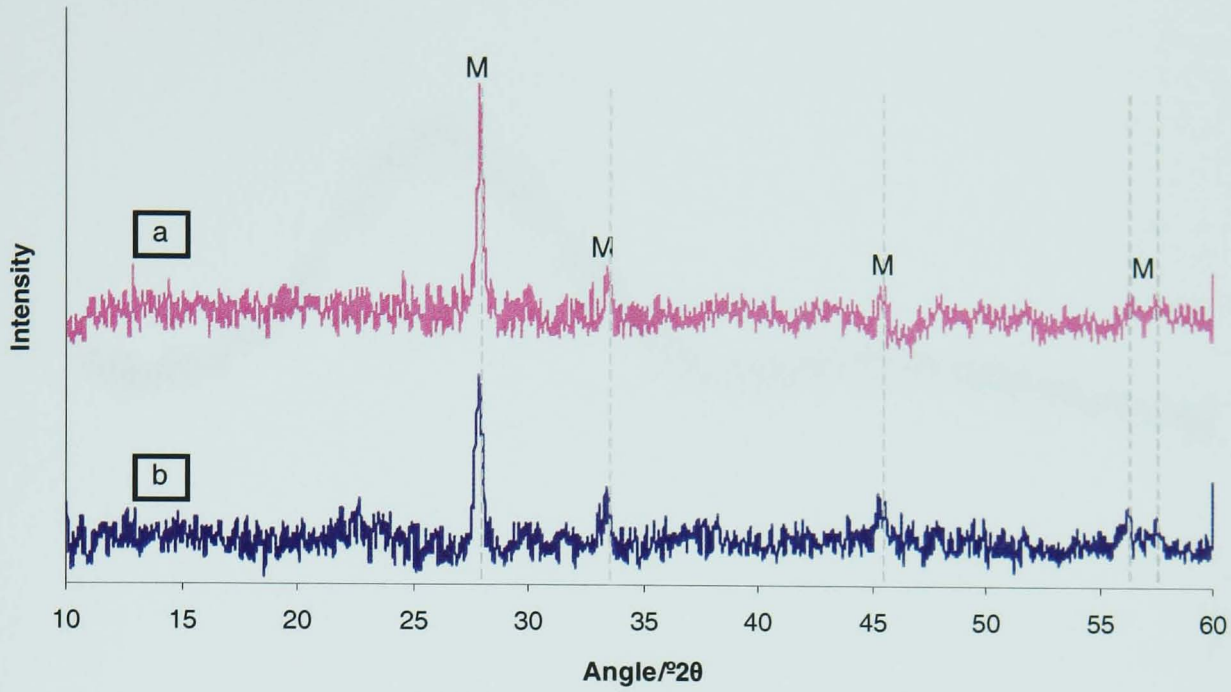

Figure 4.9 - XRD of glass 5 as cast from **(a)** crucible and **(b)** cast block

It can be seen from these traces that the major peaks (labelled "M") had the same d-spacings and were therefore caused by the same phase. The peaks could not be exactly matched to any one crystalline phase using the ICDD database, but several close matches were found for $AB(MoO_4)_2$ type molybdate compounds, where A is an alkali metal and B is a rare earth (for example $NaLa(MoO_4)_2$, card [24-1103]). It was interesting to note that this melt showed some devitrification in the as cast state, whereas all the other glasses appeared amorphous to XRD.

4.3.1.6 *Glass 6*

This glass was of an acceptable viscosity on pouring (cf glass 1 & 2), and the as-cast block was predominantly dark green in colour, although some phase separation (dark blue in colour) was apparent (see **Figure 4.1f**). XRD (**Figure 4.10**) showed the glass to be amorphous.

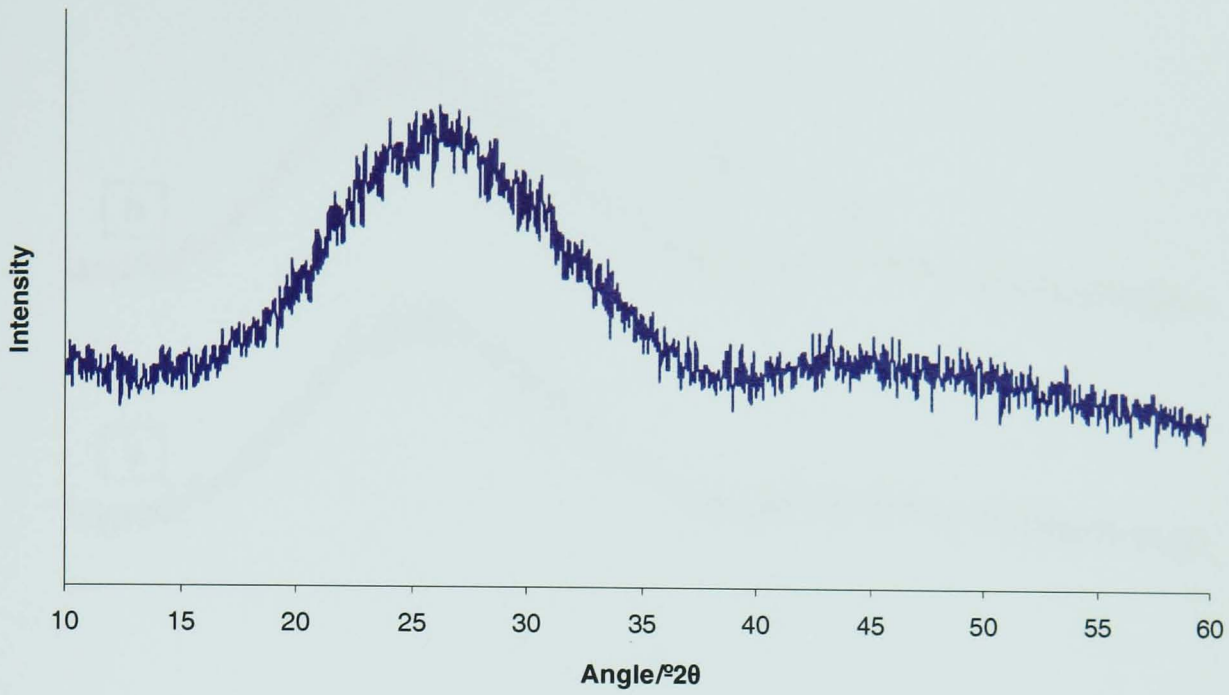

Figure 4.10– XRD of glass 6 as cast

4.3.2 As Cast Redox Effect Glasses

4.3.2.1 *Glass 7*

Glass 7(air) closely resembled glass 1 in the as cast state which was to be expected as both glasses were of the same composition and were melted in air. However, as can be seen in **Figure 4.11a,** glass 7(air) was sparged and contains many bubbles. Otherwise, glass 7(air) was a transparent dark green colour and free from any phase separation. XRD showed glass 7(air) to be amorphous (**Figure 4.12a**) and EXAFS analysis showed the presence of a coordination shell at a distance of 1.76(2)Å from the Mo centre. This had a good fit (with an R factor of 24.5) with a model of $(MoO_4)^{2-}$ tetrahedra (**Figure 4.13**) in EXCURV98 (see **Chapter 3.8**).

a **b**

Figure 4.11 – As cast samples of (**a**)glass 7(air), (**b**)glass 7(red)

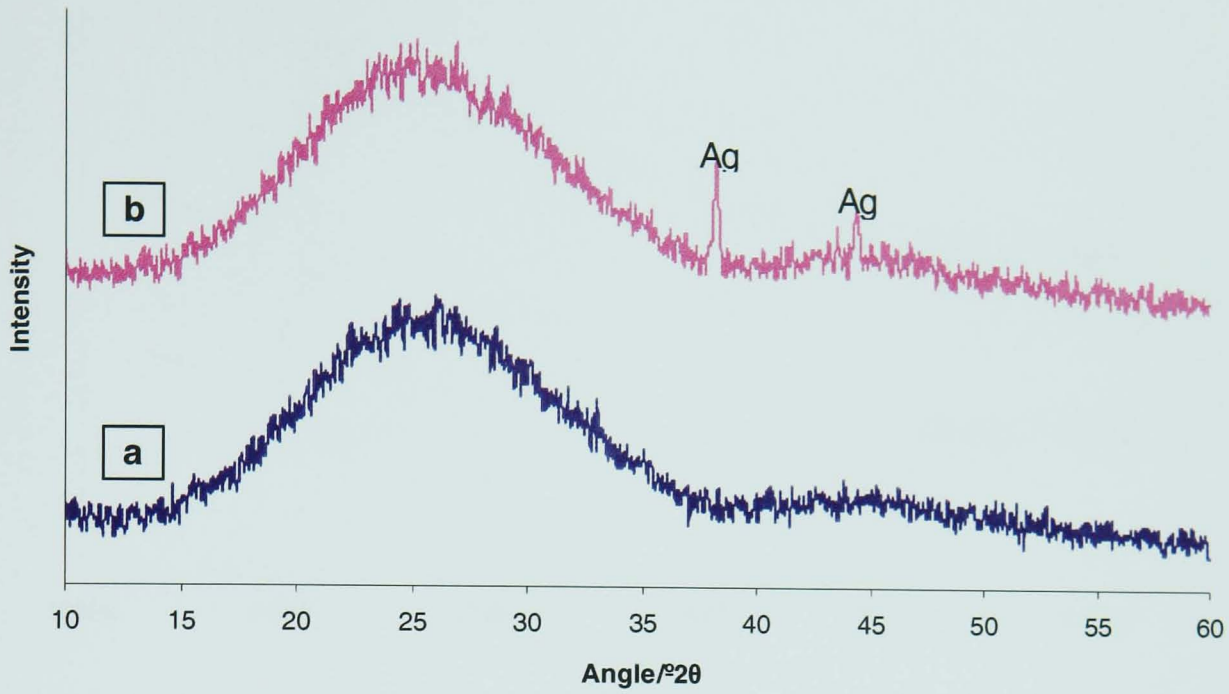

Figure 4.12 – XRD of as cast samples of (**a**) glass 7(air) and (**b**) glass 7(red)

Figure 4.11b shows that glass 7(red) did exhibit some phase separation in the as cast state despite only containing 20wt% simulated HLW, a marked difference to glass 7(air) and glass 1, also 20wt% waste glasses but which were melted in air. XRD of this sample (**Figure 4.12b**) revealed the presence of some crystalline material. The reflections at 38.2 °2θ and 44.4°2θ with d-spacings of 2.354Å and 2.04Å matched well with card [4-783] for metallic silver (d-spacings 2.3590Å and 2.0440Å) from the ICDD database, showing that the silver oxide in the batch had been reduced to metallic silver during melting. EXAFS analysis (**Figure 4.13**) again indicated a coordination shell at a distance of 1.76(2)Å from the Mo centres in this glass, which correlate well with the presence of $(MoO_4)^{2-}$ tetrahedra in the sample (R factor = 21.8). This suggests that little of the Mo^{6+} present in the glass batch was reduced to lower oxidation states during melting.

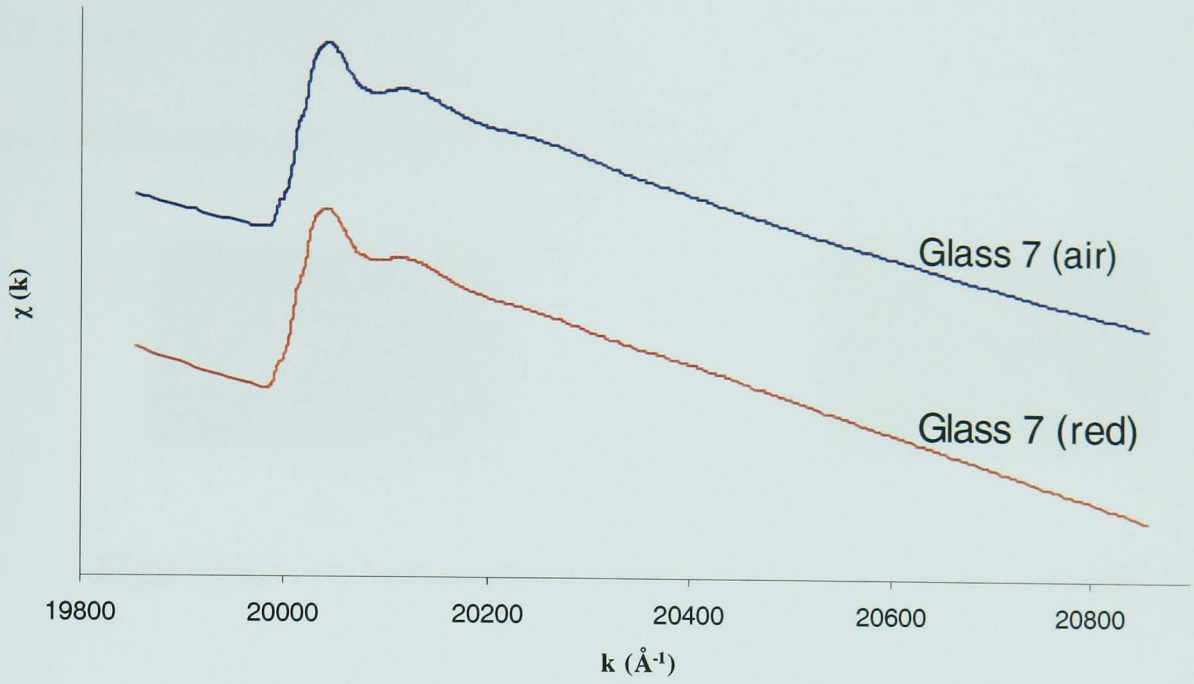

Figure 4.13a – EXAFS of glass 7(air) and glass 7(red)

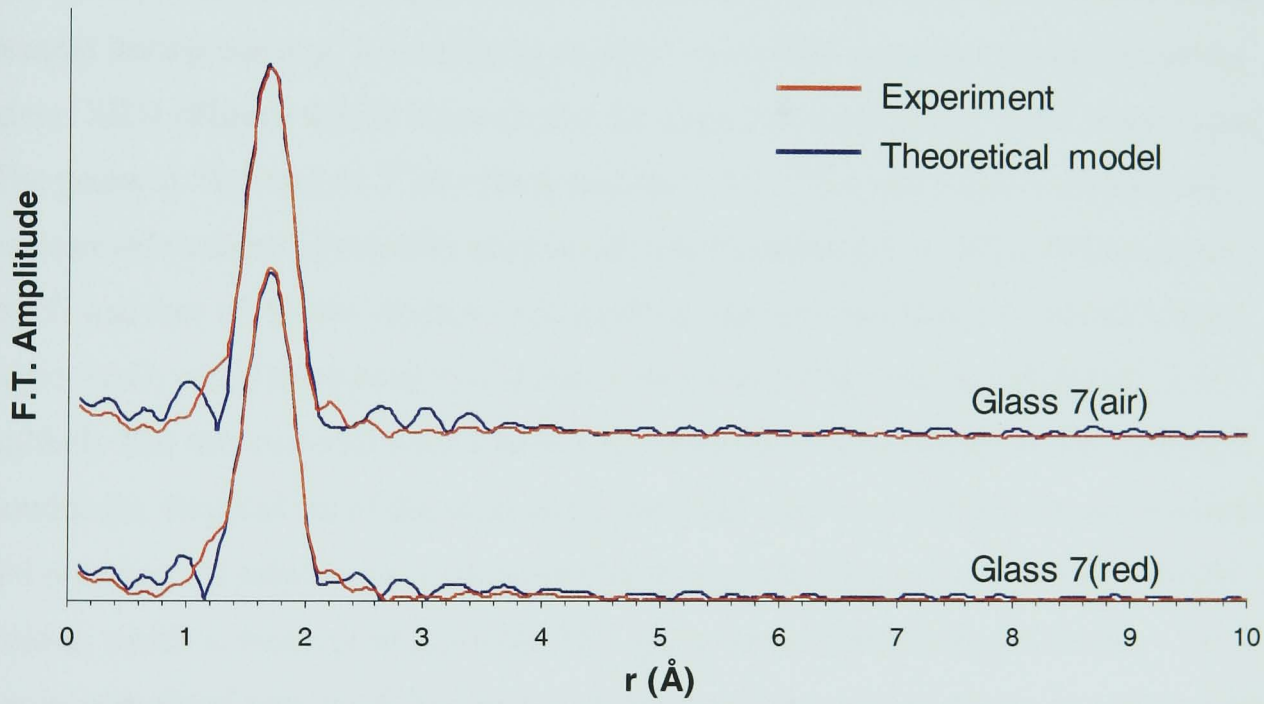

Figure 4.13b – Fourier transform of EXAFS results for glass 7(air) and 7(red)

4.3.2.2 *Glass 8*

Figure 4.14a shows glass 8(air) in the as cast state.

a **b**

Figure 4.14 – As cast samples of (**a**) glass 8(air) and (**b**) glass 8(red)

The glass appeared homogeneous, and dark green in thin section. The white particles that can be seen in **Figure 4.14a** are particles of alumina that fell into the glass when the crucible shattered during pouring. As alumina is a refractory material and was not present during melting, it is unlikely to affect any of the measured properties of the glass. XRD (**Figure 4.15a**) showed that the glass was amorphous in the as cast state. The peaks at 38.5 and 44.7°2θ with d-spacings of 2.337Å and 2.024Å respectively correspond to those of metallic aluminium (card number [85-1327]). Although the batch was free of Al, the crucible was made of alumina and thus it is possible that some Al_2O_3 could have been dissolved in the glass during melting. However, it is unlikely that this material would have been reduced to Al metal given the melting conditions. Repetitions of the scan using the XRD machine with the Cu x-ray source did not show Al reflections, indicating that these reflections arose from the sample holder, which is made of aluminium. This phenomenon only occurred in the x-ray equipment fitted with the Co source, and can therefore only be observed in those data obtained from the Co XRD.

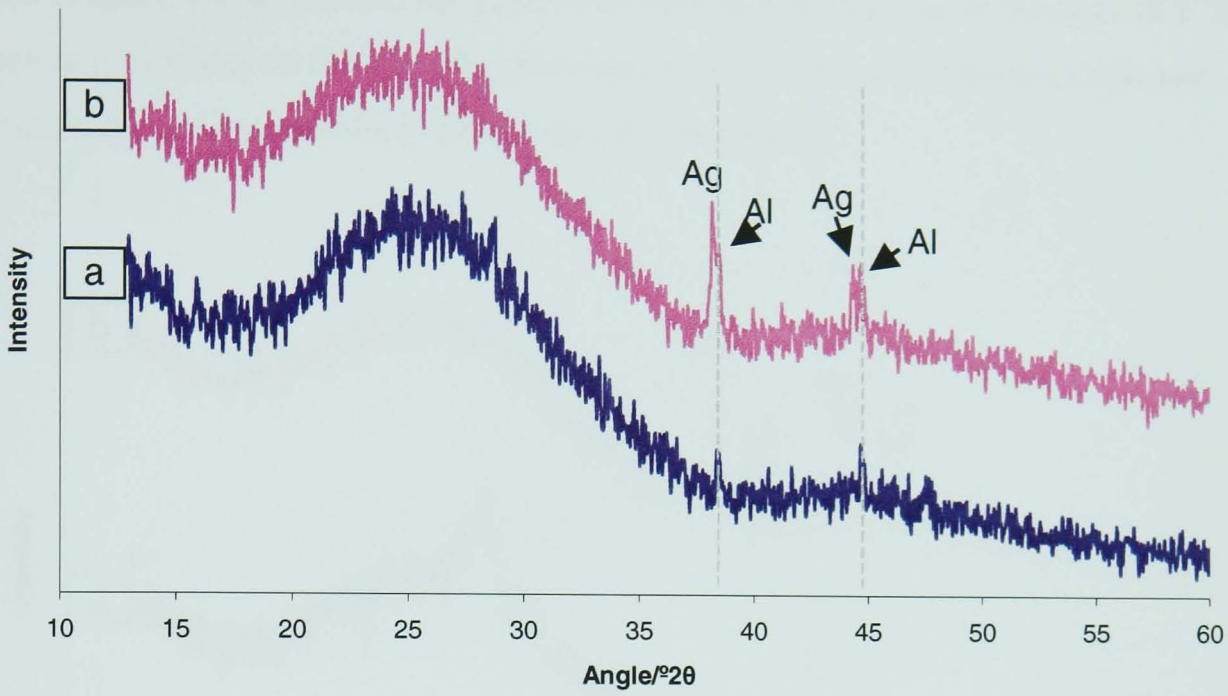

Figure 4.15 – XRD of as cast samples of (**a**) glass 8(air) and (**b**) glass 8(red)

As can be seen from **Figure 4.14b**, glass 8(red) exhibited significant phase separation during melting. XRD of this sample (**Figure 4.15b**) again showed 2 reflections at 38.2 and 44.4°2θ, revealing the presence of silver metal in the glass. These reflections are close to two other reflections at 38.5 and 44.7°2θ, which again have a good match with metallic Al. As for the XRD of glass 8(air), these reflections were caused by the sample holder and not the sample itself.

4.3.2.3 *Glass 9*

Glass 9 as cast can be seen in **Figure 4.16a** below.

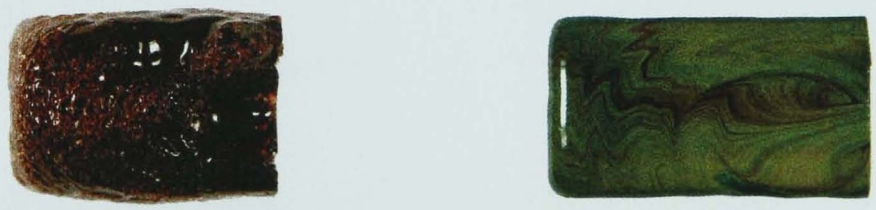

a **b**

Figure 4.16 – As cast samples of (**a**) glass 9(air) and (**b**) glass 9(red)

The glass appeared dark purple in colour and contained many bubbles from the compressed air sparge. However, no phase separation was apparent in the sample, and

XRD (**Figure 4.17a**) showed the glass to be amorphous. The 2 reflections at 38.5°2θ (seen as a shoulder on the Ag reflection) and 44.7°2θ were, as for the previous two samples, caused by the sample holder and not the sample.

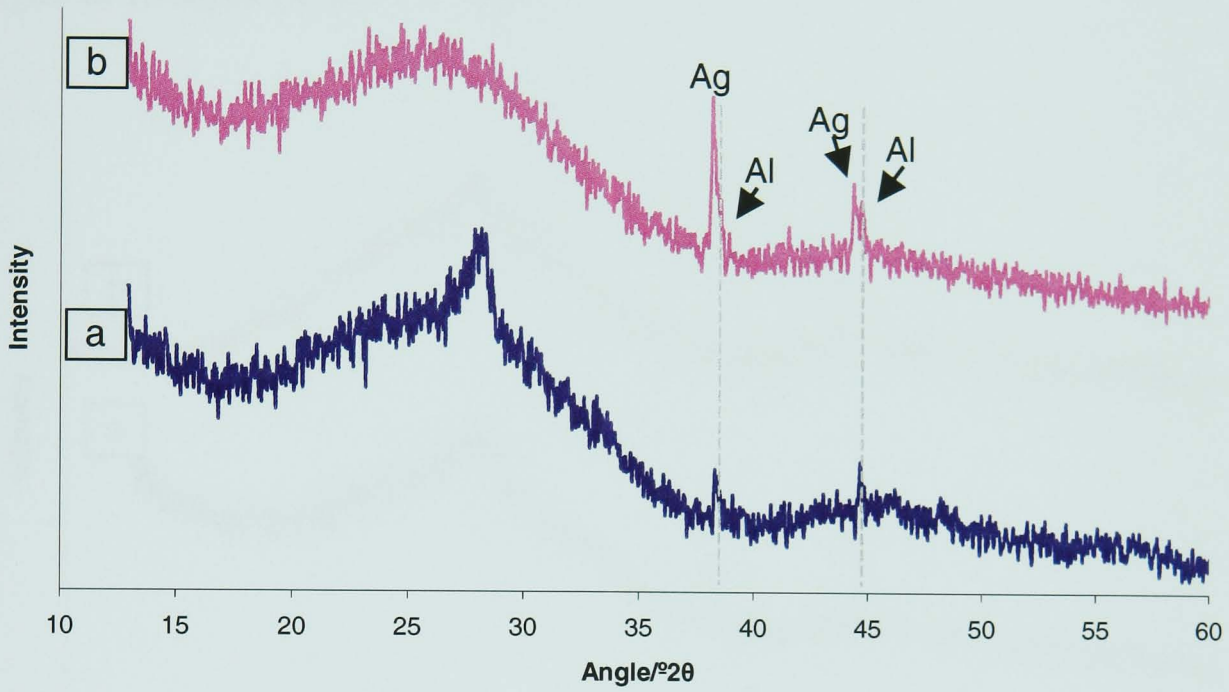

Figure 4.17 – XRD of as cast samples of (**a**) glass 9(air) and (**b**) glass 9(red)

Figure 4.16b clearly shows that glass 9(red) underwent significant phase separation during melting, with several differently coloured regions being visible in the as cast glass. XRD of this glass (**Figure 4.17b**) once again showed the presence of metallic silver in the sample, along with reflections caused by the Al sample holder.

4.3.2.4 *Glass 10*

Figure 4.18a shows glass 10(air) as cast

a **b**

Figure 4.18 – As cast samples of (**a**) glass 10(air) and (**b**) glass 10(red)

Glass 10(air) was black in colour and did not exhibit any visible phase separation in the as cast state. XRD of this sample (**Figure 4.19a**) only showed crystalline reflections for Al, an artefact of the sample holder. As for glass 7, EXAFS analysis (Figure 4.20) of glass 10(air) indicated the presence of $(MoO_4)^{2-}$ tetrahedra with bond lengths of 1.76(2)Å (R factor = 19.0).

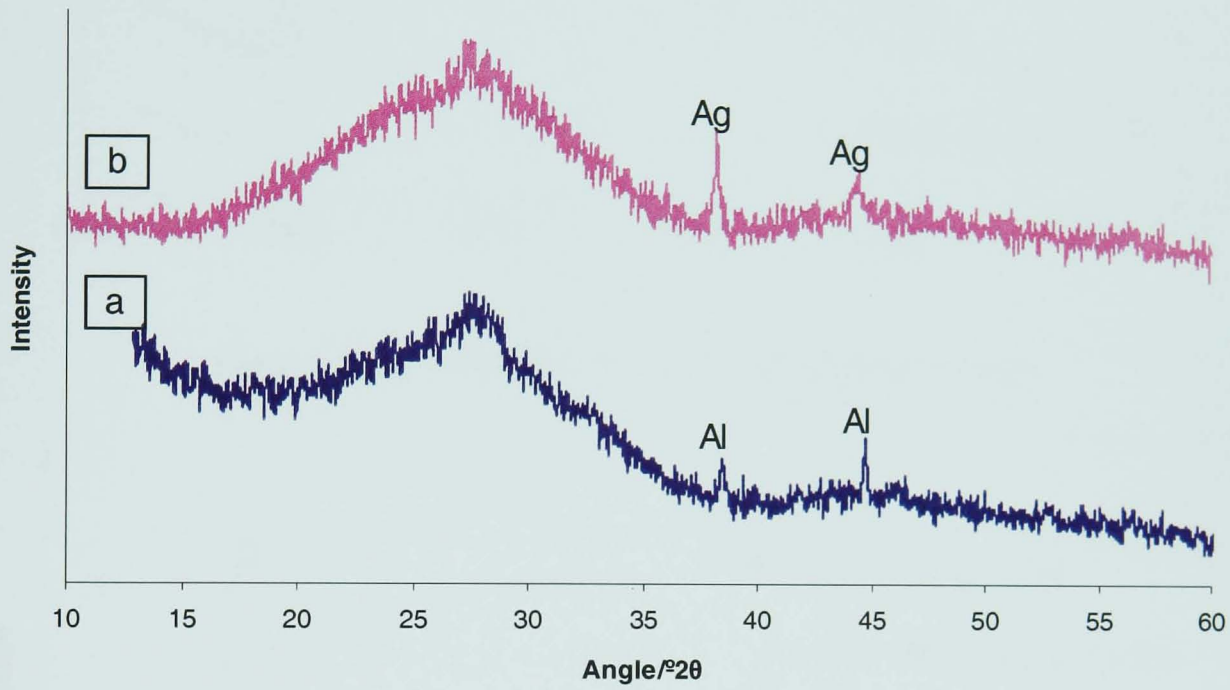

Figure 4.19 – XRD of as cast samples of (**a**) glass 10(air) and (**b**) glass 10(red)

As for all of the glasses melted under a reducing atmosphere, glass 10(red) was visibly phase separated in the as cast state (**Figure 4.18b**). The reflections at 38.2 and 44.4°2θ on the XRD of glass 10(red) (**Figure 4.19b**) show that the silver oxide in the batch was reduced to silver metal during melting. EXAFS analysis of glass 10(red) (**Figure 4.20**) again indicated the presence of $(MoO_4)^{2-}$ units in the glass, with Mo-O bond lengths of 1.76(2)Å (R factor = 34.0).

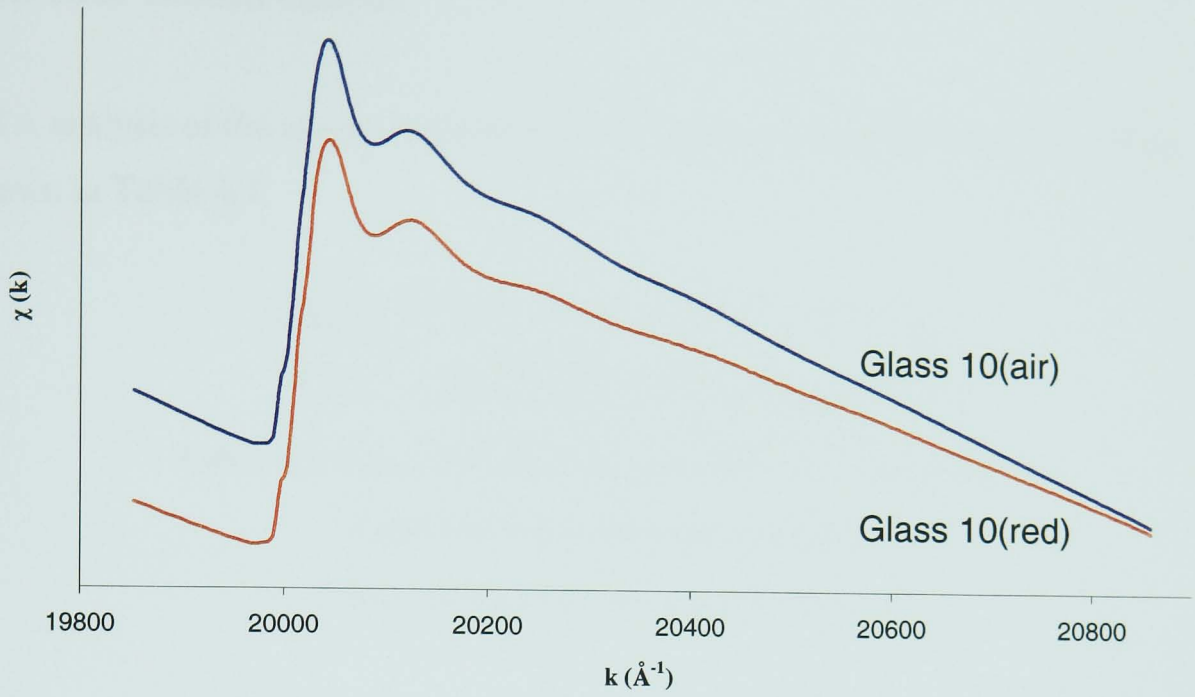

Figure 4.20a – EXAFS of glasses 10(air) and 10(red)

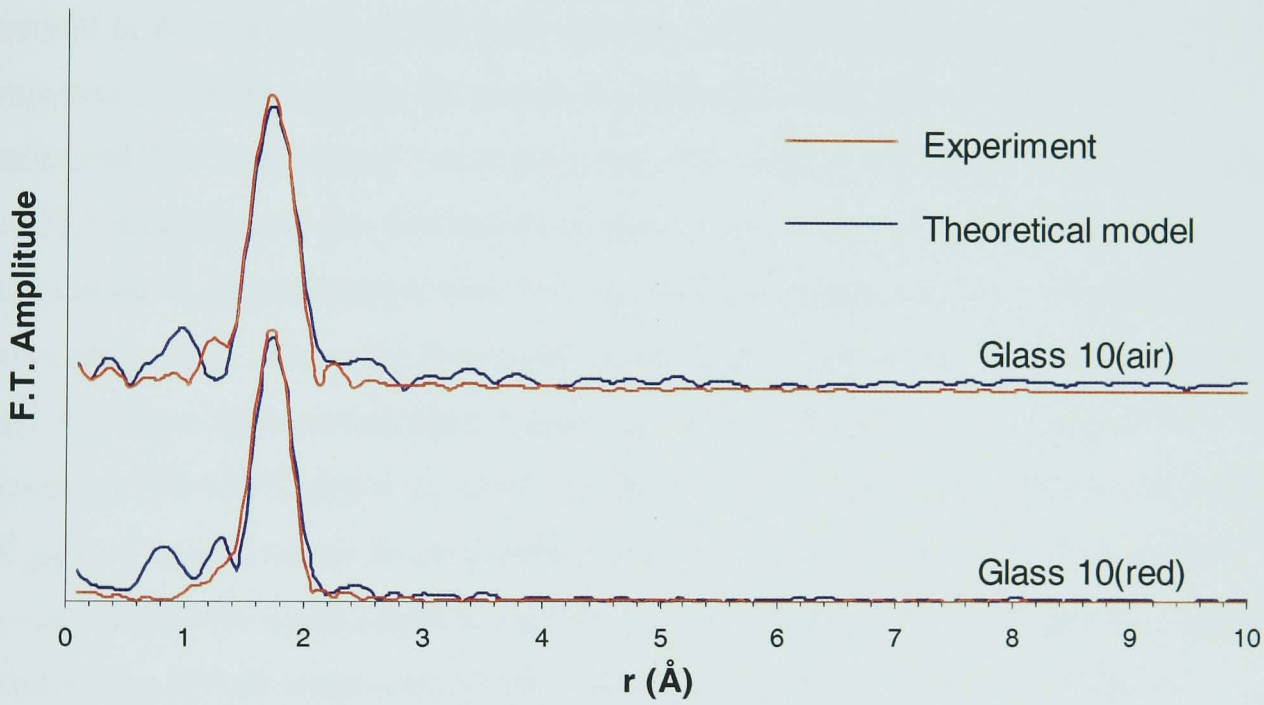

Figure 4.20b – Fourier transform of EXAFS of glasses 10(air) and 10(red)

4.3.3 Heat Treated Glasses

DTA analysis of the as-cast samples gave the glass transition temperatures (T_gs) shown in **Table 4.4**.

Glass	1†	2‡	3	4	5	6
T_g (°C)	480	480	530	545	560	515

Table 4.4. Glass transition temperatures of as-cast glasses.

† Equivalent in composition to glass 7

‡ Equivalent in composition to glass 10

For glass ceramics, the optimum growth temperature for the crystalline phase(s) in the glass is usually 100-150°C above the T_g. Therefore, to try to develop the maximum amount of devitrification in the glass samples, the heat treatment temperatures for the high waste loading samples (as shown in **Table 4.3**) were 120°C higher than the measured T_g's. Due to time constraints, only one sample of each glass was submitted to DTA analysis, and this will therefore have increased the possible experimental error in the T_g determination. However, given that the heat treatment temperatures were set at 120°C above the determined T_g's, errors of ±20°C can be accommodated and still allow the heat treatment temperature for crystal growth to be within the optimum 100-150°C above T_g range. As there was no observable difference in the T_g's of glasses 1 and 2 (equal in composition to glasses 7 and 10 and containing 20wt% waste and 35wt% waste respectively) it was assumed that the T_g's of glasses 8 and 9 (containing 25wt% waste and 30wt% waste respectively) would also be 480°C. Therefore, these glasses were heat treated at the same temperature as glasses 7 and 10 (600°C).

4.3.3.1 *Glass 1*

This glass was heat treated in air at 120°C and 200°C above its T_g for 6 hours each (the latter temperature was used to assess the possibility of a higher temperature inducing crystallisation), after which the samples showed no visible change from the as cast state. The sample treated at 680°C had flowed in the ceramic boat, but had not

devitrified. XRD analysis of these samples (**Figures 4.21a** and **4.21b**) did not show the presence of any crystalline material.

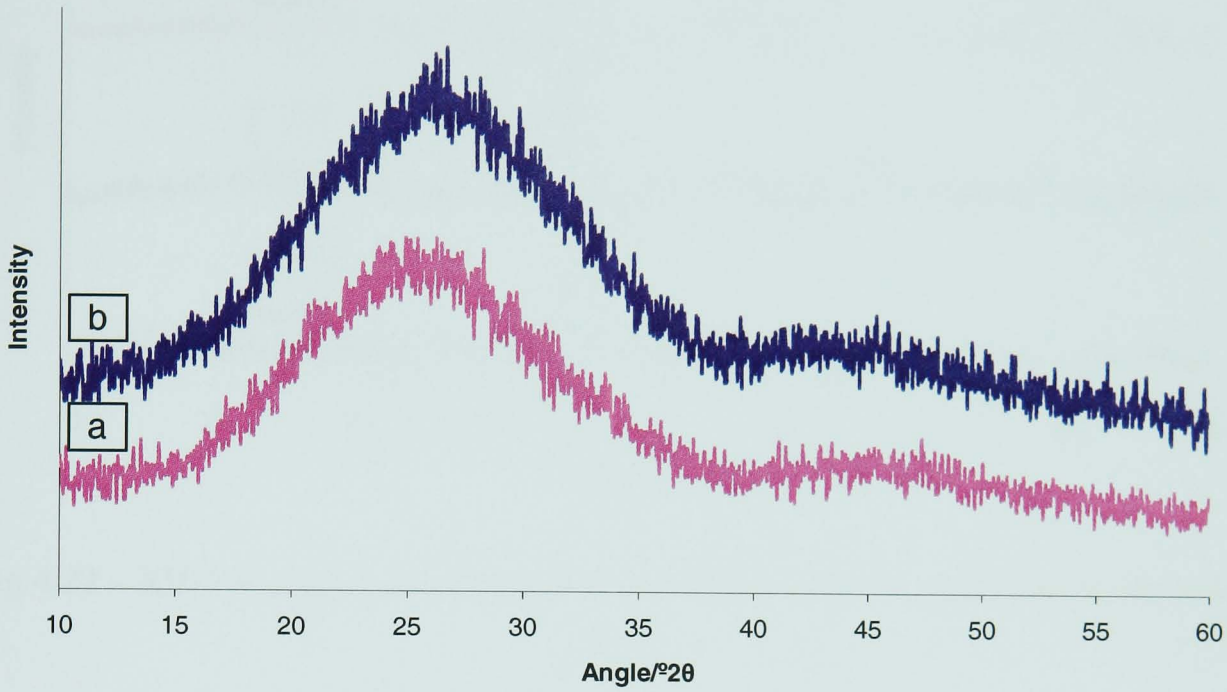

Figure 4.21 – XRD of glass 1 heat treated for 48 hours at (**a**) 600°C and (**b**) 680°C

4.3.3.2 *Glass 2*

This glass was subjected to several heat treatment programmes all of which caused a marked colour change in the sample from dark purple with some yellow streaking, to predominantly yellow. The only significant reflection on the diffraction pattern of the as-cast glass (**Figure 4.3**) had a d-spacing of 3.288Å (at 27.08 °2θ). After a 6 hour heat treatment at 600°C, much more crystallinity was apparent on the x-ray trace (**Figure 4.22a**) with the most intense reflection being at 27.09°2θ with a d-spacing of 3.289Å (i.e. as the difference is negligible, it can be assumed that the two reflections correspond to the same phase). This reflection was joined by another almost as intense reflection at 27.93°2θ with a d-spacing of 3.191Å, with the third most intense reflection being at 38.07°2θ with a d-spacing 2.362Å. This pattern was mimicked by the patterns obtained after the 12 and 48 hour heat treatments at 600°C (**Figure 4.22**) along with the increasing intensity of several other reflections as the heat treatment time (and therefore the crystal growth period) was increased.

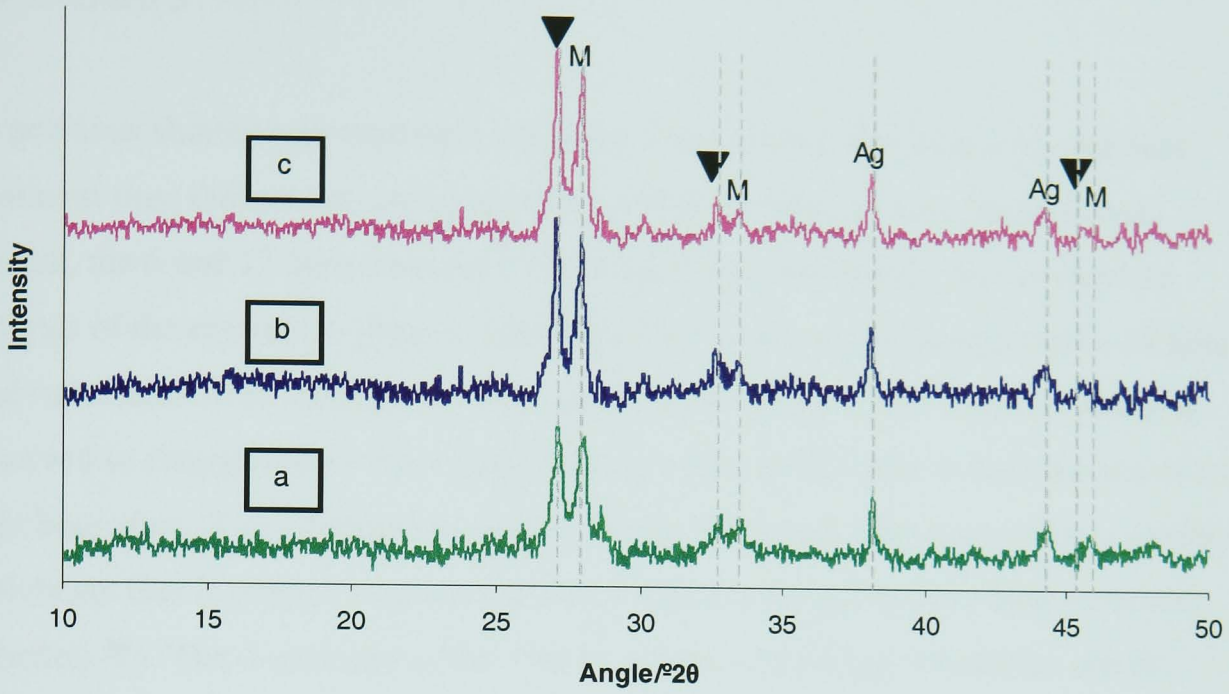

Fig 4.22 – XRD of glass 2, heat treated for (**a**) 6 hours, (**b**) 12 hours and (**c**) 48 hours at 600°C

It quickly became apparent that there were several phases present in the heat treated samples and these were identified using the search program Win XPOW. The second most intense reflection at 27.93°2θ with a d-spacing of 3.191Å, along with the reflections at 33.48°2θ and 46.02°2θ with d-spacings of 2.67Å and 1.98Å respectively (all labelled M) appear to have been caused by a tetragonal molybdate similar to powellite. Although an exact match could not be obtained from the ICDD database, several similar patterns were found which were all molybdates with the general formula $AB(MoO_4)_2$, where A = Ag^+, Na^+ or Li^+, and B = lanthanide^{3+}, for example $LiLa(MoO_4)_2$ (card number [18-734]) and $NaNd(MoO_4)_2$ (card number [25-852]).

The reflection at 27.09°2θ with a d-spacing of 3.29Å (labelled ▼) immediately suggested the presence of a silicon oxide phase, possibly some variety of quartz. However, the presence of the other ▼ reflections at 32.60°2θ and 45.58°2θ with d-spacings of 2.73Å and 2.00Å respectively indicate that this phase could also be a powellite-type phase similar to M (see discussion). Metallic silver (labelled Ag) was also present in the heat treated samples.

4.3.3.3 *Glass 3*

As previous shorter heat treatments on glass 2 had shown that increasing the heat treatment time did not encourage any new phases to form, or alter those already present, the 6 and 12 hour treatments were not deemed necessary for a complete analysis of the crystalline phases. Therefore for all subsequent samples only 48 hour heat treatments were undertaken. The sample flowed in the boat crucible, and was observed to change colour from predominantly dark green prior to heat treatment to a light blue after. X-ray diffraction of this sample (**Figure 4.23a**) shows that a similar molybdate that is present in glass 2 is also present in this glass after heat treatment (labelled ▼). The d-spacings of the 3 most intense molybdate reflections are all within 0.04Å of those in glass 2, and the doublet observed in the 27 – 28°2θ region (labelled with an arrow) is also present although at a reduced intensity.

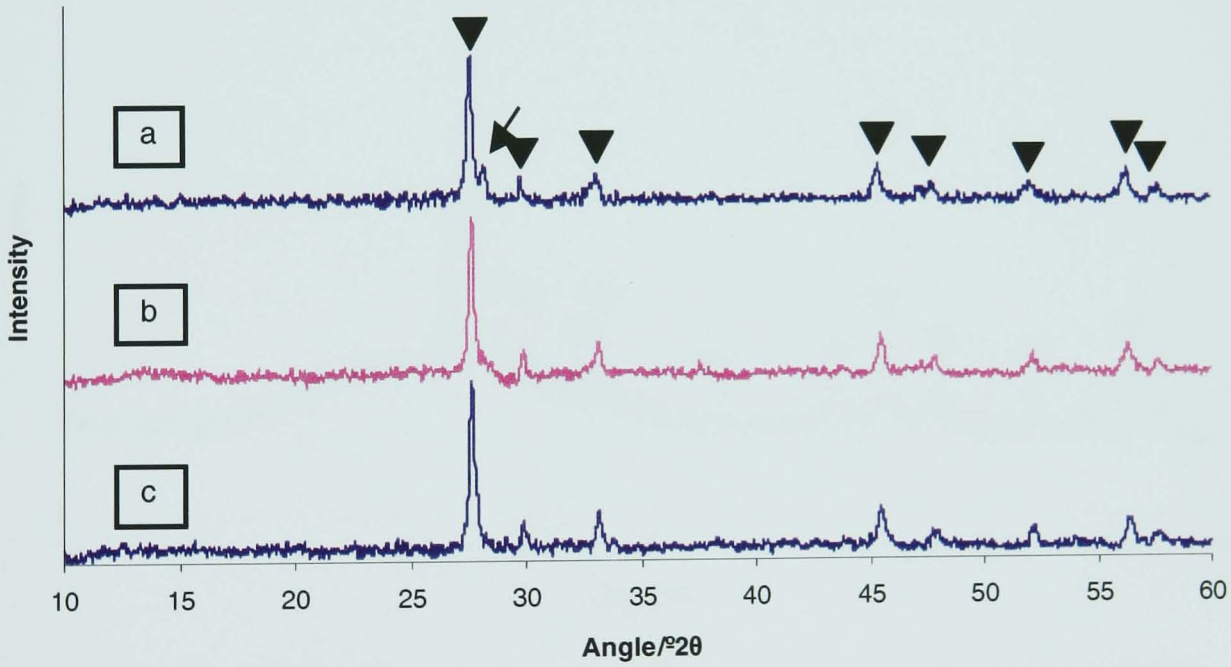

Figure 4.23 – XRD of (**a**) glasses 3, (**b**) 4 and (**c**) 5 after 48 hour heat treatments at 650°C, 665°C and 680°C respectively

4.3.3.4 *Glass 4*

The diffraction pattern of this sample (**Figure 4.23b**) showed the presence of the intense reflection in the 27.9°2θ (3.16Å) region analogous to those observed with the full Li_2O content, but did not exhibit the doublet behaviour at 27.1°2θ (3.29Å). As the

only difference between the two glasses was a reduction in the amount of lithium in the batch, this would suggest that the second reflection is Li related.

4.3.3.5 *Glass 5*

XRD of this sample (**Figure 4.23c**) again showed the presence of the powellite type molybdate phase seen in the other high waste loading glasses.

4.3.3.6 *Glass 6*

The XRD of a sample of glass 6 heat treated for 48 hours at 635°C is shown in **Figure 4.24**.

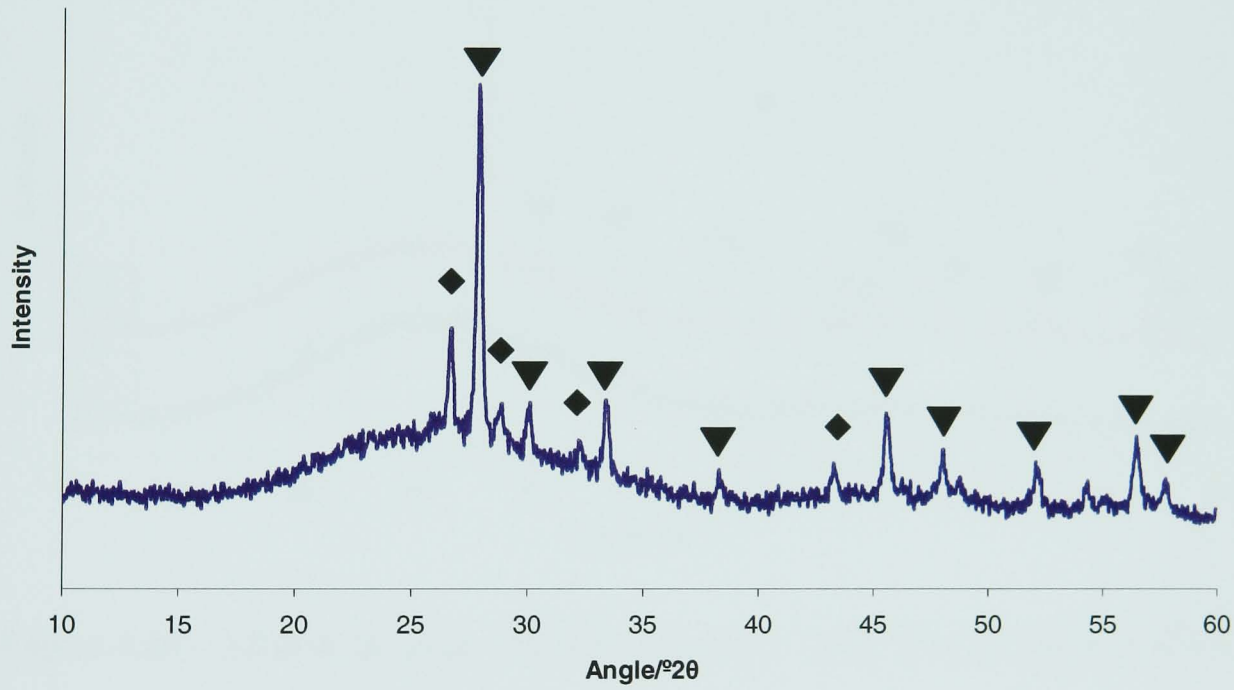

Figure 4.24 – XRD of a sample of glass 6 heat treated for 48 hours at 635°C

The sample underwent a colour change on heat treatment from predominantly dark green in colour to a much lighter green. XRD showed the presence of crystalline material in the sample and the main phase that developed (labelled ▼ in **Figure 4.24**) had the same d-spacings as one of the powellite type molybdate phases that developed in glass 2 (labelled M in **Figure 4.22**). Other reflections were also apparent in the XRD at 26.69°2θ, 28.88°2θ, 32.30°2θ and 43.27°2θ with d-spacings of 3.337Å, 3.089Å, 2.769Å and 2.089Å respectively (labelled with ♦). The first of these showed

a good match for the most intense reflection of quartz (card [85-335]), although the presence and position of the other peaks was a good indication that a second powellite type molybdate phase had developed in the glass, as seen in glass 2.

4.3.4 Heat Treated Redox Effect Glasses

4.3.4.1 *Glass 7*

Figure 4.25a shows the XRD of a heat treated sample of glass 7(air). As can be seen glass 7(air) remained amorphous to XRD upon heat treatment. A sample was also subjected to TEM analysis and no crystalline particles were observed.

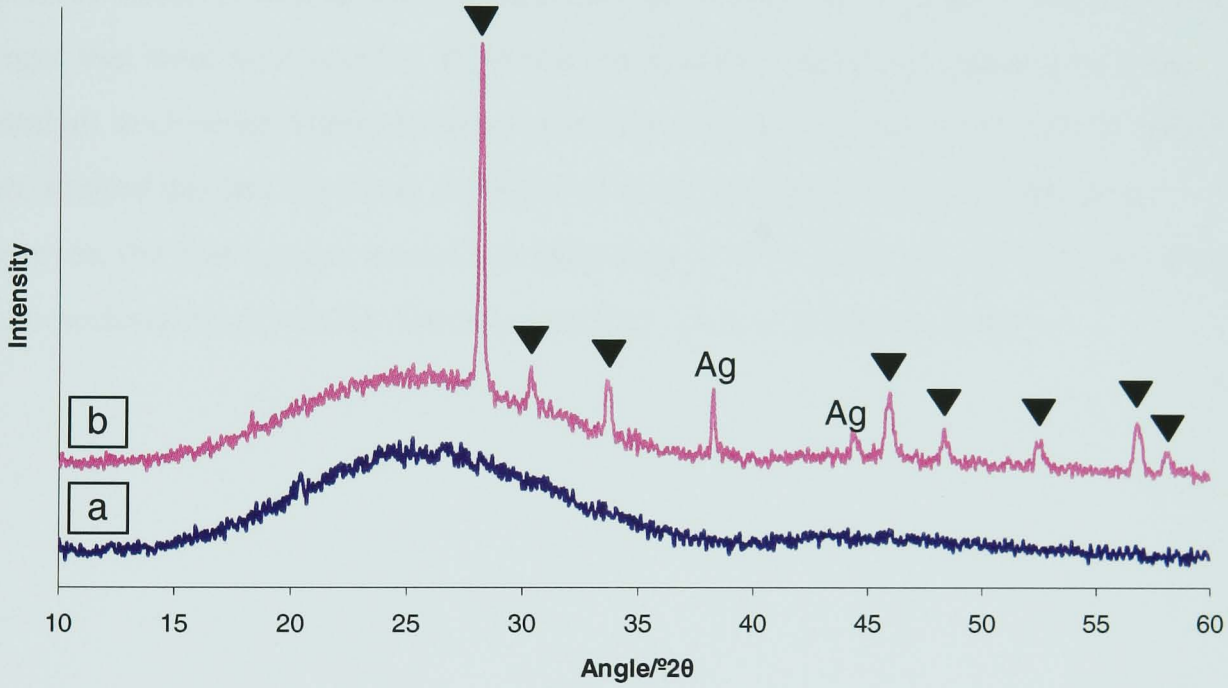

Figure 4.25 – XRD of (**a**) glass 7(air) and (**b**) glass 7(red) after 48 hours at 600°C

Figure 4.25b shows the XRD of a heat treated sample of glass 7(red). The reflections from silver metal that were observed in the as cast sample of glass 7(red) are still present in the heat treated sample. Also present in the heat treated sample are reflections from an un-identified crystalline material (labelled ▼ in **Figure 4.25**) with the 3 most intense reflections being at 28.56°2θ, 30.47°2θ and 46.09°2θ with d-spacings of 3.16Å, 2.65Å and 1.97Å respectively. These reflections were not seen in the as cast sample, but, as for the heat treated samples of glass 2-5, several good matches for powellite type molybdates were found. These were $AgNd(MoO_4)_2$ (card

[49-380]), $Nd_2(MoO_4)_3$ (card [73-1212]) and $Na_{0.5}Ce_{0.5}(MoO_4)$ (card [79-2242]). The d-spacings of the 3 most intense reflections of these compounds differ by no more that 0.005Å and all are feasible given the glass composition. Thus, it was assumed that this phase was a powellite type molybdate, although possibly a composition that had not previously been investigated and included in the ICDD database. A sample of this material was also subjected to TEM analysis. **Figure 4.26a** shows a typical portion of the thin area of the sample containing dendrites (labelled Den in **Figure 4.26a**, and repeated in **Figure 4.26b**) and spherical particles (labelled Ag in **Figure 4.26a**) in the amorphous matrix. EDS analysis of a dendrite (**Figure 4.26c**) showed these features to be much higher in Mo, Sr and lanthanides than the surrounding matrix (**Figure 4.26d**). EDS of the spherical particle (**Figure 4.26e**) showed that this particle was a crystal of silver. It was also noted from extensive observation of all of the areas of the sample that were visible using TEM that the dendritic particles tended to be more abundant in close proximity to silver particles than in the general amorphous matrix area, suggesting that the silver particles could encourage molybdate formation. However, the best images were obtainable only in those areas of thin specimen close to the perforation caused by ion beam milling (shown in **Figure 4.26a**).

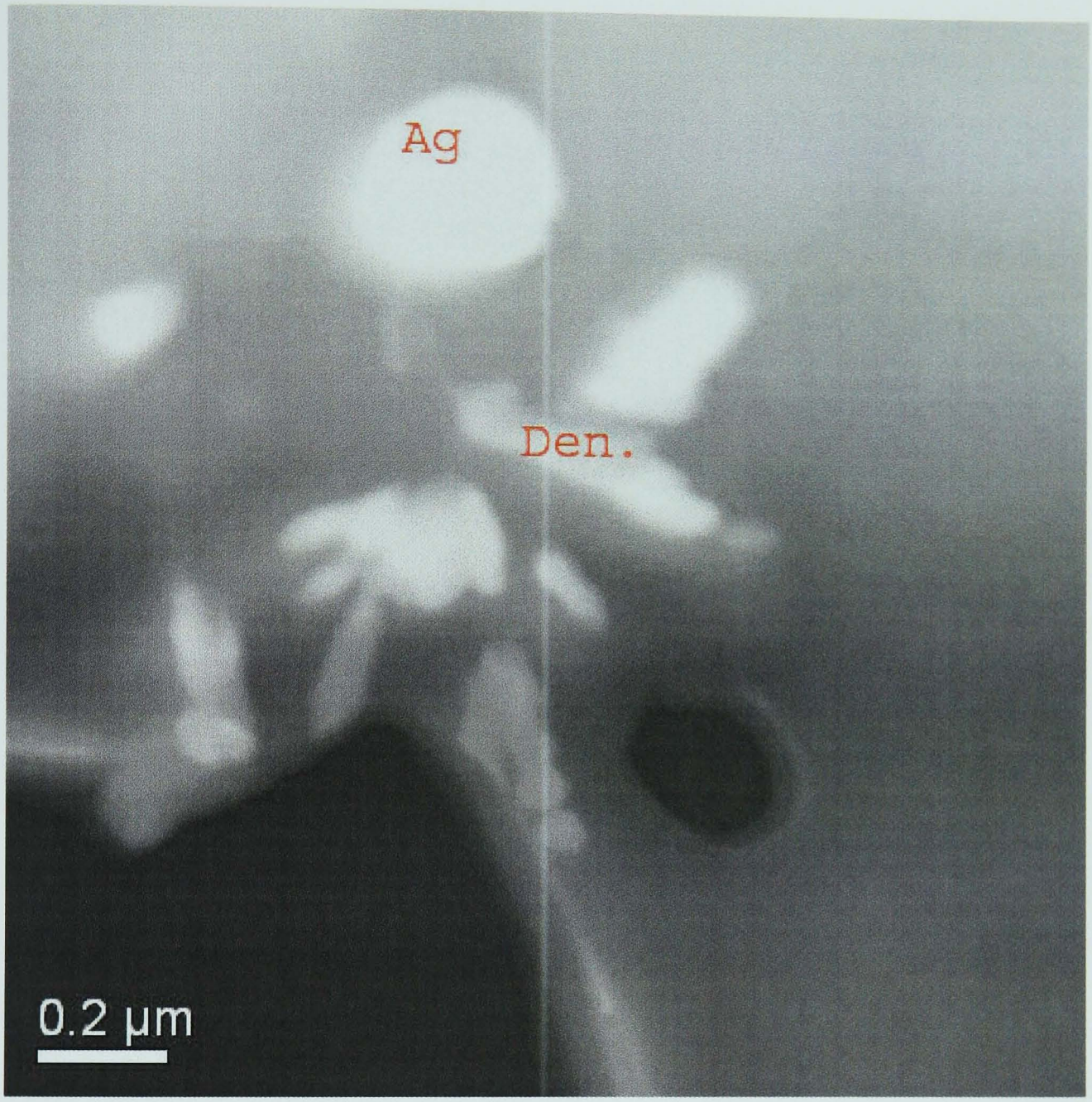

Figure 4.26a – STEM image of a typical portion of thin area of glass 7(red) after heat treatment

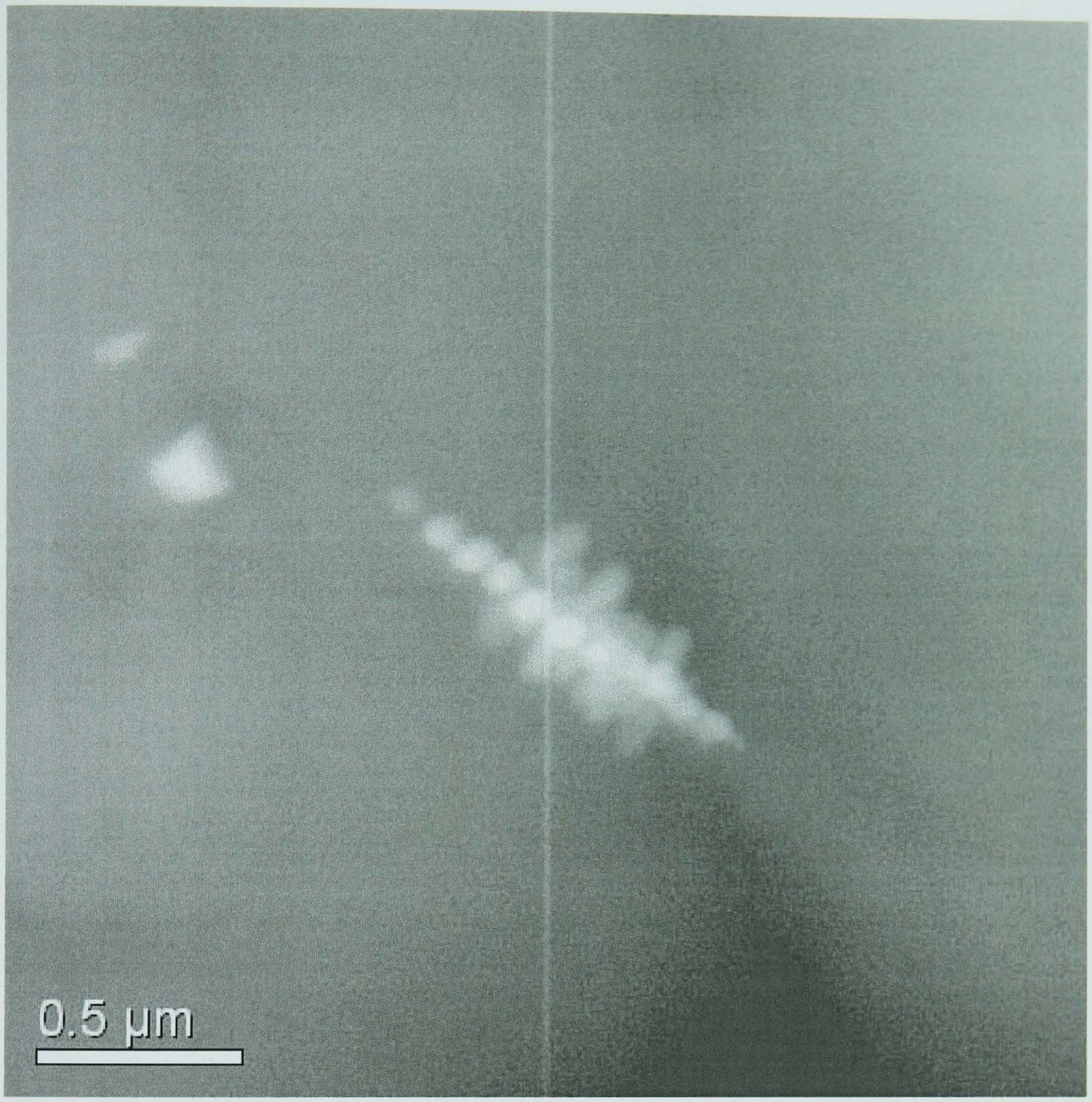

Figure 4.26b – STEM image of a dendritic molybdate particle in a heat treated sample of glass 7(red)

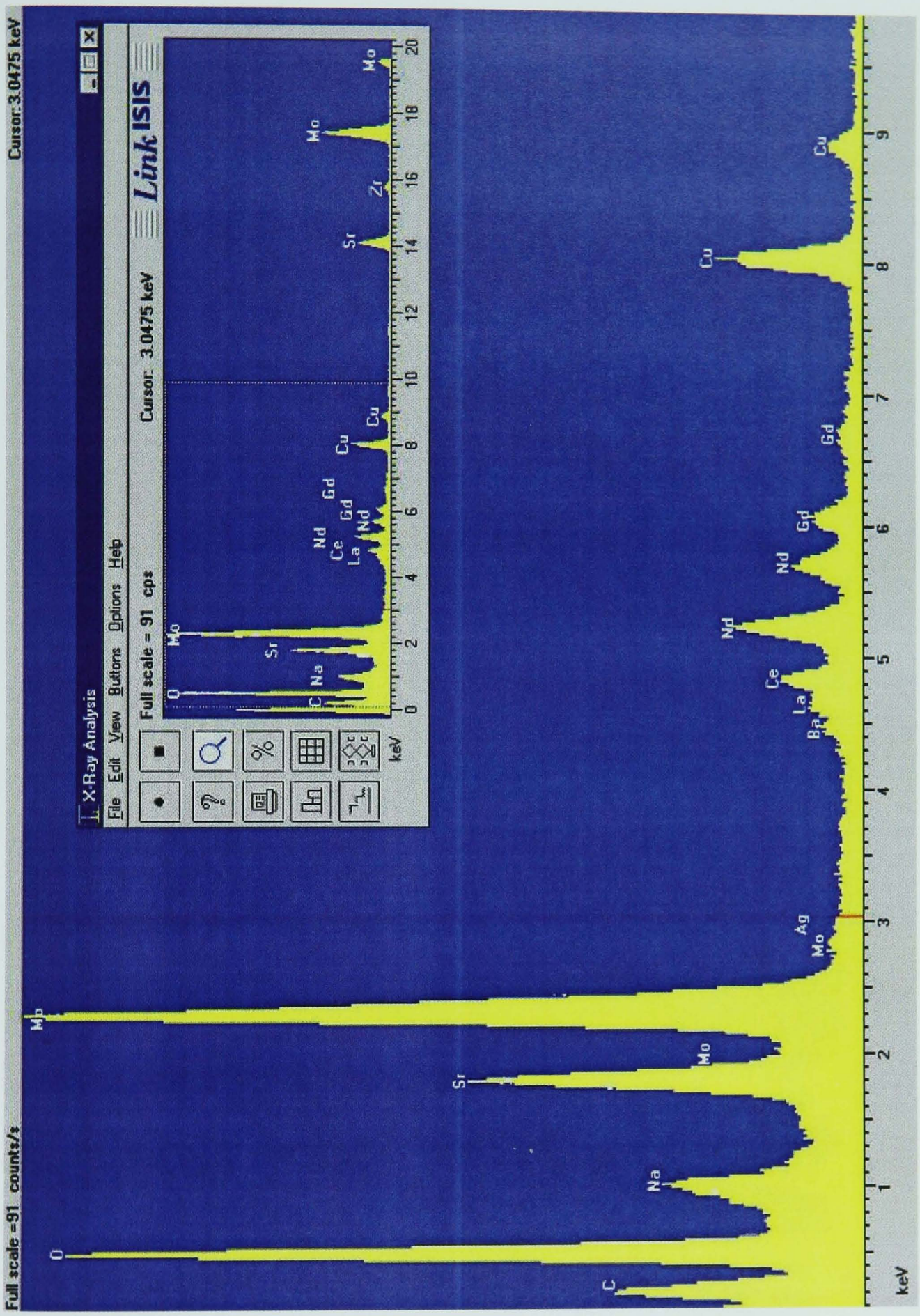

Figure 4.26c – EDS analysis of molybdate dendrites in a heat treated sample of glass 7(red)

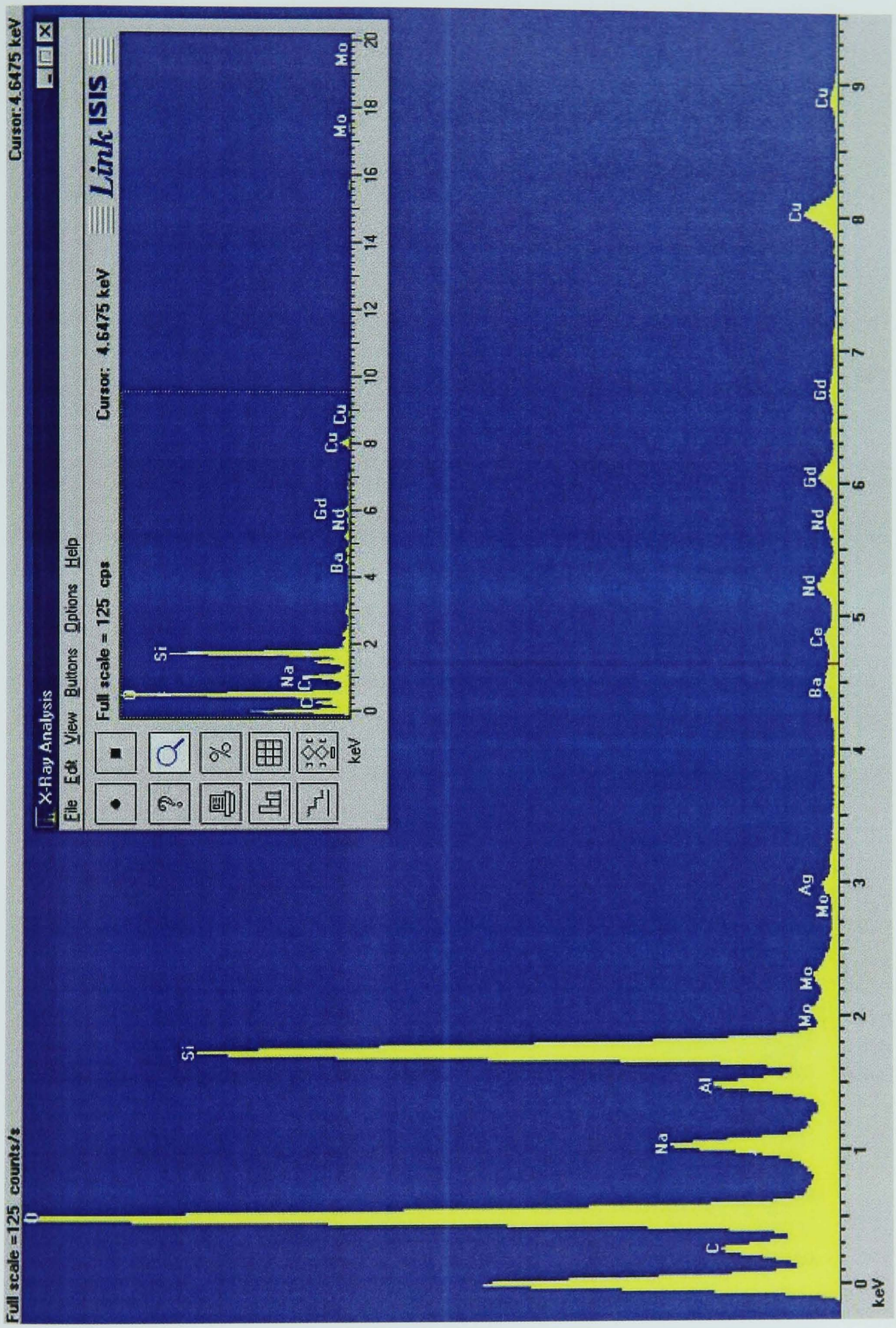

Figure 4.26d - EDS analysis of glassy area of a heat treated sample of glass 7(red)

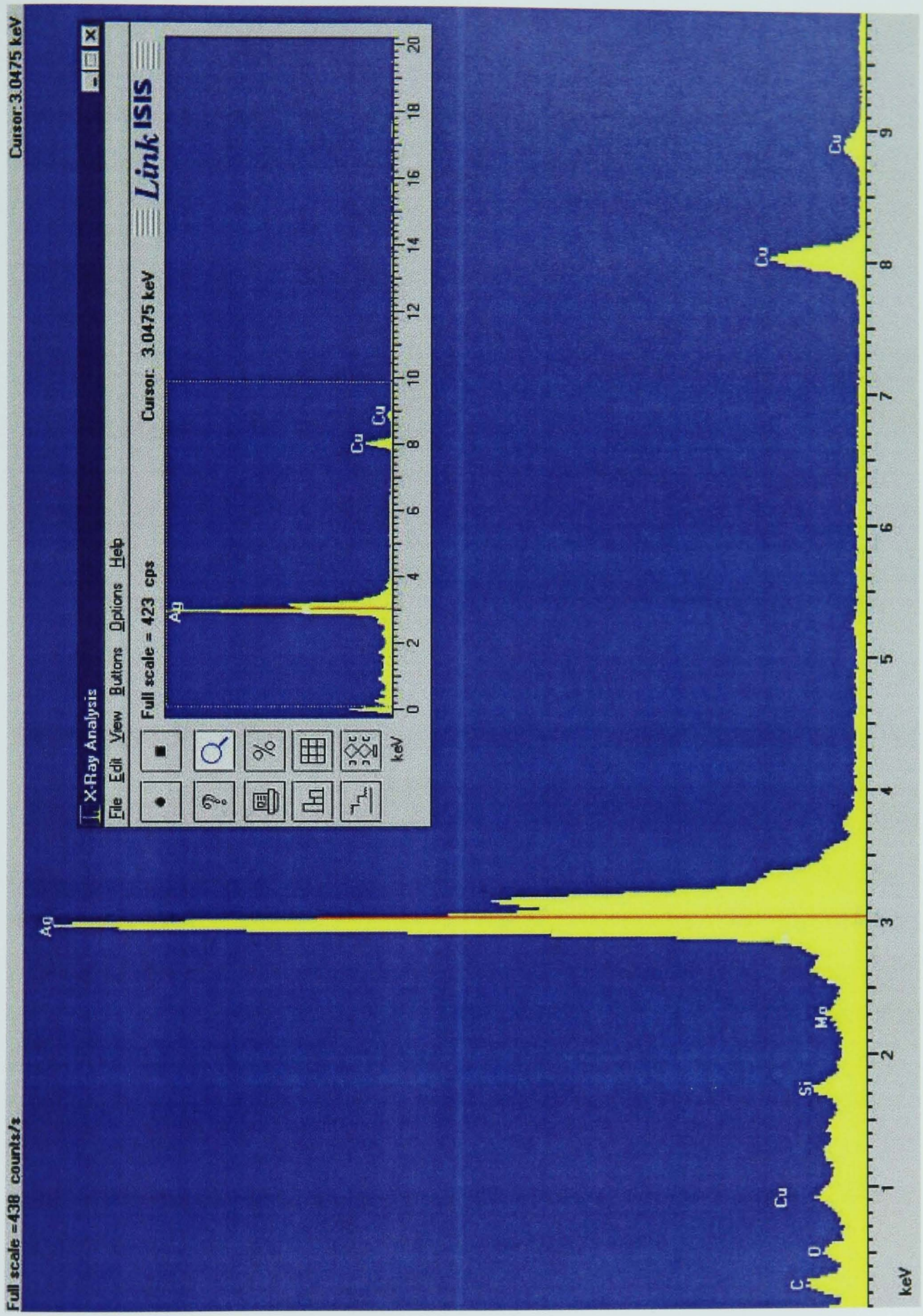

Figure 4.26e - EDS analysis of a silver particle in a heat treated sample of glass 7(red)

4.3.4.2 *Glass 8*

The XRD pattern obtained from a heat treated sample of glass 8(air) is shown in **Figure 4.27a**.

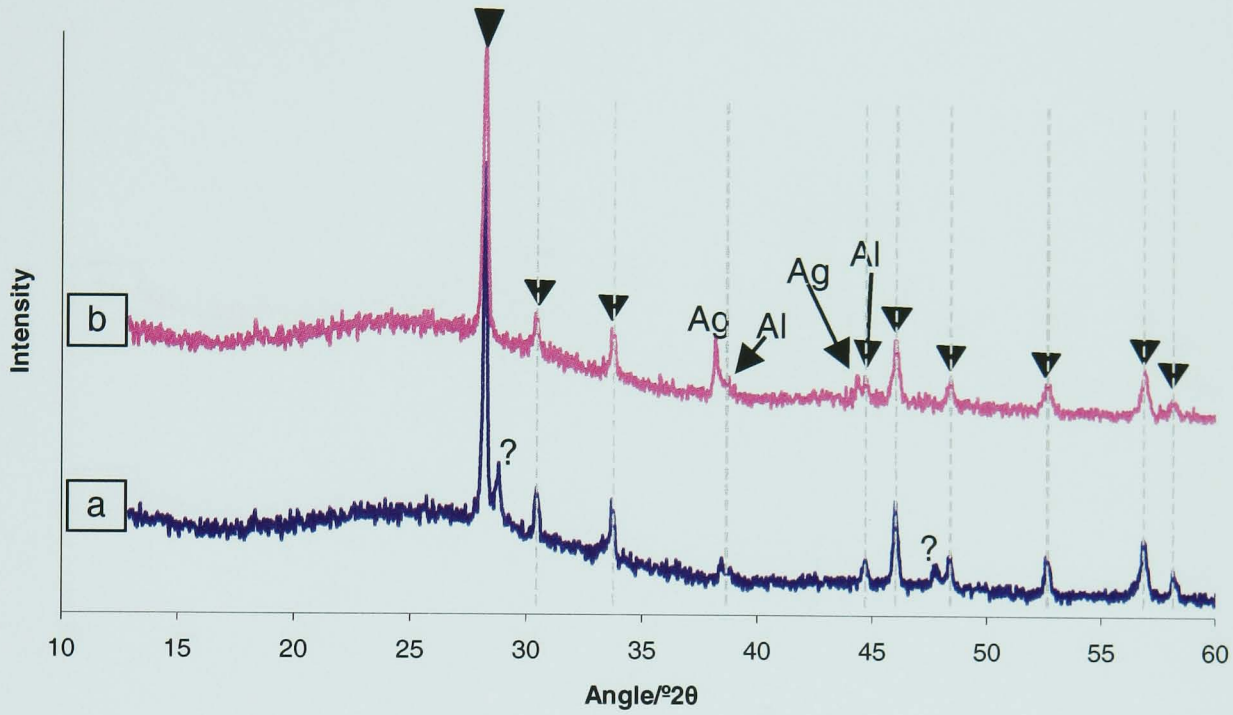

Figure 4.27 – XRD of samples of (a) glass 8(air) and (b) glass 8(red) heat treated for 48 hours at 600°C

Reflections from Al metal were observed in this glass, but (as for the as cast samples of glasses 8, 9 and 10) these arose from the sample holder used for the XRD, and not from the glass as the batch did not contain any Al. However, some crystalline material was present in the glass that resulted from the heat treatment to which the sample was subjected (labelled ▼ in **Figure 4.27**). These crystals have the same d-spacings as those seen in glass 7(red) for which several close matches were found for powellite type molybdate compounds. Two further peaks can be seen in this sample at 28.8°2θ and 47.9°2θ with d-spacings of 3.094Å and 1.904Å respectively (labelled ? in **Figure 4.27**) which could not be identified using the ICDD database**.**

XRD of a heat treated sample of glass 8(red) is shown in **Figure 4.27b.** The figure shows that as well as reflections for Ag metal (as seen in the as cast glass 8(red) sample) and Al metal (an artefact of the sample holder), the same molybdate that developed in glass 7(red) and glass 8(air) during heat treatment developed in glass 8(red) under heat treatment also.

4.3.4.3 *Glass 9*

Figure 4.28a shows the XRD of a sample of glass 9(air) after heat treatment.

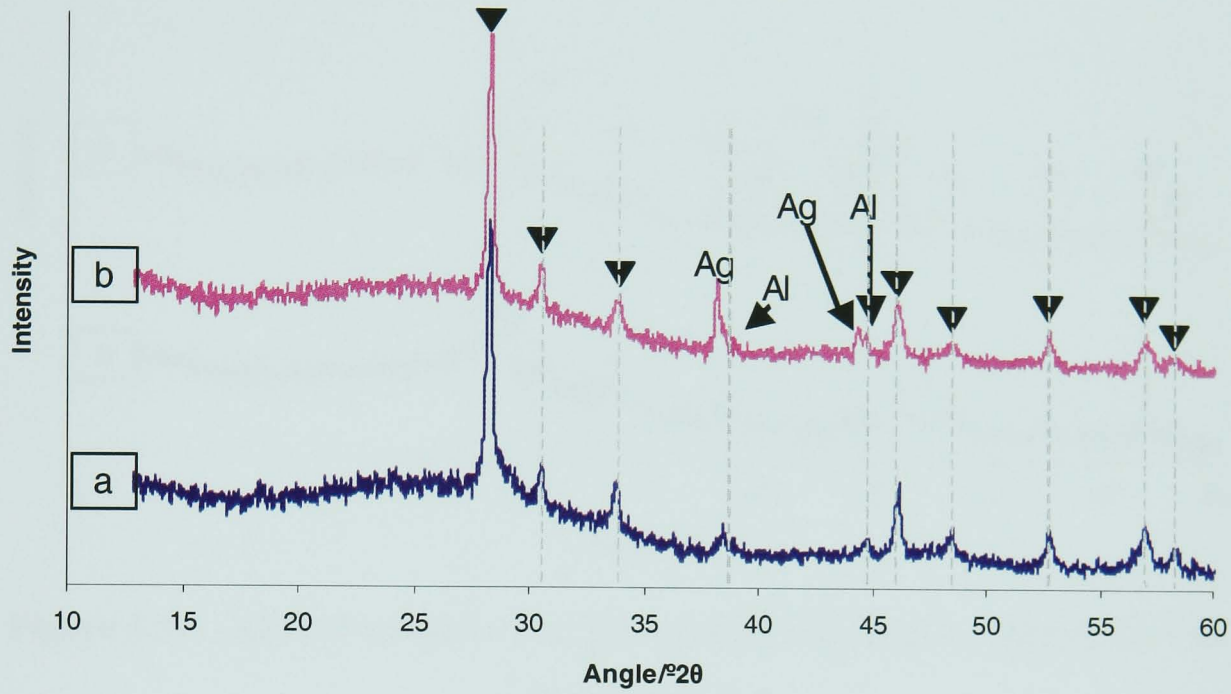

Figure 4.28 – XRD of (**a**) glass 9(air) and (**b**) glass 9(red) after 48 hours at 600°C

Once again the powellite type molybdate reflections observed in the previous heat treated samples of the sparged glasses were observed in this sample post heat treatment (labelled ▼in **Figure 4.28**). Reflections from Al metal can also be seen, again resulting from the Al sample holder used during these experiments.

The XRD of a heat treated sample of glass 9(red) is shown in **Figure 4.28b**. These data are similar to that of glass 9(air), with the same reflections (labelled ▼) from a powellite type molybdate. The data also shows reflections from metallic Ag (from the sample) and Al (arising from the sample holder).

4.3.4.4 *Glass 10*

Glass 10(air) was no exception to the general trend and also developed the molybdate phase with the major d-spacings of 3.159Å, 1.97Å and 2.655Å (28.56°2θ, 30.47°2θ and 46.09°2θ respectively) during heat treatment, as seen in the previous heat treated

sparged glasses. The reflections of this phase are labelled ▼ in the XRD of this sample, **Figure 4.29a**.

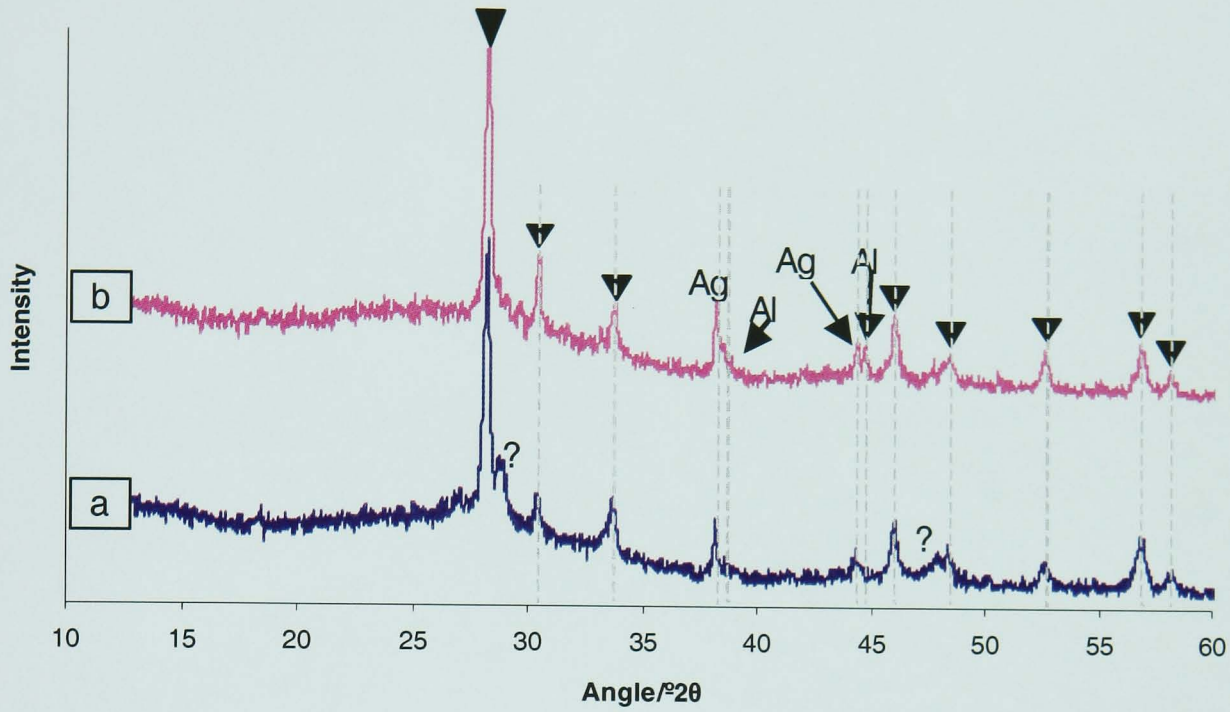

Figure 4.29 – XRD of samples of (**a**) glass 10(air) and (**b**) glass 10(red) after 48 hours at 600°C

Also seen under XRD were reflections from both metallic Al and metallic Ag. Once again, the Al reflections were caused by the sample holder, but Ag reflections had not previously been observed in the air sparged samples. It can also be seen that the reflections at 28.8°2θ and 47.9°2θ with d-spacings of 3.094Å and 1.904Å respectively (labelled ? in **Figure 4.29**) which had only previously been observed in the heat treated glass 8(air), were also present in this sample. TEM analysis of a heat treated sample of glass 10(air) (**Figure 4.30a**) showed the presence of both needle-like and spherical particles in the glass. EDS analysis of these particles showed the brighter spherical particles (labelled Ag in **Figure 4.30a**) to be silver (**Figure 4.30b**), and the darker spherical particles and needle-like particles (labelled Mo and Mo needle in **Figure 4.30a**) to contain elevated levels of Mo, Sr and lanthanides (**Figure 4.30c**) in comparison to the general matrix area (**Figure 4.30d**). This corresponds well with the XRD data indicating the presence of Ag metal and a powellite type molybdate phase in the glass.

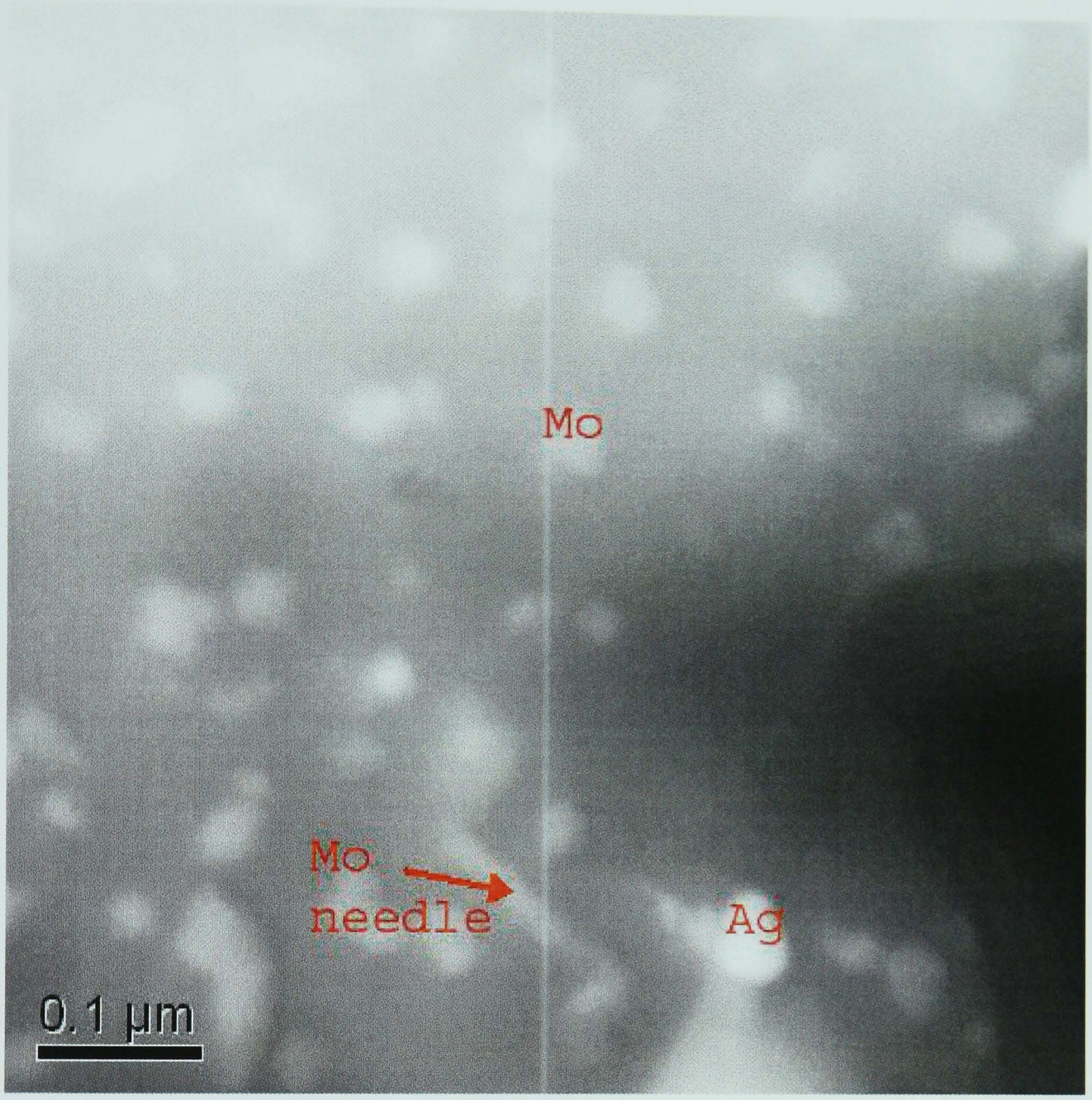

Figure 4.30a – STEM image of a heat treated sample of glass 10(air)

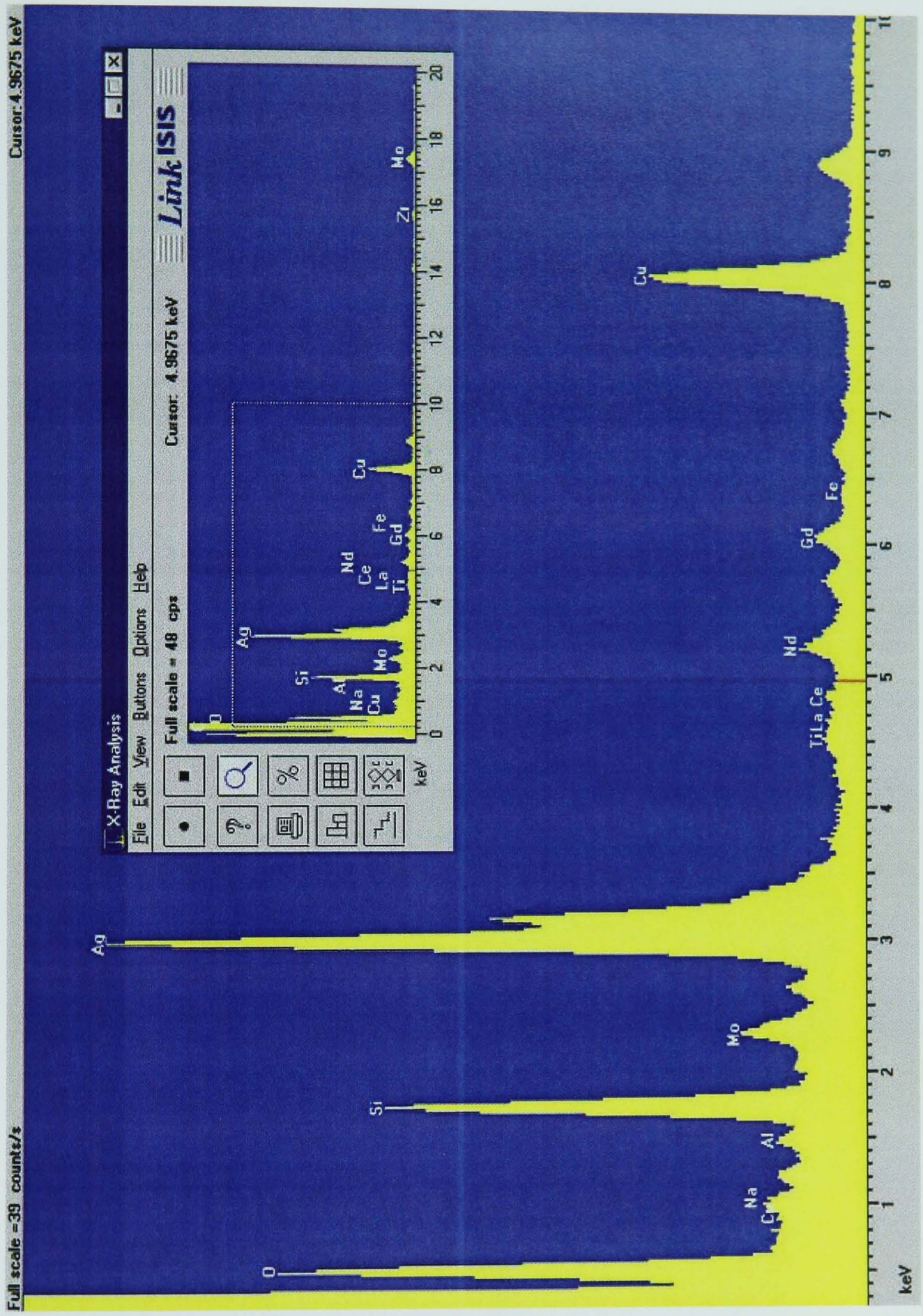

Figure 4.30b - EDS analysis of a silver particle in a heat treated sample of glass 10(air)

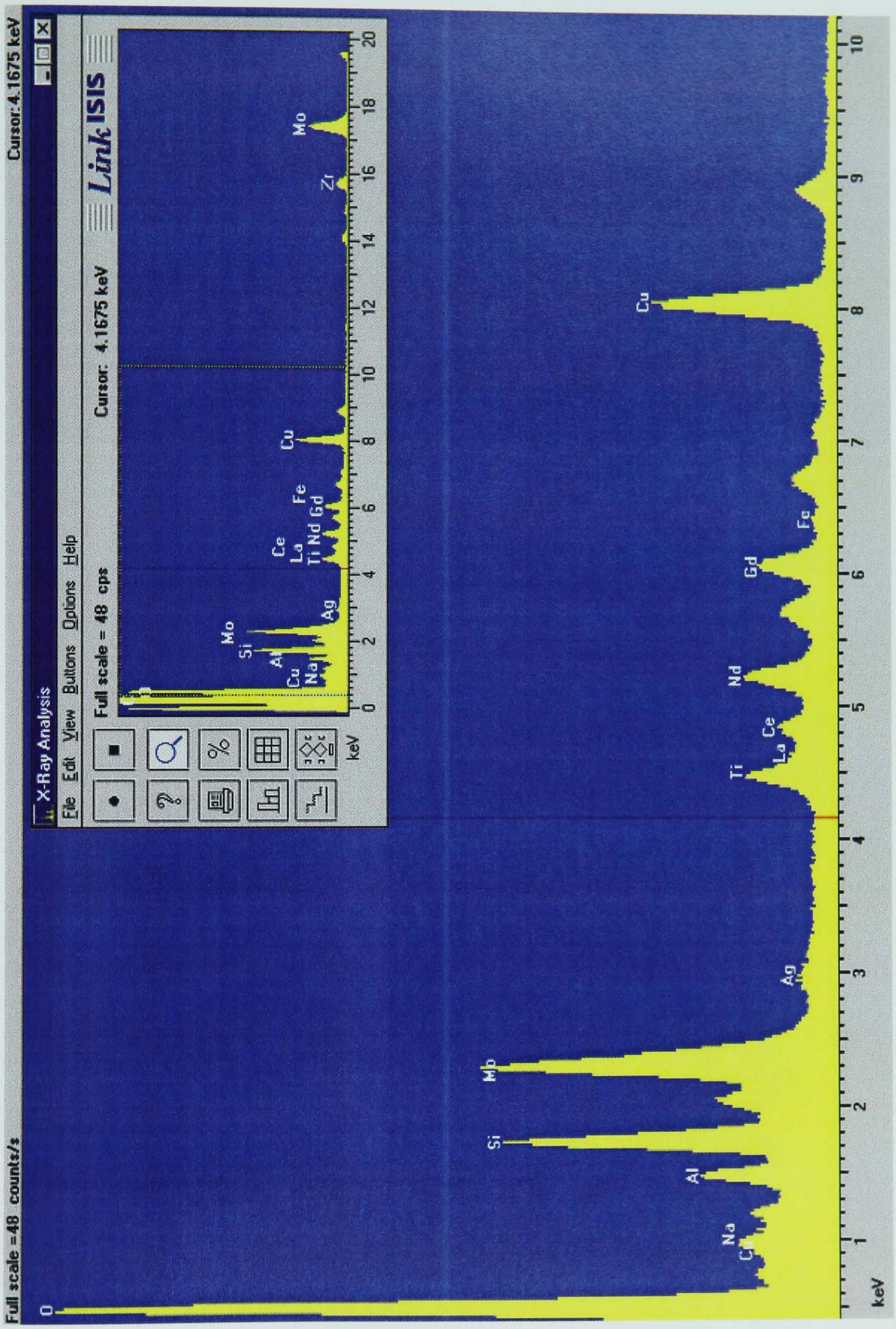

Figure 4.30c - EDS analysis of molybdate particles in a heat treated sample of glass 10(air)

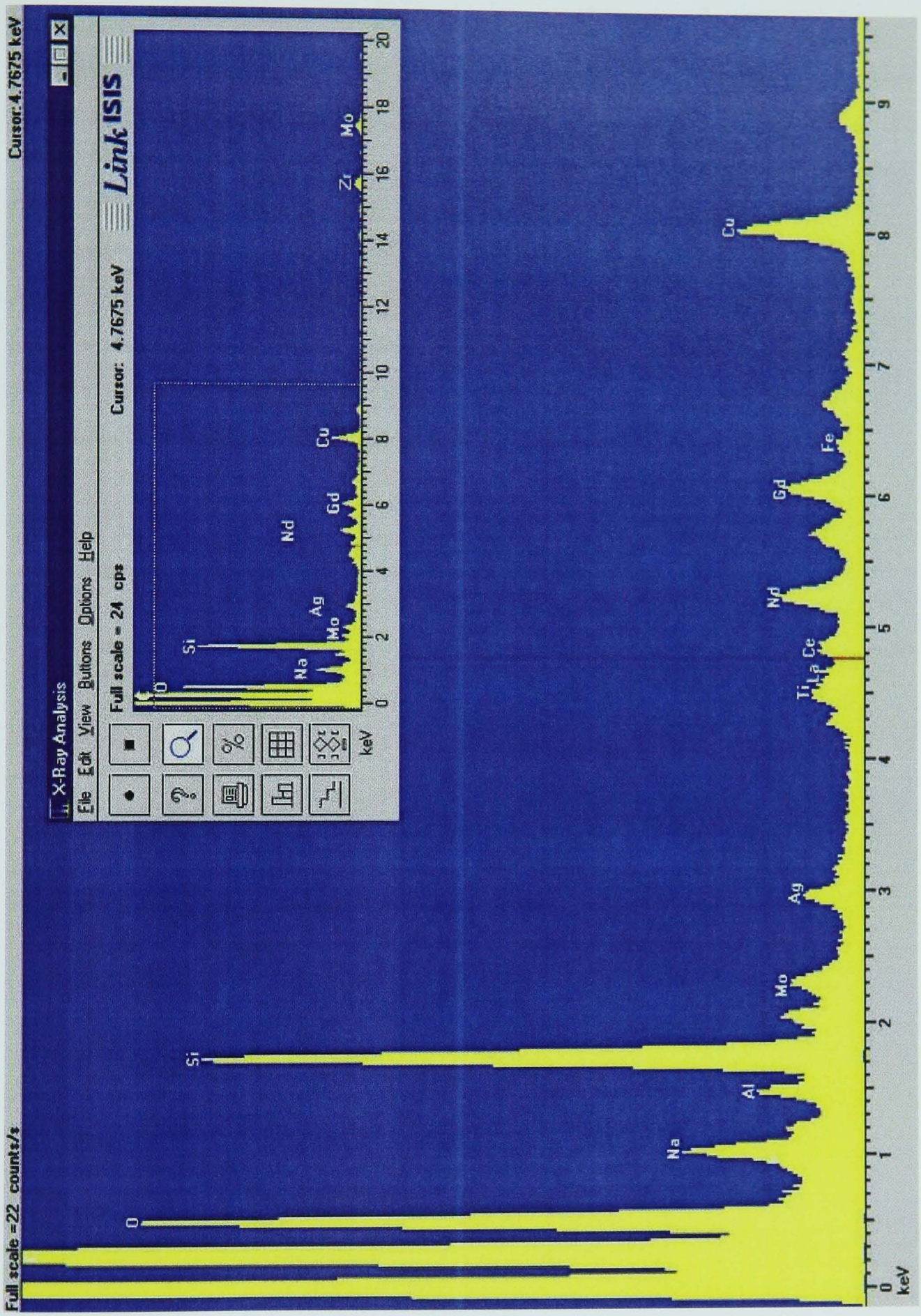

Figure 4.30d - EDS analysis of a glassy area of a heat treated sample of glass 10(air)

The XRD pattern of a heat treated sample of glass 10(red) shown in **Figure 4.29b** is similar to the previous nitrogen-hydrogen sparged heat treated samples. Reflections from metallic Ag (from the sample) and metallic Al (from the sample holder) are both

present, along with the reflections for the powellite type molybdate phase (labelled ▼) seen in the previous heat treated sparged glass samples. EXAFS analysis was also performed on this sample (**Figure 4.31a**) and a coordination shell at a distance of 1.76(2)Å from the Mo scatterer was found (**Figure 4.31b**), indicating the presence of $(MoO_4)^{2-}$ tetrahedra (R factor = 33.7). STEM analysis showed that this glass contained only spherical particles (**Figure 4.32a**), but that some were brighter than others indicating higher atomic number. EDS analysis showed that the brighter particles (labelled Ag in **Figure 4.32a**) were silver (**Figure 4.32b**), and the darker particles (labelled Mo in **Figure 4.32a**) were molybdates that were higher in Sr and lanthanide elements (**Figure 4.32c**) than the glass matrix (**Figure 4.32d**).

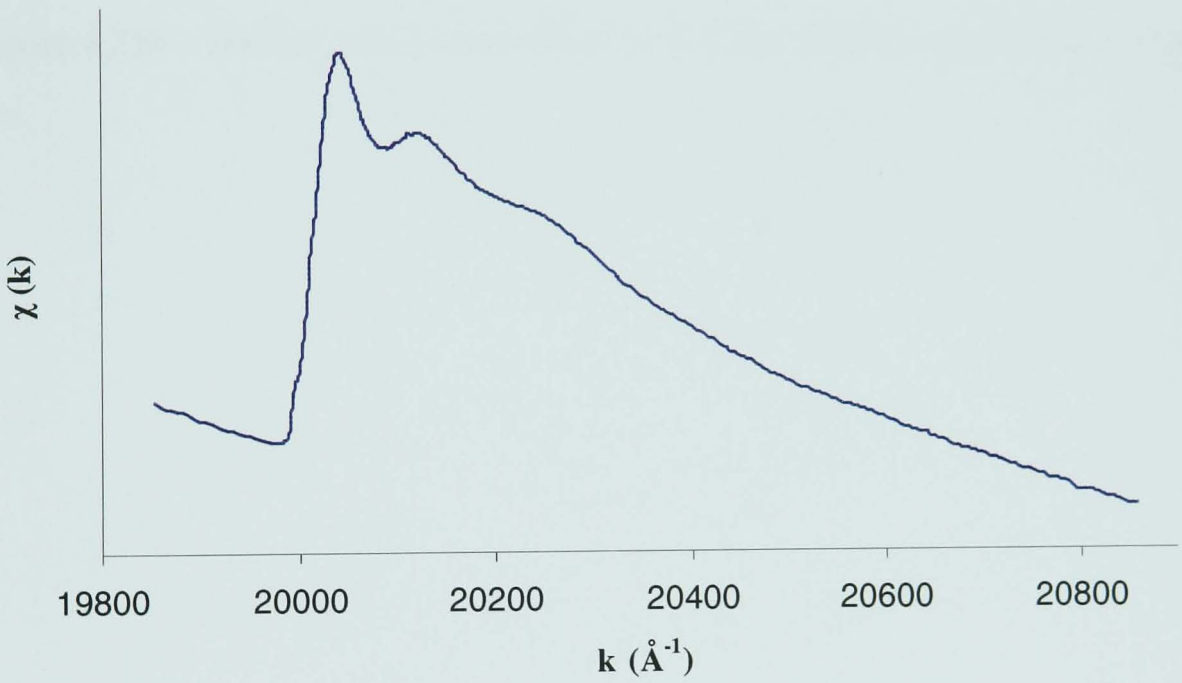

Figure 4.31a – EXAFS of a heat treated sample of glass 10(red)

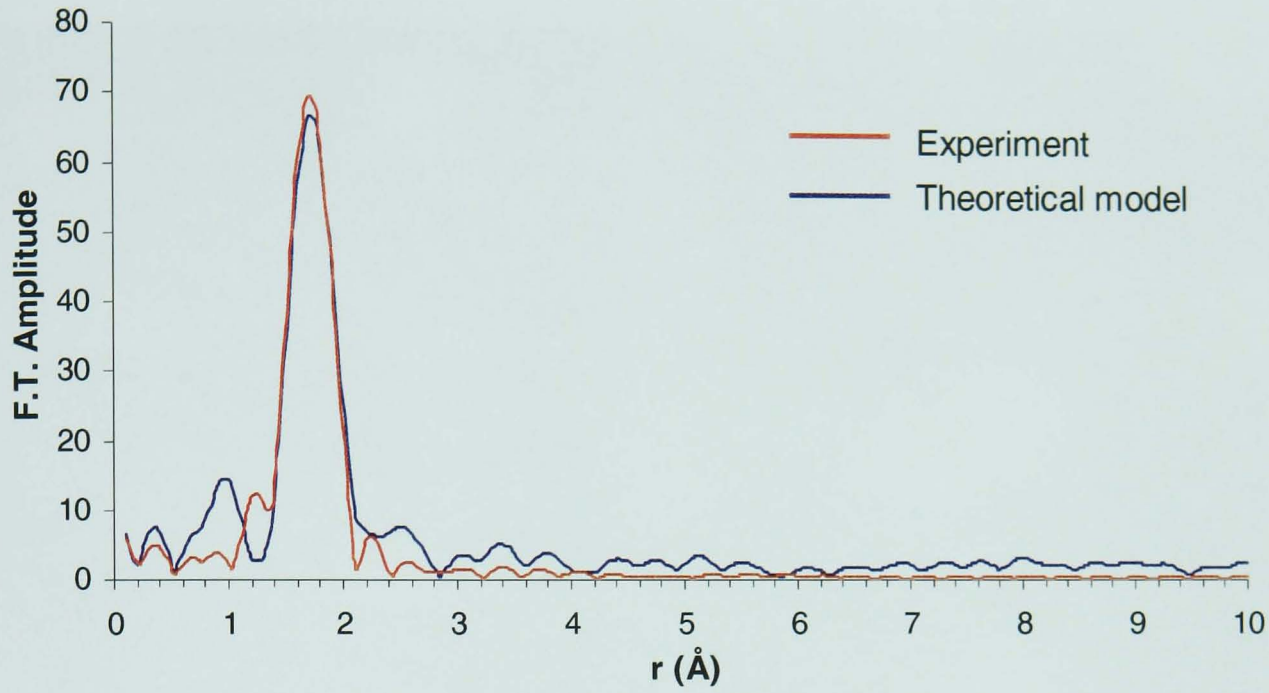

Figure 4.31b – Fourier transform of EXAFS of a heat treated sample of glass 10(red)

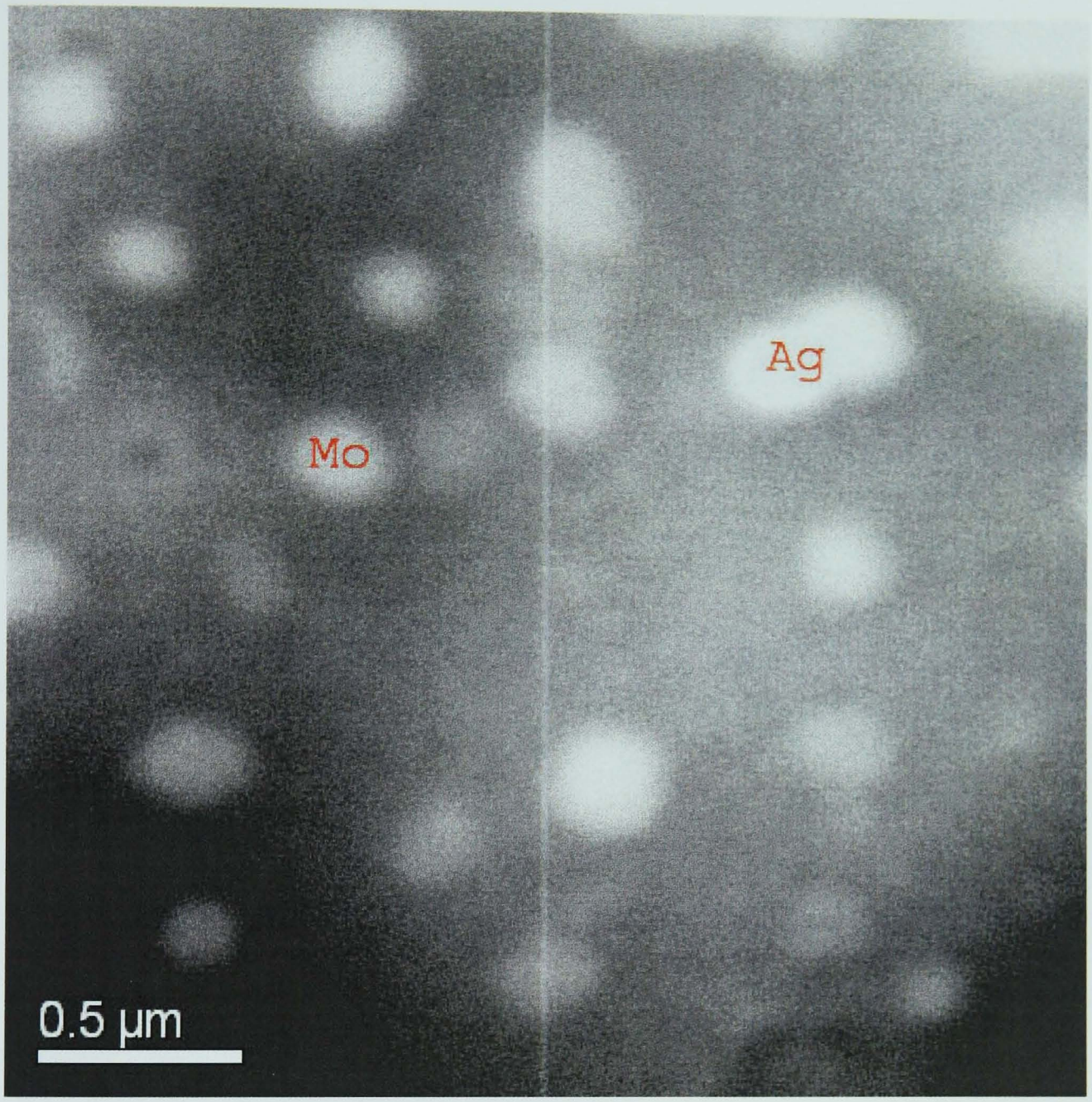

Figure 4.32a – STEM image of a heat treated sample of glass 10(red)

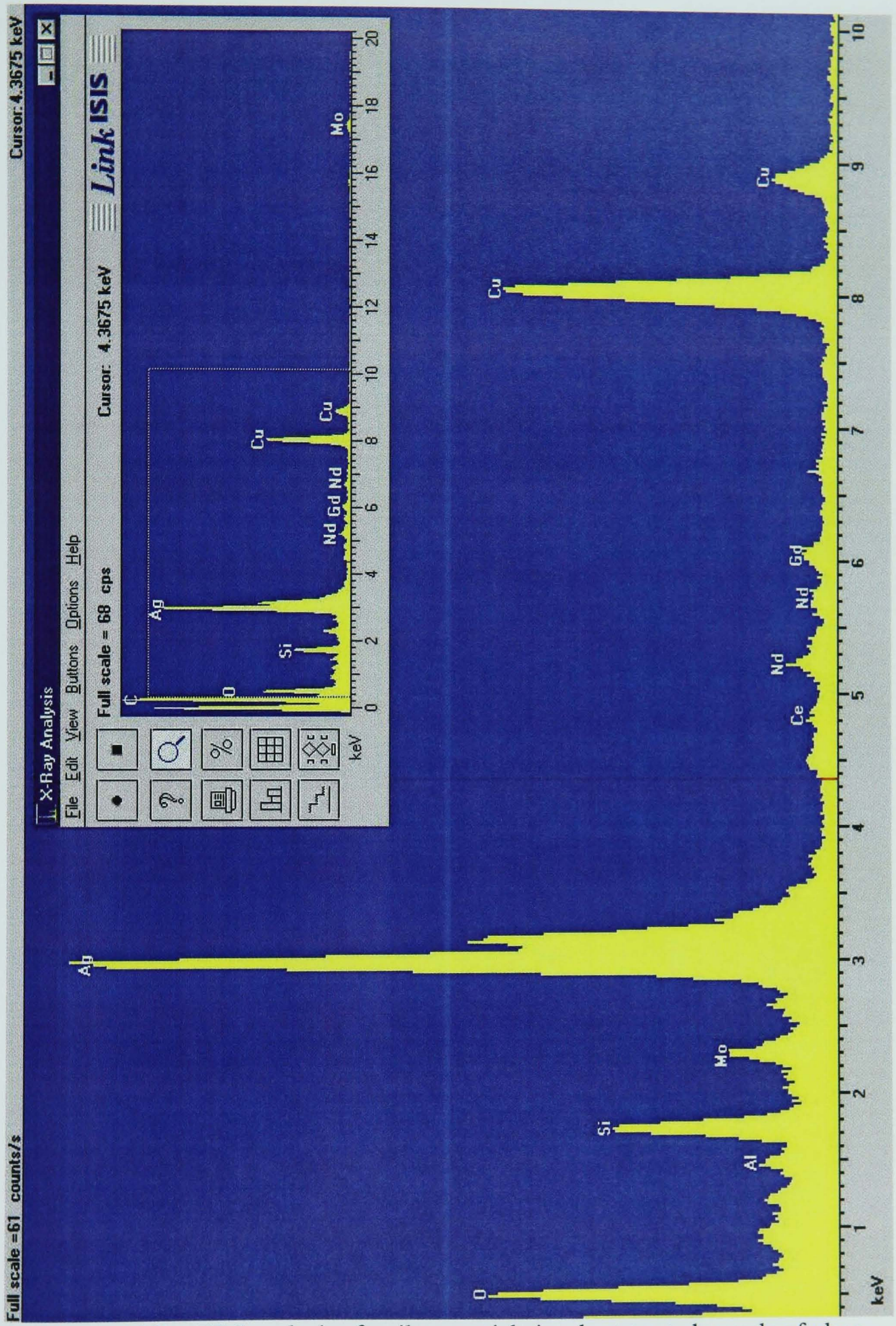

Figure 4.32b - EDS analysis of a silver particle in a heat treated sample of glass 10(red)

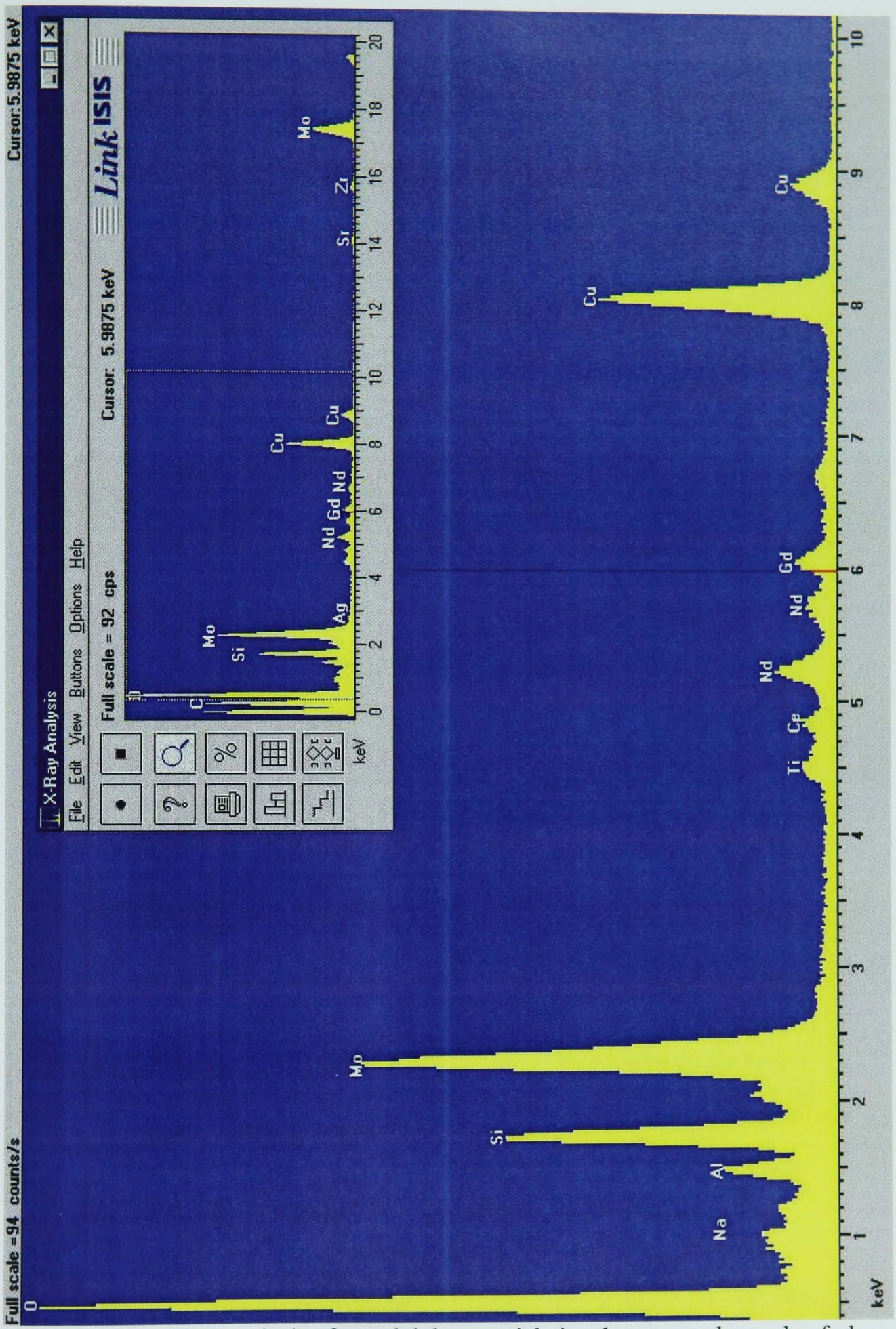

Figure 4.32c - EDS analysis of a molybdate particle in a heat treated sample of glass 10(red)

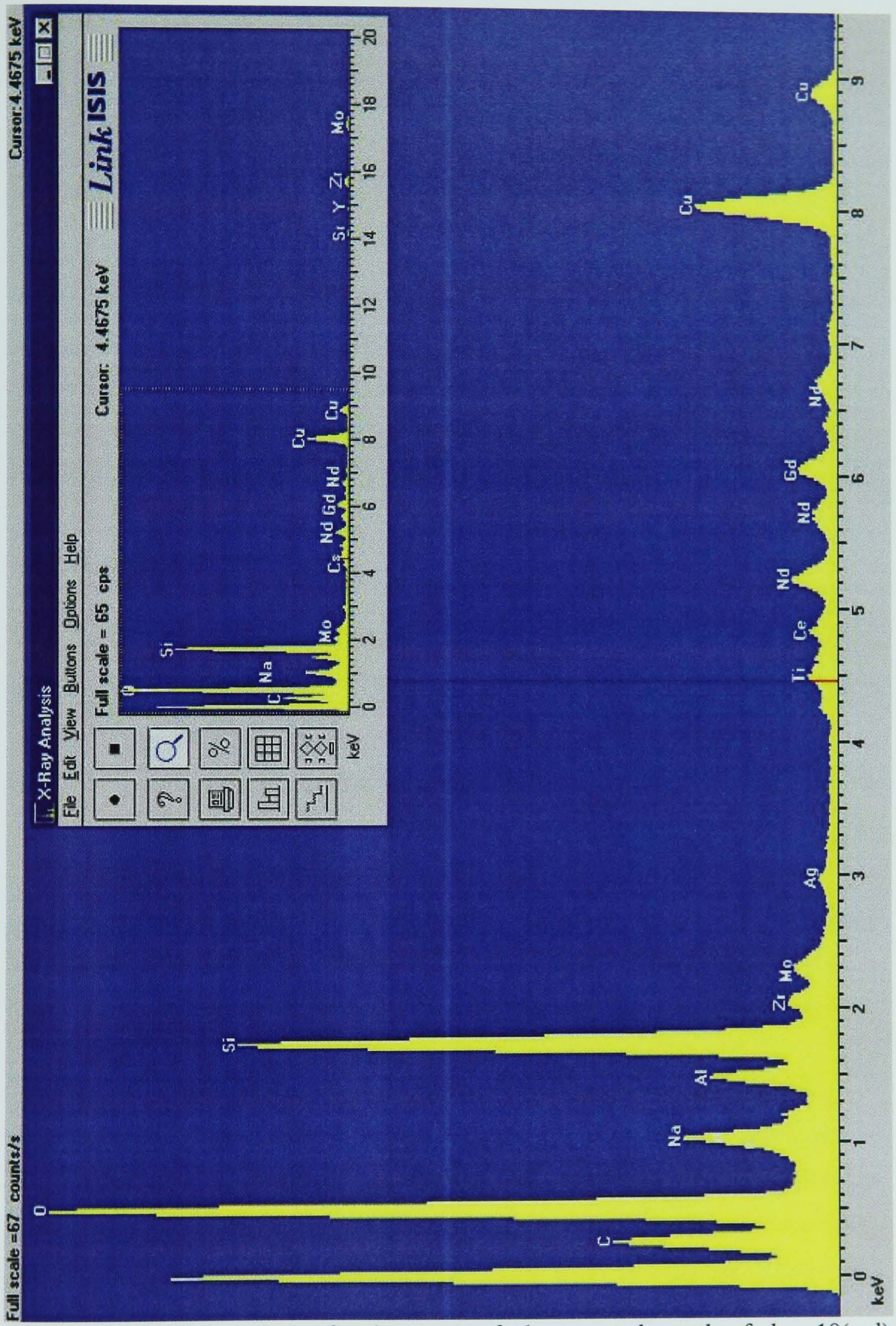

Figure 4.32d - EDS analysis of a glassy area of a heat treated sample of glass 10(red)

4.4 Discussion

4.4.1 High Waste Loading Glasses

4.4.1.1 *Glass 1*

As expected, this batch formed a homogeneous product in the as cast state that was not prone to devitrification upon heat treatment. This is consistent with analogous glasses produced on full scale vitrification lines at BNFL, and as none of the waste components exceed their solubility limits in the borosilicate glass, they are all dissolved into the matrix as intermediates or network modifiers.

4.4.1.2 *Glasses 2-5*

All of the melts performed with a 35% waste loading and varying amounts of Li_2O in the batch phase separated to a certain degree, and displayed evidence of elemental silver in the as cast state, either in the form of a dichroic effect upon splat quenching or in the form of spherical metallic particles ~1-3mm in diameter. With one exception (glass 2) these glasses appeared amorphous to XRD. The crystalline material in glass 2 (**Figure 4.3**) was too small to be seen using either optical or scanning electron microscopy, but the use of transmission electron microscopy revealed the presence of a crystalline phase (other than metallic silver). EDS indicated that this phase was higher in Mo than the surrounding matrix. The transmission electron micrograph of a heat treated sample of glass 10 (**Figure 4.30a**) which had the same nominal composition, revealed the presence of spherical particles that were Mo rich. It is therefore possible (although not proven) that the particles observed in glass 2 are related molybdates. As the other high waste glasses were of similar composition, it is likely that similar particles were present in glasses 3, 4 and 5 but were just too finely dispersed to give significant reflections on the XRD scans. In a real HLW glass, this would not be a major cause for concern as a small volume of crystalline material ($\leq$1%) can be tolerated in the vitrified product. Further evidence for crystallite presence in these as-cast glasses, is the fact that significant amounts of crystalline material developed upon heat treatment of these glasses without a nucleation step in

the heat treatment programme. Normally when synthesising a glass ceramic material, a holding step is required in the heat treatment programme at a temperature (usually) just above T_g to allow nucleation of crystalline material within the amorphous matrix. After a sufficient time, the temperature is then raised to the growth temperature (usually just below the liquidus temperature, often 100-150°C above T_g) to allow crystalline material to develop around these crystal nuclei. However, in the heat treatments performed in this work, a nucleation step was not included, which indicates the presence of crystal nuclei prior to heat treatment, i.e. in the as-cast glasses. However, it is possible that Ag crystallites alone were acting as nucleation centres in these glasses. Some support for this arises from the fact that Mo-rich dendrites were more often found adjacent to Ag crystallites in the heat treated glass 7(red) (**Figure 4.26a**).

Thermal analysis of the as-cast glasses showed an increase in the T_g of the glass as the Li_2O content decreased, ranging from 480°C for the glass with the full amount of Li_2O to 560°C for the glass with no Li_2O. This is as expected, as Li acts as a flux in glass melts thus lowering the temperatures at which the major transitions (such as the glass transition and melting) take place. It was also noted that as the amount of Li_2O was reduced, there was a reduction in intensity of some of the reflections on the XRD traces (labelled with an arrow in **Figure 4.23**). This indicates that Li was playing some part in the formation of one of the molybdate phases in the fully loaded glass. A similar phenomenon was noted by Scheetz *et al* (1982) in supercalcine ceramics in relation to powellite-type Ca-Ba-Sr molybdate phases that were forming. They found that as the amount of Ca in their batch was reduced, and the amounts of Ba and Sr were increased, the molybdate in their glass went through a 2 phase region and exhibited a doublet in the 27°2θ region of the XRD trace. This behaviour is similar to that seen in **Figure 4.23** where in glass 3 (containing the ¾ the amount of Li contained in glass 2) a doublet can clearly be seen at 28.2°2θ in the same position as in glass 2 (with the full amount of Li) although at a reduced intensity. When the Li content is reduced further in glass 4, the doublet disappears altogether. This would be consistent with the presence of 2 (similar) powellite-type molybdate phases in the high Li glasses, one of which contains Li_2O and which disappears as the quantity of Li in the glass is reduced. The molybdate phases that are forming in these high waste glasses are discussed in more detail in **Chapter 5**.

The presence of aggregates of silver in the crucibles and glass blocks indicates that the quantity of silver in the melt exceeds the solubility limit. In this situation, the metal would be precipitated rather than the oxide, as the oxide decomposes at temperatures greater than 100°C. Finely dispersed silver particles would also explain the yellow colouration observed in glass 2 (Weyl, 1959). It must be remembered however that silver oxide is being used in this simulated HLW stream as a substitute for more expensive and/or hazardous elements (such as Pt and Pd) and is thus present at much higher concentrations than would be found in a real HLW stream. Nonetheless, devitrification of the metallic elements and oxides (that Ag is used to represent) during real HLW vitrification is a well documented problem (see, for example, Marples (1988) or Donald *et al* (1997)).

4.4.1.3 *Glass 6*

XRD of the heat treated sample of glass 6 adds further weight to the proposal made above that Li is easily incorporated in a powellite type phase in these simulated HLW glasses upon heat treatment. The intensity of the reflections of this phase when compared to those of the same phase in glass 2 after the same heat treatment schedules suggests that Li is not the controlling factor in the quantity of the phase that can develop, as glass 6 contains twice as much Li yet the peak intensities are not doubled. It is possible that one of the other batch components that is incorporated in this phase (such as the Mo) could be the limiting factor. However, previous studies on simulated HLW glasses containing Ca and Mo have shown that the quantity of powellite that developed in the glass upon heat treatment was less than was theoretically possible from the sum of the Ca and Mo in the batch (Orlhac, 2000). Thus, the factor(s) limiting the maximum quantity of devitrification products that contain Mo seems to be something other than the batch composition.

The heat treatment experiments on glasses 2 – 5 show that decreasing the Li content can decrease the number of phases that form upon heat treatment. Other factors that need to be considered when altering base glass compositions are factors such as glass transition temperature, liquidus temperature and chemical durability. **Table 4.4** shows that the T_g increases on replacement of Na with Li (by comparison of the T_g's of

glasses 2 and 6), and hence the liquidus temperature would also be expected to increase. This would be a positive effect with respect to the long term storage of the waste glasses, as the higher the T_g of the glass, the lower the chances of radiogenic heating leading to the development of detrimental crystalline phases in the glass. However, it would be a drawback with respect to the efficiency of producing the glass, as more energy would need to be applied to the system to attain the same viscosity (which in turn will affect homogenisation times) compared to a glass with a lower glass transition and liquidus temperature.

The chemical durability is another important factor with respect to the overall glass quality. As previously mentioned, both Na and Li act as fluxes during melting, and due to their similar chemistry they are both included in the structure of glasses as network modifiers, and reside in the network as distinct cations, rather than being covalently bonded into the network. This makes them vulnerable to leaching should the glass come into contact with water. Doremus (1979) discusses the leaching of alkali ions from glass in terms of hydronium (H_3O^+) ion mobility through the network. He points out that the chemical durability of silicate glasses containing potassium is low, due to the similarity in size between the effective radii of K^+ and H_3O^+ (given as ~1.3Å). This similarity leads to an easier passage through the network for the hydronium ions, as they fit neatly into the holes left by the potassium ions as they diffuse out. Thus, the chemical durability of Li borosilicates is expected to be greater than that of Na borosilicates due to the closer ionic radii of Na^+ and H_3O^+ than of Li^+ and H_3O^+, and thus omitting Na from the base glass should improve the overall chemical durability of the matrix. However, Doremus also points out that adding a second alkali (e.g. Li) to a sodium silicate glass can result in an increase of chemical durability, and apportions responsibility for this to the mixed alkali effect, which has been reported and reviewed by many authors (see, for example, Isard (1968) and Day (1976)). These effects could be of most relevance to the early interdiffusion stage of leaching. Long term leaching behaviour is also composition related, but the exact relationship between composition and performance is currently the subject of debate as there is no agreement as to the exact mechanism that governs the so-called final rate (see, for example, Jégou *et al* (2000), Gin *et al* (2001), McGrail and Strachan (2001)). McGrail *et al* (2001) do however show that ion exchange is important even when the leaching solution is near saturation.

Another very important consideration with respect to altering the base glass composition is that real HLW vitrification takes place in hot cells – environments which are very difficult to work in and were designed with fairly rigid processing parameters. Thus, such a radical alteration to batch composition could be difficult to integrate into the existing technology.

It would be interesting to examine how glass 6 behaves when melted under different atmospheres (such as the reducing sparge applied to glasses 7 – 10), and to fully characterise such properties as T_g and the chemical durability. However, these avenues were not pursued in this research, as the real HLW glasses are made to strict compositional specifications, to which a variance in Na concentration is not permitted, as this would invalidate the guarantee of quality of the glass product given by BNFL to its customers (which is composition specific).

4.4.2 Effect of Redox

4.4.2.1 *Glasses 7 – 10*

The as cast appearance of the glasses sparged with a reducing gas during melting indicate that the tendency for phase separation is increased compared to glasses sparged with compressed air during melting. Even with a 20wt% waste loading, a reducing sparge leads to the formation of at least 2 distinct phases, as can be seen in **Figure 4.11b**. XRD of glass 7(red) (**Figure 4.12b**) showed that the as cast glass had also partially devitrified as reflections of metallic silver were present. This was the case for all of the as cast glasses (7- 10) sparged with the $N_2/5\%H_2$ gas composition, and it is reasonable to conclude that increasing the waste loading (and therefore the Ag content of the glasses) would lead to an increase in the quantity of devitrified material, although quantitative XRD (with samples containing well characterised standards) would need to be performed to confirm this. In comparison, the glasses sparged with compressed air remained visually homogeneous up to a 30wt% waste loading (see **Figure 4.16a**), and the XRD trace of the as cast sample of glass 10(air) (**Figure 4.19a**) shows that even at a 35wt% waste loading air sparged simulated HLW glasses remain XRD amorphous. Volf (1984) states that silver readily diffuses

into glasses as Ag^+ ions in the presence of oxygen which correlates well with the absence of silver metal in the air sparged glasses. However, the development of silver metal in the heat treated glass 10(air) sample indicates that without constant reoxidation of the metal via an oxidising sparge, the level of silver in a 35wt% waste loading is greater than the solubility limit in the glass.

The EXAFS work on the as cast glasses 7 and 10 provided important information on the immediate environment of the Mo in these samples. All of the Fourier transforms, regardless of waste loading and melting atmosphere, look similar with a large peak at ~1.76Å from the Mo centre and no other peaks at higher distances. These results have a good fit with a model of a Mo centre bonded to 4 oxygen atoms in tetrahedral coordination at equal distances of ~1.76Å. This indicates that the Mo in these glasses exists as $(MoO_4)^{2-}$ units independent of the glass network and charge balanced by random cations. If the Mo were linked to the network via a Mo-B or Mo-Si bond, then this would be apparent as a distinct peak on the Fourier transform at a distance other than 1.76Å. If the Mo was linked to the network via a bridging oxygen to a boron or silicon atom, then it should be possible to observe a second coordination shell outside of the oxygen shell. Similarly, the randomness of the charge balancing is also indicated by the lack of a second coordination shell outside of the oxygen shell. If the charge balancing was performed by the same species for all of the molybdate tetrahedra, then a second coordination shell at a distinct distance from the Mo centre would be observed (as seen in the $CaMoO_4$ and $SrMoO_4$ standards – see **Chapter 5.3.5**). Similar results were obtained by Calas *et al* (2003) upon EXAFS analysis of 3 glasses based on the SON 68 composition (the French light water reactor waste glass which has a comparable composition to the standard glass composition, glass 1, used in this work). Calas also used computer simulations of simplified HLW glass networks to show that the MoO_4 tetrahedra are likely to exist within alkali and alkaline earth rich sublattices in the network.

Upon heat treatment, the only samples that showed a marked difference in devitrification behaviour were glass 7(air) and glass 7 (red). With a waste loading of 25wt% and above (glasses 8 – 10), all of the glasses, regardless of the type of gas used for sparging, devitrified to form the same powellite type molybdate (analogous, given the simulated HLW stream composition used for these melts, to yellow phase).

However, glass 7(air) showed no evidence of devitrification after heat treatment when subjected to XRD or TEM analysis (**Figure 4.25a**) whereas the powellite type molybdate seen in the higher waste loading glasses can clearly be observed in the heat treated glass 7(red) (**Figure 4.25b**). Thus, an immediate conclusion that can be drawn from this evidence is that even for glasses with relatively low (for this work, 20wt%) waste loadings, a reducing sparge produces phase separated as cast products, which have an increased tendency to devitrify upon heat treatment when compared to air sparged glasses with identical compositions. The EXAFS analysis of the heat treated glass 10(red) sample gave the same results as those of the as-cast samples of glasses 7 and 10. The XRD and TEM data showed that this sample contained a crystalline phase incorporating Mo, and thus the absence of a second well defined coordination shell in the EXAFS data outside of the oxygen shell indicates that the powellite type molybdate phase that develops in these simulated HLW glasses upon heat treatment also has a random arrangement of cations in its structure. The EDS analysis of the crystalline molybdate performed under TEM also shows that the phase incorporates Sr and lanthanide elements, and it is also possible that Li is present in this phase although this element is too light to be detected using the EDS system and thus cannot be observed in the results. However, the phase may only contain di and trivalent cations (in the form of Sr and lanthanides) with the charge imbalance being accounted for by the presence of vacancies on the A site of the compound (see **Chapter 2.3**).

The XRD and EXAFS data contradicts the suggestion made by Lutze (1988) that melting in a reducing atmosphere could reduce the oxidation state of the Mo in the glasses, and thus decrease the tendency for yellow phase formation. It would appear that the reducing sparge did not reduce enough of the Mo^{6+} in the batch during melting to prevent it from forming $(MoO_4)^{2-}$ units in the glass, which are then incorporated into the powellite type molybdates (analogous to yellow phase) that form when the glasses are heat treated. It is unlikely that the Mo in the reduced sample could have reoxidised during the heat treatment (even though it was performed in an air atmosphere), as the temperature was not sufficient to allow the glass to flow, and therefore the bulk of the sample would not have been exposed to oxygen in the furnace. Furthermore, the reducing sparge caused a glass with a 20wt% loading to devitrify upon heat treatment, whereas the same glass melted under an air atmosphere showed no evidence of devitrification upon heat treatment. This fact suggests that the

reducing sparge increases the number of potential nucleation sites for powellite type molybdates in the glasses. An obvious candidate for these nuclei is metallic silver which was present in the as cast glass 7(red), but not in as cast glass 7(air). However, no metallic silver was observed in the XRD of as cast samples of glasses 8 – 10(air), and all of these glasses developed the same powellite type molybdate phase that was observed in the reduced samples after heat treatment. It is possible that metallic silver could have developed in the air sparged glasses upon heat treatment and then served as a nucleation centre for the molybdate phase – Weyl (1959) reports that silver particles increase in size in phosphate glasses under heat treatment, and it was noted during TEM of a heat treated sample of glass 7(red) that the molybdate dendrites tended to be more abundant in close proximity to silver particles than in the rest of the matrix. A further experiment that could answer this question would be to re-melt glasses 7-10 but with Ag omitted from the batch (time constraints made this experiment unfeasible in the present work). The reduction of Mo^{6+} in simulated HLW glasses is discussed further in **Chapter 6**.

The only evident drawback of the compressed air sparge seems to be the tendency for the glasses to retain bubbles prior to pouring. All of the glasses were melted at the same temperature with the same gas flow rate through the glass, but **Figures 4.11a** and **4.16a** clearly show that glasses 7(air) and 9(air) were of increased viscosity relative to the other melts performed in this section, as they contain significantly more bubbles. This would be a problem if it were to occur in the real vitrification process as it would decrease the mechanical strength of the glass and, more importantly, would increase the volume of a given weight of glass, a property that ideally needs to be decreased to promote efficiency in the vitrification process as a whole. The reason for this apparent increase in viscosity is at present unclear, but could be due to a cooling effect caused by the gas sparge. However, the differences in bubble retention in glasses 7(air) and 9(air), and 8(air) and 10(air) demonstrate a strong dependence of glass quality on outside factors (such as the partial pressure of oxygen in the atmosphere on any given day). Further work which could possibly furnish an answer to this problem would be to perform the same melts in a closed system (such as an autoclave) in which the prevailing factors such as pO_2 could be closely controlled (again, a lack of time made prevented these experiments from being carried out for this thesis).

It is apparent that the sparge applied during melting can strongly affect the quality of the glass produced. Currently, a compressed air sparge is used in the UK, but this is primarily for promoting mixing and homogeneity in the melt, and to try to prevent heal formation in the melter. The formation of heels (a layer of metallic fission products and oxides with greater density than the overall melt that can form at the bottom of the melter) is a problem that needs to be avoided to increase the efficiency of the vitrification process, as once they reach a certain depth the melter can no longer be used for vitrification as pouring the glass from it become impossible. Processing of the concentrated heel glass is also a problem. It is possible that tailoring the composition of the gas used for sparging could help to reduce or prevent heal formation. It is known that the French AVM process (which is very similar to that used in Sellafield) employs an argon sparge during melting (Vernaz, private communication), although the reason for this is unclear. Although Ar is a noble gas and would not therefore create a reducing atmosphere, purging the melting atmosphere of all other gases would prevent oxygen from the atmosphere affecting the redox state of the elements in the glass. However, given a real HLW stream composition, it would appear that a reducing sparge would tend to increase the likelihood of yellow phase formation (although there is some contrary evidence for this, see **Chapter 6**), and would tend to increase the tendency for the formation of heavy metals such as Pt, Pd etc (for which Ag is used as an analogue in this work) in the melt, and therefore worsen the problem of heel formation.

4.5 Conclusions

• Simulated HLW glasses melted under a reducing sparge tend to phase separate even at low (20wt%) waste loadings.

• Glasses containing a 20wt% waste loading and melted in an air atmosphere produce homogeneous glasses that show no tendency to devitrify upon heat treatment.

• Glasses with low (20wt%) waste loadings show an increased tendency to phase separate during melting and to devitrify upon heat treatment when sparged with a reducing gas during melting, compared to those sparged with compressed air.

• Glasses containing ≥25wt% waste tend to devitrify upon heat treatment to produce powellite type molybdate phases analogous to yellow phase, regardless of the melting atmosphere.

• The powellite type molybdate phase contains elevated levels Sr and lanthanide elements.

• Reducing the Li content of glasses containing 35wt% waste reduces the number of crystalline phases formed upon heat treatment.

• Mo is present as distinct $(MoO_4)^{2-}$ units charge balanced by random cations in simulated HLW glasses, regardless of melting atmosphere and subsequent heat treatments.

5. Molybdate Formation

5.1 Introduction

As mentioned in **Chapter 4**, the formation of molybdates in HLW glass production usually leads to a deterioration in the quality of the product. In full scale simulated HLW glass products, the molybdates are usually found in yellow phase, a mixture of alkali sulphates, chromates and molybdates. As was seen in the previous chapter, the molybdates that have been identified in the heat treated HLW glass simulations in this work have all been powellite-type molybdates. Powellite has a tetragonal unit cell and with the space group $I4_1/a$. Powellite is a calcium molybdate with the formula $CaMoO_4$ and is analogous to the more widely known mineral scheelite, $CaWO_4$. Indeed, powellite and its derivatives (such as $SrMoO_4$, $BaMoO_4$ etc) are often referred to as scheelites, or scheelite-type molybdates. The unit cell of powellite is shown in **Figure 2.2**, and the structure is outlined below in **Figure 5.1.**

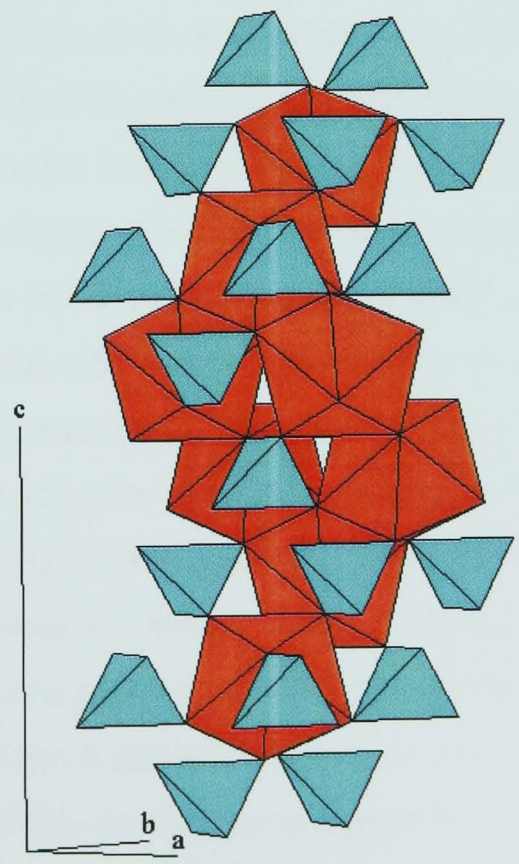

Figure 5.1 – Outline of powellite structure showing molybdate tetrahedra (blue) and calcia octahedra (red)

Much of the published literature surrounding powellite type molybdates stems from interest in their optical properties for use in applications such as solid state lasers (Christofilos *et al*, 1995). Indeed, these molybdates exhibit a great deal of diversity with respect to the ions they are capable of incorporating into the powellite type structure. If the general formula is taken as $AMoO_4$, then from the literature alone one can find many distinct ions, and combinations of ions, that can occupy the A site whilst the molybdate retains its powellite type structure. For example, Schieber and Holmes (1964) grew a range of $Na_{0.5}Ln_{0.5}MoO_4$ (where Ln = Nd→Yb) crystals and $Ag_{0.5}Ln_{0.5}MoO_4$ (where Ln = La→Nd and Sm) compounds were made by Shi *et al* (1995). Li derivatives of these compounds have also been synthesised by Schieber, (1965), along with molybdates containing both divalent and trivalent cations such as $Sr_{0.9}Gd_{0.1}MoO_4$. The author explained the charge imbalance in the latter case by proposing either a reduction in oxidation state of the hexavalent Mo, or the presence of vacancies on some of the di and trivalent cation sites. The presence of pentavalent Mo is suggested by Preziosi *et al* (1962) to account for charge imbalances in the molybdates they studied, although the presence of vacancies on the alkali and rare earth sites is the explanation that tends to be favoured when accounting for charge imbalance in the more recent papers on the subject (e.g. Teller, 1992). In all cases where comments are made on the cation (and vacancy) distribution within the crystal structure, the consensus is that they are randomly distributed rather than ordered. Muller (1974) devotes a chapter of his book on ternary structures to ABX_4 compounds and discusses the scheelite structure at length, especially in relation to the range of cations (and combinations of cations) that can occupy the A and B sites of scheelite structured ABX_4 compounds. He also discusses crystallographic relationships between the scheelite structure and other related ABX_4 structures such as wolframite and fergusonite, for example the transition to a scheelite structure that occurs for many M-fergusonite structures at high temperature. Muller illustrates these relationships between crystal structures mainly through the use of structure field maps charting the ionic radii of the A and B site cations in relation to the structures that they form. An example of this can be seen in **Figure 5.2**.

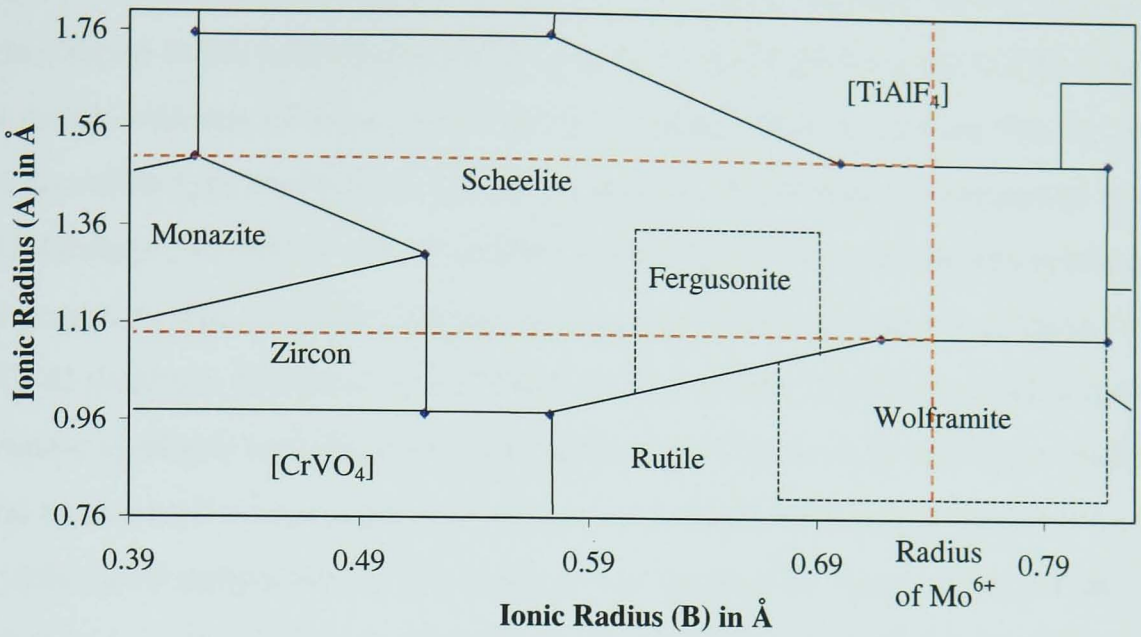

Figure 5.2 – Enlargement of scheelite region of ABO_4 structure field map (from figure 22, Muller, 1974)

Given the composition of the simulated HLW glasses in this work, there is a large scope for molybdate formation. The molybdates that could theoretically be formed from the HLW glass composition and that have files in the ICDD database are shown in **Table 5.1**.

$SrMoO_4$ [85-586]	$Sr_{0.5}Ba_{0.5}MoO_4$ [30-157]	$Li_{0.5}Y_{0.5}MoO_4$ [17-773]	$Na_{0.5}Y_{0.5}MoO_4$ [82-2368]	
$BaMoO_4$ [29-193]		$Li_{0.5}La_{0.5}MoO_4$ [18-734]	$Na_{0.5}La_{0.5}MoO_4$ [79-2243]	$Ag_{0.5}La_{0.5}MoO_4$ [49-384]
		$Li_{0.5}Ce_{0.5}MoO_4$ [84-539]	$Na_{0.5}Ce_{0.5}MoO_4$ [79-2242]	$Ag_{0.5}Ce_{0.5}MoO_4$ [49-381]
		$Li_{0.5}Nd_{0.5}MoO_4$ [23-1195]	$Na_{0.5}Nd_{0.5}MoO_4$ [25-852]	
		$Li_{0.5}Sm_{0.5}MoO_4$ [18-745]		$Ag_{0.5}Sm_{0.5}MoO_4$ [49-383]
		$Li_{0.5}Gd_{0.5}MoO_4$ [18-728]	$Na_{0.5}Gd_{0.5}MoO_4$ [25-828]	

Table 5.1 - Relevant powellite type molybdate phases that have been fully characterised in the ICDD database. The relevant card numbers are shown as [#].

As was mentioned in the previous chapter, several close matches for the molybdates that developed in the heat treated HLW glasses were found from the ICDD, but no exact match with any of these phases could be made. Thus, it is likely that the phase was a powellite type molybdate, but of a composition that was not contained in the ICDD database. To aid the identification of this phase, it was decided to synthesise some powellite type molybdate phases with compositions alternative to those found in the ICDD database. Previous workers had used a number of different techniques for molybdate synthesis including the flux method, the Czochralski technique (pulling a crystal from a melt whilst rotating it) and slow cools from stoichiometric melts. For the synthesis of molybdates in this work, it was decided to sinter mixed oxide powders in a similar fashion to Mokhosoev *et al* (1969) who prepared rubidium-rare earth molybdates, as this seemed to be the least complicated method and to give satisfactorily pure phases.

5.2 Experimental

The synthesis method for the molybdate compounds is described fully in **Chapter 3.9**. The compositions of these molybdates were chosen for the following reasons:

5.2.1 Ag Series – Having observed the wide range of alkali-rare earth powellite type molybdates that had previously been synthesised, it was suspected that it would be possible to mix two rare earth ions on the A site of this structure, hence the Ag-La-Gd composition. $Ag_{0.5}Ce_{0.5}MoO_4$ was prepared as a firing schedule test compound (as has already been explained in **Chapter 3.9**), and $Ag_{0.5}Gd_{0.5}MoO_4$ was prepared for comparison purposes (as is explained fully in the results section of this chapter).

5.2.2 Nd Series – These compositions were chosen in order to attempt to establish limiting ionic radii for the alkali metal ions that could occupy the A site. Nd was used as the rare earth in all cases as it is the most prevalent rare earth in the simulated waste stream.

5.2.3 Di-alkali Series – The molybdate compositions for this series were chosen to further explore the cation mixing possibilities on the A site of these compounds. Again, Nd was used as the rare earth for the same reason as noted above.

5.2.4 Triple Valency Series – To test further the cation incorporation properties of these molybdates, compositions including mono, di and trivalent cations were prepared.

5.2.5 Yellow Phase and Standards – A sample of yellow phase material (~0.5g) was removed from a sample of simulated Magnox waste glass melted in a full scale vitrification plant at Sellafield. This material was analysed by XRD and EXAFS along with samples of $CaMoO_4$ and $SrMoO_4$ used as standards for comparison. The composition of the Magnox waste glass is given in **Table 5.2** below.

Oxide	Weight %	Oxide	Weight %
SiO_2	46.10	SrO	0.30
TiO_2	0.01	NiO	0.37
Al_2O_3	6.58	B_2O_3	15.9
Fe_2O_3	3.00	Li_2O	4.07
CaO	0.01	RuO_2	0.70
MgO	5.74	MoO_3	1.62
K_2O	0.01	Cs_2O	1.11
Na_2O	8.29	Nd_2O_3	1.44
P_2O_5	0.26	Sm_2O_3	0.22
Cr_2O_3	0.58	CeO_2	0.84
ZrO_2	1.45	La_2O_3	0.48
HfO_2	0.02	Pr_6O_{11}	0.44
BaO	0.50	Y_2O_3	0.10

Table 5.2 – Composition of Magnox waste glass with a 25.62wt% waste loading melted on the full scale vitrification plant at Sellafield, from which yellow phase sample was taken.

5.3 Results

5.3.1 Ag Series

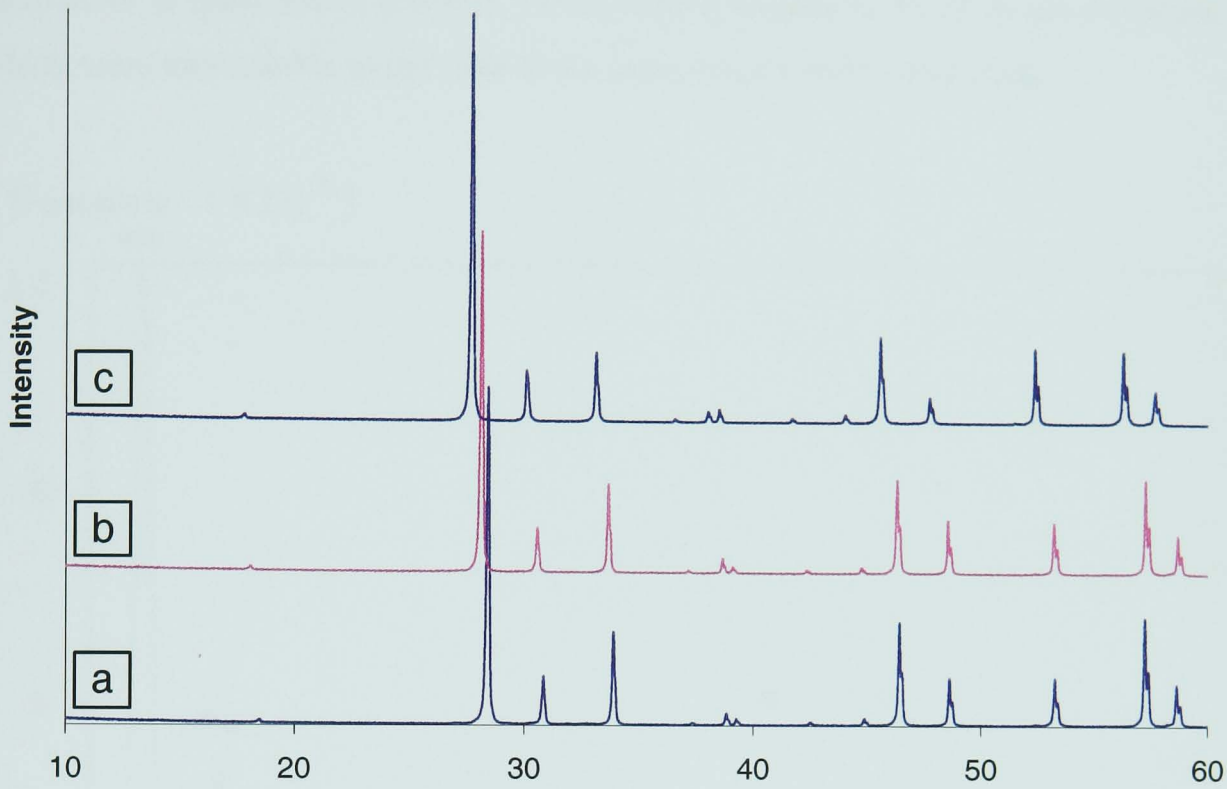

Figure 5.3 – XRD of (**a**)$Ag_{0.5}Gd_{0.5}MoO_4$, (**b**)$Ag_{0.5}La_{0.25}Gd_{0.25}MoO_4$ (**c**)$Ag_{0.5}Ce_{0.5}MoO_4$

As can been seen from **Figure 5.3**, the x-ray diffraction patterns of the Ag series of molybdates indicate that all 3 batches formed single phase powellite type molybdates on firing. In the case of the Ag-Ce molybdate (**Figure 5.3c**), this can be inferred from the d-spacings of the reflections on the XRD pattern, all of which match those recorded in the ICDD database for that compound (card [49-381]) to within 0.05Å. There are no reflections present on the XRD that cannot be accounted for by comparison with the Ag-Ce molybdate file from the ICDD database (although some of the reflections at higher angles did exhibit $k\alpha_2$ splitting). The XRD patterns of the Ag-Gd and Ag-La-Gd molybdates are similar to that of the Ag-Ce molybdate although shifted to slightly lower angles (for the Ag-La-Gd as compared to the Ag-Ce, and the Ag-Gd as compared to the Ag-La-Gd) and therefore slightly higher d-spacings. This was to be expected as larger ions were being substituted into identical unit cells.

An EDS analysis was also performed on the Ag-La-Gd molybdate (**Figure 5.4**). By examining the heights of the elemental peaks, it can be seen that there are similar amounts La and Gd in this powder, approximately twice the amount of Ag and approximately four times the amount of Mo. These results are however only qualitative as quantitative analysis would require standards for all of the elements, which were unavailable at the time these experiments were conducted.

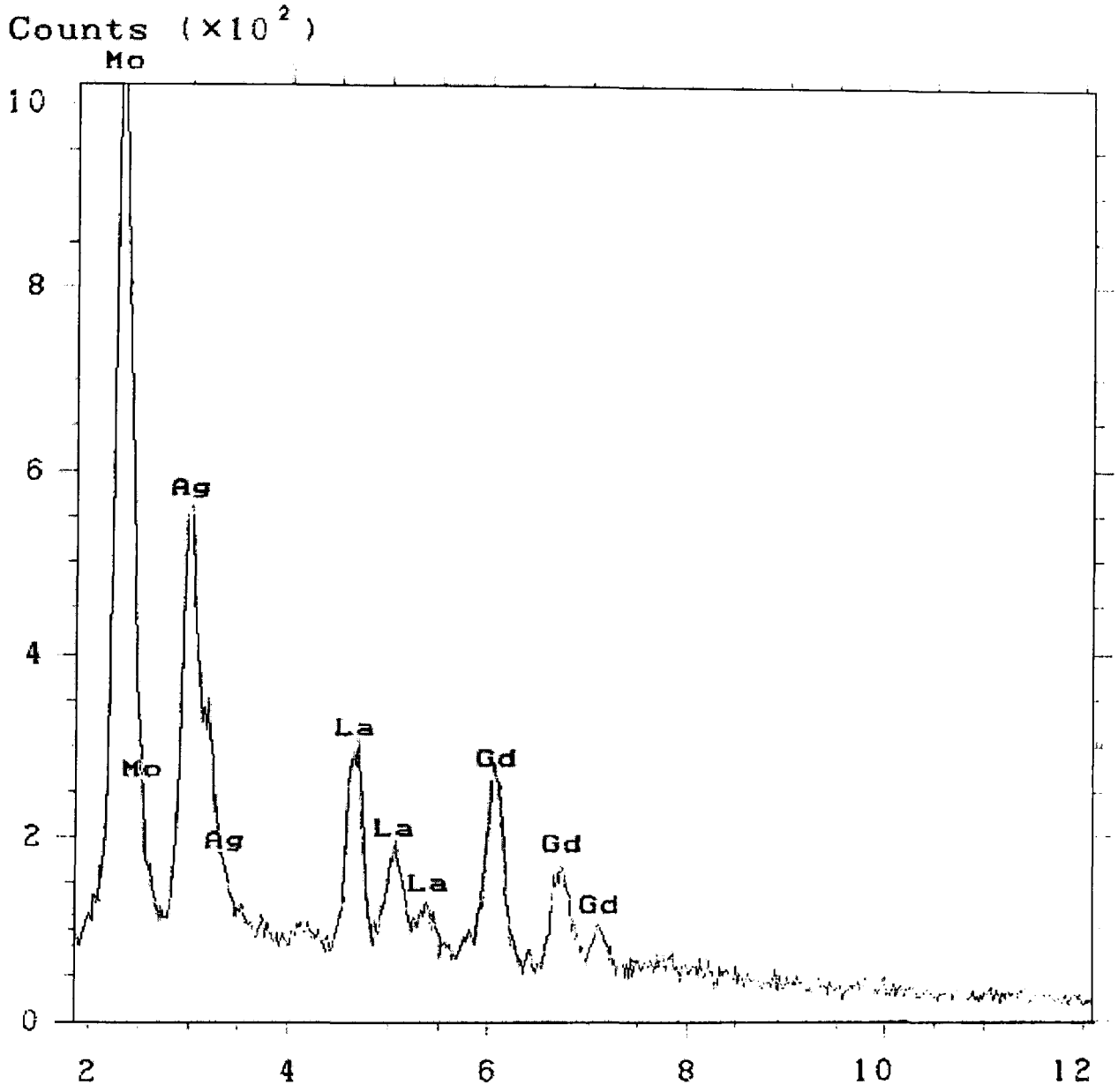

Figure 5.4 – EDS analysis of $Ag_{0.5}La_{0.25}Gd_{0.25}MoO_4$

Further evidence for the formation of single phase molybdates in the cases of the Ag-Gd and Ag-La-Gd molybdates was obtained by constructing a theoretical model of the unit cells of these compounds using the crystallography program Carine 3.1. The cells were assigned a tetragonal $I4_{1/a}$ space group and the atomic positions were obtained from the well characterised $CaMoO_4$ unit cell (with the relevant cations being substituted onto the Ca positions and given the appropriate occupancy). The XRD

patterns of the sintered Ag-Gd and Ag-La-Gd molybdate compounds were indexed by comparison to the Ag-Ce pattern (assuming that both the Ag-Gd and Ag-La-Gd compounds were single phase) and the lattice parameters for the theoretical cells were derived from the d-spacings of the assigned (200) and (004) planes. **Figures 5.5a** and **5.5b** below show the XRD patterns generated by Carine from the theoretical Ag-Gd and Ag-La-Gd unit cells respectively, superimposed on the actual XRD patterns from the sintered compounds.

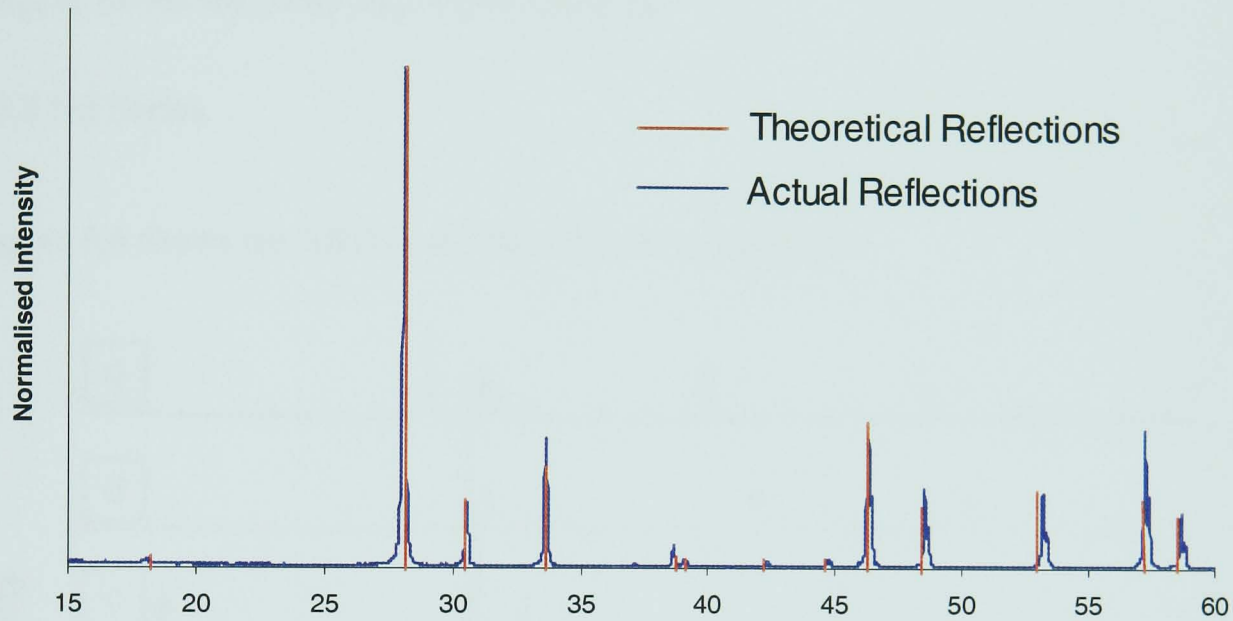

Figure 5.5a – Comparison of ideal and real $Ag_{0.5}Gd_{0.5}MoO_4$ XRD patterns

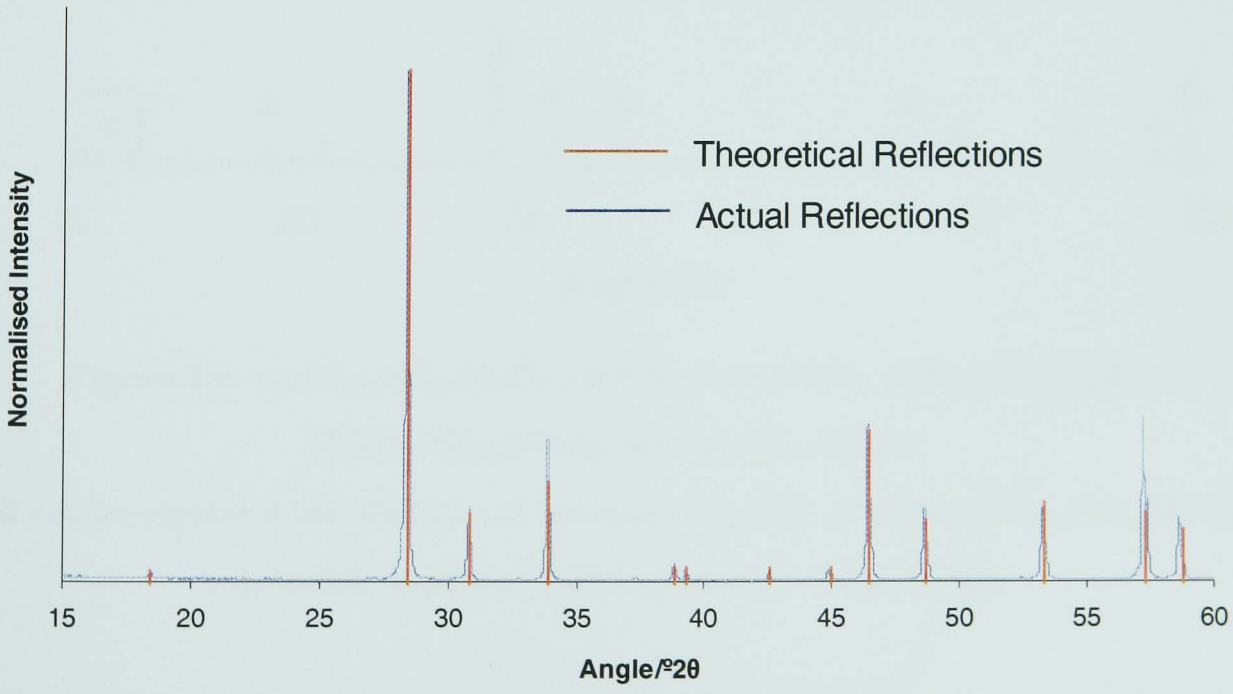

Figure 5.5b – Comparison of ideal and real $Ag_{0.5}La_{0.25}Gd_{0.25}MoO_4$ XRD patterns

The comparisons show that the sintered compounds are close to the ideal compositions as the reflections overlap, although there is a slight deviation of the positions of the reflections at higher angles for the ideal Ag-Gd molybdate (**Figure 5.5a**) and the real sintered compound. This could be due to slight errors in the lattice parameter calculation for the ideal cell, which would be more accurate if they were derived from the (008) and (400) d-spacings of the sintered compound. However, at the time of print, the sintered compounds had not been x-rayed over a large enough range to obtain the (008) and (400) reflections.

5.3.2 Nd Series

Figure 5.6 shows the XRD of the Nd series of molybdates.

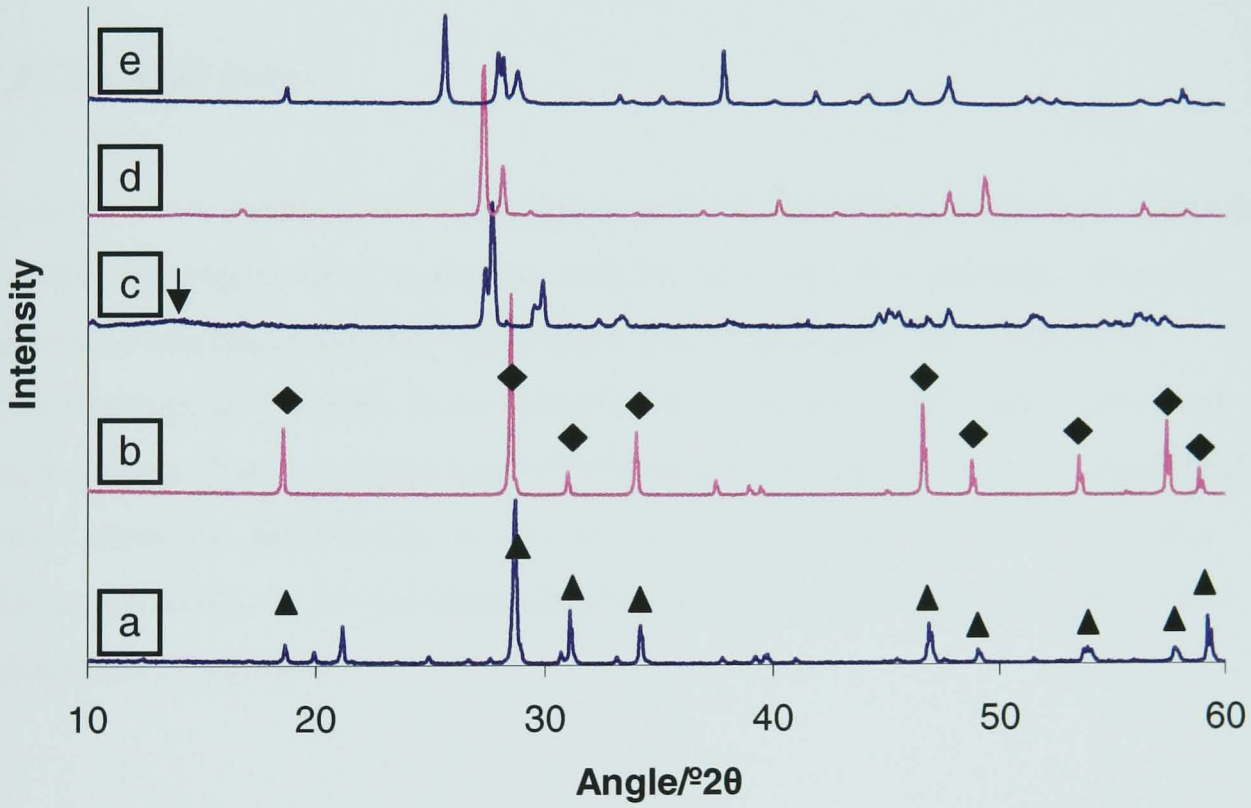

Figure 5.6 – (**a**)$Li_{0.5}Nd_{0.5}MoO_4$, (**b**)$Na_{0.5}Nd_{0.5}MoO_4$, (**c**)$K_{0.5}Nd_{0.5}MoO_4$, (**d**)$Rb_{0.5}Nd_{0.5}MoO_4$, (**e**) $Cs_{0.5}Nd_{0.5}MoO_4$.

▲s & ♦s represent the positions of the major $Li_{0.5}Nd_{0.5}MoO_4$ and $Na_{0.5}Nd_{0.5}MoO_4$ powellite-type molybdate reflections respectively

Both the Li and Na-Nd molybdates (**a** and **b** in **Figure 5.6**) formed compounds with good matches to the ICDD files for these compositions (cards [23-1195] and [25-852] respectively). However, 2 small reflections at 20°2θ and 22°2θ on the Li-Nd

molybdate pattern indicate that not all of the batch components were incorporated into the $Li_{0.5}Nd_{0.5}MoO_4$ structure. The K-Nd composition (**c** in **Figure 5.6**) showed a good match to the ICDD file [32-817], a monoclinic crystal, although the presence of a small amorphous hump in the 12-17 $^{o}2\theta$ region of the XRD trace (labelled with an arrow in **Figure 5.6c**) indicates that the compound was not single phase in this case. The Rb-Nd molybdate (**d** in **Figure 5.6**) produced a large number of reflections under XRD, although no matches for any of these could be found in the ICDD files. The reflections do not appear to correspond well to other powellite-type molybdate patterns, so it can be assumed that this phase is not a powellite-type molybdate structure. The Cs-Nd molybdate (**e** in **Figure 5.6**) showed a good match with card [49-1015] for $CsNd(MoO_4)_2$, which has an orthorhombic structure with a Pccm space group.

5.3.3 Di-alkali Series

As there are no entries in the ICDD database for di-alkali type molybdates, it was not possible to compare them to previous data for these type of compounds. Thus, to determine whether or not they were single phase and if they were likely to be powellite-type molybdates, direct comparisons to the above diffraction patterns of known single phase powellite-type molybdate compositions were made. **Figure 5.7** below shows the XRD results of scans of the di-alkali series, and also shows the diffraction pattern of an identified powellite-type molybdate ($Na_{0.5}Nd_{0.5}MoO_4$) for comparative purposes.

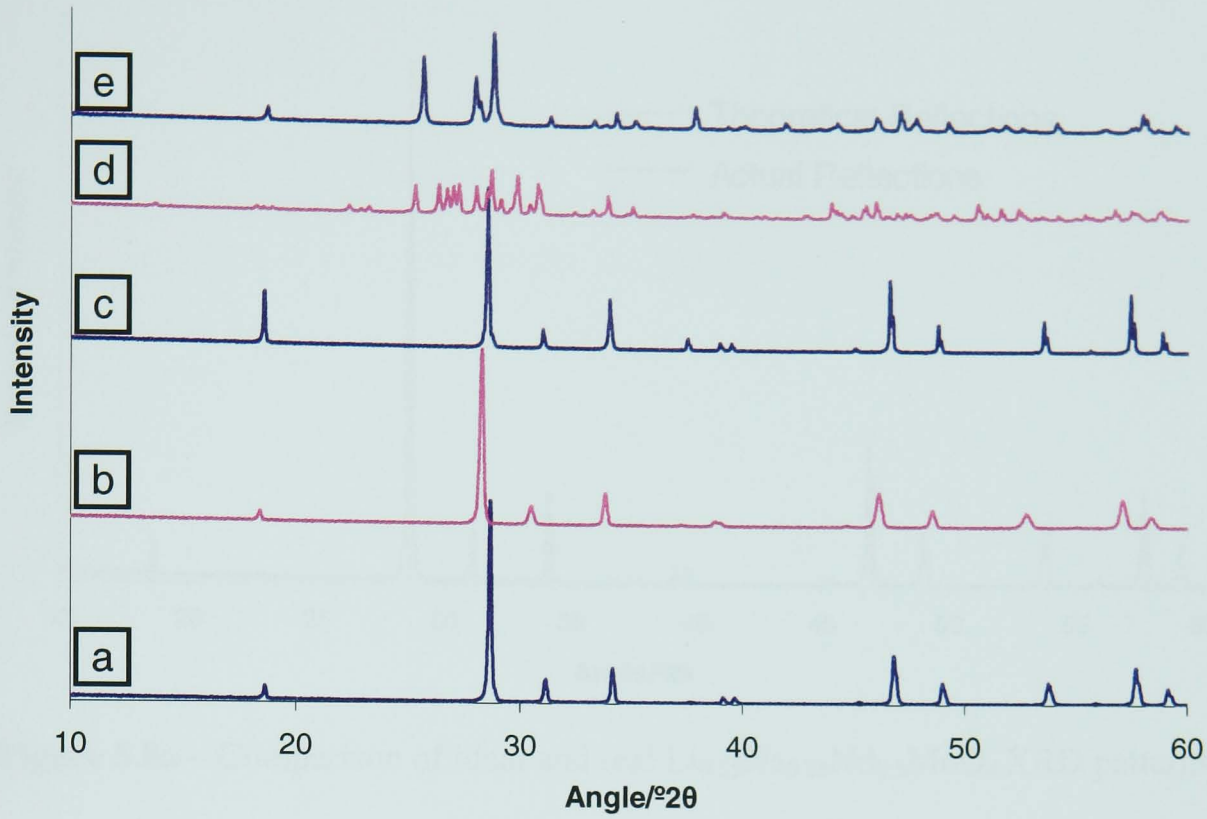

Figure 5.7 – (**a**)$Li_{0.25}Na_{0.25}Nd_{0.5}MoO_4$, (**b**)$Li_{0.25}K_{0.25}Nd_{0.5}MoO_4$, (**c**)$Na_{0.5}Nd_{0.5}MoO_4$ (for comparison), (**d**)$Li_{0.25}Rb_{0.25}Nd_{0.5}MoO_4$, (**e**)$Li_{0.25}Cs_{0.25}Nd_{0.5}MoO_4$,

As can be seen, the reflections caused by the Li-Na-Nd and Li-K-Nd molybdates (**a** and **b** respectively in **Figure 5.7**) are similar to the known single phase Na-Nd molybdate reflections, although the reflections are slightly shifted to lower angles (an effect caused by having larger ions and correspondingly larger d-spacings in the same unit cell). However, the Li-Rb-Nd and Li-Cs-Nd compositions (**d** and **e** respectively in **Figure 5.7**) appear to have formed multiphase powders upon sintering judging by the number of reflections, and do not correspond well to previous powellite-type molybdate diffraction patterns. No good matches were obtained when these reflections were compared to those in the ICDD database.

Theoretical unit cells were constructed for the Li-Na-Nd and Li-K-Nd molybdates using the same method as described in **section 5.3.1**. **Figures 5.8a** and **5.8b** show the theoretical reflections from the idealised unit cells superimposed upon the real XRD patterns obtained from the Li-Na-Nd and Li-K-Nd molybdates respectively.

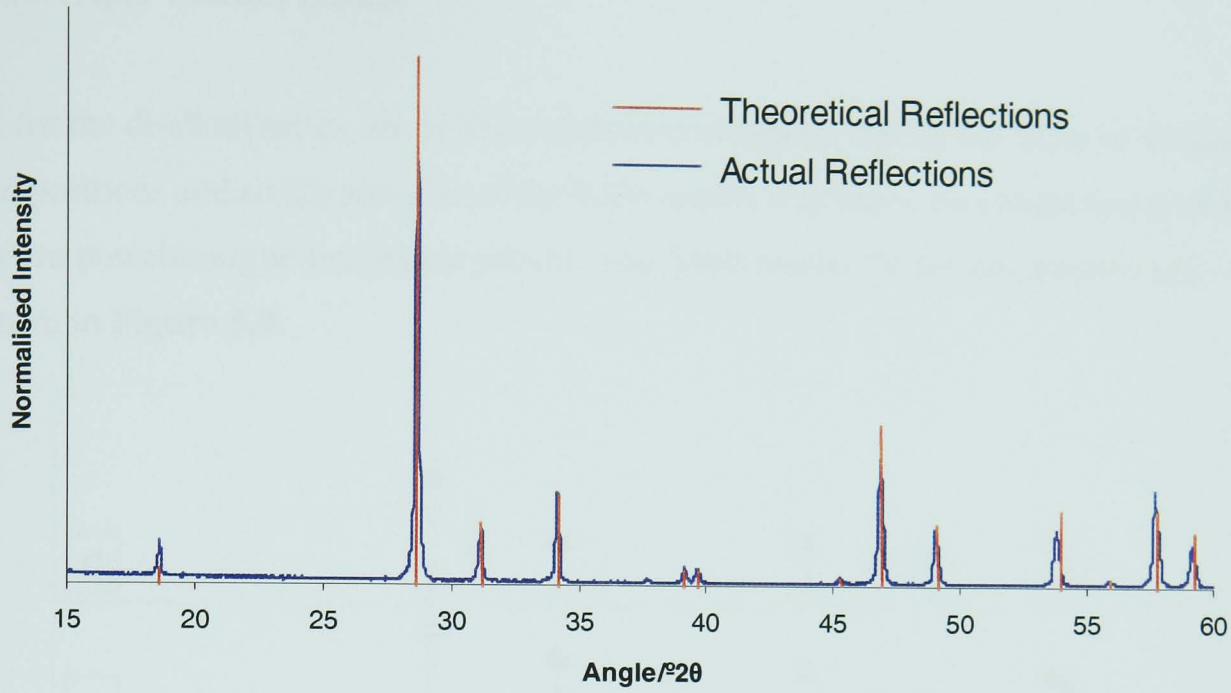

Figure 5.8a – Comparison of ideal and real $Li_{0.25}Na_{0.25}Nd_{0.5}MoO_4$ XRD patterns

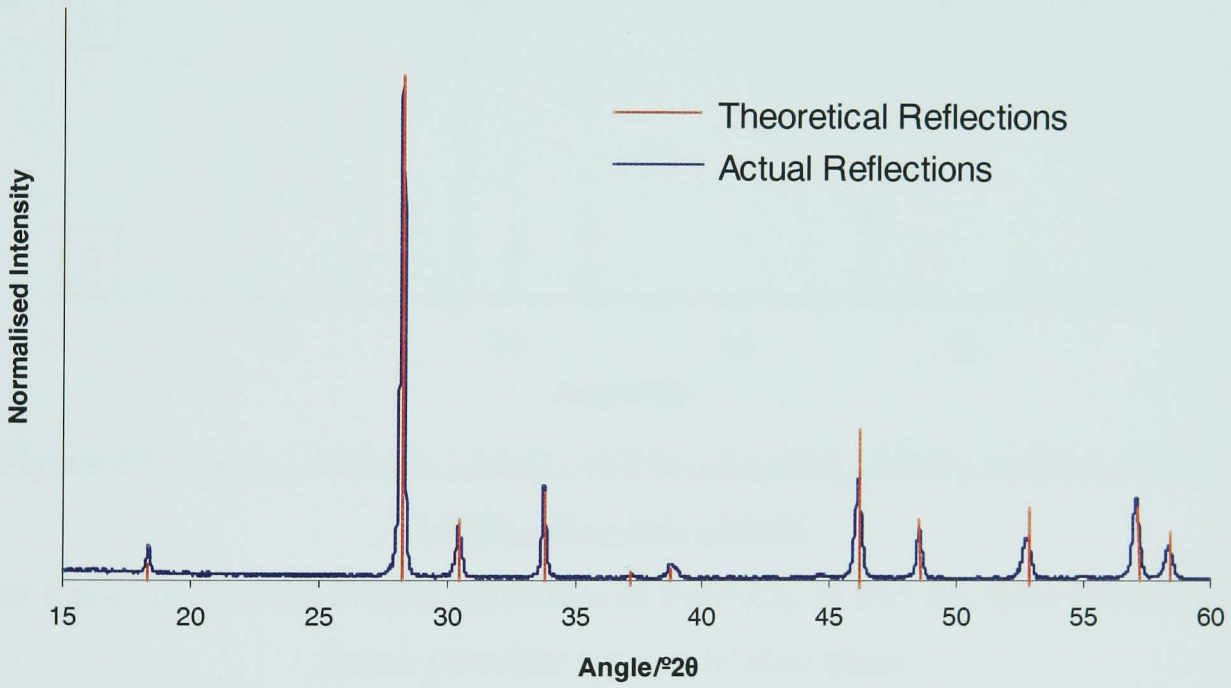

Figure 5.8b – Comparison of ideal and real $Li_{0.25}K_{0.25}Nd_{0.5}MoO_4$ XRD patterns

As for the Ag-Gd and Ag-La-Gd molybdates, there is a close overlap of the calculated XRD reflections for the ideal Li-Na-Nd and Li-K-Nd molybdate unit cells, and the real XRD patterns from the sintered molybdates. This indicates that the sintered compounds are close to the ideal powellite type structures for these compositions.

5.3.4 Triple Valency Series

As for the di-alkali series, the ICDD database contains no entries for these or similar compositions and so the analysis of the XRD results was based on comparisons with known powellite-type molybdate phases. The XRD results for the compounds are shown in **Figure 5.9.**

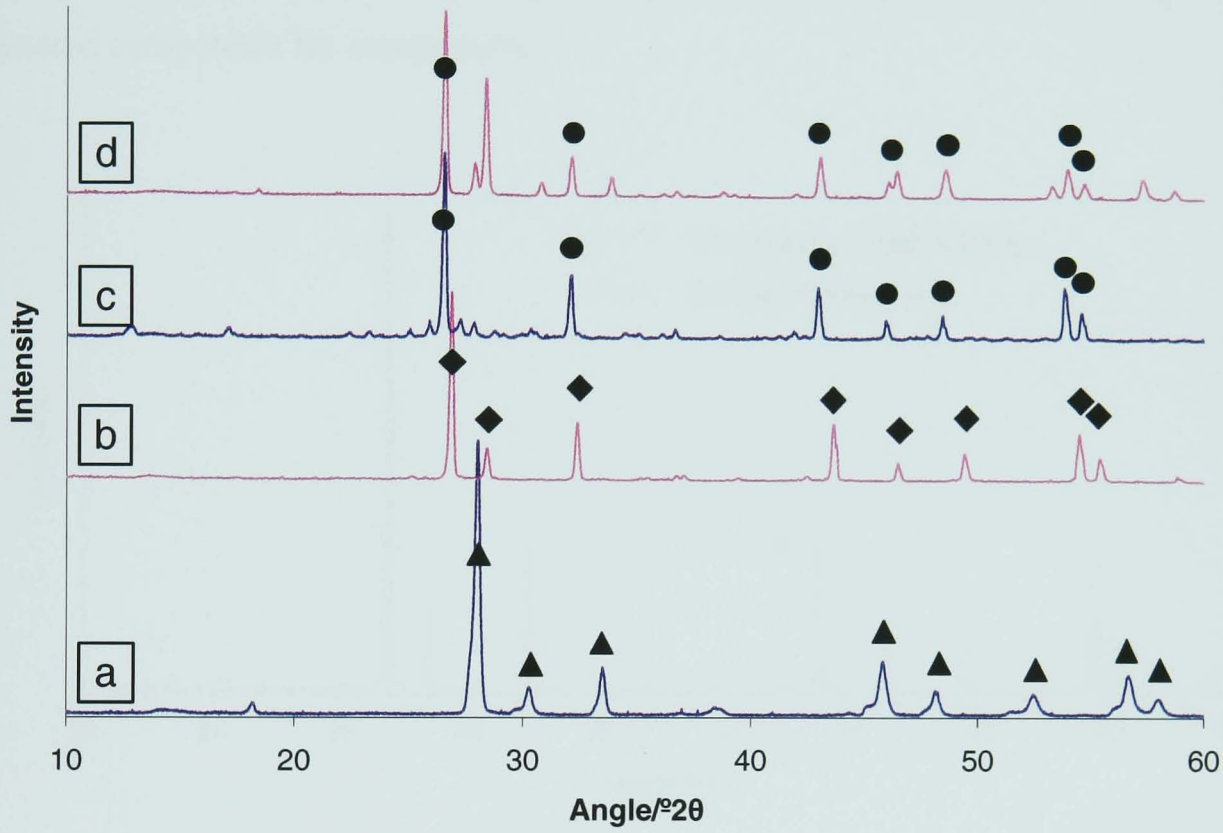

Figure 5.9 – (**a**)$K_{0.25}Ba_{0.5}La_{0.25}MoO_4$, (**b**)$Na_{0.25}Sr_{0.5}Nd_{0.25}MoO_4$, (**c**)$KBa_{0.5}MoO_4$, (**d**)$Na_{0.25}Ba_{0.5}Nd_{0.25}MoO_4$

●s represent the most intense reflections of $BaMoO_4$, ♦s and ▲s show reflections from a powellite type molybdate phase

It can be seen from the XRD data that the K-Ba-La and Na-Sr-Nd molybdates (**a** and **b** respectively in **Figure 5.9**) both display diffraction patterns similar to that for the known powellite-type molybdate $Na_{0.5}Nd_{0.5}MoO_4$ (**Figure 5.6**), and the lack of extraneous peaks suggest that these compounds are single phase. The K-Ba and Na-Ba-Nd molybdate compositions (**c** and **d** respectively in **Figure 5.9**) displayed a large number of reflections, some of which (labelled ● in **Figure 5.9**) matched those of $BaMoO_4$ (card [29-193] from the ICDD database) indicating that this compound had formed preferentially over the intended K-Ba and Na-Ba-Nd molybdate compositions. Thus, the other unidentified reflections in **Figures 5.9c** and **5.9d** are likely to have

been caused by K and Na-Nd rich phases respectively, and their presence confirms that these compounds are not single phase molybdates.

Theoretical unit cells were constructed for the ideal $K_{0.25}Ba_{0.5}La_{0.25}MoO_4$ and $Na_{0.25}Sr_{0.5}Nd_{0.25}MoO_4$ powellite type compositions using the same method described in **section 5.3.1**. The calculated XRD reflections of the ideal unit cells are presented in **Figures 5.10a** and **5.10b** superimposed upon the XRD patterns from the real sintered compounds for comparison.

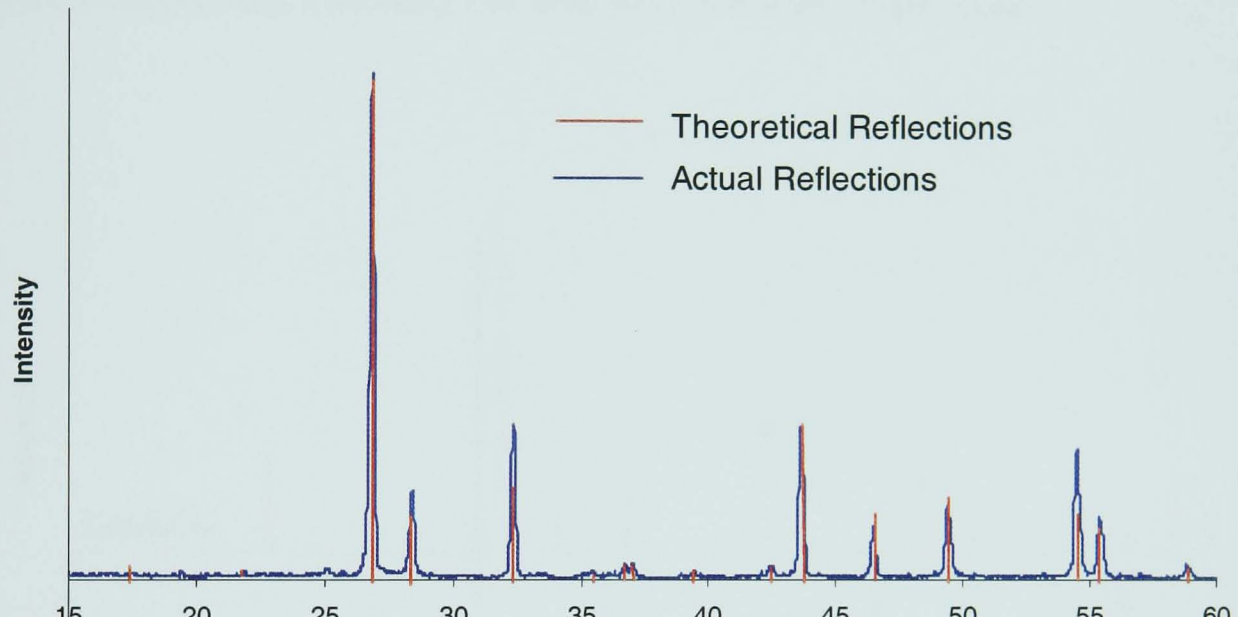

Figure 5.10a – Comparison of ideal and real $K_{0.25}Ba_{0.5}La_{0.25}MoO_4$ XRD patterns

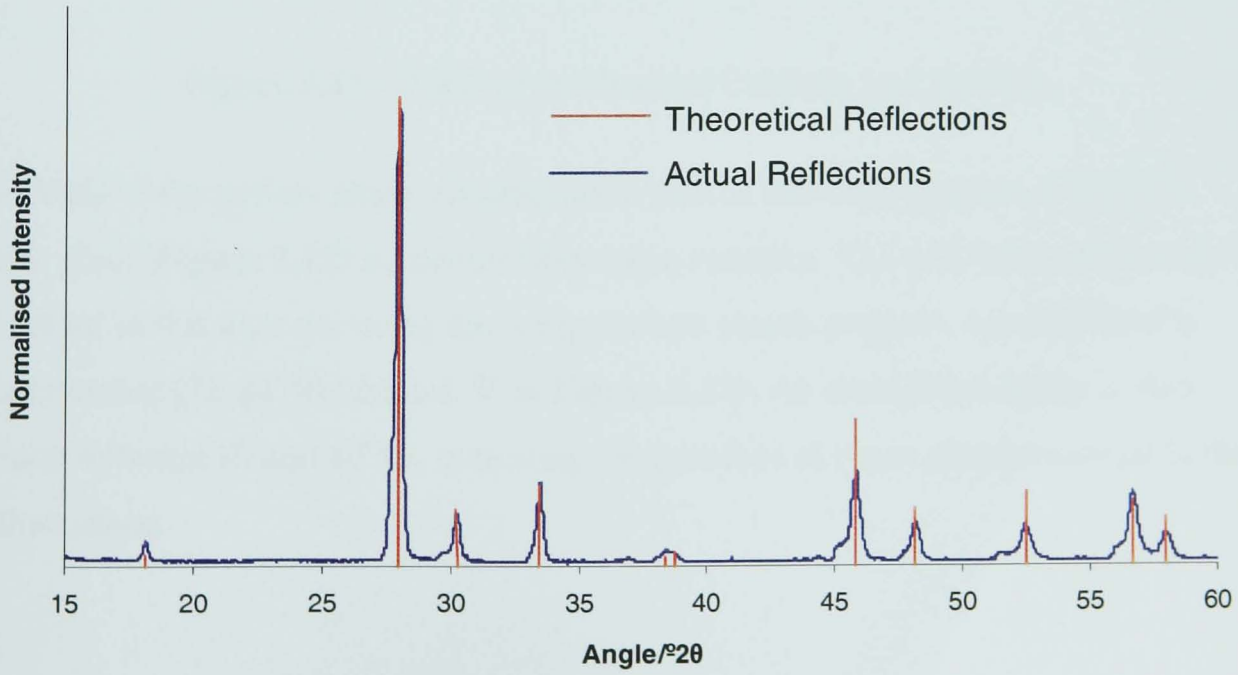

Figure 5.10b – Comparison of ideal and real $Na_{0.25}Sr_{0.5}Nd_{0.25}MoO_4$ XRD patterns

As for the previous comparisons of idealised and real XRD patterns, there is a good over lap of reflections in **Figures 5.10a** and **5.10b** indicating that the sintered molybdates are close to the ideal compositions and structures.

5.3.5 Yellow Phase and Standards

Figure 5.11 shows the XRD of Ca and Sr molybdate standards. All of the reflections can be matched to the ICDD database cards [85-546] and [8-482] for $CaMoO_4$ and $SrMoO_4$ respectively, indicating that both standards were single phase.

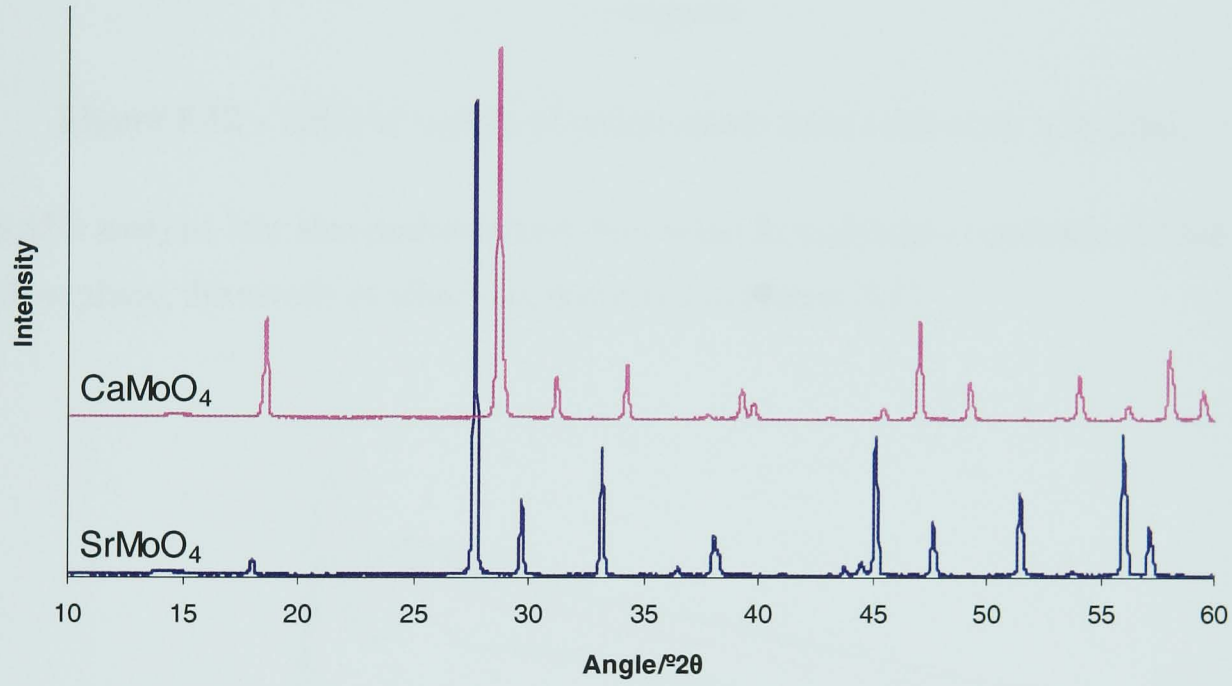

Figure 5.11 – XRD of synthesised $CaMoO_4$ and $SrMoO_4$

The XRD of the yellow phase material taken from a full scale simulated Magnox waste glass (**Figure 5.12**) is considerably more complex. The only phase that could be identified in this material using the computerised search program was $LiCsMoO_4$ (card number [72-2479] labelled ▼ in **Figure 5.12**). An amorphous hump is also present between 10 and 40°2θ, indicating the presence of some glassy material in the yellow phase.

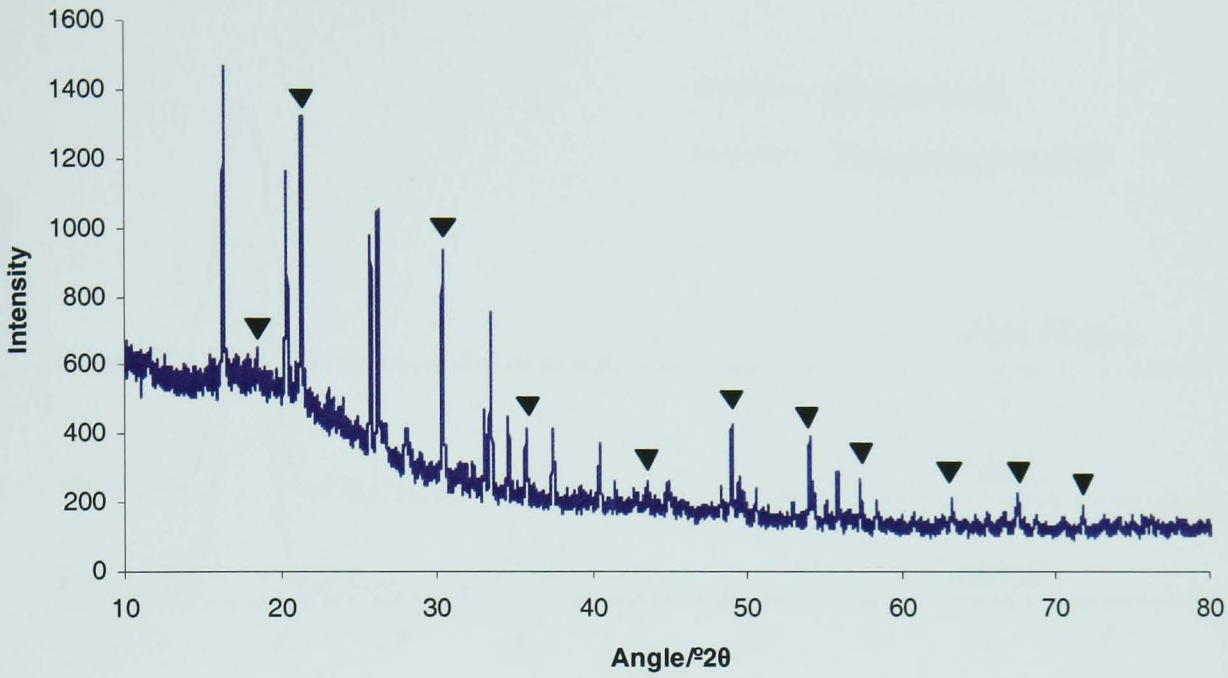

Figure 5.12 – XRD of sample of yellow phase from a full scale V26 glass

EXAFS analysis was also performed on the Ca and Sr molybdate standards and the yellow phase, the results of which are presented in **Figure 5.13**

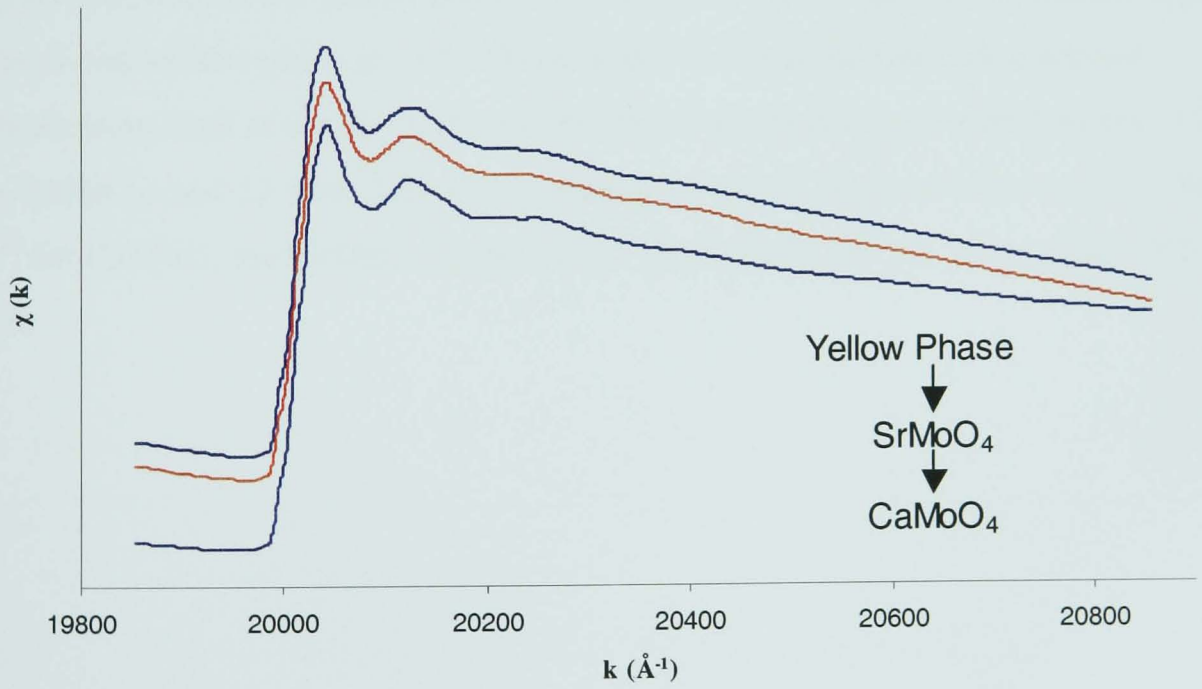

Figure 5.13a – Summed EXAFS of yellow phase, $SrMoO_4$ and $CaMoO_4$

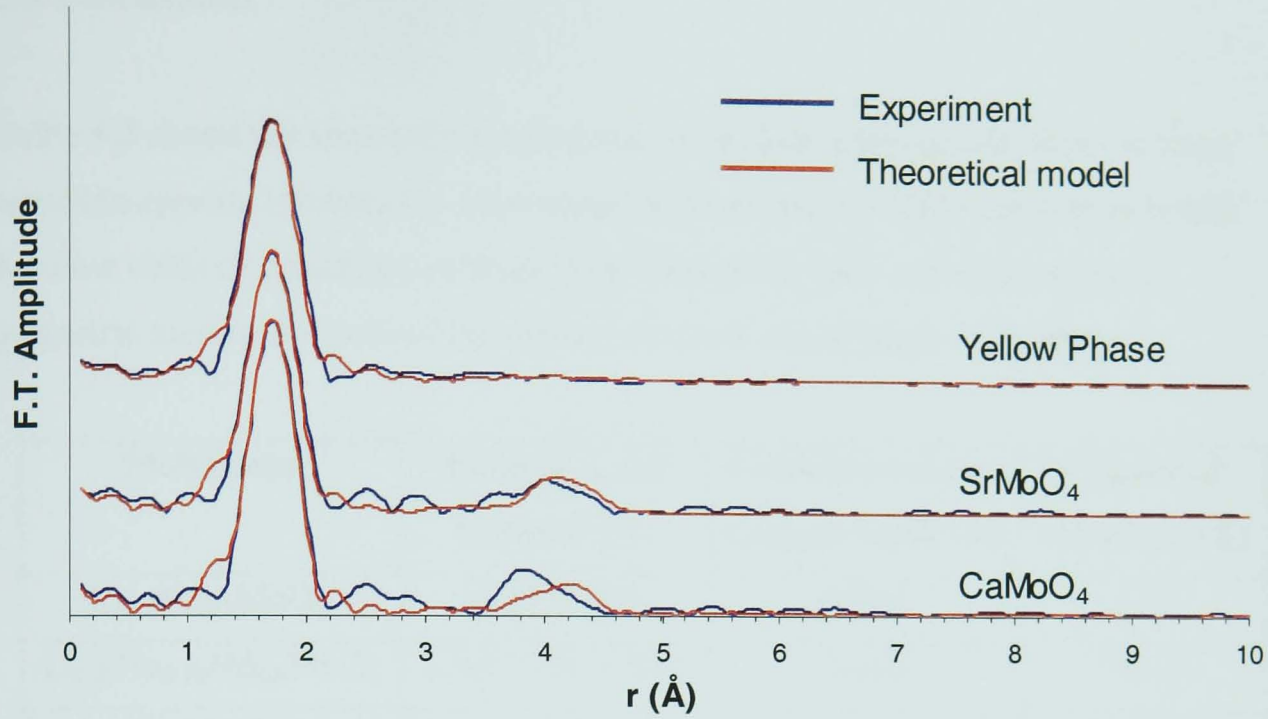

Figure 5.13b – Fourier transforms of yellow phase, $SrMoO_4$ and $CaMoO_4$ EXAFS

The Fourier transforms (FT) of the EXAFS results from all of the samples show a large peak at ~1.76Å, which fits well with a model of 4 oxygen atoms in tetrahedral coordination to, and equidistant from, the Mo centre. Whilst this is the only significant peak on the yellow phase FT, the FTs of the Ca and Sr molybdates have second noteworthy peaks at ~4Å. These peaks can be modelled with a second coordination shell of 8 cations around the MoO_4 tetrahedra to give an R factor of 24.5 for $CaMoO_4$, and 22.5 for $SrMoO_4$ indicating a good fit. These cations are Ca^{2+} and Sr^{2+} for $CaMoO_4$ and $SrMoO_4$ respectively. The R factor for the yellow phase FT fit is 21.9.

5.4 Discussion

Table 5.3 shows the shows the synthesised molybdate compositions that did form powellite-type molybdates (as determined by matching the XRD patterns to ICDD database cards or calculated patterns from theoretical ideal unit cells) and the geometric mean ionic radii of the cations on the A site of those molybdates.

Molybdate	Radii of A site Cations* (Å)	Geometric mean cationic radii (Å)	d-space of 112 plane (Å)
$Li_{0.5}Nd_{0.5}MoO_4$	0.88, 1.123	0.994	3.12
$Li_{0.25}Na_{0.25}Nd_{0.5}MoO_4$	0.88, 1.16, 1.123	1.065	3.116
$CaMoO_4$	1.14	1.14	3.1023
$Na_{0.5}Nd_{0.5}MoO_4$	1.16,1.123	1.141	3.141
$Ag_{0.5}Gd_{0.5}MoO_4$	1.29, 1.078	1.179	3.112
$Na_{0.25}Sr_{0.5}Nd_{0.25}MoO_4$	1.16, 1.27, 1.123	1.204	3.183
$Ag_{0.5}La_{0.25}Gd_{0.25}MoO_4$	1.29, 1.185, 1.078	1.207	3.139
$Ag_{0.5}Ce_{0.5}MoO_4$	1.29, 1.15	1.218	3.17
$Li_{0.25}K_{0.25}Nd_{0.5}MoO_4$	0.88, 1.52, 1.123	1.229	3.156
$SrMoO_4$	1.27	1.27	3.222
$K_{0.25}Ba_{0.5}La_{0.25}MoO_4$	1.52, 1.50, 1.185	1.419	3.317

Table 5.3 - Some parameters of powellite-type synthesised molybdates

* Shannon and Prewitt radii used

A trend of increasing lattice parameters with increasing mean cationic radius is expected in these molybdates, as larger ions are inserted into the same unit cell. This relationship is seen within the various molybdate "families" (i.e. the 112 d-spacing of the Li-La molybdate is greater than the Li-Sm, which in turn is greater than the Li-Gd etc). However, as can be seen from **Table 5.3**, this relationship is not strictly linear. For example, the mean ionic radii for the A-site cations in $Na_{0.5}Nd_{0.5}MoO_4$ is 1.141Å and for $Ag_{0.5}Gd_{0.5}MoO_4$ is 1.179Å, and yet the 112 d-spacing for the former is larger than that of the latter. Often, large size differences in cationic radii can strain crystal structures which could lead to an increase in unit cell parameters. However, as the size difference between Ag and Gd is greater than that between Na and Nd, the

reduction in the unit cell parameters for the Ag-Gd molybdate as compared to the Na-Nd molybdate is probably due to differences in the effective nuclear charge. Ag^+ is a significantly larger ion than Na^+ and Ag^+ contains many more protons in its nucleus than Na^+. Ag^+ also has a larger number of electrons in the shells surrounding the nucleus, hence its larger size. However, the effectiveness of these shells at shielding the high positive charge of the Ag nucleus is not as high as the smaller number of shells that shield the smaller positive charge of the Na nucleus. Therefore, the Ag^+ ion has a stronger attraction to the negatively charged O^{2-} anions to which it is bonded than the Na^+ ion has, therefore the resultant lattice parameters are smaller.

Muller (1974) produced a structure field map for ABO_4 compounds, and an enlargement of the scheelite region of this map is shown in **Figure 5.2**. As can be seen from the map, Muller indicates that scheelites can form when cations with radii between 1.14Å and 1.5Å can be placed on the A site of these compounds with Mo^{6+} (radius 0.74Å) as the cation on the B site. Our experiments have shown that cations with radii outside of this range (eg. Li^+ - radius 0.88Å and K^+ - radius 1.52Å) can occupy this site when combined with other elements to bring the mean cationic radius to within 0.99Å – 1.42Å. They have also shown that the range of mono, di and trivalent cations that can be combined on this site is wide, and of the 16 elements present in the simulated waste stream and batch used in this work that have valencies in +1 to +3 range, 10 of them can be incorporated into these type of molybdates. This helps to explain why the molybdate that forms in the glass containing the full simulated waste stream could not be identified, as the range of possible compositions and stoichiometries (given 10 elements that are potential molybdate formers) is large. As a real waste stream would contain upwards of 40 different elements, this would only widen the scope for molybdate formation.

However, from the field map it is expected that the $Li_{0.25}Rb_{0.25}Nd_{0.5}MoO_4$ and $Li_{0.25}Cs_{0.25}Nd_{0.5}MoO_4$ compositions should have formed single phase scheelite compounds as the average radii for the A site cations in these cases are 1.160Å and 1.195Å. These values are well within the range in which scheelite type molybdates were found to form in this work, and yet a single phase molybdate could not be produced using these compositions. This indicates that there are factors other than mean ionic radii that can limit molybdate formation. In this case it is likely that the

limiting factor may have been the size difference between the cations. A single phase molybdate could be produced using the $Li_{0.25}K_{0.25}Nd_{0.5}MoO_4$ composition, where the size difference between the largest and smallest A site cations (K^+ and Li^+ respectively) was 0.64Å. However the size difference between Li^+ and Rb^+ is 0.75Å, and it is proposed that this size difference could overstrain the scheelite unit cell and therefore make the structure energetically unstable.

The EXAFS results from the yellow phase analysis lend further weight to the random cationic distribution proposal for the molybdates that are forming in the simulated HLW glasses melted in this project. If there was a regular distribution of cations around the MoO_4 tetrahedra in this material (i.e. if the molybdate structure favoured one particular cation to charge balance the $(MoO_4)^{2-}$ units), then a second coordination shell would be observed at a distance of ~4Å (depending on the cationic species) from the Mo centre. This phenomenon can be observed in the EXAFS of the Ca and Sr molybdate standards, where the structure (and composition) is regular.

5.5 Conclusions

• Powellite type molybdates of the form $AMoO_4$ can incorporate mono, di and trivalent cations on the A site

• Multiple cations with a geometric mean radius of 0.99Å – 1.42Å can be incorporated onto the A site of powellite type molybdates to form single phase compounds.

• Cations with radii between 0.88Å and 1.52Å can be incorporated onto the A site of powellite type molybdates providing the mean cationic radii of all of the A site cations falls within the 0.99Å – 1.42Å range.

•Cations with a difference in radii of greater than 0.64Å tend to overstrain the lattice and do not tend to produce single phase powellite type molybdates.

6. Redox Effects on Simplified Batches

6.1 Introduction

As was discussed in **Chapter 4**, a powellite type molybdate forms upon heat treatment of glasses containing full simulated HLW streams which have been melted in an air atmosphere and stirred during melting. This phase proved hard to identify due to the large number of elements present in the simulated HLW stream which were capable of being incorporated into the phase in conjunction with one another in varying amounts. However, this phase is analogous to the alkali molybdate part of the yellow phase material found in the full scale simulated melts performed at the Sellafield vitrification plant. The alkali chromates and sulphates that give the phase its yellow colouration will not be found in this work as the simulated waste stream contains only a very small (0.09mol%) amount of Cr_2O_3 and no sulphur at all. It was also shown in **Chapter 4** that glasses containing the full simulated HLW stream and sparged with a reducing gas during melting, tended to develop the same powellite type molybdate phase upon heat treatment as identical compositions sparged with compressed air. In this chapter, the oxidation state and environment of the Mo in the glass are examined more closely.

It has been suggested (Lutze, 1988) that by reducing the oxidation state of Mo in HLW glasses from (predominantly) Mo^{6+} to lower valence states, it would be possible to increase the solubility of the Mo, and therefore decrease the tendency for yellow phase formation. Experiments on soda lime silica glasses doped with small (≤1mol%) quantities of Mo and reduced using tannic acid (Camara *et al*, 1980) have shown that Mo^{3+} quantities are increased relative to the values observed for the same glasses melted without the reducing agent. It was also observed by Horneber *et al* (1982) that in glasses with compositions similar to those used by Camara *et al*, Mo solubility increased when the glass was melted under reducing conditions. Kawamoto *et al* (1981) studied the phase separation of sodium borosilicate glasses containing small MoO_3 and MoO_2 additions and melted under oxidising and reducing conditions of air and argon respectively. Kawamoto notes that when Mo^{4+} is present in the glasses, the tendency for crystalline MoO_2 needles to form in the glass upon heat treatment is

increased. He also reports that some of the glasses phase separated into 2 phases, one of which was Mo rich, and the immiscibility temperature of the 2 phases depend on the [Mo^{5+}/Mo_{Total}]. This is important with respect to the field of waste vitrification because, if the immiscibility temperature between two different phases in glass can be brought down to below the liquidus, it may be possible to form a metastable product that does not exhibit phase separation if the correct cooling regime is applied. Thus, as yellow phase in HLW glasses originates from a liquid-liquid phase separation the immiscibility temperature of which is above the liquidus of the glass, it may be possible to avoid yellow phase formation using a combination of reducing melt conditions and cooling regimes.

The solubility of transition metal ions in glasses is approached using a modified aqueous chemistry theory by White (1985), who designates higher valency transition metals as being present as distinct molecules in the glass. For example, Mo^{6+} would be present as $(MoO_4)^{2-}$ complexes that would retain the bonds with the O^{2-} anions with which they were associated when they entered the batch. However, as the valency of the transition metal ions is decreased, they take up more of a network former role, initially becoming linked to the network via ionic bonds with oxygen anions connected to the network, and eventually by bridging oxygens or even direct metal-silicon bonds. Thus, this approach is also compatible with Lutze's theory of increasing solubility via a reduction in oxidation state.

The preliminary experiments in this section were based on those of Camara and Horneber, but designed for the HM4 composition. It was decided to use simplified batches for the initial experiments in order to ease the analysis of the results, and to use different gas sparges to create the different redox conditions that would prevail during melting (as opposed to chemical reductants, such as tannic acid, that were used by the authors noted above). This was done to keep the experimental procedure as representative as possible to the real vitrification process at Sellafield where the melt is sparged with air to aid mixing and homogenisation.

6.2 Experimental

Glass batches were made with the compositions shown in **Table 6.1**.

Glass	**11**	**12**	**13**	**14**
	1%Mo glasses	Cs-Nd glasses	Cs-Nd glasses	Cs-La glasses
Oxide	Weight (g)	Weight (g)	Weight (g)	Weight (g)
SiO_2	61.18	46.35	45.92	45.92
B_2O_3	21.68	16.43	16.28	16.28
Na_2O	10.89	16.5	16.35	16.35
Li_2O	5.25	n/a	n/a	n/a
MoO_3	1.00	2.99	4.79	4.79
Cs_2O	n/a	1.94	3.11	3.11
Nd_2O_3	n/a	8.47	13.55	n/a
La_2O_3	n/a	n/a	n/a	13.55

Table 6.1 – Compositions of simplified batches used for redox effect experiments

6.2.1 Glass 11 – 1%Mo Glasses

The purpose of this batch was for initial observation of the redox behaviour of Mo using several different techniques. The batch contains Mo and those elements necessary to form the base glass frit, but none of the other elements that would normally be present in a simulated HLW stream were included. These were omitted from the batch to simplify the analysis of, for example, ESR and XPS results, and to allow the observation of Mo behaviour when influenced only by the base glass composition. This composition was melted using sparges of oxygen (and hence forth will be denoted "Glass 11(ox)"), compressed air ("Glass 11(air)"), argon ("Glass 11(arg)"), and nitrogen mixed with 5% hydrogen ("Glass 11(red)").

6.2.2 Glass 12 – 25%Cs-Nd Glasses

This batch was formulated to represent a HLW glass containing a 25wt% waste loading, but avoiding the inclusion of many of the waste stream elements (again, to

simplify analysis of the results). The quantities of Cs and Nd in the batch have been increased to account for the lack of other mono and trivalent elements that would normally be found in the HLW stream. Li has been omitted from the base glass and replaced with an equal amount of Na. The batch does however contain all the elements necessary for powellite type molybdate formation. This batch was melted using sparges of O_2 ("glass 12(ox)"), compressed air ("glass 12(air)") and $N_2/5\%H_2$ ("glass 12(red)").

6.2.3 Glass 13 – 35%Cs-Nd Glasses

As for glass 12, but with quantities of Mo, Cs and Nd increased to be representative of a 35wt% waste loading, melted using O_2, compressed air and $N_2/5\%H_2$ sparges ("glass 13(ox)", "glass 13 (air)" and "glass 13(red)" respectively).

6.2.4 Glass 14 – 35%Cs-La Glasses

This glass was formulated as an analogue for glass 13 for XPS experimentation. It was discovered during XPS of glass 13 that the Nd signal interfered with the Mo signal, thus complicating the experimental analysis. Therefore it was decided to replace the Nd in the batch with an equal quantity of La, an element of very similar atomic mass and similar chemistry, but one that would not cause interference with Mo during XPS. Batches of this composition were sparged with compressed air ("glass 14(air)") and $N_2/5\%H_2$ ("glass 14(red)") during melting.

6.2.5 Heat Treatments

Glasses 12(ox), 12(air), 12(red) 13(ox), 13(air) and 13(red) were all subjected to heat treatments of 48 hours at 650°C in order to observe the differences in the crystallisation behaviour (if any) between these samples.

6.2.6 ESR

Glasses 11(air), 11(red), 11(arg) and 13(red) were subjected to ESR analysis. The oxygen sparged glasses were omitted from the ESR investigation as they were

expected to give the same results as the air sparged glasses using this technique. Glasses with the glass 12 and glass 14 compositions were omitted from the ESR experiments as they were expected to behave in an identical manner to the glass 13 compositions with respect to ESR.

6.2.7 XPS

Glasses 11(air), 11(red), 14(air) and 14(red) were analysed using XPS. The glass 12 and glass 13 compositions were unsuitable for analysis using this technique due to the presence of Nd, although they were expected to give similar results to the glass 14 compositions when melted using the same sparges. No oxygen sparged glasses were analysed by XPS as they were unlikely to give different results to the air sparged glasses.

6.2.8 EXAFS

Glasses 11(air), 11(arg), 11(red), 13(air) and 13(red) were subjected to EXAFS analysis to examine the immediate environment of Mo (on an atomic scale) in these glasses. It was assumed that the glasses melted in the oxygen atmosphere would give the same results as those melted in the air atmosphere (due to the abundance of O_2 in air), and thus these samples were not analysed using EXAFS.

6.3 Results

6.3.1 As Cast Glasses

6.3.1.1 *Glass 11*

Figure 6.1a shows the oxygen sparged 1wt% Mo glass in the as cast state.

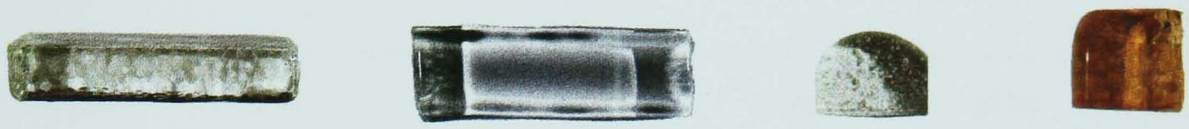

a **b** **c** **d**

Figure 6.1 –(**a**)Glass 11(ox) as cast, (**b**)Glass 11(air) as cast, (**c**)Glass 11(arg) and (**d**)Glass 11(red) as cast

In this batch, the only element present that was capable of affecting a colour change under the given melting conditions was Mo. As glass 11(ox) was clear and colourless it can be assumed from this that the Mo was predominantly in the +6 oxidation state. **Figure 6.1b** shows that glass 11(air) was a clear colourless glass, again an indication that the majority of the Mo in this glass was present as Mo^{6+}, and this is also the case for glass 11(arg) (**Figure 6.1c**). From **Figure 6.1d** it can be seen that glass 11(red) was a smokey brown colour upon casting. This colouration indicates that the there has been at least a partial reduction of the Mo in this batch from Mo^{6+} to Mo^{3+} (Camara, 1979).

The ESR data for glass 11(air), glass 11(arg) and glass 11(red) is shown in **Figures 6.2a**, **6.2b** and **6.2c** respectively.

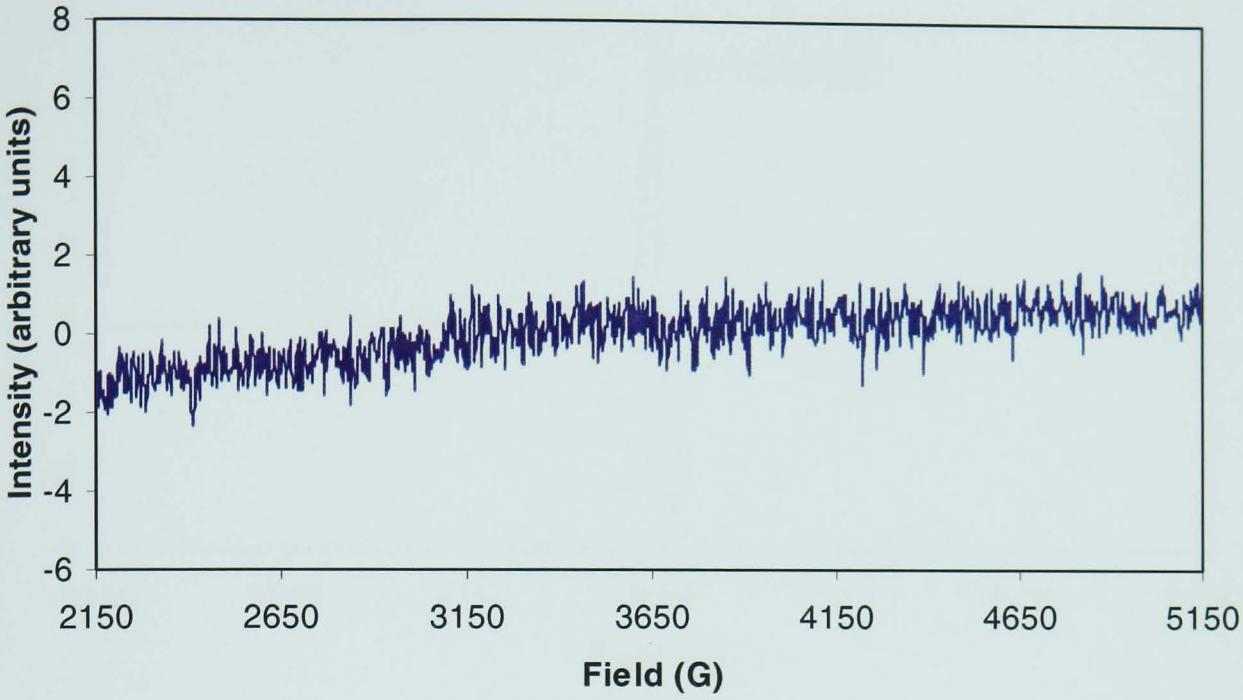

Figure 6.2a – ESR of glass 11(air)

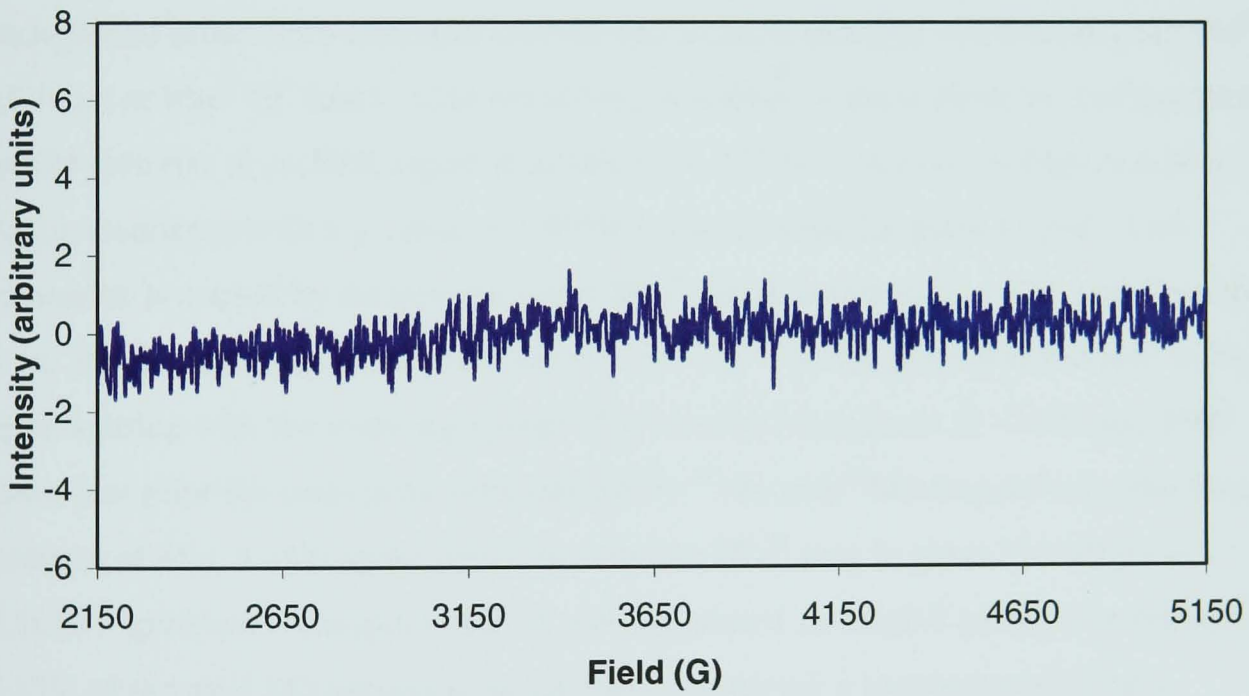

Figure 6.2b - ESR of glass 11(arg)

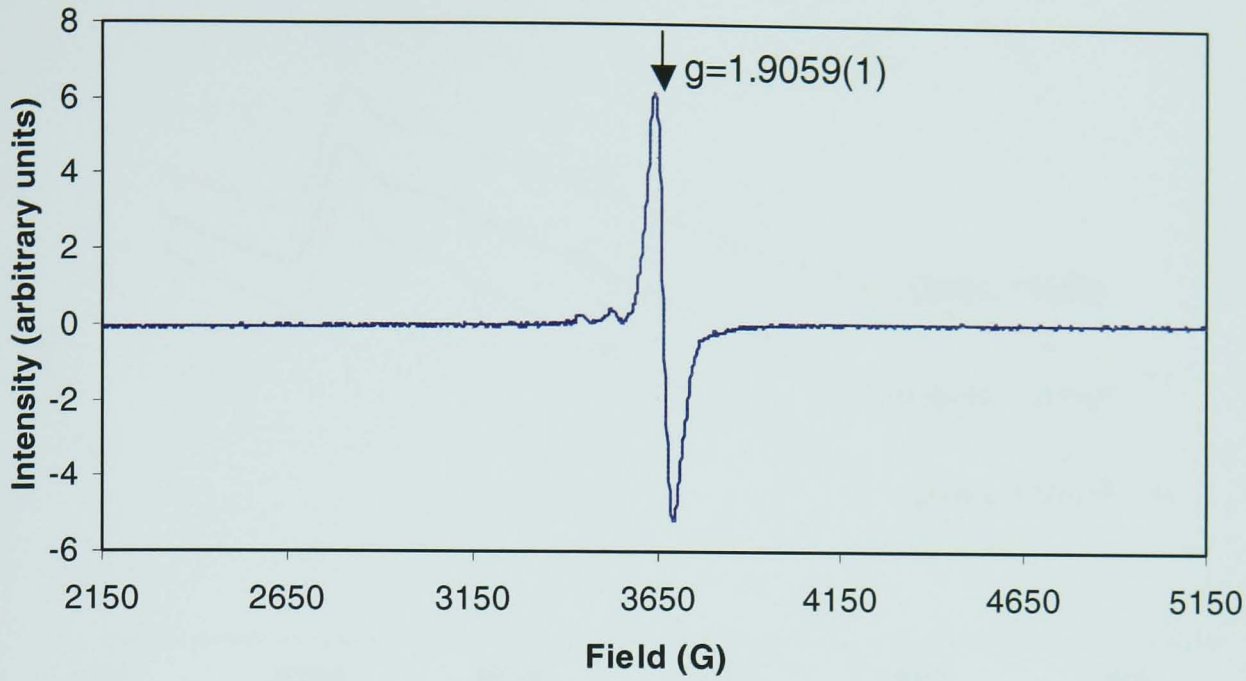

Figure 6.2c - ESR of glass 11(red)

Glasses 11(air) and 11(arg) (**Figures 6.2a** and **6.2b** respectively) only show background noise. This indicates that the Mo in these samples was in either the Mo^{6+} (d^0 ions) or Mo^{4+} (d^2 ions) oxidation states, as neither of these electron configurations would give rise to an ESR signal (Camara *et al*, 1979). However, in **Figure 6.2c** a strong resonance with a *g* value of 1.9059(1) can be seen for glass 11(red). This resonance is caused by the paramagnetic Mo^{3+} ion (Camara *et al*, 1979, and Horneber *et al*, 1982) indicating that at least some of the Mo^{6+} in this glass was reduced to Mo^{3+} upon melting with the reducing sparge. The smaller resonances at ~3400 and 3500 gauss just prior the main peak were caused by ^{97}Mo and ^{95}Mo respectively, the natural isotopes of Mo. A spin count performed for the Mo^{3+} ions in glass 11(red) gave $2.3x10^{18}$ spins/cm^3. The glass density was calculated as 2.5±0.2 g/cm^3, this equates to 2.25% of the total Mo present as being Mo^{3+} (assuming a homogeneous glass).

The EXAFS analysis (**Figures 6.3a**, **6.3b**) of the air, argon and nitrogen/hydrogen sparged 1wt% Mo glasses all gave the same result, with the Fourier transform showing a regular arrangement of atoms at a distance of ~1.74Å from the Mo atoms in the glasses. This has a good fit with a model of the molybdenum atoms being surrounded by 4 oxygen atoms in a tetrahedral arrangement with R factors of 36.7, 19.0 and 29.7 for the air, argon and nitrogen/hydrogen sparged glass 11 samples respectively. This indicates that the majority of the Mo in all of these samples (including glass 11(red)) was in the +6 oxidation state.

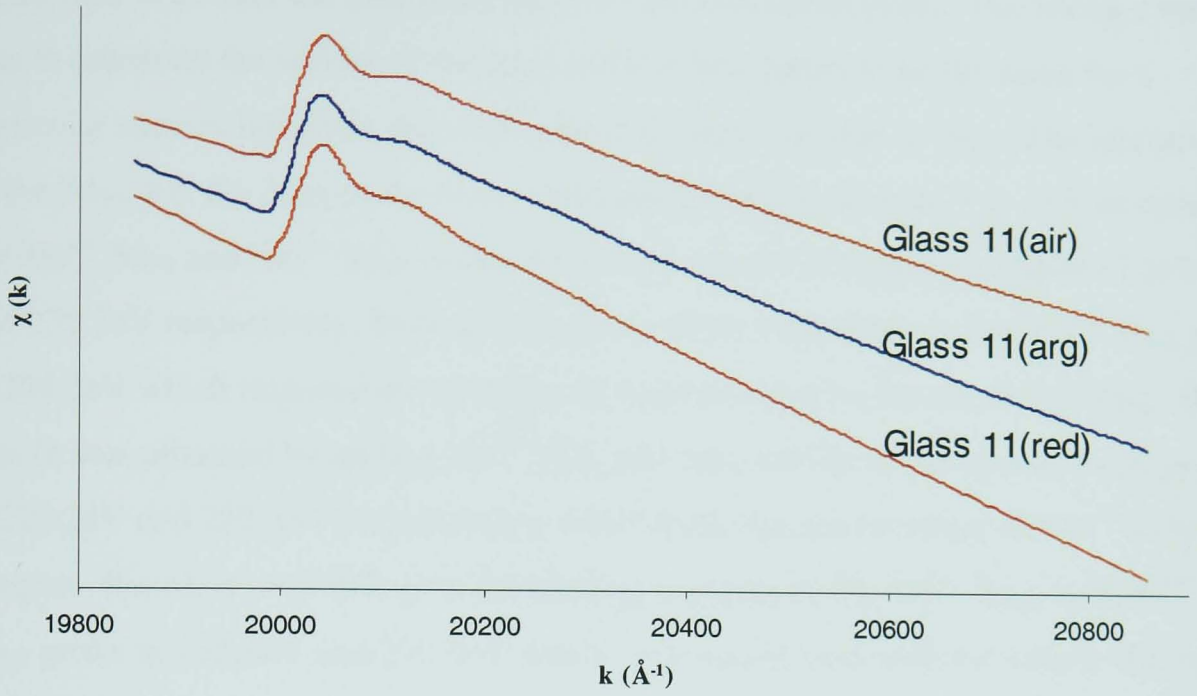

Figure 6.3a – EXAFS of glass 11(air), glass 11(arg) and glass 11(red)

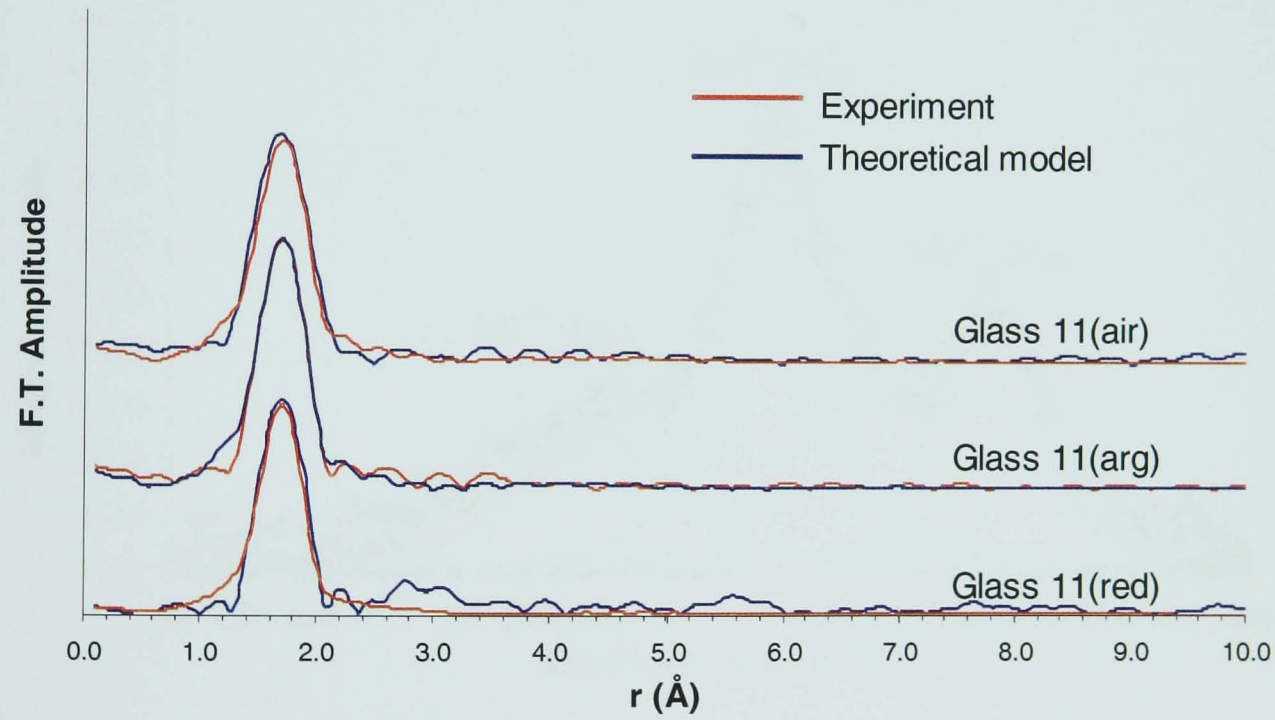

Figure 6.3b – Fourier transformed EXAFS results for glass 11(air), glass 11(arg) and glass 11(red)

Figures 6.4a and **6.4b** show the results of the XPS analysis of glass 11(air) and 11(red) respectively. The results have been normalised to an integrated intensity, and fitted using the Origin curve fitting program. The data were un-smoothed and were initially corrected for charge shifting by comparison with the position of the C 1s peak which arose from adventitious carbon deposited from the vacuum system. This peak

was assigned the binding energy value 284.6eV and the observed offset from this value used to correct the data from the other photoelectron peaks. The fitting strategy was to constrain the widths of the $3d_{5/2}$ and the $3d_{3/2}$ peaks to be the same for a particular species but allow the widths from different species to vary. The intensities of the $3d_{5/2}$ and the $3d_{3/2}$ peaks were constrained to have the ratio 3:2. In both spectra, the Mo^{6+} $3d_{5/2}$ and Mo^{6+} $3d_{3/2}$ peaks are clearly present at binding energies of 232.0eV and 235.2eV respectively. Both spectra also exhibit a shoulder on the Mo^{6+} $3d_{5/2}$ peak at 229.2eV which required the presence of a second species for accurate fitting. The best fit was obtained by adding Mo^{4+} $3d_{5/2}$ and $3d_{3/2}$ curves to the spectra (with peaks at 229.2eV and 232.8eV respectively), which indicates the presence of Mo^{4+} in both samples. Barath *et al* (1999) give the binding energies of the Mo^{6+} $3d_{3/2}$ and Mo^{4+} $3d_{3/2}$ peaks as 235.8eV and 232.9eV which correspond well with the values obtained in this work. The calculated quantities (to within ±3.5%) of each species are shown in **Table 6.2**.

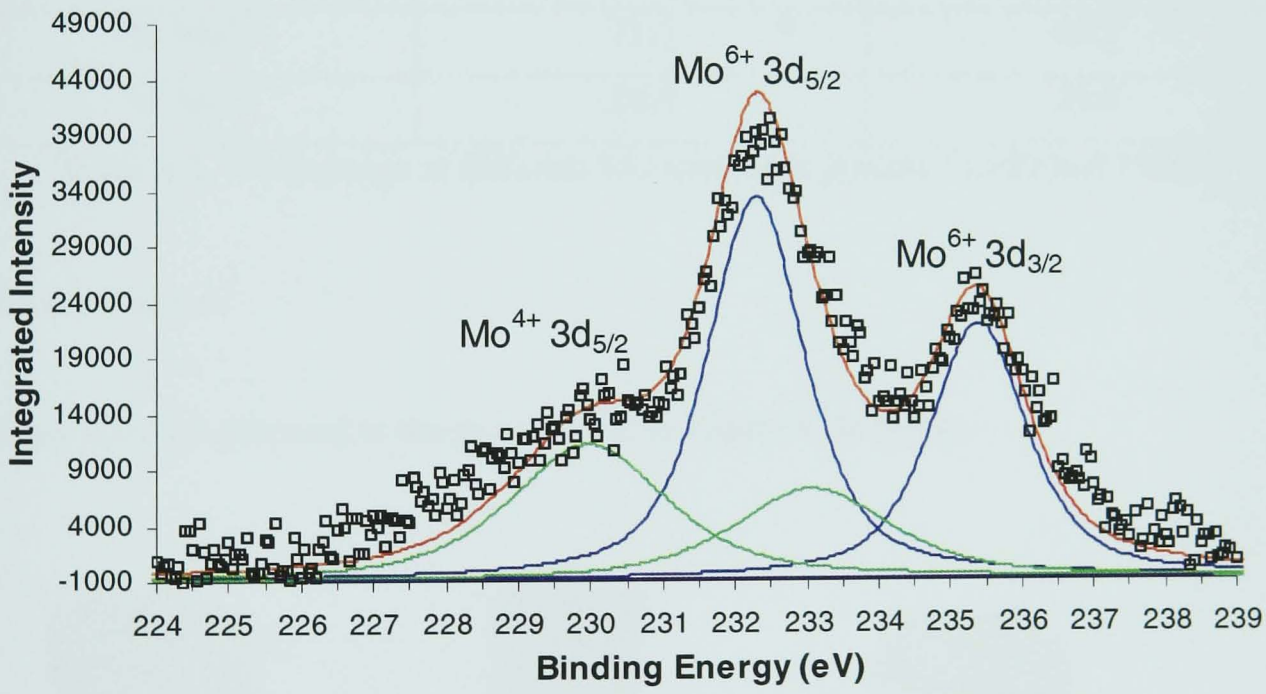

Figure 6.4a – XPS spectra of glass 11(air)

□ = Data points, —— = Fitted data, —— = Mo^{6+} fits, —— = Mo^{4+} fits

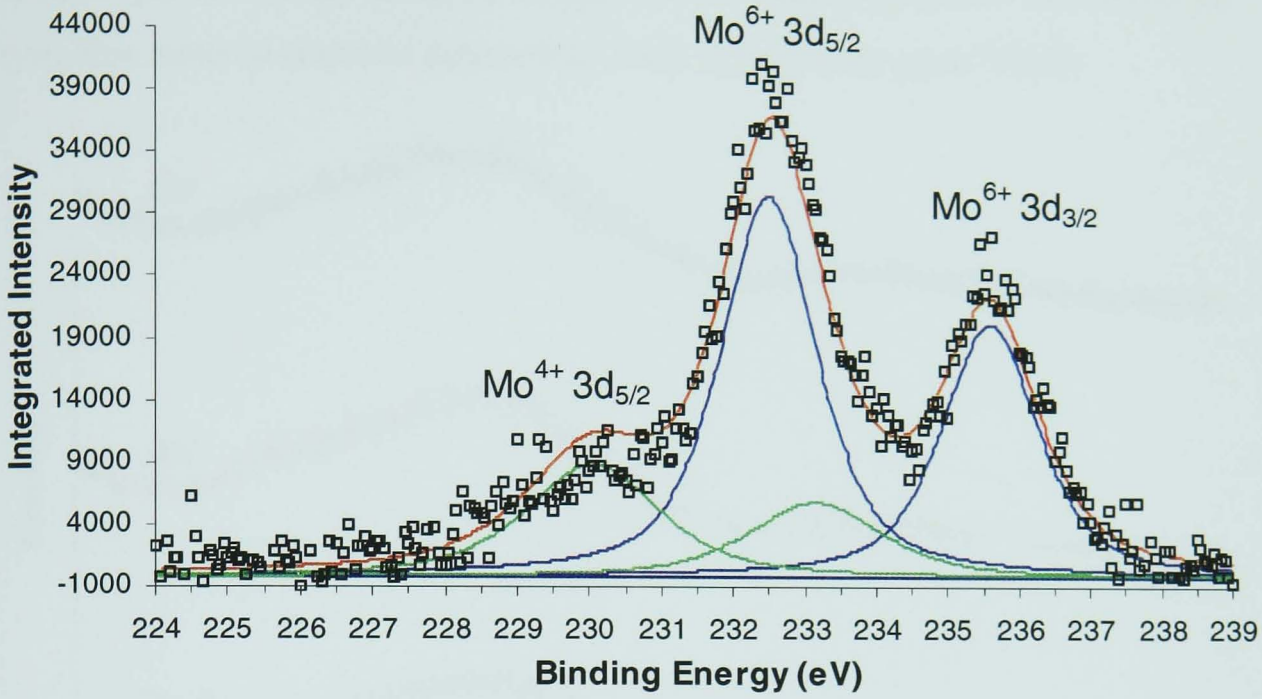

Figure 6.4b – XPS spectra of glass 11(red)

□ = Data points, — = Fitted data, — = Mo^{6+} fits, — = Mo^{4+} fits

	Glass 11(air)	**Glass 11(red)**
% Mo^{6+}	71.5	64.1
% Mo^{4+}	28.5	35.9

Table 6.2 – Percentage of different Mo species in glasses 11(air) and 11(red)

6.3.1.2 *Glass 12*

Glass 12(ox) is pictured in the as cast state in **Figure 6.5a** below.

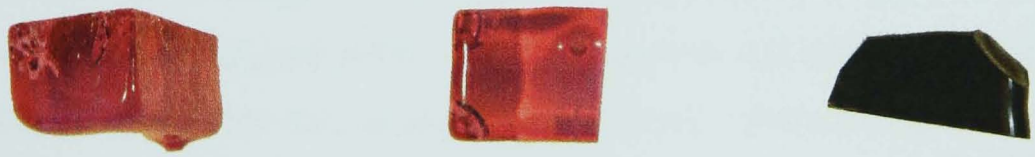

a **b** **c**

Figure 6.5 – (**a**)Glass 12(ox) as cast, (**b**)Glass 12(air) as cast, (**c**)Glass 12(red) as cast

The intense red/violet colour of this glass is due to the presence of Nd in the batch. As the colour of Nd originates from inner shell electron transitions, it is independent of the oxidation state of the Nd ion (Weyl, 1959). As there are no other colours present in this glass other than that which can be attributed to Nd, it can again be assumed that

the Mo is predominantly in the +6 oxidation state. **Figure 6.6** below shows that no crystalline material could be detected by XRD in the as cast glass 12(ox).

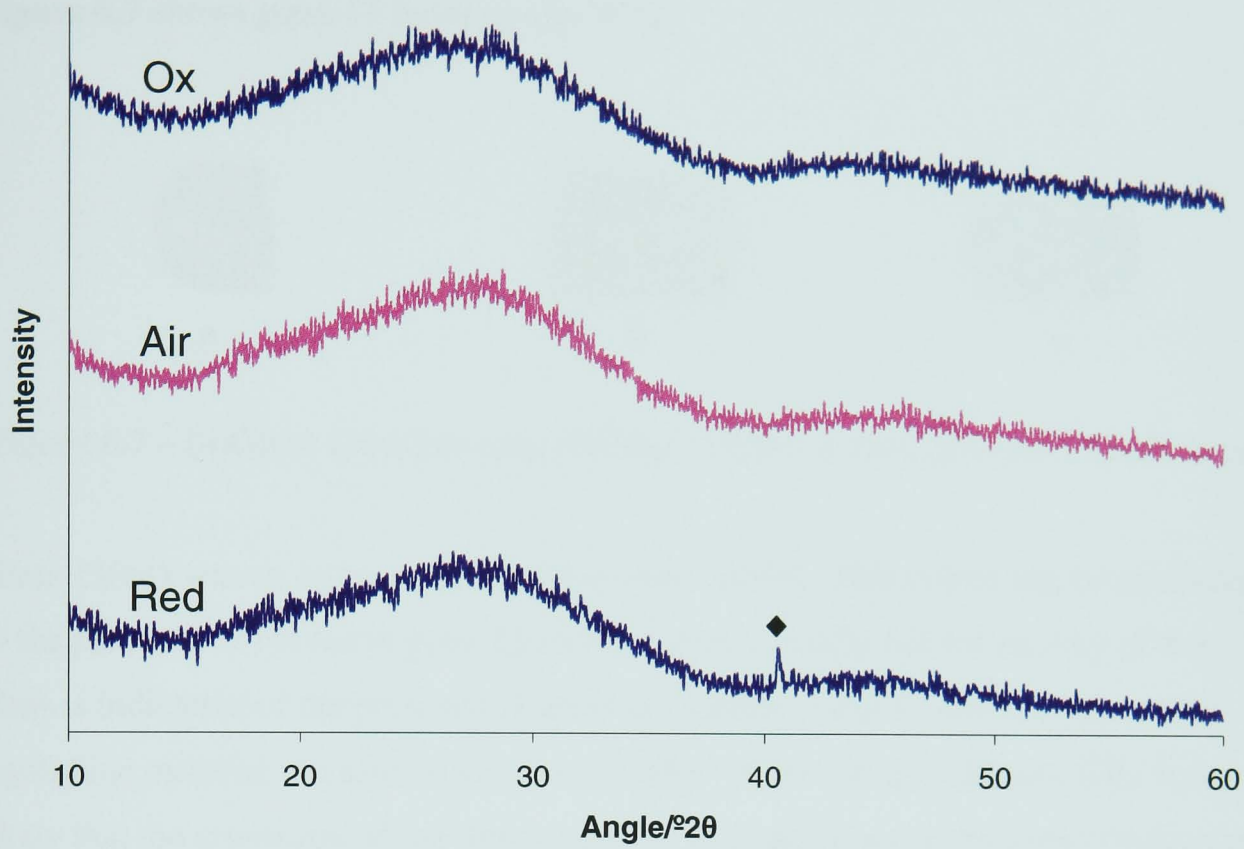

Figure 6.6 – XRD of as cast samples of glass 12(ox), glass 12(air) and glass 12 (red).
♦ shows crystalline reflection in glass 12(red)

Glass 12(air) was similar in appearance to glass 12(ox), again indicating that the majority of the Mo was present as Mo^{6+} (**see Figure 6.5b**). XRD of this sample (**Figure 6.6**) indicates that the sample is amorphous.

A marked colour change to an opaque dark grey/black was apparent in the reduced 25%Cs-Nd glass (**Figure 6.5c**). It is likely that this was due to a reduction in the oxidation state of Mo that, as seen in glass 11(red), produces a smokey brown colour when present as Mo^{3+}. It is also known to produce dark blue and green colours in reduced glasses (Camara, 1979), and any of these colours combined with the purple Nd colour could produce the colour observed in glass 12(red). XRD (**Figure 6.6**) did detect some crystalline material in this sample, and the reflection at 42.6°2θ has a good match with the (110) reflection of Mo metal (ICDD card [42-1120]), although a definite match cannot be assigned from a single reflection.

6.3.1.3 *Glass 13*

Figure 6.7 shows glass 13 in the as cast state.

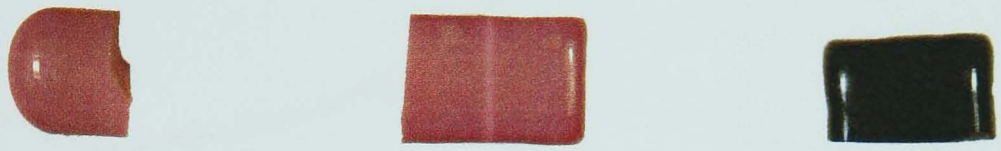

a **b** **c**

Figure 6.7 – (a) Glass 13(ox) as cast, **(b)**Glass 13(air) as cast, **(c)**Glass 13(red) as cast

Glass 13(ox) was an opaque violet colour upon casting. This colour can be attributed to the presence of Nd (as in glass 12(ox) and glass 12(air)), but the opacity of the glass is indicative of the presence of some crystalline material. Some evidence for crystalline material can also be seen on the XRD of this sample (**Figure 6.8**). It is likely that the crystalline phase developed due to the increase in the concentration of the simulated HLW stream elements (Cs, Nd and Mo) in this glass compared to glass 12, although it was not possible to make a positive identification of the phase from a single reflection.

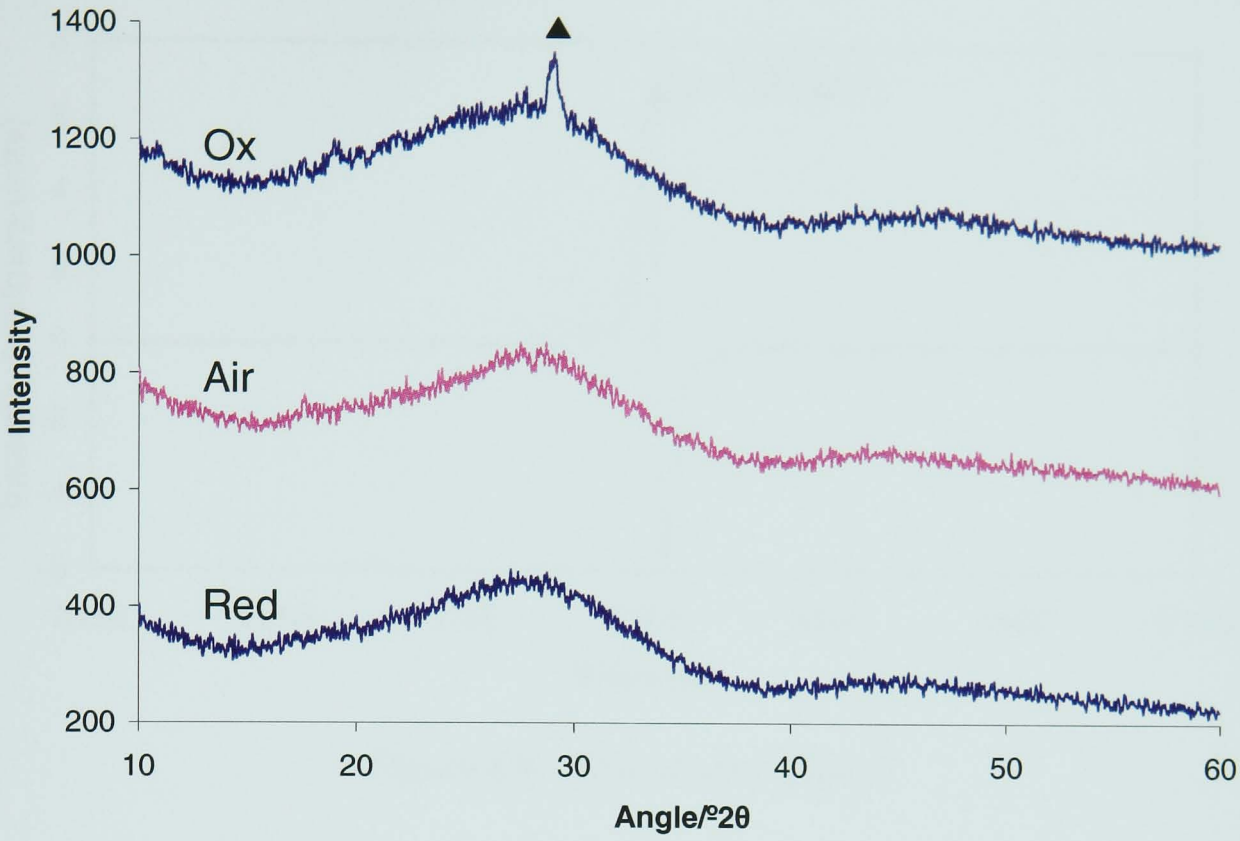

Figure 6.8 – XRD of as cast samples of glass 13(ox), glass 13(air) and glass 13(red). ▲shows position of crystalline reflection in glass 13(ox).

The as cast appearance of glass 13(air) (**Figure 6.6b**) was the same as that of glass 13(ox). Again, the violet colour indicates that Mo was acting as a colourant in these melts, which is a good indication that it is primarily present as Mo^{6+}. However, the XRD of this sample (**Figure 6.8**) did not indicate the presence of any crystalline material. **Figure 6.7c** shows that glass 13(red) was an opaque black colour upon casting. As with glass 12(red), this colour change indicates a reduction in the Mo^{6+} oxidation state during the melt with a reducing gas sparge. XRD showed this sample to be amorphous (**Figure 6.8**), although the opacity of the glass would suggest the presence of some crystalline material. It is possible that the volume of crystalline material was not sufficient to give dominant reflections under XRD.

Figure 6.9 below shows the ESR data for glass 13(red).

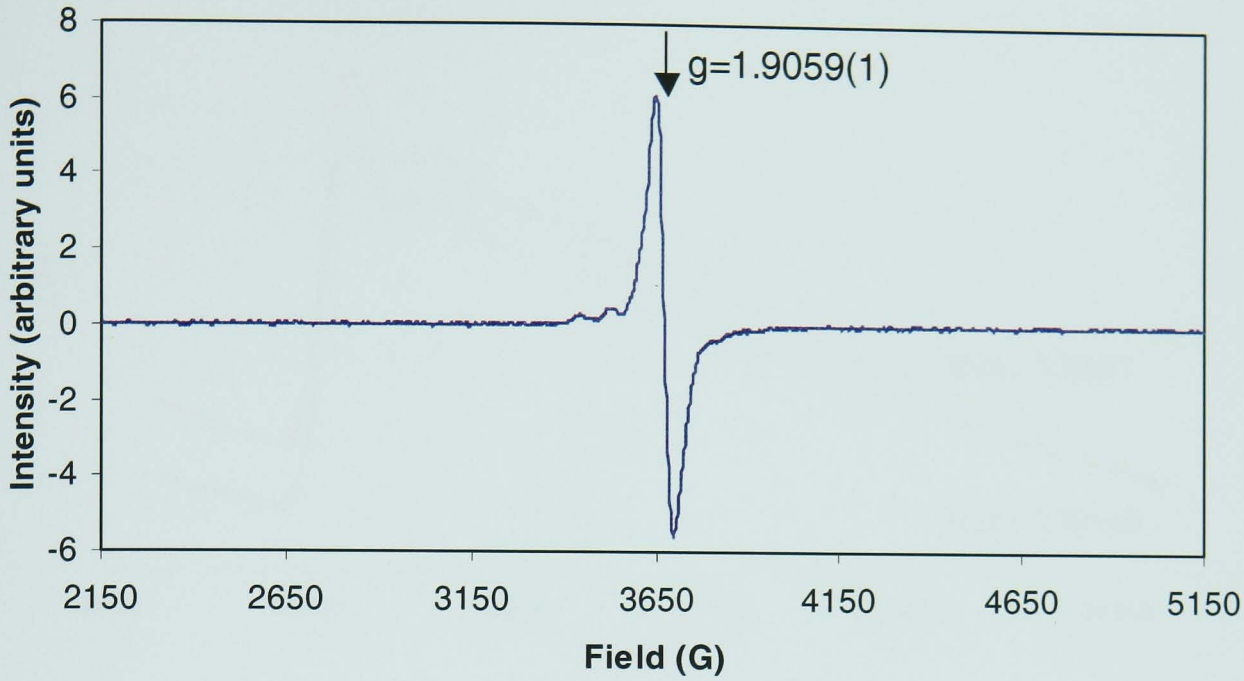

Figure 6.9 – ESR of glass 13(red)

As with glass 11(red), a resonance at g = 1.9059(1) can be seen in the ESR of glass 13(red). Once again, this resonance is indicative of the presence of Mo^{3+} in this glass.

EXAFS analysis of glasses 13(air) and 13(red) (**Figures 6.10a** and **6.10b**) revealed a regular arrangement of atoms at distances ~1.74Å and ~1.75Å respectively from the Mo atoms in the samples. As for glass 11, this indicates that the Mo atoms were surrounded by 4 oxygen atoms in a tetrahedral arrangement (with R factors of 25.0 and 32.2 for glass 13(air) and glass 13(red) respectively), hence Mo^{6+} must be the most prevalent species in both the air sparged and reduced samples.

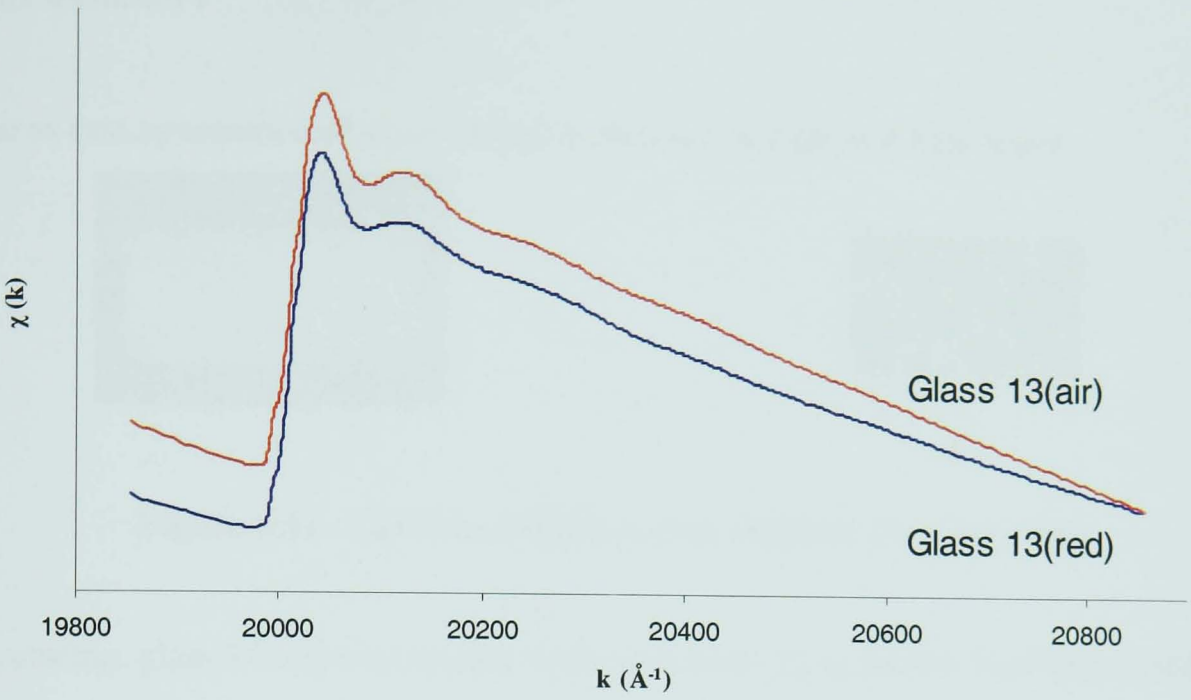

Figure 6.10a – EXAFS of glass 13(air) and glass 13(red)

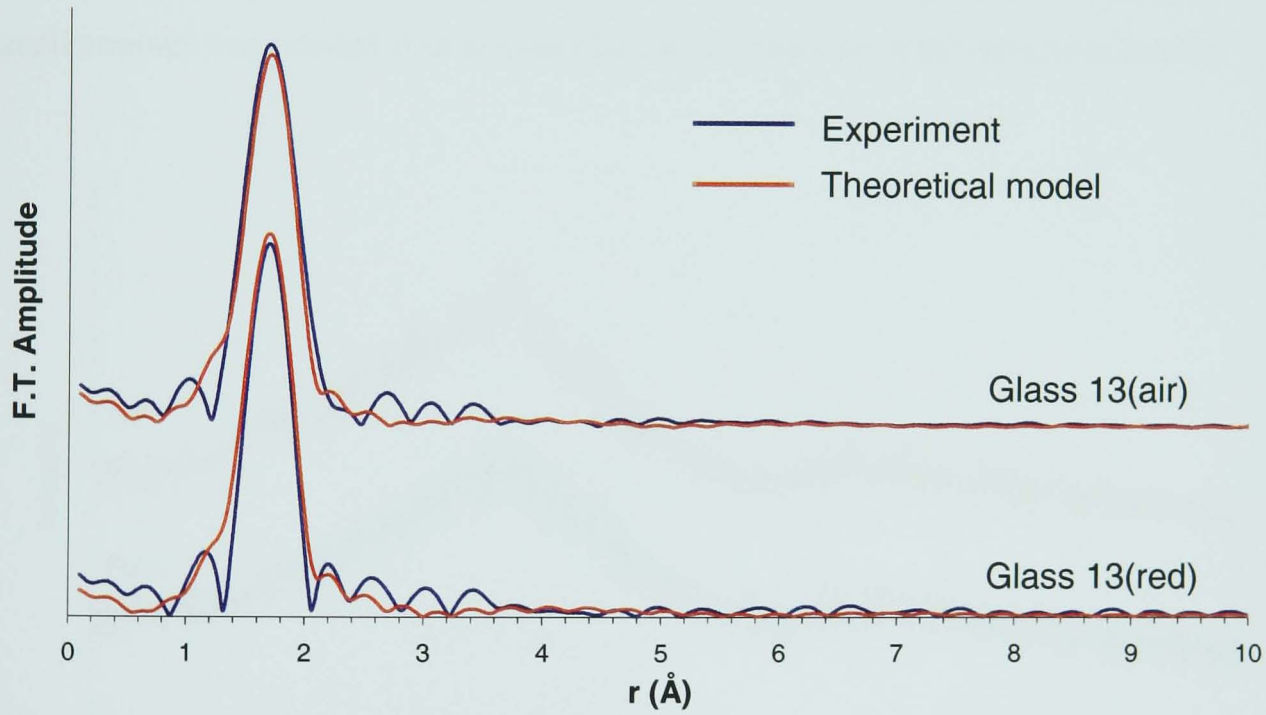

Figure 6.10b – Fourier transformed EXAFS results of glass 13(air) and glass 13(red)

6.3.1.4 *Glass 14*

The as cast appearance of glass 14(air) is pictured in **Figure 6.11a** below.

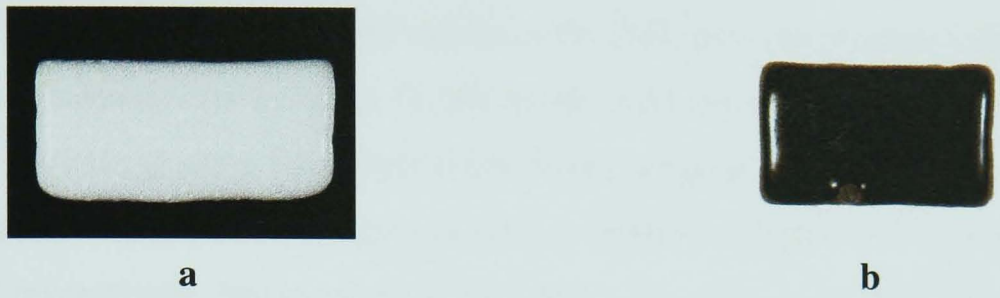

a **b**

Figure 6.11 – (**a**)Glass 14(air) as cast, (**b**)Glass 14(red) as cast

On casting, glass 14(air) was opaque white in colour. La is known to produce white glasses, although the opacity of this glass could also be due to the presence of crystalline material or amorphous phase separation. No crystalline material registered on the XRD analysis of this sample (see **Figure 6.12**), although it is possible that a small amount was present (but in quantities lower than the XRD detection limit).

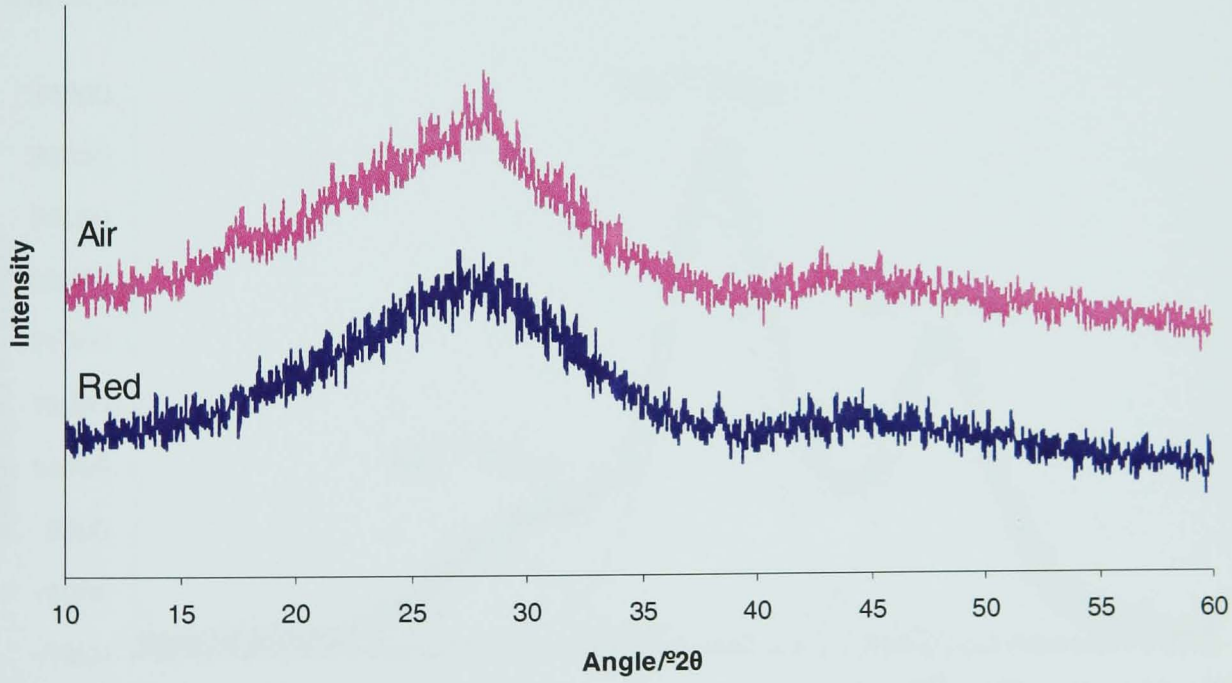

Figure 6.12 – XRD of as cast samples of glass 14(air) and 14(red)

It can be seen from **Figure 6.11b** that glass 14(red) was black in the as cast state, indicting that at least some of the Mo^{6+} was reduced during melting. The opacity of the glass (even in thin section) also indicated that either there was some crystalline

material present in glass 14(red) (although not enough to register on the XRD analysis, see **Figure 6.12**), or that amorphous phase separation occurred in this glass.

Figures 6.13a and **6.13b** show the results of the XPS analysis of glass 14(air) and 14(red) respectively. As for glass 11, the results have been normalised to an integrated intensity, and fitted using the Origin curve fitting program. In both spectra, the Mo^{6+} $3d_{5/2}$ and Mo^{6+} $3d_{3/2}$ peaks are again present at binding energies of 232.0eV and 235.2eV respectively. Both spectra also exhibit a shoulder on the Mo^{6+} $3d_{5/2}$ peak at 229.2eV which required the presence of a second species for accurate fitting. The best fit was obtained by adding Mo^{4+} $3d_{5/2}$ and $3d_{3/2}$ curves to the spectra (with peaks at 229.2eV and 232.8eV respectively), which indicates the presence of Mo^{4+} in both samples. To accurately fit the glass 14(red) spectra, a third species also needed to be added, and the best fit was given by adding the Mo^{5+} $3d_{5/2}$ and $3d_{3/2}$ curves with peaks at 230.6eV and 233.9eV respectively, signifying the presence of Mo^{5+} in this sample. Barath *et al* (1999) give the Mo^{5+} $3d_{3/2}$ binding energy as 234.7eV. The calculated quantities (to within ±2%, as estimated by the data spread) of each species are shown in **Table 6.3**.

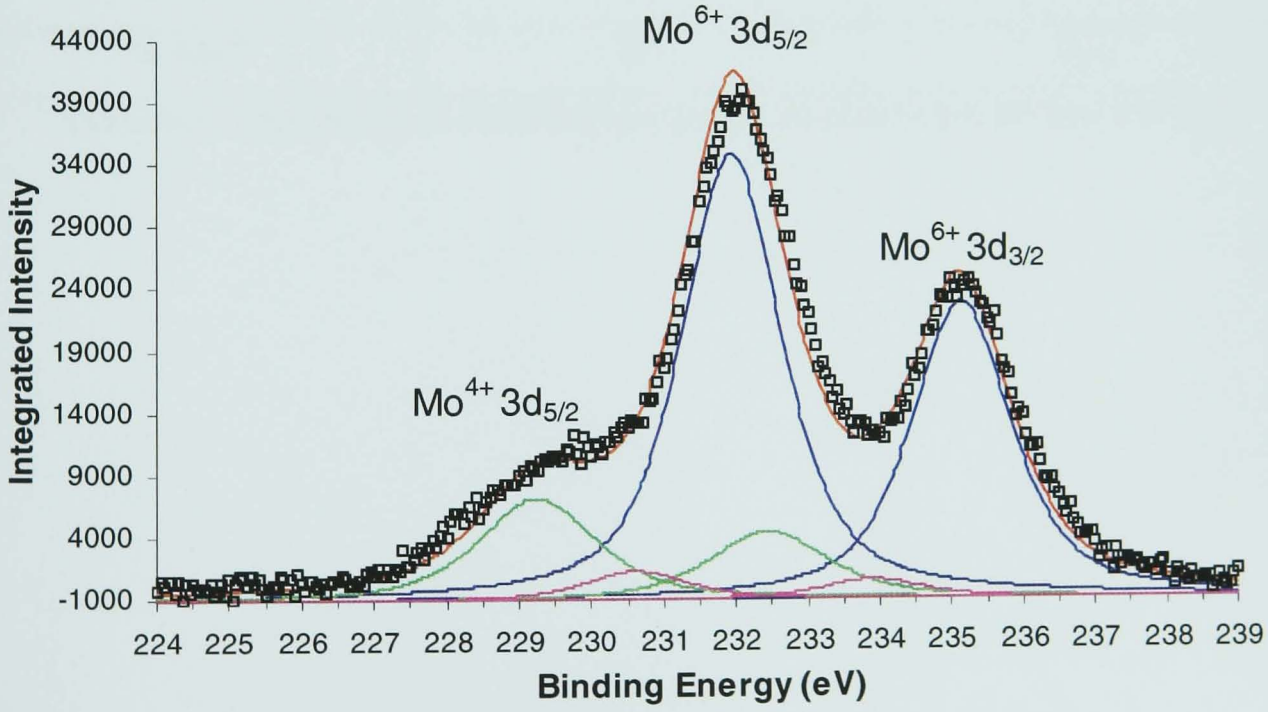

Figure 6.13a – XPS spectra of glass 14(air)

□ = Data points, — = Fitted data, — = Mo^{6+} fits, — = Mo^{5+} fits, — = Mo^{4+} fits

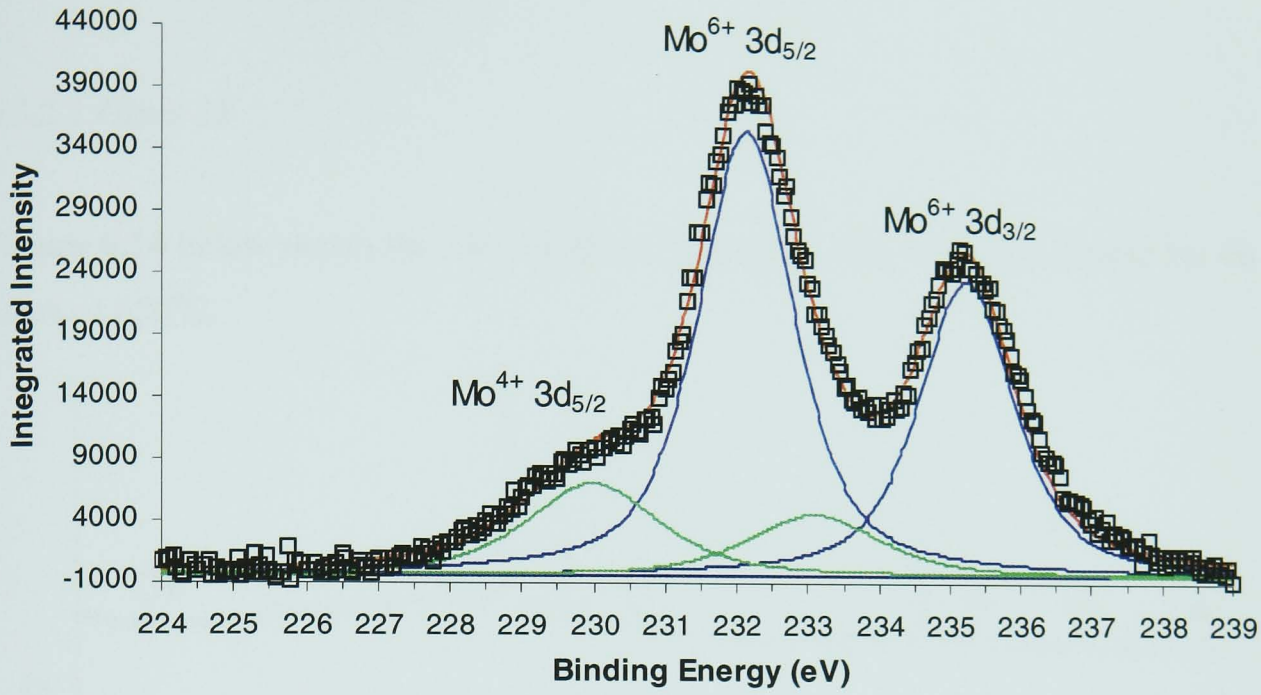

Figure 6.13b – XPS spectra of glass 14(red)

□ = Data points, —— = Fitted data, —— = Mo^{6+} fits, —— = Mo^{4+} fits

	Glass 14(air)	Glass 14(red)
% Mo^{6+}	75	78.3
% Mo^{5+}	5	-
% Mo^{4+}	20	21.7

Table 6.3 - Percentage of different Mo species in glasses 14(air) and 14(red)

6.3.2 Heat Treated Glasses

6.3.2.1 *Glass 12*

Figure 6.14 below shows the XRD of glass 12 samples that were heat treated for 48 hours at 650°C.

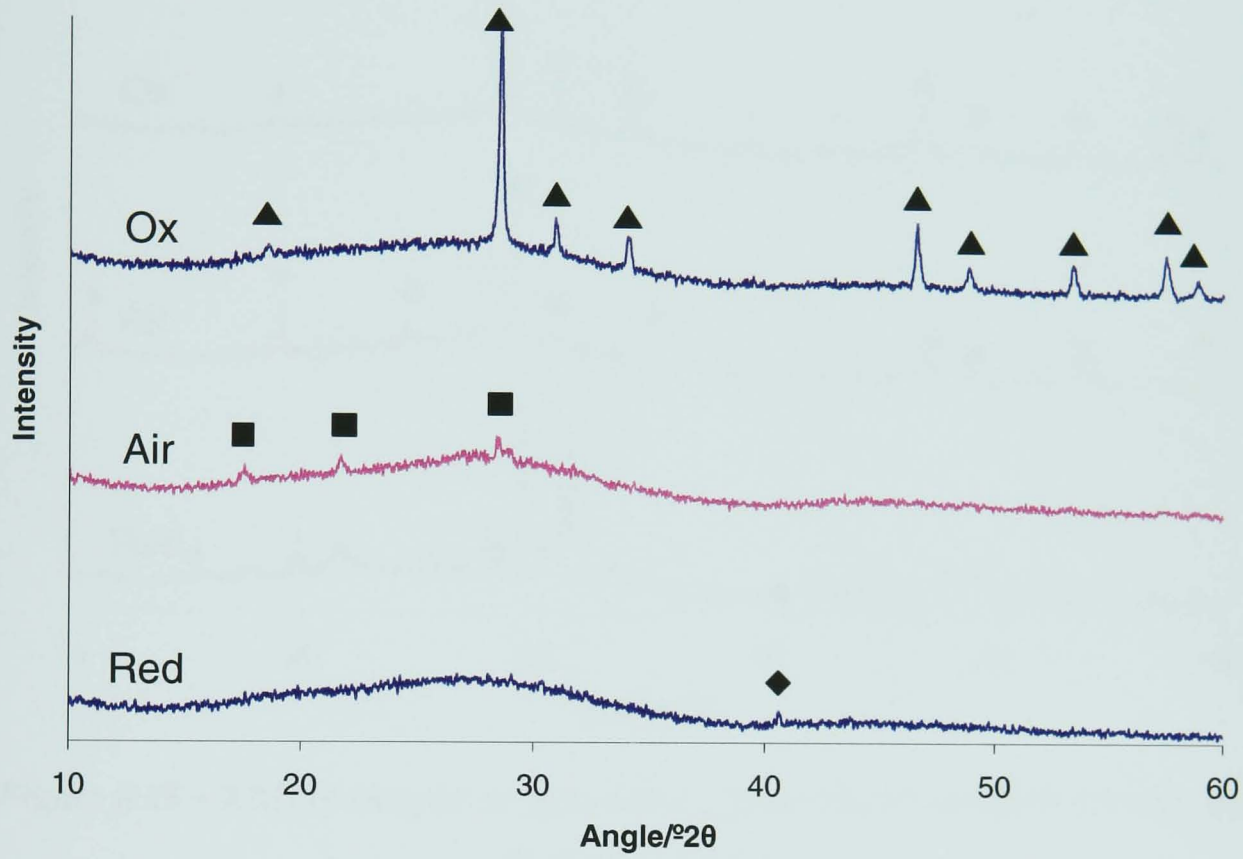

Figure 6.14 – XRD of samples of glass 12(ox), glass 12(air) and glass 12(red) which were heated to 650°C for 48 hours.

It is apparent from the XRD traces that glass 12(red) did not undergo any further crystallisation upon heat treatment than was seen in the as cast glass (denoted by the ♦ in **Figure 6.14**). Some crystallisation has taken place in glass 12(air) (labelled ■ in **Figure 6.14**), although no matches were obtained for this phase from the ICDD database. A significant amount of crystalline material developed in glass 12(ox) during heat treatment. This phase (labelled ▲ in **Figure 6.14**) is a tetragonal scheelite type phase and good matches were obtained from the ICDD database for $(Nd_2(MoO_4)_3)_{1.333}$ and $Na_{0.5}Nd_{0.5}(MoO_4)$ (card numbers [73-498] and [25-852] respectively), both of which are of the same space group ($I4_1/a$) and have d-spacings for the same planes that differ by ~0.01Å.

6.3.2.2 *Glass 13*

XRD of heat treated samples of glass 13 (heated to 650°C for 48 hours) is shown in **Figure 6.15**..

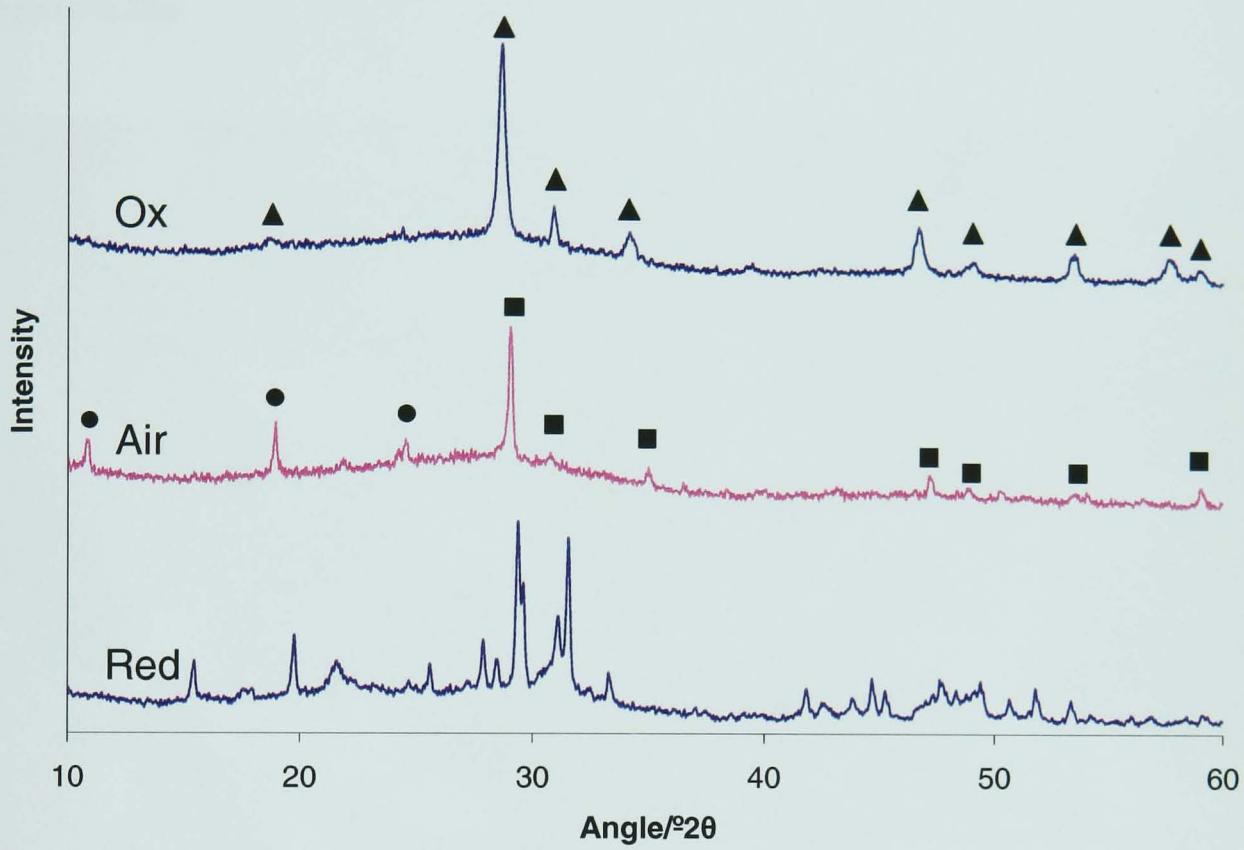

Figure 6.15 – XRD of samples of glass 13(ox), glass 13(air) and glass 13(red) after 48 hours at 650°C

The XRD data shows that significant crystallisation took place upon heat treatment in all of the glass 13 samples, regardless of melting atmosphere. It is also apparent that the type of sparge strongly affected the type of crystalline phase that developed in these samples. The phase that devitrified in glass 13(ox) (denoted by ▲ symbols in **Figure 6.15**) is the same as that seen in the heat treated glass 12(ox) samples, and has been identified as either $(Nd_2(MoO_4)_3)_{1.333}$ or $Na_{0.5}Nd_{0.5}(MoO_4)$ by matching to cards [73-498] and [25-852] from the ICDD database. Glass 13(air) also shows evidence of the phase that developed in glass 12(air) (denoted by ● in **Figure 6.15**). However, the reflections denoted by ■ in **Figure 6.15** indicate the presence of a scheelite type phase in this glass also. This phase could not be matched to any of the ICDD database cards, although the intensities and periodicity of the reflections strongly suggest the presence of a scheelite type molybdate phase as seen in the heat treated glass 13(ox) above. The complexity of the XRD data for the heat treated glass 13(red) sample suggested that

more than one crystalline phase was present in this material, although no matches were obtained for any of the reflections from the ICDD database. TEM analysis of a heat treated sample of glass 13(red) revealed the presence of spherical, needle-like particles and laths(**Figure 6.16a**). Heavier elements are shown as lighter colours in **Figure 6.16a**.

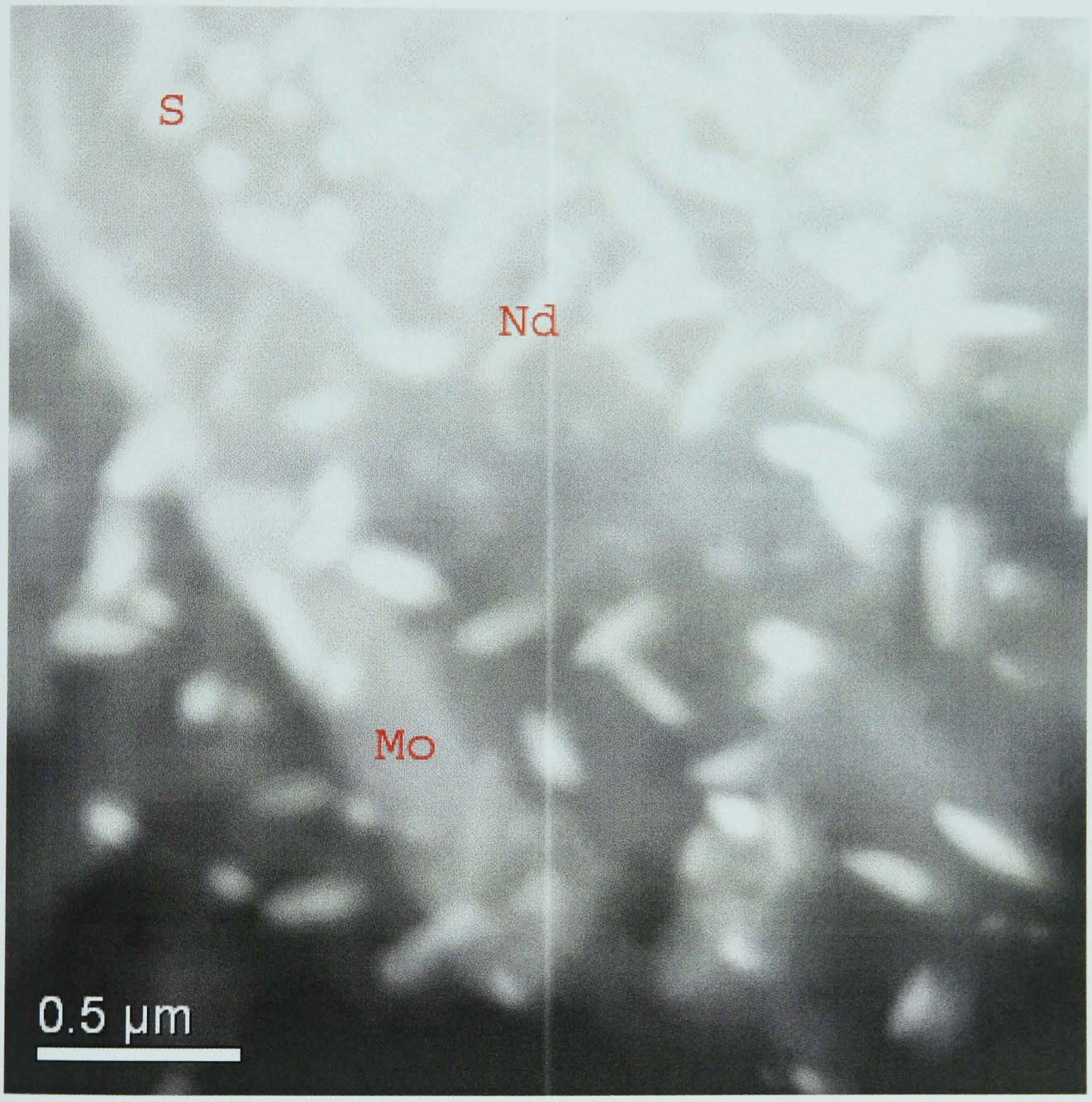

Figure 6.16a – TEM image of a heat treated sample of glass 13(red)

Nd = Needle-like particles high in Nd and O

Mo = Laths high in Mo, Na and O

S = Cross section of needle-like particles

EDS was performed on the sample, and the needle-like particles (labelled "Nd" in **Figure 6.16a**) were found to be high in Nd and O, the laths (labelled "Mo" in **Figure**

6.16a) were high in Mo, Na and O, and the spherical particles were cross sections of the needle-like particles. An EDS map of a portion of the area shown in **Figure 6.16a** illustrating these findings is shown in **Figure 6.16b**.

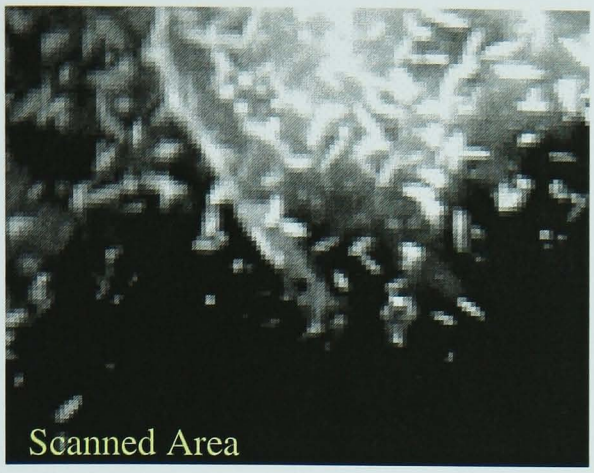

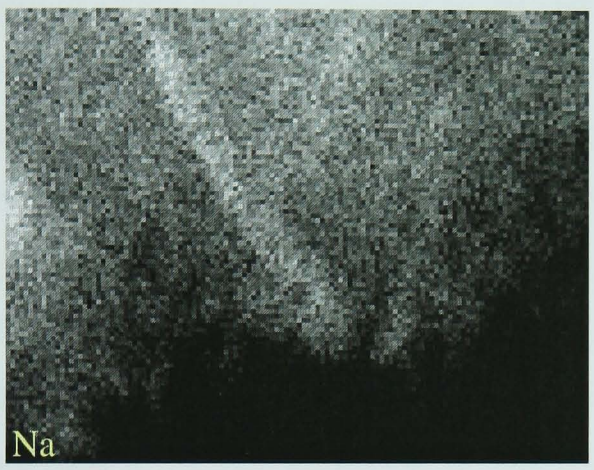

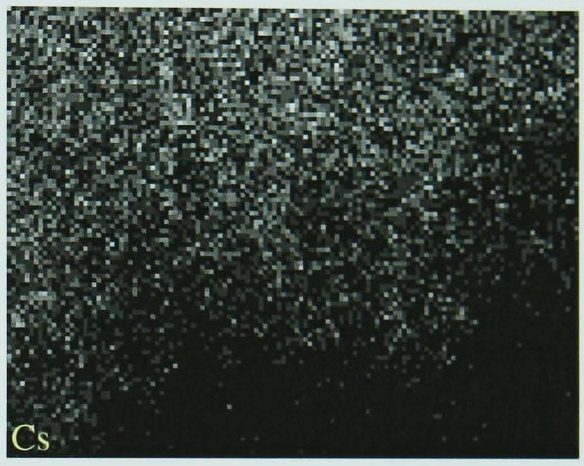

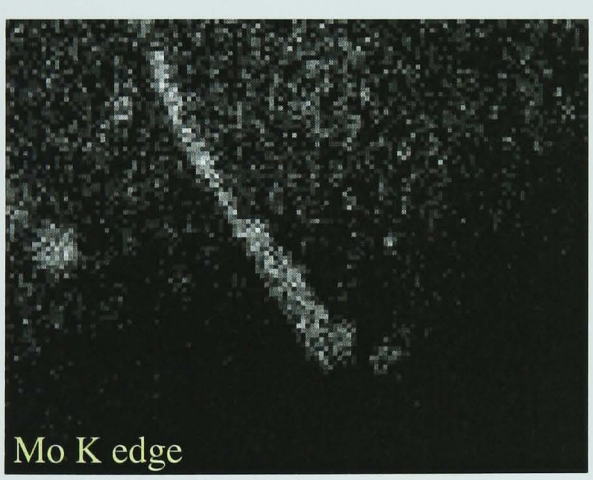

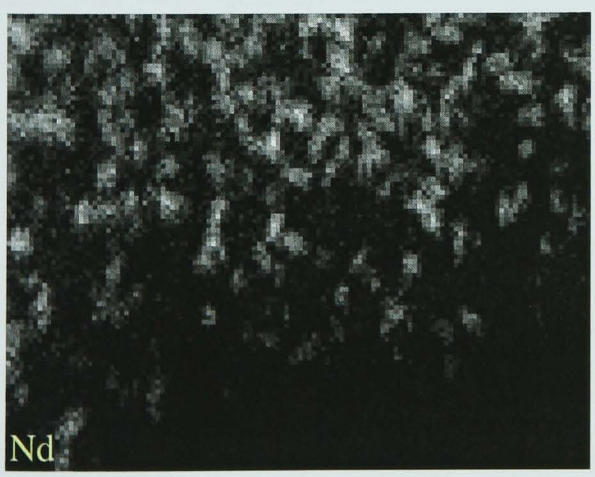

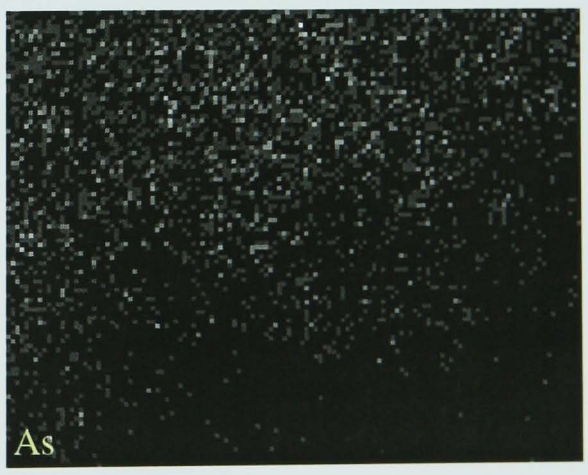

Figure 6.16b – EDS map of a heat treated sample of glass 13(red) – Arsenic was scanned for as a background reference

6.4 Discussion

6.4.1 As Cast Glasses

The appearance of the as cast glasses in this chapter show that colour alone can be a good indication of the effect of different melting atmospheres on the oxidation state of the Mo in these glasses. Mo was the only element present in glasses 11-14 that was likely to effect a colour change as the reduction of Si or B which are strongly bonded to oxygens in the network (the Si-O and B-O bond strengths are 799.6±13.4kJ/mol and 808.8±20.9kJ/mol respectively, CRC Handbook (2000)) was unlikely, and Na, Li and Cs are unstable in their elemental state and would quickly re-oxidise at any opportunity. Also the colouration due to lanthanide elements is independent of oxidation state (Weyl, 1959). Thus, the striking differences in colour between the glasses melted with oxygen or air sparges with those melted using a reducing sparge are a clear indication that some change in the oxidation state of Mo has taken place. This qualitative evaluation is reinforced by the ESR data which clearly shows the presence of Mo^{3+} in the reduced glass 11 and 13 samples via the strong resonance at g = 1.9059(1). However, it is also widely known that small quantities of certain transition metal ions are capable of causing strong colouration in glasses (see, for example, Weyl (1959)), and thus the colour of glasses 11-14 does not give any indication of the proportion of Mo^{6+} (as it is found in the batch) that has been reduced. The spin count from the ESR experiment performed on glass 11(red) shows that the quantity of Mo^{3+} present was low, approximately 2.3% of the total Mo. The XPS scans confirm this result, as no Mo^{3+} was detected in either glass 11(red) or glass 14(red). Thus, the quantity of Mo^{3+} in the reduced glasses was less than the detection limit of the XPS. However, an unexpected result of the XPS analysis was the presence of Mo^{4+} in the air sparged glass 11 and glass 14 samples. Although the overall quantity of reduced Mo species was higher in the reduced glass 11 and glass 14 samples than in the air sparged glass 11 and glass 14 samples, this result did show that some reduction of Mo^{6+} had occurred in glasses melted in atmospheres with abundant oxygen. The EXAFS experiments performed on these glasses agreed with the ESR results, as they gave similar data regardless of the sparge applied. These data showed that in all of the analysed glasses there was only one regular coordination shell around

the Mo ions at a distance of ~1.75Å, corresponding to the presence of $(MoO_4)^{2-}$ groups. Therefore the majority of the Mo in all of the samples must have been hexavalent (as was also shown by XPS). These results again correspond well with those of Calas (2003) (discussed fully in **Chapter 4.4.2**).

XRD of the as cast samples revealed little difference between the glasses melted in oxygen rich and oxygen poor atmospheres. Only glasses 12(red) and 13(ox) showed any evidence of the presence of crystalline material, and neither traces exhibited enough reflections to positively identify the material causing them. In the case of glass 12(red), the one reflection does have a good match with that of the 110 plane Mo metal, although the absence of this reflection in glasses 13(red) and 14(red), both of which contain more Mo than glass 12(red) and were melted under the same conditions, suggest that this may be a spurious result. The most significant conclusion that can be drawn from the XRD data of the as cast samples of glasses 11-14 is that the bulk of the material was amorphous regardless of melting atmosphere.

6.4.2 Heat Treated Samples

Upon heat treatment it became apparent that there were significant differences in the crystallisation behaviour of glasses 12 and 13 with respect to the sparge applied during melting. Glass 12 (a composition designed to represent that of the standard HLW glass (glass 1) containing 25% waste, although greatly simplified) only showed a tendency to develop a scheelite type molybdate phase (as seen in the fully waste loaded glasses in **Chapter 4.3.4**) upon heat treatment after melting in an oxygen atmosphere. The same composition melted in an air atmosphere did undergo some crystallisation (but the phase could not be identified), although no evidence of a scheelite type phase was apparent. Glass 12(red) only gave one reflection under XRD after heat treatment, in the same position as that seen in glass 12(red) prior to heat treatment but at a reduced intensity, indicating that in this sample the quantity of crystalline material actually decreased upon heat treatment. The comparative intensities of the reflections (**Figure 6.14**) of all of the heat treated glass 12 samples clearly shows that increasing the amount of oxygen available to the glass during melting increases the quantity of crystalline material formed during heat treatment.

Thus, for this composition, melting under a reducing sparge is beneficial with respect to the devitrification properties of the glass.

Upon moving to glass 13 (a composition designed to represent that of the standard HLW glass (glass 1) containing 35% waste but again, greatly simplified), the difference between XRDs of the heat treated oxygen and air sparged glasses is less striking than for glass 12. The results show that a scheelite type molybdate phase has developed in glass 13(ox) and strongly suggest (by comparison to those results discussed in **Chapter 5**) that a structurally similar but compositionally different scheelite type molybdate is present in glass 13(air). Glass 13(red) also underwent considerable devitrification upon heat treatment and EDS showed that two distinct crystalline phases developed, one neodymium oxide phase and one sodium molybdenum oxide. These crystalline phases could not be identified from the XRD patterns using the ICDD database, although several entries are present for neodymium oxides and sodium molybdates. The entries for sodium molybdates cover the majority of the lattice types (i.e. cubic, hexagonal, monoclinic, triclinic, orthorhombic and rhombohedral) and have compositions ranging from $NaMoO_2$ to $Na_{0.93}Mo_6O_{17}$. Those for neodymium oxides show cubic, hexagonal and monoclinic structures with compositions ranging from NdO to Nd_6O_{11}. Thus, the scope for the compositions and structures of sodium molybdates and neodymium oxide phases is broad, and it is likely that the phases formed in the heat treated glass 13(red) sample have not been previously characterised and filed in the ICDD database. However, the XRD results do indicate that no powellite type molybdate phase was present in the heat treated glass 13(red). In all of the previous samples containing a powellite type molybdate phase, a (200) reflection is present at ~5.5°2θ after the (112) reflection (which is always the most intense reflection for the powellite type molybdates seen previously). The XRD trace of the heat treated glass 13(red) does not exhibit this reflection, regardless of which of the 2 most intense peaks is theoretically assigned as being the (112) reflection. However, this does not indicate that the crystals in glass 13(red) would be any more appropriate in a HLW glass composition, as this would depend on their chemical durability, thermal expansion properties etcetera as compared to the glass matrix. Thus, glass 13(ox) behaved in the same manner as glass 12(ox), whilst the increase in the simplified waste loading of glasses 13(air) and 13(red) compared to 12(air) and 12(red) increased their tendency to form crystalline material upon heat

treatment. Given the likely mismatches in thermal expansion coefficients between the glass matrix and the crystalline material (regardless of the type of crystals that develop) and the inevitable segregation of at least some of the elements into rich and poor domains that has to occur upon crystallisation, devitrification of the glass would ideally be avoided. This indicates that even when melted under a reducing sparge, a waste loading of 35wt% is too great to be incorporated into a product that is likely to remain amorphous upon heat treatment.

Interestingly, the French vitrification programme uses an argon sparge (Vernaz, 2002) which might be expected to create a mildly reducing melting atmosphere during melting. On the evidence from the various works previously mentioned in this chapter, this would be expected to be beneficial from a Mo point of view as it would decrease the tendency for yellow phase formation in the melt. The reason that BNFL swapped from an argon to an air sparge on purchasing the AVM process from the French is at present unclear, although it must be remembered that there are many other elements contained in the HLW stream whose oxidation states will also be affected by melting atmosphere. Some of these elements (such as Ru and Pd for example) need to be kept in higher oxidation states in the melt, or may otherwise precipitate out as detrimental crystalline phases (such as needles of RuO_2 or even elemental metals) which can form a heel in the melter which eventually becomes a reason for scrapping it.

6.5 Conclusions

• Sparging simplified HLW glasses with a reducing atmosphere can partially reduce the oxidation state of Mo in the glass from +6 to +3

• Even with a reducing sparge, the majority of the Mo in simplified HLW glasses remains as Mo^{6+}.

• At 25wt% waste loadings, simplified HLW glasses have a greater tendency to devitrify upon heat treatment if they are melted under oxidising conditions than if they are melted under reducing conditions

• At 35wt% waste loadings, simplified HLW glasses devitrify upon heat treatment regardless of the sparge applied during melting.

• Simplified 35wt% waste loaded HLW glasses melted under a reducing sparge do not form powellite molybdates upon heat treatment.

7. Conclusions and Suggestions for Further Work

7.1 Relevance to Real HLW Glasses

As discussed in **Chapter 3**, the glasses used in this work were composed with the intention of simulating a real HLW vitrification matrix. However, for much of the research the composition had to be modified to obtain the best results from the analysis techniques used, or in order to observe the effect of changing the composition on the Mo incorporation. The HM4 composition (glass 1) is the most representative composition of the real HLW glasses currently being produced by BNFL. The base glass composition (the Si, B, Na and Li quantities) used was close to that used by BNFL, although the quantity of Li was boosted slightly to account for the Li added to the HLW stream during calcination in the real process. Whenever possible, the ratios of these 4 basic elements were kept constant to maintain the relevance of the work to real HLW vitrification, although some of the experiments did require alteration of the ratios in order to observe the consequences of such an action.

The HLW stream itself is intrinsically more complicated to simulate. The composition of a real HLW stream is constantly changing due to the radioactive decay process, and the settling of heavier elements during storage of the liquid waste in tanks. Therefore, the composition of the liquor taken from the top of a given tank is considerably different to that taken from the bottom. Experiments (mainly durability studies) have been performed using glasses doped with various radionuclides. However, batching a glass containing all the radionuclides found in a real HLW stream would be an extremely costly and difficult process which would have to be carried out robotically in a hot cell (or an equivalently radiation shielded environment), as would melting and any further analysis of the glass. These restrictions made using an accurate active simulant unfeasible given the facilities available at the time the work was carried out. Yet it was possible to mimic the behaviour of the typical radioactive HLW components using inactive elemental isotopes, or by using elements that have similar chemistry. Thus, many of the radioactive actinides that could not be used were

accounted for by increasing lanthanide levels, ^{135}Cs and ^{90}Sr were replaced with ^{133}Cs and ^{88}Sr (the natural stable isotopes), Tc was simulated by Ti and Ag was used to simulate the more toxic and expensive heavy metals such as Cd, Pd and Rh. Another problem in making a direct comparison between the simulated waste stream used here and the real HLW stream which it replicates, is that the stream used here was based on a predicted future waste stream that will be used should BNFL decide to start vitrifying a 4:1 blend of high burn up:MOX reprocessed fuel, and thus no real waste stream actually existed with which to make a comparison. If all of these factors are taken into account, it can be concluded that although the simulated waste stream used for these experiments is a reasonable model of a real HLW stream, its direct relevance to BNFL operation cannot be judged until (or unless) the plant moves to vitrifying such a stream. An important consideration is that the stream contains a high concentration of Mo, and was therefore of a suitable and appropriate composition for studying the incorporation of Mo in HLW glasses.

7.2 Molybdate Formation

The sample of yellow phase taken from a full scale simulated HLW glass melted on line 3 (prior to the line going into production of active HLW glass) at the Sellafield vitrification plant, was shown by XRD to be a complex mix of crystalline and amorphous material (**Chapter 5.3.5**). Previous analysis of similar samples of yellow phase have shown it to be composed of various mixtures of sulphates, chromates and molybdates, although the exact composition of the phase will always depend on the composition of the waste stream from which it develops. Thus, the crystalline material that was found in many of the compositions in this work is representative of the composition of the batch from which it ultimately developed. It is therefore unlikely to be of a similar overall composition to yellow phase samples found in glasses currently melted on full scale vitrification lines using simulated HLWs representing current liquors, as the HLW simulant used in this work did not contain any sulphur and virtually insignificant amounts of chromium, the compounds of which tend to make up over 50% of yellow phases from full scale melts.

This made it necessary to examine the relevance of the molybdates produced to the real yellow phase composition. As mentioned earlier, previous authors have shown yellow phase to be partially composed of molybdates, and so the presence of scheelite type molybdates in samples of the simulated HLW glasses produced in this work was a good indication that similar phases were developing. Further evidence for the similarity of the scheelite molybdates to the real yellow phase molybdates comes from the Mo K edge EXAFS analysis of the yellow phase compound and of the 2 alkali earth molybdates that were sintered for standardisation purposes, $CaMoO_4$ and $SrMoO_4$. The results of alkali earth molybdate analysis (**Chapter 5.3.5**) clearly show 2 coordination shells around the Mo scatterer, one representing a 4 fold coordination to oxygen ions at ~1.76Å, and then another showing an 8 fold coordination to the alkali earth metal ions at a distance of ~4Å. The EXAFS of the yellow phase, however, crucially only shows evidence of the 4 fold coordination of the oxygen atoms around the Mo centres, and does not indicate the presence of a regular second coordination shell around these Mo-O tetrahedra. Thus, the arrangement of these cations is likely to be irregular, as some cations have to be in close proximity to

$(MoO_4)^{2-}$ units to balance the charge. This model fits well with the proposed scheelite-type molybdate structure with a random arrangement of cations on the A site (**Chapter 5**) for the crystalline material that was found in the simulated HLW glasses melted in this work. Therefore, it can be concluded that the scheelite type molybdates that were referred to as being analogous to yellow phase in earlier chapters are representative of the composition of the "yellow phase" that would be produced should this HLW stream ever be fed into the vitrification process. It can also be concluded that these molybdates are similar to the molybdate portion of the yellow phase sample taken from the full scale line 3 glass melted at Sellafield. However, until BNFL vitrify a waste stream (on a full scale plant) that represents the predicted composition of 4:1 blend of oxide/magnox waste used in this study, it will be impossible to make a direct comparison between the molybdates formed in these experiments and the yellow phase that will develop in these glasses with the reduced Cr and S levels.

7.3 Effect of Altering the Base Glass Composition

In **Chapter 4.3.3.2** it was shown that upon heat treatment of the standard simulated HLW glass containing a 35% waste loading, 2 scheelite type molybdate phases develop in the glass. Further experimentation (**Chapter 4.3.3.3**) showed that by reducing the Li content of the base glass composition, the number of scheelite-type molybdates that developed upon heat treatment could be reduced to 1. This effect would initially suggest that a reduced Li base glass would be a better composition to use as a matrix for HLW vitrification, as it reduced the potential for crystalline formation. However, altering the base glass composition can have significant effects on other glass properties. From a vitrification standpoint, the most problematic effect of a reduction in Li is likely to be seen as an increased viscosity at any given temperature, as Li acts as a flux during glass making (an effect apparent in this work as an increase in T_g of the reduced Li glasses 3-5). This would mean that the glass would need to be melted at a higher temperature to attain an equivalent level of homogeneity compared to the current vitrification matrix, and to attain the equivalent degree of viscosity required upon pouring. Any increase in melting temperature would be associated with an increase in cost (an important factor in HLW vitrification), and would be likely to lead to a decrease in melter lifetime due to the extra thermal load on the system, and as previously mentioned, replacing melters in hot cells is time consuming and costly.

From a long term storage standpoint, the viscosity increase would have the advantage of increasing the T_g of the glass, which would decrease the potential for crystalline phase formation (as the crystallisation process cannot proceed at temperatures lower than T_g in silicate systems). The Li reduction, as mentioned above, would also have the advantage of reducing the potential number of crystalline phases that could develop in the glass. However, the chemical durability of the glass is arguably the most important factor when considering long term storage in repository conditions, and this too can be greatly affected by a change in composition. In the standard base glass composition, the Li and Na may work together to produce a mixed alkali effect. It is widely known that adding 1/2x moles of alkali A and 1/2x moles of alkali B to a silicate glass can produce a more durable matrix than the equivalent silicate

containing x moles of either A or B. Thus it can be concluded that removing the Li from the HLW base glass composition could have a detrimental effect on the chemical durability of that glass.

The process of eliminating Li from the base glass would also lead to other problems for HLW vitrification. For example, Li is currently added to the HLW prior to the calcination process to reduce refractory oxide formation during calcination. This process is currently under consideration for redundancy in order to increase the available storage area in the highly active liquor storage tanks at Sellafield (as the pre-calcination Li feed tank is currently located in the liquor storage tanks). However, a reduction in Li (rather than a total elimination) has been shown to decrease the amount of crystalline material formed (glasses 3 and 4), and so a total elimination may not be necessary. Thus we can conclude from the work performed on the affects of base glass alteration, that a reduction in Li would be advantageous from a molybdate crystallisation point of view (i.e. less of it could potentially form and higher temperatures would be required during storage for it to form), but this advantage would need to be weighed against the increase in melting temperature required and the possible reduction in durability (with respect to aqueous attack) of the matrix.

7.4 Effect of Changing the Melting Atmosphere

It has been proposed by previous authors that reducing the oxidation state of the Mo in HLW glasses could increase the solubility of the Mo in the matrix via a reduction in field strength, and thus lead to a reduction in yellow phase formation. Field strength (z/a^2) can be used as a measure of the interaction between a cation and an adjacent O^{2-} anion, at a distance a from the cation (where z is the valency of the cation). By reducing the valency of Mo^{6+} to Mo^{5+}, Mo^{4+} or Mo^{3+} and keeping a the same, it is possible to see that the field strength of the cation would be reduced, although in reality a would be likely to increase as z decreased, as the radius of the Mo ion would increase due to an increase in the effective nuclear shielding of the electron shells with decreasing valency. In relation to glass melting, it has also been suggested (Weyl, 1962) that the greater the difference in field strengths between 2 cations, the more likely that a stable compound can be formed between those 2 cations. Thus, in a silicate network, reducing the field strength of the Mo should (assuming the field strength of Si stays the same) lead to a greater chance of the Mo being incorporated into the silicate network rather than it forming independent structures in network holes (i.e. not chemically bonded to the silicate network).

This hypothesis was examined by melting a range of simulated HLW glass compositions in various atmospheres. The ESR analysis performed on the reduced simplified batches containing only the base glass with 1wt% Mo in **Chapter 6.3.1.1** showed that it was possible to reduce some of Mo^{6+} found in the glass batch to Mo^{3+} by melting the glasses in a reducing atmosphere. However, the ESR spin counts along with the EXAFS analysis showing the presence of $(MoO_4)^{2-}$ tetrahedra in the reduced glasses, indicated that the majority of the Mo was still in the +6 valence state. However, the heat treatments performed on the simplified glasses containing a partial waste stream at a 25wt% waste loading (**Chapter 6.3.2.1**) did show that melting in a reducing atmosphere decreased the tendency for crystalline formation compared to glasses melted in an atmosphere containing an abundance of oxygen. When the waste loading of the reduced simplified batch was boosted to 35wt% (**Chapter 6.3.2.2**), the development of a scheelite-type molybdate phase still did not occur upon heat treatment, although there was a significant crystalline presence in the sample. Thus, it

would appear from experiments on the simplified batches that melting in a reducing atmosphere would be beneficial in terms of reducing the tendency to form a scheelite type molybdate structure. Whether this is an overall benefit would depend on the properties of the phase formed in the reduced case.

The heat treatments performed on the simulated glasses containing various loadings of the full simulated waste stream and melted in reducing and air atmospheres gave the opposite results (**Chapter 4.3.4**). At a 20% waste loading, the glass melted in the air atmosphere showed no tendency for crystallisation upon heat treatment, whereas a scheelite-type molybdate phase did develop upon heat treatment of the same composition melted in a reducing atmosphere. Even in the as-cast state metallic silver was found in glass 7(red) via XRD analysis (**Chapter 4.3.2.1**), a problem that did not occur in the air sparged glasses until the waste loading was increased to 35wt%. Thus, the experiments on glasses containing the full simulated HLW stream show that melting these batches in a reducing atmosphere increases the tendency for scheelite-type molybdate formation upon heat treatment. That said, it is also possible to conclude that these experiments (i.e. melting glasses 7 to 10 in reducing atmospheres) did not succeed in their intention of assessing whether reduced Mo is more easily incorporated into the matrix, as the ESR and EXAFS results indicated that the majority of the Mo remained in the +6 oxidation state, and was not therefore reduced during melting.

Extrapolation of these results leads to the conclusion that melting in a reducing atmosphere would be detrimental to the real vitrification process. As was mentioned earlier, the formation of metallic silver in the reduced glasses 7-10, was a phenomenon that is unlikely to occur in a real HLW glass as the percentage of silver in a real HLW stream would be much lower. But it does seem to be important with regards to the formation of scheelite-type molybdates in these glasses. When the heat treated glass 7(red) sample was examined using TEM, it was noted that the molybdate particles were significantly more abundant in areas close to silver particles than in areas where no silver was observable. Thus, silver particles seem to act as nucleation centres for the molybdate phase, although the presence of molybdate particles in glasses where no silver particles were found indicates that molybdate formation is not

exclusively linked to silver. Silver was added to these glasses as a substitute for chemically similar elements such as Pd or Rh, so if a real HLW glass were to be melted in a reducing atmosphere it is likely (based on the results presented here) that these elements would be more susceptible to reduction than the Mo, and could act as nucleation sites for Mo-containing crystalline phases. Further problems would also be created in a real vitrification plant by formation of metallic particles during melting. They would be denser than the melt and would thus tend to sink to the bottom of the melter, which would add to the problem of heel formation, a phenomenon that can eventually require the replacement of the melter. Metallic particles can also lead to drilling of the melting vessel (Watts, 2001) – a problem where a particle gets stuck against the side of the vessel and is caused to rotate by the convection currents in the melter, thus drilling into the lining and potentially causing melter failure.

If all of the Mo^{6+} could be selectively reduced to Mo^{3+} without altering the oxidation state of the other elements in the glass, then this would be a valid method of preventing scheelite-type molybdate formation, as $(MoO_4)^{2-}$ tetrahedra would not be able to form in the melt and thus the scheelite unit cell could not develop. However, due to the compositions of the current and predicted real HLW streams, it is always likely that there will be elements present that are more susceptible to reducing agents than Mo, and plenty of transition metals that would be likely to form redox couples. Therefore, it seems that reduction of Mo via sparging with a reducing atmosphere is unlikely to be beneficial to the overall composition.

7.5 Summary

In the high (35wt%) waste loaded simulated HLW glasses melted for this project, a scheelite-type molybdate phase containing a random arrangement of Sr, lanthanide elements and possibly the alkali metals Li and Na on the A site, tends to form upon heat treatment. This phase is analogous to the yellow phase compound found in full scale simulated HLW glasses melted at the Sellafield vitrification plant, although the specific phases found are particular to the composition studied here. Reducing the quantity of Li in the base glass reduces the number of crystalline phases formed upon heat treatment, but increases the viscosity of the glass at a given temperature. Melting the glass using a reducing sparge as opposed to a compressed air sparge can partially reduce the Mo^{6+} to Mo^{3+}, although the majority of the Mo remains in the +6 oxidation state. This method of reduction also leads to the formation of metallic particles in the glass, and tends to increase the likelihood of scheelite type-molybdate formation upon heat treatment of glasses containing the full HLW stream.

7.6 Further work

The work performed for this project highlights the necessity for further fundamental research in this area. There were also several experiments that I would like to have performed during the course of this work, but unfortunately did not get done due to the time constraints associated with conducting PhD research. The major areas that I would like to expand upon with more research are listed below.

- Analysis of more samples of yellow phase from various full scale simulated HLW melts in order to fully characterise the chemical properties in relation to batch composition.

- SEM and TEM analysis of the glass-glass phase separation observed in many of the compositions melted containing the full simulated HLW stream. If a significant compositional difference could be observed between the different phases, this could lead to a greater understanding of both the precursors of molybdate formation and the chemical durability of the system.

- Further studies on the effects of base glass composition alteration. This could lead to the formulation of a base glass composition that has a reduced tendency for molybdate formation, and yet retains the favourable physical properties (e.g. liquidus temperature, glass transition temperature) of the current composition.

- More work in the field of Mo reduction. It may be possible to reduce more of the Mo^{6+} if the glass was melted in a more strongly reducing atmosphere, or possibly to target Mo specifically with a chemical reducing agent rather than relying on a sparge which affects the whole batch.

- Remelt the more significant glasses from the base glass alteration and Mo reduction experiments using a more accurate (i.e. closer to a real) HLW stream composition to see if the theories proposed earlier (such as the reduction of heavy metal oxides to elements during melting with a reducing sparge) hold true.

- Chemical durability studies on all of the significant compositions are necessary. Although likely changes in chemical durability have been inferred from glass theory for many of the compositions studied in this work, experiments simulating the long term corrosion of any possible HLW vitrification matrix are indispensable. Whilst the author acknowledges that simulating many hundreds of thousands of years in an underground repository is a task that rarely promotes agreement between scientists on the best method of simulating it, it is an essential undertaking.

- Investigate the possibility of chemical additions to the glass batch that may act as a suppressant to the formation of molybdates.

References

Amphlett, C.B., Treatment and Disposal of Radioactive Wastes, Ed. Dunworth, J.V., (Permagon Press), 1961

Bando, Y., Iijima, S., Kawamoto, Y., Tomozawa, M., Application of STEM to Elemental Analysis in Glass, Journal of Non-crystalline Solids, Vol. 42, 1980, p.151-156

Barath, F., Turki, M., Keller, V., Maire, G., Catalytic Activity of Reduced MoO_3/α-Al_2O_3 for Hexanes Reforming, Journal of Catalysis, Vol. 185, 1999, p. 1-11

Berkhout, F., Radioactive Waste: Politics and Technology, (Routledge, London) 1991

Bobkova, N. M., Rakov, I. L., Solovei, N. P., Spectroscopic Study of Molybdenum Containing Glass Structure, Journal of Non-crystalline Solids, Vol. 111, 1989, p.98-102

Briggs, D., Seah, M. P., Practical surface analysis - Vol.1 : Auger and X-ray photoelectron spectroscopy (Chichester, Wiley), 1990

Buhler, P., Thermodynamics of Redox Reactions Between Oxides of Glass Melt and Oxygen: V. Coupled Redox Reactions, Glass Physics and Chemistry, Vol. 25, No. 2, 1999, pp.172-175

Calas, G., Le Grand, M., Galoisy, L., Ghaleb, D., Structural Role of Molybdenum in Nuclear Glasses: An EXAFS study, Journal of Nuclear Materials, Vol. 322, 2003, p. 15-20

Calestani, G., Ferraguti, E., Montenero, A., Ingletto, G., Bettinelli, M., Influence of Simulated Waste Oxides on the Durability of a Borosilicate Glass, , Inorganica Chimica Acta, Vol. 94, February 1984, pp.125-126.

Camera, B., Lutze, W., Lux, J., 1980, Scientific Basis for Nuclear Waste Management, MRS Symposium Proceedings Vol. 2, Boston, 1979 ed. C.J.M. Northrup Jr (Plenum Press, New York)

Christofilos, D., Kourouklis, G. A., Ves, S., A High Pressure Study of Calcium Molybdate, Journal of Physics and Chemistry of Solids, Vol. 56, 1995, pp.1125-1129

Clauβen, O., Rüssel, C., Thermodynamics of Some Transition Metal Ions in a Borosilicate Glass Melt, Phys. Chem. Glasses, 1997, Vol. 38 (5), pp. 227-231

Clark, D.E., Maurer, C.A., Jurgensen, A.R., Urwongse, L., Effects of Waste Composition and Loading on the Chemical Durability of a Borosilicate Glass, Scientific Basis for Nuclear Waste Management V, Ed. W. Lutze, (North-Holland, Amsterdam) 1982, pp. 1-13.

CRC Handbook of Chemistry and Physics 80th Edition, Ed. Lide, D.R. (CRC Press, London), 2000

Day, D. E., Mixed Alkali Glasses – Their Properties and Uses, Journal of Non-Crystalline Solids, Vol. 21, 1976, p.343-372

DEFRA – Department for Environment, Food and Rural Affairs, Managing Radioactive Waste Safely – Proposals for developing a policy for managing solid radioactive waste in the UK, September 2001, pp 14-15

Donald, I.W., Metcalfe, B.L., Taylor, R.N.J., The Immobilisation of High Level Radioactive Wastes Using Ceramics and Glasses, Journal of Materials Science, Vol. 32, 1997, p.5851-5887

Donald, I. W., Metcalfe, B. L., Bradley, D. J., Hill, M. J. C., McGrath, J. L., Bye, A. D., The Preparation and Properties of some Lithium Borate Glasses, Journal of Materials Science, Vol. 29, 1994, p. 6379-6396

Donald, I. W., Metcalfe, B. L., Morris, A. E. P., Influence of Transition Metal Oxide Additions on the Crystallisation Kinetics, Microstructures and Thermal Expansion Characteristics of a Lithium Zinc Silicate Glass, Journal of Materials Science, Vol. 27, 1992, p.2979-2999

Doremus, R. H., Treatise on Materials Science and Technology, Volume 17, Glass II (Academic Press, London) 1979, p.58-61

Duffy, J.A., Stability of Metal Ions in Molten Glass: the Definition of Reduction and Oxidation, Phys. Chem. Glasses, 1999, Vol. 40, April 1999, 54-56

Ewing, R.C., Weber, W.J., Clinard, F.W.Jr., Radiation Effects in Nuclear Waste Forms for High-Level Radioactive Waste, Progress in Nuclear Energy, 1995, Vol. 29, No. 2, pp.63-127

Feng, X., Pegg, I.L., Saad, E., Cucinell, S., Barkatt, Aa., Redox Effects on the Durability and Viscosity of Nuclear Waste Glasses, Nuclear Waste Management 3, Ceramic Transactions, Vol. 9, 1989

Fortner, J.A., Buck, E.C., Ellison, A.J.G., Bates, J.K., EELS Analysis of Redox in Glasses for Plutonium Immobilisation, Ultramicroscopy, Vol. 67, 1997, pp. 77-81

Gibb, F. G. F., High Temperature, Very Deep, Geological Disposal: A Safer Alternative for High Level Radioactive Waste?, Waste Management, Vol. 19, 1999, p. 207-211

Gin, S., Jollivet, P., Mestre, J. P., Jullien, M., Pozo, C., French SON 68 Nuclear Glass Alteration Mechanisms on Contact with Clay Media, Applied Geochemistry, Vol. 16, 2001, p. 861-881

Goldman, D.S., Brite, D.W., Redox Characterisation of Simulated Nuclear Waste Glass, Journal of the American Ceramic Society, Vol. 69 (5), 1986, p. 411-413

Guinier, A., X-ray Diffraction in Crystals, Imperfect Crystals and Amorphous Bodies (New York, Dover), 1994

Harbour, J.R., Volatility of Simulated High-Level Nuclear Waste Glass by Thermogravimetric Analysis, Journal of the American Ceramic Society, Vol. 75 [3], 1992, pp.507-513

Hayward, P.J., The use of Glass Ceramics for Immobilising High Level Wastes from Nuclear Fuel Recycling, Glass Technology, Vol. 29, Nº 4 August 1988

Holzwarth, S., Russel, C., Tomandl, G., Corrosion of Molybdenum Electrodes in an Aluminosilicate Glass Melt, Glastech. Ber., Vol. 64, 1991, p. 195-198

Horneber, A., Camera, B., Lutze, W., 1982, Scientific Basis for Nuclear Waste Management V, ed. W. Lutze (North Holland, Amsterdam) Vol. 11, 1982,

Isard, J. O., The Mixed Alkali Effect in Glass, Journal of Non-Crystalline Solids, Vol. 1, 1969, p.235-261

Iwase, M., Okumura, T., Kawamura, K., Miyamoto, Y., Oh-uchi, H., Oxidation-reduction Equilibrium of Fe^{3+}/Fe^{2+} in a Candidate Glass for the Immobilisation of High Level Nuclear Waste, Glass Technology, Vol. 39, (4), 1998, p. 142-146

Jantzen, C.M., Nuclear Waste Glass Durability: 1, Predicting Environmental Response from Thermodynamic (Pourbaix) Diagrams, Journal of the American Ceramic Society, Vol. 75 [9], 1992, p. 2433-2448

Jégou, C., Gin, S., Larché, F., Alteration Kinetics of a Simplified Nuclear Glass in an Aqueous Medium: Effects of Solution Chemistry and of Protective Gel Properties on Diminishing the Alteration Rate, Journal of Nuclear Materials, Vol. 280, 2000, p. 216-229

Johnson, K. D. B., Marples, J. A. C., Glasses and Ceramics for Immobilisation of Radioactive Wastes for Disposal, UK Atomic Energy Authority Report R-9417, 1979, p. 1

Johnson. W., Park, Y. S., Butt, D. P., Castro, R., Petrovic, J., Durability of Molybdenum Disilicide in Molten Alkali Borosilicate Glass, Materials Science and Engineering A, A261, 1999, p.278-283

Kawamoto, Y., Clemens, K., Tomozawa, M., The Effect on Phase Separation of the Oxidation State of Molybdenum in a Na_2O-B_2O_3-SiO_2 Glass, Physics and Chemistry of Glasses, 1981, Vol. 22, No.5, p.110-114

Krause, Ch., Luckscheiter, B. Properties and Behaviour of the Platinum Group Metals in the Glass Resulting From the Vitrification of Simulated Nuclear Fuel Reprocessing Waste. J. Mat. Res., Vol. 6, Nº 12, December 1991 2535-2546

Lutze, W., Ewing, R.C. Radioactive Waste Forms for the Future (North Holland, Amsterdam) 1988

Mackenzie, R.C., Differential Thermal Analysis Vol. 1: Fundamental Aspects (London, Academic Press), 1970

Marples, J.A.C., The Preparation, Properties, and Disposal of Vitrified High Level Waste from Nuclear Fuel Reprocessing, Glass Technology, Vol. 29, Nº 6 December 1988

Matzke. H. J., Actinide Behaviour and Radiation Damage Produced by α-Decay in Materials to Solidify Nuclear Waste, Inorganica Chimica Acta, Vol. 94, February 1984, pp.142-143.

McGrail, B. P., Icenhower, J. P., Shuh, D. K., Liu, P., Darab, J. G., Baer, D. R., Thevuthasen, S., Shutthanandan, V., Englehard, M. H., Booth, C. H., Nachimuthu, P., The Structure of Na_2O-Al_2O_3-SiO_2 Glass: Impact on Sodium Ion Exchange in H_2O and D_2O, Journal of Non-crystalline Solids, Vol. 296, 2001, p. 10-26

Medlin, M.W., Sienerth, K.D., Schreiber, H.D., Electrochemical Determination of Reduction Potentials in Glass-Forming Melts. Journal of Non-Crystalline Solids, Vol. 240 (1998) 193-201

Min'ko, N. I., Zhernovaya, N. F., Tkachenko, O. I., Krasavin, V. Y., Baskova, Z. P., The effect of Process Parameteres on the Stability of Molybdenum Electrodes in Glass Melting Furnace, Glass and Ceramics, Vol. 57, 2000, p. 333-337

Mokhosoev, M.V., Get'man, E.I., Alekseev, F.P., Double Molybdates of Rubidium and Rare-earth Elements of Composition $RbLn(MoO_4)_2$, Russian Journal of Inorganic Chemistry, Vol. 14, 1969, p.1691-1694

Muller, O., The Major Ternary Structural Families (Springer-Verlag, Berlin) 1974, p. 83-152

Orlhac, X., Fillet, C., Brec, R., Deniard, P., Phalippou, J., Proceedings of the International Conference ATLANTE, 2000, p.5.04.0

Paul, A., Oxidation – Reduction Equilibrium in Glass, Journal of Non-Crystalline Solids, 123, 1990, p.354-362

Preziosi, S., Soden, R.R., Van Uitert, L.G., Large Alkali Metal and Alkali Earth Tungstate and Molybdate Crystals for Resonance and Emission Studies, Journal of Applied Physics, Vol. 33, 1962, p. 1893

Raman, S.V., The Effect of Mixed Modifiers on Nuclear Waste Glass Processing, Leaching, and Raman Spectra, J. Mater. Res., Vol.13, No. 1, Jan 1998.

Scheetz, B. E., Freeborn, W. P., Pepin, J., White, W. B., The System $SrMoO_4$-$BaMoO_4$-$CaMoO_4$: Compatibility Relations, The Implications for Supercalcine Ceramics, Scientific Basis for Nuclear Waste Management, Ed. Topp, S. V. (North Holland, New York) 1982, p.155-162

Schieber, M., Growth of Rare Earth Scheelites by the Flux Method, Inorganic Chemistry, Vol. 4, 1965, p.762-763

Schieber, M., Holmes, L., Crystal growth and Magnetic Susceptibilities of Some Rare Earth Sodium Molybdenum Scheelites, Journal of Applied Physics, Vol. 35, 1964, p.1004-1005

Schiewer, E. Rabe, H. Weisenburger, 1982, Scientific Basis for Nuclear Waste Management V, Ed. Topp, S. V., MRS Symposium Proceedings Vol. 11, Berlin 1982

Schlesinger, M. E., Lynch, D. C., Effect of VB and VIB Oxides on Nucleation Parameters in Lithium Disilicate Glass, Journal of Non-crystalline Solids, Vol. 108, 1989, p.237-248

Schreiber, H.D., Balazs, G.B., Carpenter, B.E., Kirkley, J.E., Minnix, L.M., Jamison, P.L., An Electromotive Force Series in a Borosilicate Glass-forming Melt, Communications of the American Ceramic Society, June 1984 C106-C108

Schreiber, H.D., Fowler, R.W., Ward, C.C., Sulphate as a Selective Redox Buffer for Borosilicate Melts, Physics and Chemistry of Glasses, Vol. 34, No. 2, 1993, pp. 66-70

Shi, F., Meng, J., Ren, Y., Preparation Structure and Physical Properties of New Silver Lanthanide Molybdenum Oxides, Materials Research Bulletin, Vol. 30, 1995, p.1401-1405

Smith, P.A., Vienna, J.D., Hrma, P., The Effects of Melting Reactions on Laboratory-scale Waste Vitrification, Journal of Materials Research, Vol. 10, Nº 8, August 1995 p. 2137-2149

Soper, P.D., Walker, D.D., Plodinec, M.J., Roberts, G.J., Lightner, L.F., Optimisation of Glass Composition for the Vitrification of Nuclear Waste at the Savannah River Plant, Bulletin of the American Ceramic Society, Vol. 62, No. 9, 1983, p. 1013-1018

Stedman, N.J., Cheetham, A.K., Battle, P.D., Crystal Structures of Two Sodium Yttrium Molybdates: $NaY(MoO_4)_2$ and $Na_5Y(MoO_4)_4$, Journal of Materials. Chemistry, Vol. 4 (5), 1994, p. 707-711

Stemprock, M., Voldan, J., Homogeneous Silicate Glasses in Systems Na_2O-SiO_2-WO_3 and Na_2O-SiO_2-MoO_3, Journal Silikaty, Vol. 18, 1974, p.19

Strachan, D. M., Glass Dissolution: Testing and Modelling for Long-term Behaviour, Journal of Nuclear Materials, Vol. 298, 2001, p. 69-77

Teller, R.G., Refinement of some $Na_{0.5-x}M'_{0.5+x/3}\square_{2x/3}MoO_4$, M = Bi, Ce, La, Scheelite Structures with Powder Neutron and X-ray Diffraction Data, Acta Cryst. 1992, C**48**, 2101-2104

Teo, B.K., Joy, D.C., EXAFS Spectroscopy: Techniques and Applications (London, Plenum), c1981

Tilquin, J.Y., Duveiller, P., Gilbert, J., Claes, P., Comparison Between High Temperature UV-Visible Spectroscopy and Electrochemistry for the In-situ Study of Redox Equilibria in Glass-Forming Melts, Journal of Non-Crystalline Solids, 224, 1998, pp. 216-224

Trocellier, P., Chemical Durability of High Level Nuclear Waste Forms, Ann. Chim. Sci. Mat, 2001, 26(2), pp.113-130

Van Der Wielen, J. C. Th. G. M., Stein, H. N., Stevels, J. M., Glass formation in Alkali Molybdate Systems, Journal of Non-crystalline Solids, Vol. 1, 1968, p.18-28

Vernaz, E, Private Communication, 2002

Volf, M.B., Chemical Approach to Glass, Glass Science and Technology 7 (Elsevier, Oxford), 1984

Wang, T.H., Hand, R.J., James, P.F., "Redox Control in H/M Waste Glasses", 17th Quarterly Report, University of Sheffield, June 2000

Watt, I.M., The Principals and Practice of Electron Microscopy (Cambridge University Press), 1985

Watts, I., Private communication, 2001

Wertz, J.E., Electron Spin Resonance: Elementary Theory and Practical Applications (London, Chapman and Hall), 1986

Weyl, W. A., Coloured Glasses, Society of Glass Technology (Dawsons, London) 1959, p.403

Weyl W. A., Marboe, E. C., The Constitution of Glasses, A Dynamic Interpretation, (John Wiley and Sons, New York) 1962

Weyl, W. A., Marboe, E. C., The Constitution of Glasses – A Dynamic Interpretation (John Wiley and Sons, London) Vol. 2 Part 1, 1964, p.508

White, W.B., Knight, D.S., Transition Metal Ions in Glass: A Comparison of Optical Absorption and Luminescence Evidence, MRS Symposia Proceedings Vol. 61 of the Defects in Glasses Symposium, Boston, Dec, 1985.

Williams, D. B., Cater, B., Transmission Electron Microscopy: A Textbook for Materials Science (Plenum, London), 1996

Young, H. D., Freedman, R. A., Sear and Zemansky's University Physics with Modern Physics 11th Edition (Pearson/Addison Wesley), 2004, p.1653

Glass Compositions

Glass		Oxide (g)								
		SiO_2	B_2O_3	Na_2O	Li_2O	Waste[†]	MoO_3	Cs_2O	Nd_2O_3	La_2O_3
1	HM4 20%	49.44	17.52	8.80	4.24	20	-	-	-	-
2	HM4 35%	40.17	14.24	7.15	3.45	35	-	-	-	-
3	HM4 35% 3/4Li_2O	40.73	14.43	7.25	2.58	35	-	-	-	-
4	HM4 35% 1/2Li_2O	41.29	14.63	7.35	1.72	35	-	-	-	-
5	HM4 35% No Li_2O	42.42	15.03	7.55	-	35	-	-	-	-
6	HM4 35% No Na_2O	40.17	14.24	-	6.9	35	-	-	-	-
7 air/red	HM4 20%	49.44	17.52	8.80	4.24	20	-	-	-	-
8 air/red	HM4 25%	46.35	16.43	8.25	3.98	25	-	-	-	-
9 air/red	HM4 30%	43.26	15.33	7.7	3.71	30	-	-	-	-
10 air/red	HM4 35%	40.17	14.24	7.15	3.45	35	-	-	-	-
11 ox/air/arg/red	1%Mo glasses	61.18	21.68	10.89	5.25	-	1.00	-	-	-
12 ox/air/red	Cs-Nd glasses	46.35	16.43	16.5	-	-	2.99	1.94	8.47	-
13 ox/air/red	Cs-Nd glasses	45.92	16.28	16.35	-	-	4.79	3.11	13.55	-
14 air/red	Cs-La glasses	45.92	16.28	16.35	-	-	4.79	3.11	-	13.55

[†]See **Table 3.2** for full waste composition

Suffixes **ox**, **air**, **arg** and **red** denote glasses sparged with oxygen, compressed air, argon and nitrogen/5%hydrogen gases respectively during melting